Polyamide 1010 and 2D Nanomaterials-Based Hybrid Multifunctional Nanocomposites

By

Gabriel Matheus PINTO

MANUSCRIPT-BASED THESIS PRESENTED TO ÉCOLE DE TECHNOLOGIE SUPÉRIEURE AND MACKENZIE PRESBYTERIAN UNIVERSITY IN PARTIAL FULFILLEMENT FOR THE DEGREE OF DOCTOR OF PHILOSOPHY
Ph.D.

MONTREAL, NOVEMBER 15th, 2024

ÉCOLE DE TECHNOLOGIE SUPÉRIEURE
UNIVERSITÉ DU QUÉBEC

BOARD OF EXAMINERS

THIS THESIS HAS BEEN EVALUATED
BY THE FOLLOWING BOARD OF EXAMINERS

Mrs. Nicole R. Demarquette, Thesis Supervisor
Department of Mechanical Engineering, École de Technologie Supérieure

Mr. Guilhermino J. M. Fechine, Thesis Supervisor
School of Engineering, Universidade Presbiteriana Mackenzie, Brazil

Mr. Éric David, Thesis Co-supervisor
Department of Mechanical Engineering, École de Technologie Supérieure

Mr. Hélio Ribeiro, Thesis Co-supervisor
School of Engineering, Universidade Presbiteriana Mackenzie, Brazil

Mr. Bora Ung, President of the Board of Examiners
Department of Electrical Engineering, École de Technologie Supérieure

Mr. Lucas Abia Hof, Member of the jury
Department of Mechanical Engineering, École de Technologie Supérieure

Mrs. Emna Helal, Member of the jury
Department of Mechanical Engineering, École de Technologie Supérieure

Mr. Ricardo J. E. Andrade, Member of the jury
School of Engineering, Universidade Presbiteriana Mackenzie, Brazil

Mr. Patrick Lee, External Evaluator
Department of Mechanical and Industrial Engineering, University of Toronto, Canada

THIS THESIS WAS PRENSENTED AND DEFENDED
IN THE PRESENCE OF A BOARD OF EXAMINERS AND PUBLIC
ON NOVEMBER 6th, 2024
AT ÉCOLE DE TECHNOLOGIE SUPÉRIEURE

ACKNOWLEDGMENTS

I would like to express my deepest gratitude to everyone who has supported me throughout this journey.

Firstly, I want to thank my family for their unwavering support and encouragement. Their belief in me has been a constant source of motivation.

To my wife, Nathalie, thank you for being by my side through every step of this journey. Your love, patience, and understanding have been invaluable.

I am deeply grateful to my advisors and all other professors with whom I was able to collaborate for their guidance. Their expertise and encouragement have greatly contributed to the completion of this work.

A special thanks to my colleagues for their friendship and camaraderie. Your support and collaboration have made this experience enriching and enjoyable.

I would like to express my gratitude to Eder, Josué, and Daria, who have served as great sources of inspiration. I have adopted them as role models, and their influence has been profoundly impactful.

I would like to acknowledge the laboratory technicians, especially Serge Plamondon, for all the technical support. Serge's efforts in assembling the environmental chamber for the mechanical tests at low temperature were crucial to the success of my research.

A heartfelt thank you to Emna Helal for the insightful discussions. Your wisdom and perspective have been greatly appreciated.

Thank you all for your contributions and support.

Nanocomposites Multifonctionnels Hybrides à Base de Nanomatériaux 2D et Polyamide 1010

Gabriel Matheus PINTO

RÉSUMÉ

Cette thèse de doctorat se concentre sur le développement de nanocomposites polymères en utilisant une matrice de polyamide 1010 (PA 1010) biosourcée et de divers nanomatériaux bidimensionnels (2D). Pa 1010 a été choisi pour son potentiel d'application diversifié dans plusieurs domaines et son caractère respectueux de l'environnement par rapport aux polyamides traditionnels. Les charges nanométriques sélectionnés - l'oxyde de graphène (GO), le nitrure de bore hexagonal (h-BN) et le disulfure de molybdène (MoS_2) - ont été choisis pour leur compatibilité chimique avec les groupes amide du polyamide et leurs structures 2D, ce qui conduit à leur surface élevée et à leurs propriétés exceptionnelles. Cependant, un défi clé dans l'utilisation de charges nanométriques 2D est d'obtenir une dispersion appropriée dans la matrice polymère. Par conséquent, cette thèse propose la nouvelle approche de combiner différentes particules 2D dans un seul composite pour améliorer la dispersion mutuelle et promouvoir des effets synergiques.

Les nanocomposites ont été produits par fusion dans une extrudeuse double vis. Tout d'abord, de faibles quantités (0,1, 0,3 ou 0,5 % en poids) des nanoparticules exfoliées précédemment ont été déposées sur les particules de polymère au sol par une technique appelée *solid-solid deposition*. Ensuite, ce mélange de poudre a été introduit à l'extrudeuse pour mélanger la matrice polymère avec les charges nanométriques à l'état fondu, formant ainsi un mélange homogène. Ce processus facilite considérablement la mise à l'échelle, car il est compatible avec l'infrastructure de traitement des polymères industriels existante, permettant son intégration dans les lignes de production actuelles et ouvrant la voie à des applications commerciales.

Des études sur la dynamique moléculaire ont été menées pour élucider les interactions entre les charges nanométriques et la matrice de polyamide, en se concentrant sur le processus de relaxation du polymère lors de la transition vitreuse, le volume des chaînes impliquées dans la transition de Brill pendant la fusion et l'énergie nécessaire pour séparer les chaînes polymères des feuilles nanométriques. Les résultats ont indiqué que GO et h-BN présentent des interactions plus fortes avec la matrice polymère par rapport au MoS_2, ce qui se reflète également dans les performances de leurs respectifs composites hybrides.

La microstructure de la matrice polymère, un facteur critique influençant les propriétés des matériaux à base de polymères, a été examinée par des analyses microstructurales. Ces analyses ont révélé que l'ajout des charges nanométriques a affecté l'ordre semi-cristallin de la matrice polymère. Bien que la transition de phase de α à γ n'ait pas été observée, h-BN et MoS_2 se sont avérés pour diminuer à la fois la fraction cristalline globale et l'organisation des domaines cristallins. Au contraire, go n'a pas affecté de manière significative la microstructure de polymère. Cependant, avec ses feuilles plus grandes et sa forte affinité chimique, GO a

conduit à la plus grande amélioration de la ténacité à la traction à température ambiante (plus de 120% à 0,5% en poids). Fait intéressant, cette amélioration n'a pas été observée à basse température (-40 ° C), où la diminution de l'ordre microstructural était la principale raison d'augmentation de la ténacité de la PA 1010, avec seuls les composites renforcés par h-BN conservant certaines caractéristiques d'augmentation de la ténacité d'origine.

Enfin, pour démontrer la multifonctionnalité des nanocomposites développés, il a été démontré que l'incorporation de faibles quantités (moins de 0,5 % en poids) de ces charges nanométriques 2D permettait aux nanocomposites de conserver les propriétés diélectriques et tribologiques originales du PA 1010 tout en améliorant la conductivité thermique de près de 10%. Ces résultats soulignent le potentiel de ces nanomatériaux en tant qu'additifs à faible teneur pour des applications avancées, où l'obtention de propriétés spécifiques sans compromettre les autres présente un défi important.

Mots-clés: Nanocomposites polymères; Polyamide 1010; Oxyde de graphène; Nitrure de bore hexagonal; Disulfure de molybdène; Propriétés multifonctionnelles

Hybrid Multifunctional Nanocomposites Based on Polyamide 1010 and 2D Nanomaterials

Gabriel Matheus PINTO

ABSTRACT

This PhD thesis focuses on the development of polymer nanocomposites using a bio-sourced polyamide 1010 (PA 1010) matrix and various two-dimensional (2D) nanomaterials. PA 1010 was chosen for its diverse application potential across multiple domains and its environmentally friendly character compared to traditional polyamides. The selected nanofillers - graphene oxide (GO), hexagonal-boron nitride (h-BN), and molybdenum disulfide (MoS_2) - were chosen for their chemical compatibility with the polyamide's amide groups and their 2D structures, which leads to their high surface area and exceptional properties. However, a key challenge in utilizing 2D nanofillers is achieving proper dispersion within the polymer matrix. Therefore, this thesis proposes a novel approach of combining different 2D fillers within a single composite to enhance mutual dispersion and promote synergistic effects.

The nanocomposites were produced through melt blending in a twin-screw extruder. First, low amounts (0.1, 0.3, or 0.5 wt%) of the previously exfoliated nanofillers were deposited on the ground polymer particles by a technique called solid-solid deposition. Then, this powder mixture was fed to the extruder to properly mix the polymer matrix with the nanofillers in the melt, thus forming a homogeneous mixture. This process significantly facilitates scalability, as it is compatible with existing industrial polymer processing infrastructure, enabling its integration into current production lines and paving the way for commercial applications.

Molecular dynamics investigations were conducted to elucidate the interactions between the nanofillers and the polyamide matrix, focusing on the polymer relaxation process at the glass transition, the volume of chains involved in the Brill transition during melting, and the energy required to separate polymer chains from the nanosheets. The results indicated that GO and h-BN exhibit stronger interactions with the polymer matrix compared to MoS_2, which is also reflected in the performance of their respective hybrid composites.

The microstructure of the polymer matrix, a critical factor influencing the properties of polymer-based materials, was examined through microstructural analyses. These analyses revealed that the addition of the nanofillers affected the polymer matrix's semi-crystalline order. Although the phase transition from α to γ was not observed in the Polyamide crystals, h-BN and MoS_2 were found to decrease both the polymer's overall crystalline fraction and the organization of its crystalline domains. On the contrary, GO did not significantly affect the polymer microstructure. However, with its larger sheets and strong chemical affinity, GO led to the greatest enhancement in tensile toughness at room temperature (over 120% at 0.5 wt%). Interestingly, this enhancement was not observed at low temperatures (-40 °C), where the decreased microstructural order was the predominant reason for the toughening of PA 1010, with only h-BN composites retaining some of the original toughening characteristics.

Finally, to demonstrate the multifunctionality of the developed nanocomposites, it has been demonstrated that incorporating low amounts (less than 0.5 wt%) of these 2D nanofillers allowed the nanocomposites to retain the original dielectric and tribological properties of PA 1010 while enhancing thermal conductivity by nearly 10%. These findings underscore the potential of these nanomaterials as low-content additives for advanced applications, where achieving specific properties without compromising others presents a significant challenge.

Keywords: Polymer nanocomposites; Polyamide 1010; Graphene oxide; Hexagonal-boron nitride; Molybdenum disulfide; Multifunctional properties

Nanocompósitos Multifuncionais Híbridos à Base de Poliamida 1010 e Nanomateriais 2D

Gabriel Matheus PINTO

RESUMO

Esta tese de doutorado se concentra no desenvolvimento de nanocompósitos poliméricos usando uma matriz de poliamida 1010 (PA 1010) de origem biológica e múltiplos nanomateriais bidimensionais (2D). A PA 1010 foi escolhida por sua potencial aplicação em vários campos e seu caráter ecológico em comparação às poliamidas tradicionais. As nanocargas selecionadas - óxido de grafeno (GO), nitreto de boro hexagonal (h-BN) e dissulfeto de molibdênio (MoS_2) - foram escolhidas por sua compatibilidade química com os grupos amida da poliamida e suas estruturas 2D, o que leva à sua alta área superficial e propriedades excepcionais. No entanto, um dos principais desafios na utilização de nanocargas 2D é alcançar a dispersão adequada dentro da matriz polimérica. Portanto, esta tese propõe uma nova abordagem ao combinar de diferentes cargas 2D em um único compósito para aumentar a dispersão mútua e promover efeitos sinérgicos.

Os nanocompósitos foram produzidos por mistura no estado fundido em uma extrusora dupla-rosca. Primeiramente, pequenas quantidades (0,1, 0,3 ou 0,5% em peso) dos nanomateriais previamente esfoliados foram depositados nas na superfície do polímero moído por uma técnica chamada *solid-solid deposition*. Em seguida, essa mistura em pó foi alimentada na extrusora para promover uma mistura adequada da matriz polimérica com as nanocargas no estado fundido, formando assim uma mistura homogênea. Este processo facilita significativamente a escalabilidade, pois é compatível com a infraestrutura industrial existente de processamento de polímeros, permitindo sua integração nas linhas de produção atuais e abrindo caminho para aplicações comerciais.

Investigações de dinâmica molecular foram conduzidas para elucidar as interações entre as nanocargas e a matriz de poliamida, com foco no processo de relaxamento do polímero na transição vítrea, no volume de cadeias envolvidas na transição Brill durante a fusão e na energia necessária para separar as cadeias poliméricas das nanofolhas. Os resultados indicaram que GO e h-BN exibem interações mais fortes com a matriz polimérica em comparação com MoS_2, o que também se reflete no desempenho de seus respectivos compósitos híbridos.

A microestrutura da matriz polimérica, um fator crítico que influencia as propriedades dos materiais à base de polímeros, foi examinada por meio de análises microestruturais. Essas análises revelaram que a adição das nanocargas afetou a ordem semicristalina da matriz polimérica. Embora a transição de fase de α para γ não tenha sido observada nos cristais de poliamida, verificou-se que o h-BN e o MoS_2 diminuem a fração cristalina do polímero, assim como a organização de seus domínios cristalinos. Pelo contrário, o GO não afetou

significativamente a microestrutura do polímero. No entanto, com suas folhas maiores e forte afinidade química, o GO levou ao maior aumento na tenacidade à tração à temperatura ambiente (mais de 120% a 0,5% em peso). Curiosamente, esse aumento não foi observado em baixas temperaturas (-40 °C), onde a menor ordem microestrutural foi a razão predominante para a tenacificação da PA 1010, com apenas os compósitos de h-BN parcialmente mantendo algumas de suas características tenacificantes.

Finalmente, para demonstrar a multifuncionalidade dos nanocompósitos desenvolvidos, foi demonstrado que a incorporação de baixas quantidades (menos de 0,5% em peso) desses nanomateriais 2D permitiu que os nanocompósitos mantivessem as propriedades dielétricas e tribológicas originais da PA 1010, enquanto a condutividade térmica foi aumentada em quase 10%. Essas descobertas ressaltam o potencial desses nanomateriais como aditivos de baixo teor para aplicações avançadas, onde alcançar propriedades específicas sem comprometer outras apresenta um desafio significativo.

Palvras-chave: Nanocompósitos poliméricos; Poliamida 1010; Óxido de grafeno; Nitreto de boro hexagonal; Dissulfeto de molibdênio; Propriedades multifuncionais

TABLE OF CONTENTS

Page

LIST OF TABLES

Page

LIST OF FIGURES

Page

ABBREVIATIONS LIST

2DM	Two-dimensional materials
ABS	Acrylonitrile butadiene styrene
AFM	Atomic Force Microscopy
BDS	Broadband dielectric spectroscopy
$CaCO_3$	Calcium carbonate
CF	Carbon fiber
COF	Friction coefficient
CT	Cryogenic temperatures
CTE	Coefficient of thermal expansion
CVD	Chemical vapor deposition
DC	Direct current
DFT	Density functional theory
DMA	Dynamic mechanical analysis
DMF	Dimethylformamide
DOE	Design of experiments
DSC	Differential scanning calorimetry
DV	Double-vacancy
EC	Electrical conductivity
EG	Expanded graphite
EMA	Ethylene methyl acrylate copolymer
EME	Extensional mixing elements
EMI	Electromagnetic interference
EVA	Ethylene-vinyl acetate
FLG	Few layer graphene
FPA	Fluorinated polyamide
FWCNT	Few-wall carbon nanotube
GNP	graphene nanoplatelets
GO	Graphene oxide

GRM	Graphene related materials
h-BN	Hexagonal boron nitride
HDPE	High-density polyethylene
ITC	Interfacial thermal conductivity
ITR	Interfacial thermal resistance
KB	Kneading blocks
LAMMPS	Large-scale atomic/molecular massively parallel simulator
LLDPE	Linear low-density polyethylene
LOI	Limiting oxygen index
LVR	Linear viscoelastic regime
MAH	Maleic anhydride
MD	Molecular dynamics
mGO	Multilayer graphene oxide
MGW	Multi-layer graphene web
MMT	Montmorillonite
MoS_2	Molybdenum disulfide
$MoSe_2$	Molybdenum selenide
MTPS	Modified transient plane source method
MV	Multi-vacancy
MWCNT	Multi-wall carbon nanotubes
MWS	Maxwell-Wagner-Sillars
NfG	NH_2-functionalized graphene
NIR	Near infrared
NMP	n-methyl-2-pyrrolidone
NPT	Isothermal-isobaric ensemble
NVT	Canonical ensemble
OMMT	Organic montmorillonite
PA 1010	Polyamide 1010
PA 12	Polyamide 12
PA 6	Polyamide 6

PA 66	Polyamide 66
PA	Polyamide
PAni	Polyaniline
PC	Polycarbonate
PDMS	Poly(dimethylsiloxane)
PES	Poly(ether sulfone)
PET	Poly(ethylene terephthalate)
PLA	Polylactic acid
PMMA	Poly(methyl methacrylate)
POMOE	Poly[oxymethylene-(oxyethylene)]
PP	Polypropylene
PPy	Polypyrrole
PS	Polystyrene
PTA	Polythioamide
PTP	polythiophene
PU	Polyurethane
PVA	Poly(vinyl alcohol)
PVC	Poly(vinyl chloride)
rGO	Reduced graphene oxide
RNEMD	Reverse non-equilibrium molecular dynamics
RT	Room temperature
SE	Shielding effectiveness
SEM	Scanning electron microscopy
SPM	Scanning Probe Microscopy
SRF	Solid rectangular fixture
STEM	Scanning transmission electron microscopy
STM	Scanning Tunneling Microscopy
SV	Single-vacancy
SW	Stone-Wales
TC	Thermal conductivity

TGA	Thermogravimetric analysis
TIM	Thermal interface material
TiO_2	Titanium dioxide
TMD	Transition metal dichalcogenide
TRGA	Thermally reduced graphene aerogel
UHMWPE	Ultrahigh molecular weight polyethylene
VFT	Vogel-Fulcher-Tammann
WS_2	Tungsten sulfide
WSe_2	Tungsten selenide
XRD	X-ray diffraction

SYMBOLS LIST

ε''_{tot}	Total dielectric loss
$\emptyset_f$	Filler volume fraction
ΔH_B	Enthalpy of the melting peak after PA 1010's Brill transition
ΔH_m	Overall enthalpy related to the melting of PA 1010
$\tan \delta_c$	Composite's damping factor
$\tan \delta_m$	Neat polymer's damping factor
E_a	Activation energy
$I_{(hkl)}$	Intensity of diffraction peak related to *hkl* crystalline plane
$L_{(hkl)}$	Crystalline lamella thickness related to *hkl* crystalline plane
T_g	Glass transition temperature
T_{mc}	Temperature at the peak of crystallization
T_{on}	Temperature at the onset of crystallization
T_v	Vogel-Fulcher temperature
X_c	Polymer crystallinity
k_B	Boltzmann's constant
$t_{1/2}$	Time to reach half-crystallinity
α_k	Width parameter characteristic to the slope at the low frequency side of the relaxation peak
β_k	Asymmetry parameter
ε'	Real part of dielectric permittivity (dielectric constant)
ε''	Imaginary part of dielectric permittivity (dielectric loss)
ε''_{rel}	Dielectric losses related to relaxation processes
ε_0	Permittivity of free space
$\varepsilon_{\infty k}$	Residual dielectric constant at "infinitely" higher frequencies than the one of relaxation process *k*
η_r	Relative viscosity
σ'	Real part of the complex conductivity

σ_{DC}	Direct current conductivity
τ_0	Relaxation time at infinite temperature
τ_k	Relaxation time of relaxation process k
$\Delta\varepsilon_k$	Dielectric strength of relaxation process k
n	Exponential factor between 0 and 1
A	Adhesion factor
B	Full width at half maximum of the diffraction peak (rad)
C	Solution concentration
K	Mark-Houwink constant
M	Molecular weight
T	Temperature
X	Cooling rate.
a	Mark-Houwink exponent
k	Thermal conductivity
η	Intrinsic viscosity
θ	Diffraction angle
λ	X-ray wavelength
ω	Angular frequency

INTRODUCTION

In this section, a concise context will be presented to provide background information on the thesis' topic, elucidating the significance and relevance of polymer nanocomposites based on polyamide 1010 (PA 1010) and 2D nanomaterials. Following this contextual overview, the specific objectives of the research are outlined, detailing the aims of the study while explaining how these were systematically addressed in each subsequent chapter.

0.1 Context

Polymer nanocomposites represent a cutting-edge class of materials that combine the properties and processability of polymers with the enhanced functionalities provided by nanoscale fillers. These nanocomposites can offer significant improvements over traditional composites in terms of mechanical strength, thermal and electrical conductivity, and other functional properties, all while maintaining lightweight characteristics. The integration of nanoscale fillers into polymer matrices allows for the development of materials with a tailored balance of properties, making them suitable for a wide range of applications, including aerospace, automotive, electronics, and biomedical (Abd Malek et al., 2020; Aghajani, Ehsani, Khajavi, Kalaee, & Zaarei, 2022; Ashok & Kalaichelvan, 2020; J. Bai et al., 2019; Bragaglia et al., 2021; Xing Chen et al., 2009; Dong et al., 2022; Du et al., 2010; Garcia et al., 2021; George, Joy, & Anas, 2021; Horváth et al., 2011; Hu et al., 2019; Hussain, Hojjati, Okamoto, & Gorga, 2006; Jang, Youn, Song, & Lee, 2016; Kumar, Goel, & Kumar, 2017; Lei et al., 2014; P. Li, Zhang, Yang, Yuan, & Jiang, 2021; Q. Li et al., 2016; C. Liu et al., 2019; Md Said et al., 2021; X. Meng, Wang, Cong, Ye, & Zhou, 2019; Naskar, Keum, & Boeman, 2016; Nie et al., 2022; Öner, Keskin, Kızıl, Pochat-Bohatier, & Bechelany, 2019; Peddamallu, Sridharan, Nakayama, & Sarathi, 2019; Pham, Li, Bekyarova, Itkis, & Mulchandani, 2019; Qu, Fan, Mukerabigwi, Liu, & Cao, 2021; Radisavljevic, Radenovic, Brivio, Giacometti, & Kis, 2011; Ramezani et al., 2022; Salunke & Gopalan, 2021; Santhosha, Nayak, Pollok, Langenhorst, & Adelhelm, 2019; Sarkar et al., 2019; Seki, Kizilkan, İşbilir, Sarikanat, & Altay, 2021; Shin, Shin, & Choi, 2020; Sorrentino et al., 2015; L. S. Su & Tsai, 2021; Vikraman et al., 2019;

Yinrui Wang & Xie, 2020; S. N. Wei et al., 2022; Woodward et al., 2017; X. Wu, Liu, Shi, Yang, & Zhang, 2022; L. Xu, Tan, Xu, Xie, & Lei, 2019; Z. Yu & Drzal, 2020; S. Zhou, Shi, Bai, Liang, & Zou, 2020).

Polyamide 1010 (PA 1010), derived from renewable resources, is an environmentally friendly polymer known for its excellent mechanical properties, thermal stability, and good resistance to chemicals and abrasion. PA 1010 is a long-chain aliphatic polyamide that not only supports sustainability initiatives but also offers desirable features such as high strength, durability, and flexibility. These properties make it an ideal candidate for developing high-performance composites (A. Kausar, 2017; Ayesha Kausar, 2017, 2018; Kuciel, Kuźnia, & Jakubowska, 2016; Kuciel, Kuźniar, & Liber-Kneć, 2012; Levinta et al., 2020; Wanli Li et al., 2008; McKeen, 2012; S.-L. Zhang, Wang, Jiang, Wang, Ma, & Wu, 2005; Zhishen, Qingbo, Jinhua, Hongfang, & Donglin, 1993).

Among nanoscale fillers, 2D nanomaterials have emerged as revolutionary components in the field of composites due to their extraordinary properties. Among these, graphene oxide (GO), hexagonal boron nitride (h-BN), and molybdenum disulfide (MoS_2) have been extensively studied for their unique characteristics, e.g., remarkable mechanical strength, large specific surface area, high thermal conductivity and stability, electrical insulation and/or semiconducting behavior, and outstanding lubricating character (Blase, Rubio, Louie, & Cohen, 1994; Brent, Savjani, & O'Brien, 2017; Dean et al., 2010; Furimsky, 1980; Holinski & Gänsheimer, 1972; Kinloch, Suhr, Lou, Young, & Ajayan, 2018; P. Liu et al., 2018; Luo et al., 2017; Rasul, Kiziltas, Arfaei, & Shahbazian-Yassar, 2021).

However, there is still a great challenge regarding filler agglomeration in the production of polymer nanocomposites due to the large specific surface area these nanomaterials exhibit, which favors their restacking when they are embedded in a polymer matrix. A recent approach proposed in the literature to mitigate this effect is the employment of hybrid nanofillers. This concept involves the simultaneous incorporation of multiple nanofillers into a polymer matrix by carefully selecting and combining fillers such as GO, h-BN, and MoS_2. This approach aims

to harness the synergistic effects that can arise from the distinct properties of different fillers, potentially leading to superior material performance compared to single-filler systems (X. Cui et al., 2015; Kavimani et al., 2021; Ribeiro, Trigueiro, Lopes, et al., 2018; Ribeiro, Trigueiro, Owuor, et al., 2018; Ribeiro et al., 2019, 2020a).

Another important issue is that, up to this date, most works in the literature have employed significant high amounts of nanofillers (> 20 wt%) when studying nanocomposites with thermoplastic matrices such as PA 1010, which is detrimental for some intrinsic properties of the neat polymer, such as flexibility and ductility.

Therefore, this PhD thesis aims to develop low-content polymer nanocomposites based on PA 1010 and various 2D nanomaterials, specifically GO, h-BN, and MoS_2. The study covers both single-filler systems and hybrid composites, where pairs of these nanomaterials are combined to evaluate potential synergistic effects. The composites were fabricated using the conventional melt-blending technique in a twin-screw extruder, following a preliminary solid-solid deposition method to coat the polymer powder with the nanomaterials, thereby enhancing dispersion uniformity prior to extrusion. By employing low nanofiller contents (< 0.5 wt%), the intent is to achieve enhancements in functional properties such as thermal conductivity while not compromising the inherent mechanical properties of the polymer matrix. Additionally, molecular dynamics and microstructural characterizations were performed to gain insights into the interactions between each nanofiller and the polymer matrix, offering a deeper understanding of the nanocomposites' structural and functional characteristics.

0.2 Objectives and Outline

The general aim of this thesis is to develop and characterize polymer nanocomposites based on PA 1010 and 2D nanomaterials (GO, h-BN, and MoS_2) at extremely low contents (0.1 – 0.5 wt%), focusing on three key areas: (I) physical interactions between polymer chains and the nanofillers; (II) changes in the polymer microstructure; and (III) multifunctional properties.

To achieve these objectives, a thorough literature review on the subject was performed, which is presented in this thesis' Chapter 1 and published in *Polymer Composites*. This literature review was also selected as the cover article for the issue in which it was published. Then, polymer nanocomposites based on PA 1010 and GO, h-BN, or MoS_2, applied both individually and in pairs, were produced through melt blending in a twin-screw extruder. Three contents were investigated, i.e., 0.1, 0.3, and 0.5 wt%, with the final content being kept the same for the hybrid composites while applying a ratio of 1:1 for each nanofiller. After acquiring the nanocomposites, the different degrees of interaction between each nanofiller and the polymer matrix were investigated by studying how the relaxation processes of the polymer chains were affected by the presence of the nanofillers. This first study is presented in this thesis' Chapter 2 and was published in *Polymer*. Then, the microstructural changes in the semi-crystalline structure of PA 1010 promoted by the addition of the nanofillers, as well as the mechanical behavior of the nanocomposites under tensile stress and different environmental conditions were investigated. The results of this second study are presented in this thesis' Chapter 3 and were published in *Polymer Composites*. Lastly, important functional properties for engineering applications, i.e., dielectric behavior, tribological aspects, and thermal conductivity were investigated. These results are reported in this thesis' Chapter 4 and were published in *Journal of Applied Polymer Science*.

CHAPTER 1

FROM TWO-DIMENSIONAL MATERIALS TO POLYMER NANOCOMPOSITES WITH EMERGING MULTIFUNCTIONAL APPLICATIONS: A CRITICAL REVIEW

Gabriel M. Pinto[1,2,3], Josué M. O. Cremonezzi[1,2], Hélio Ribeiro[2], Ricardo J. E. Andrade[1,2], Nicole R. Demarquette[3], Guilhermino J. M. Fechine[1,2]

[1] Mackenzie Institute for Research in Graphene and Nanotechnologies – MackGraphe, Mackenzie Presbyterian University. Rua da Consolação. 896. São Paulo - SP. 01302-907. Brazil
[2] Engineering School, Mackenzie Presbyterian University. Rua da Consolação. 896. São Paulo - SP. 01302-907. Brazil
[3] École de Technologie Supérieure (ÉTS), Mechanical Engineering Department, 1100, rue Notre-Dame Ouest, Montréal, Québec, H3C 1K3, Canada

Paper published in *Polymer Composites*, 2023
DOI: https://doi.org/10.1002/pc.27213

ABSTRACT

2D materials are a very up-and-coming class of additives in the field of polymer composites due to their versatility and exceptional intrinsic properties. This enables researchers to create a variety of nanocomposites that can be employed in a myriad of emerging multifunctional applications. The performance of such nanocomposites depends heavily on the quality of the 2D materials, their interactions with the polymer matrix, as well as on their dispersion and morphology when embedded in the polymer. In order to control these variables, one needs to choose wisely between the available synthesis techniques and mixing strategies, playing with the process-structure-property relationships, while keeping in mind the compatibility with current industrial infrastructure. Therefore, this paper presents a brief review on the 2D materials most used in polymer nanocomposites, the main synthesis techniques and mixing routes developed, the state of the art on the most sought-after properties in different systems, and what are the effects of the morphology evolution. In each section, the main challenges are highlighted, and possible strategies to overcome them are presented, e.g., the advent of hybrid 2D nanostructures, which promote synergistic effects, enabling the combination of properties that were not previously achievable on the final material. Finally, the paper ends by presenting a perspective of the current state in the development of these emerging multifunctional nanocomposites and what are the most important steps that need to be taken, not only academically, but also industrially, in order for these materials to start being widely applied and become staples in the daily life of humanity.

Keywords: Polymer Nanocomposites; Multifunctional Materials; 2D Materials

1.1 Introduction

Multifunctional materials with specific features are starting to be considered one of the fundamental pillars in many industries, such as in mobility systems, wearable electronic devices, energy storage and conversion, and environmental rehabilitation. In that sense, composites based on nanoscale fillers incorporated in a polymeric matrix constitute a very interesting class of advanced materials with multifunctional properties. Two-dimensional materials (2DM), commonly represented by graphene, with a thickness of just one atomic layer, have become steadily more important for composite applications because of their considerable surface areas and exceptional physical properties (Kinloch et al., 2018; P. Liu et al., 2018).

In the last decades, many new 2DM have emerged beyond graphene, e.g., hexagonal boron-nitride (h-BN) (Luo et al., 2017), numerous transition metal dichalcogenides (TMDs), such as molybdenum disulfide (MoS_2), among others (Brent et al., 2017), with their combined distinctive optical, electromagnetic, and conductive properties contributing to flexibility and mechanical resistance. Figure 1.1 presents the bidimensional structure of these aforementioned materials.

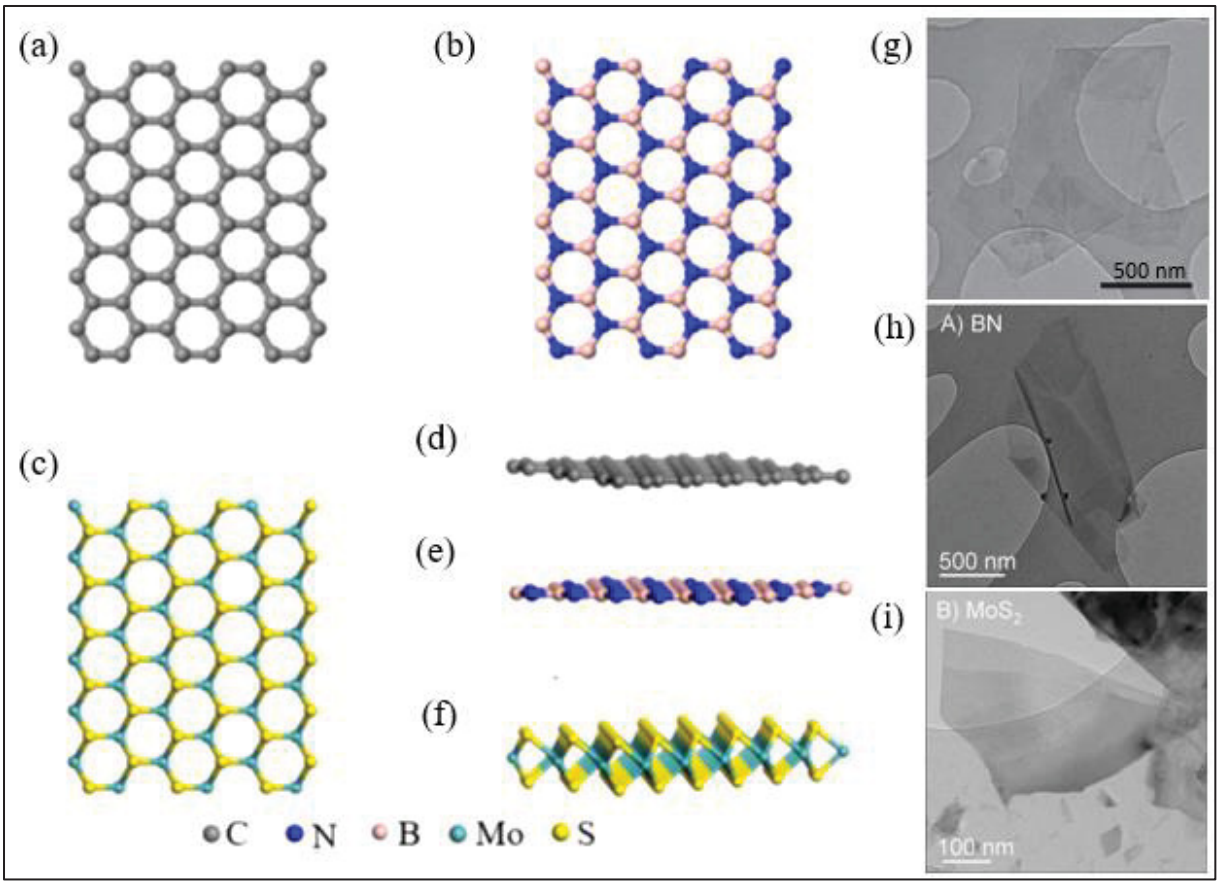

Figure 1.1 – Top view (a-c), lateral view (d-f), and TEM images (g-i) of the structure of graphene, h-BN, and MoS_2, respectively. Reproduced with permission from (Coleman et al., 2011; Hernandez et al., 2008; Jialin Liu, Hui, & Lau, 2022)

Ideally, the use of these materials could result in nanocomposites with impressive multifunctional attributes, which explains the astounding increase in the annual number of publications with "polymer" and, "graphene", "boron nitride", or "MoS_2" as keywords from 2005 to 2022, as presented in Figure 1.2.

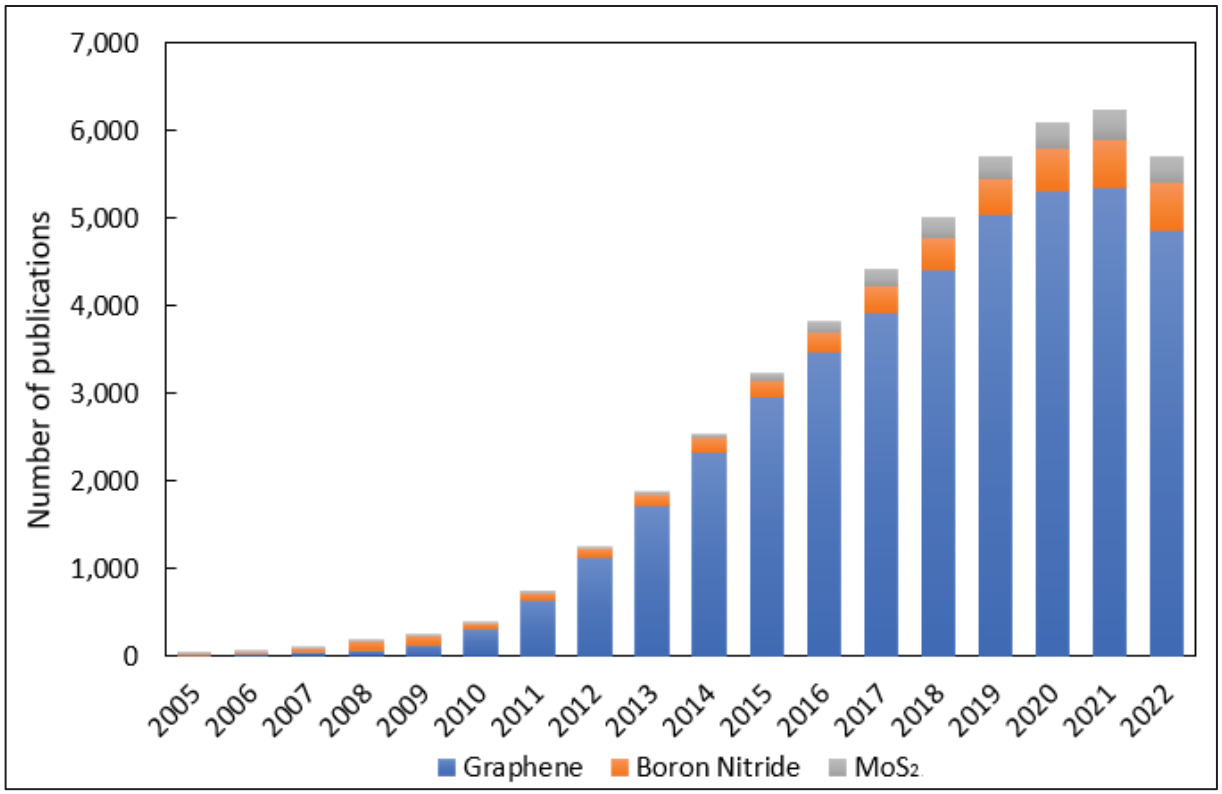

Figure 1.2 – Annual number of publications with keywords "polymer" and, "graphene", "boron nitride", or "MoS_2" from 2005 to 2022. Source: Scopus. Accessed in November 2022

Moreover, as the maturity of 2DM's mass production techniques develops (L. Yang, Chen, Yu, & Liu, 2021), the emergence of new products with relevant industrial applications shows that the technology is accelerated towards the market (Barkan, 2019; Kong et al., 2019; Reiss, Hjelt, & Ferrari, 2019). Thus, the scientific efforts regarding 2DM-reinforced polymer composites may now change from a purely technology-pushed to a market-pulled approach.

However, it is still a challenge to fully transfer the excellent properties of 2DMs to polymeric matrices using traditional processing methods, which involve the direct mixture of the nanofillers with polymers in the melt (Mittal, Dhand, Rhee, Park, & Lee, 2015; Yoo, Shin, Yoon, & Park, 2014). There are two main limitations: (i) production of 2DM with a controlled number of layers, lateral dimensions and surface functionalities, and (ii) obtaining uniform dispersions with as little agglomeration as possible, as well as controlling the final morphology, i.e., relative orientations, distribution and content inside the polymer matrix (Ma, Siddiqui, Marom, & Kim, 2010; Potts, Dreyer, Bielawski, & Ruoff, 2011).

Despite the efforts to develop new methodologies to achieve different composites' morphologies using 2DM, there is still a lack of understanding of how to optimize the final composites for specific applications, which require multiple properties. This can be partially attributed to the large variation of 2DM features in terms of geometry, structural defects and functional groups induced by different syntheses (Ma et al., 2010). Moreover, the ideal composite morphologies strongly depend on the specific application. For example, aligned 2DM maximize barrier properties, while an interconnected 3D network with low percolation threshold is preferable for homogeneous electrical/thermal conductivity (X. Shen, Zheng, & Kim, 2021). Therefore, multifunctional applications can demand exclusive morphologies. Another practical example is in electroactive actuators and in energy storage: it is particularly desired materials with high dielectric constant and low dielectric loss, but these two properties are generally mutually exclusive (Q. Li et al., 2015). Therefore, aiming to attend the strict demands required by multifunctional applications, it is extremely important to establish a complete comprehension of the process-structure-property relation.

On that account, this paper aims at presenting a critical review on the use of 2DM in polymer nanocomposites, more specifically, graphene-related materials (GRM), h-BN, and MoS_2. The paper starts with a brief definition of these 2DM, addressing some of the interesting properties that they present, which makes them so appealing for polymer nanocomposites. Then, the biggest and most important challenges to be overcome for the production of 2DM/polymer-based nanocomposites are presented. These go from the synthesis of nanomaterials, which highly influence their intrinsic properties, to the available mixing routes, which define the fillers dispersion and their viability for mass production. Afterwards, an individual section is given for three of the most fundamental properties towards emerging multifunctional demands, i.e., mechanical reinforcement, thermal properties (conductivity and stability), and electrical conductivity (EC). Some other miscellaneous properties might be presented throughout this manuscript if the specific nanomaterial exhibits an interesting characteristic that is not addressed by the main topics. Additionally, the combination of these 2DM as hybrid fillers is

also tackled, enlightening why these 2D hybrid materials show even more promise than their individual constituents for some applications.

1.2 2DM Intrinsic Properties

The differentiated properties arising from 2DM are the main reason for their possible applications in multifunctional systems. These properties, ranging from mechanical strength to electrical behavior, have been evaluated using Scanning Probe Microscopy (SPM) techniques, such as Atomic Force Microscopy (AFM) in nanoindentation mode and Scanning Tunneling Microscopy (STM) (M. Zeng, Xiao, Liu, Yang, & Fu, 2018). In this context, monolayer graphene without structural defects is regarded as one of the most rigid materials due to its σ graphitic bonds (C. Lee, Wei, Kysar, & Hone, 2008). Although other 2DM, such as h-BN (Falin et al., 2017), and MoS_2 (Bertolazzi, Brivio, & Kis, 2011; Castellanos-Gomez et al., 2012) have inferior moduli and ultimate strengths than graphene, these are still significantly higher than polymeric materials, as can be verified in Table 1.1.

Table 1.1 – Young's moduli of 2DM obtained from simulations

2D Material	Young's modulus (GPa)	Ref.
Graphene	1000	(C. Lee et al., 2008)
GO	200-250	(Suk, Piner, An, & Ruoff, 2010)
rGO	250-300	(Gómez-Navarro, Burghard, & Kern, 2008)
h-BN	271	(Falin et al., 2017)
MoS_2	~ 300	(Bertolazzi et al., 2011; Castellanos-Gomez et al., 2012)

GO = graphene oxide; rGO = reduced graphene oxide; MoS_2 = molybdenum disulfide; h-BN = hexagonal boron-nitride.

The structure and type of bonds present in these nanostructures are not only responsible for their excellent mechanical properties, but they are also the base for their multifunctionality. For instance, the EC of these 2DM varies in orders of magnitude, going from extremely conductive graphene to semiconductor MoS_2, and insulating h-BN. Such a vast array of

properties theoretically allows the modification of the final composites' characteristics at will. This could be done by choosing the appropriate 2DM or even their hybrids in an adequate association.

Regarding the thermal conductivity (TC), monolayer graphene shows a very high value, surpassing that of diamond, which distinguishes it as the highest among current materials. Even though h-BN has a lower TC than graphene, its low EC makes it useful for applications that require TC associated with electrical insulation, e.g., in thermal interface materials (TIMs), electrical cables insulation, refractory crucibles, and electronics packaging (Kuang et al., 2015; Rasul et al., 2021). This excellent TC arises from the innate crystalline structure of 2DMs, which allows the phonons to be transported without much scattering (X. Shen et al., 2021). While GRM and h-BN are considered highly thermally conductive fillers, MoS_2 has been less explored in this field due to its three-atom lamellar structure, which generates higher phonon scattering (I. Jo, Pettes, Ou, Wu, & Shi, 2014; Wu Li, Carrete, & Mingo, 2013; Yafei Wang et al., 2021). Table 1.2 summarizes the EC of these materials and Table 1.3 their TC.

Table 1.2 – Electrical properties of the addressed 2DM and some derivatives. Values reproduced from (Tokarczyk et al., 2014; Turchanin et al., 2009)

2D Material	Electrical property
Graphene	Conductive (resistivity < 10 Ω/sq)
GO	Insulating
rGO	Conductive (resistivity = 10-20 kΩ/sq)
h-BN	Insulating
MoS_2	Semiconductor (*band gap* = 1.4 – 1.9 eV)

GO = graphene oxide; rGO = reduced graphene oxide; MoS_2 = molybdenum disulfide; h-BN = hexagonal boron-nitride.

Table 1.3 – Thermal conductivity of the addressed 2DM and some derivatives

2D Material	Thermal Conductivity ($Wm^{-1}K^{-1}$)	Ref.
Graphene	5000	(Balandin et al., 2008)
GO	72 – 670	(Junjie Chen & Li, 2020)
rGO	30 – 2600	(Y. Zeng et al., 2019)
h-BN	360	(I. Jo et al., 2013)
MoS_2	40 - 50	(I. Jo et al., 2014; Wu Li et al., 2013; Yafei Wang et al., 2021)

GO = graphene oxide; rGO = reduced graphene oxide; MoS_2 = molybdenum disulfide; h-BN = hexagonal boron-nitride.

Although this class of materials present high conductivities along the basal plane direction, they show elevated anisotropy. Graphite's TC in its thickness is just ~ 6 $Wm^{-1}K^{-1}$, i.e., three orders of magnitude lower than in its basal plane direction. This occurs due to the increased phonon scattering across the van der Waals' interlayer forces (Balandin, 2011). This trend is not exclusive to TC. For example, the EC and mechanical performance also manifest substantial anisotropy, promoting uneven properties in polymer composites (Z. Wang et al., 2015; Yousefi et al., 2013, 2014). Some details for each family of 2DM are given below.

1.2.1 Graphene-Related Materials

Graphene is a bidimensional sheet of sp^2 hybridized carbon atoms organized in a honeycomb structure. As already mentioned, it is considered the "thinnest and strongest material in the universe" having exceptional physical and chemical characteristics, which leads to its impressive properties. It also has a very large specific surface area (2360 m^2g^{-1}), which exceeds TiO_2 by more than one order of magnitude (33.3 – 174.5 m^2g^{-1}). Therefore, high-performance nanocomposites are thought to benefit from using it as a filler (Gouzman et al., 2019; X. Sun et al., 2021; Young, Kinloch, Gong, & Novoselov, 2012; X. Yu et al., 2017; Zhu et al., 2010). In addition, some tailored forms of graphene, such as reduced graphene oxide (rGO), present some very interesting optical properties, e.g., the capacity to absorb light energy at visible or

near-infrared (NIR) wavelengths and convert it to phonon energy (Leeladhar, Raturi, & Singh, 2018; Shi et al., 2015; J. Wei et al., 2017). These latter properties have motivated the engineering of some photothermal nanocomposites such as actuators (D. D. Han et al., 2015; L. Yu & Yu, 2015) and solar steam generators (Liang et al., 2019; G. Wang et al., 2017; H. Wang, Mi, Li, & Zhan, 2020).

All of these characteristics made GRM the most employed nanofillers to obtain nanocomposites over the last few years (Ashok & Kalaichelvan, 2020; Dong et al., 2022; Garcia et al., 2021; George et al., 2021; Hu et al., 2019; C. Liu et al., 2019; Md Said et al., 2021; Seki et al., 2021; L. S. Su & Tsai, 2021; Z. Yu & Drzal, 2020), as can be seen in Figure 1.2. It's also important to note that by 2019, papers on graphene/polymer composites account for about 50% of all articles on graphene-based composites. The reason for that is the much wider range of possible applications for polymer nanocomposites compared to metallic or ceramic nanocomposites due to the chemical modifications that this nanomaterial can undergo (X. Sun et al., 2021).

1.2.2 Hexagonal Boron Nitride

Of the three crystalline forms, h-BN is the most stable among boron-nitride materials (hexagonal, cubic, and wurzite). It can be found in 0D fullerenes, 1D nanotubes, and the 2D nanosheets. Similar to graphene, its atomic structure has boron and nitrogen atoms bonded by strong covalent bonds in an hexagonal pattern. In spite of that, its layers are stacked by weaker van der Wall’s forces and Lip-Lip bonds, with boron and nitrogen atoms positioned above and below one another in neighboring layers. (Golberg et al., 2010; W. Meng, Huang, Fu, Wang, & Zhi, 2014; Weng, Wang, Wang, Bando, & Golberg, 2016).

One of the significant material classes with several uses is h-BN/polymer composites (Aghajani et al., 2022; Bragaglia et al., 2021; Nie et al., 2022; Öner et al., 2019; Qu et al., 2021; Salunke & Gopalan, 2021; S. N. Wei et al., 2022; X. Wu et al., 2022; S. Zhou et al., 2020), encompassing fields like health care and medicine (Xing Chen et al., 2009; Horváth et al., 2011), energy storage (Lei et al., 2014; Q. Li et al., 2016), electronic engineering (Jang et

al., 2016), and the mobility sector (automotive (Naskar et al., 2016) and aerospace (Hussain et al., 2006)). While graphene/polymer nanocomposites have received a lot of attention, less focus has been placed on h-BN/polymer composites. However, h-BN is a very interesting 2DM to be explored, because, differently from other 2D nanofillers, it is a dielectric due to a wide bandgap (~5.6 eV) (Blase et al., 1994; Dean et al., 2010). In addition to this higher electronic bandgap, h-BN has better thermal stability than graphene, which makes it the perfect candidate for electrical insulation applications (Rasul et al., 2021). Another intriguing feature is that B-N (Lip-Lip) bonding's partial ionic electronic structure may be beneficial for molecular interactions with polymers, as has been already demonstrated by molecular dynamics (MD) simulations (Xiaoming Chen et al., 2015). Finally, it also differentiates itself from its carbonaceous counterparts by being white, which enables the dying of its composites (Zhi et al., 2006).

1.2.3 Molybdenum Disulfide

Molybdenum disulfide (MoS_2) is one of the more than 40 possible types of transition metal dichalcogenides (TMD). A monolayer of MoS_2 structure is formed by a prismatic trigonal arrangement of S–Mo–S, constituted of 2 planes of hexagonally arranged sulfur atoms that sandwich an also hexagonal plane of molybdenum atoms. These three planes are strongly bonded through ionocovalent interactions. Even so, the lamellae are associated to its neighbors through van der Waals interactions (Coleman et al., 2011; Dickinson & Pauling, 1923; Mak, Lee, Hone, Shan, & Heinz, 2010).

Depending on the lamellae disposition, four different polytypes of MoS_2 can be formed, the 2H (hexagonal), 3R (rhombohedral), and 1T (tetragonal) being the most studied. Among them, the most common phase is the thermostable 2H, that occurs naturally as molybdenite, being a diamagnetic semiconductor. The 3R phase has the same coordination as the 2H polytype in its layers, however, they are arranged in a rhombohedral arrangement. (Singh et al., 2018). The 1T-MoS_2 is conductive and shows a metastable arrangement, being obtained only via synthetic

routes (Singh et al., 2018; Wypych & Schöllhorn, 1992). Figure 1.3 illustrates these different allotropic forms.

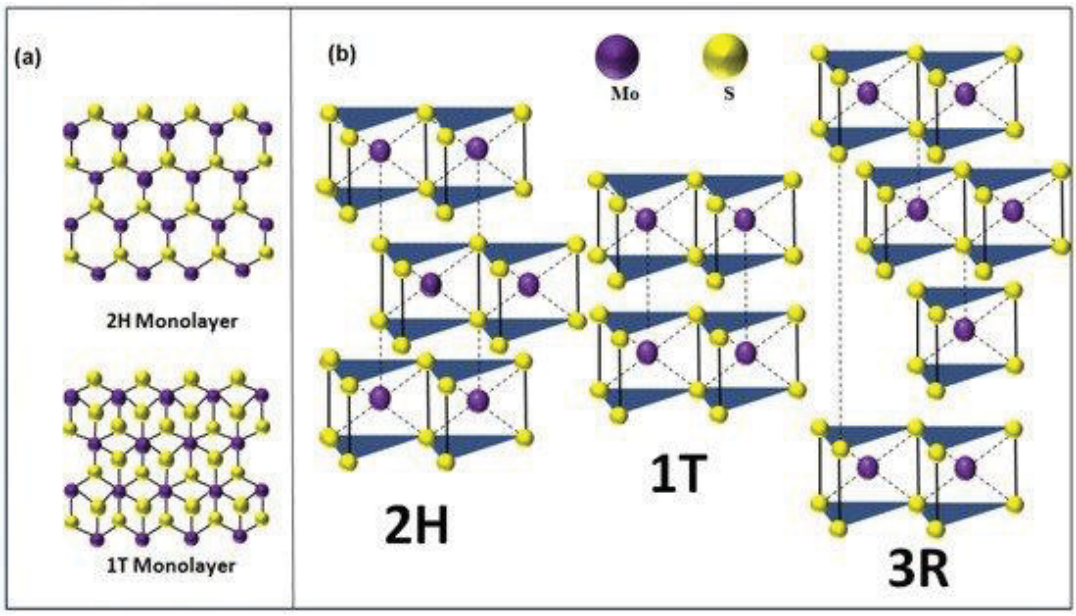

Figure 1.3 – (a) Top view of 2H and 1T MoS_2 monolayers; (b) Polymorphic structures of MoS_2. Reproduced with permission from (Mouloua et al., 2021)

MoS_2 has been used as a solid-state lubricant and catalyst for hydrogen evolution and hydrodesulfurization in bulk form for a very long time (Furimsky, 1980; Holinski & Gänsheimer, 1972). However, although the exfoliation of MoS_2 to monolayer was performed for the first time in 1986 (Joensen, Frindt, & Morrison, 1986), major attention to the material was drawn only after the emergence of graphene (P. Li et al., 2021; X. Meng et al., 2019; Peddamallu et al., 2019; Ramezani et al., 2022; Sorrentino et al., 2015; L. Xu et al., 2019). As soon as Geim and Novoselov's (Novoselov et al., 2004) discussion on the "electric field effect in atomically thin carbon films" gained momentum, several researchers devoted their attention to MoS_2 and other TMDs.

Due to its superior optoelectronic properties, exfoliated MoS_2 is mainly used for optoelectronic applications (Rao, Maitra, & Waghmare, 2014). Among promising applications are devices such as transistors (Radisavljevic et al., 2011), solid-state lithium-ion batteries (J. Bai et al., 2019; Du et al., 2010; Santhosha et al., 2019), supercapacitors (Sarkar et al., 2019; Yinrui

Wang & Xie, 2020), solar cells (Abd Malek et al., 2020; Shin et al., 2020; Vikraman et al., 2019) and sensors (Kumar et al., 2017; Pham et al., 2019). Moreover, the non-linear susceptibility of monolayer MoS_2, which may be ~ 3.4 times higher than that of monolayer graphene, brings opportunities for the material in integrated frequency conversion, nonlinear switching, and signal processing in telecommunications (Woodward et al., 2017).

1.3 Current Challenges

Although it is known that the mastery of the process-structure-property triad relation is essential to achieve multifunctional characteristics in polymer nanocomposites, controlling it is still an enormous challenge. In the case of nanocomposites containing 2DM, this hardship mainly originates from two reasons: (i) control of the quality during the synthesis of these 2DM; (ii) viability of mixing techniques in different polymer systems and scalability. Some aspects of these two challenges are reviewed below.

1.3.1 Structural Defects

A characteristic that affects 2DM properties is related to structural defects, or presence of functional chemical groups that can promote the breakage of the nanostructures symmetry (Addou & Colombo, 2022). For instance, edge effects and folding of the nanosheets in graphene can lead to a lower modulus, ~ 500 GPa, almost half of a defect-free monolayer graphene sheet (Q.-Y. Lin et al., 2013; Ruiz-Vargas et al., 2011). The moduli of graphene's chemical derivatives graphene oxide (GO) and reduced graphene oxide (rGO) are also significantly lower, as shown in Table 1.1 (Gómez-Navarro et al., 2008; Suk et al., 2010). Although these values are below those of pure graphene, they are nevertheless superior to those of conventional fillers, e.g., carbon black and titanium dioxide (TiO_2), which are in the order of 4.1 - 27.6 GPa and 230 - 288 GPa, respectively (T. Chen, Qiu, Zhu, & Li, 2016; Dittrich, Wartig, Hofmann, Mülhaupt, & Schartel, 2013).

Graphene's EC and TC are substantially reduced by defects, as well as by the presence of functional groups, as can be seen in Table 1.2 and Table 1.3. This occurs due to electron and phonon scattering, where the sp^2 hybridization of the carbon atoms changes to sp^3 (Jung, Dikin, Piner, & Ruoff, 2008; X. Shen, Wang, Wu, Liu, & Kim, 2016). It is well known that GO presents lower EC and TC than neat graphene. Therefore, it is often reduced to partially recover graphene's characteristic C=C bonds (Jung et al., 2008). However, even after reduction, both conductivities remain much lower than those of pristine graphene. The inherent properties of 2DM are thus adversely affected by functionalization, despite the fact that functional groups are required to increase their dispersion and interfacial dynamics with polymer matrices. In order to balance the interfacial quality of nanomaterials in composites with their inherent qualities, a compromise must be made.

Although defect structures are more discussed in GRM due to the great interest in graphene's chemical derivatives, the other 2DM are not exempt from it. In the case of h-BN, defects are usually formed during its synthesis. There are three main types of defects that are more common for this 2DM, i.e., N and B vacancies (V_N and V_B), antisites (N_B and B_N), which is when a N atom takes the place of a B atom and vice-versa, and carbon substitution (C_N and C_B), which is when a C atom takes the place of either a N or B atom.

These defects have been investigated theoretically through density functional theory (DFT) simulations and experimentally observed (Azevedo, Kaschny, De Castilho, & De Brito Mota, 2007; Jiménez et al., 1998, 1997). It has been noticed that C_N/C_B are the most stable defects, while antisites are more likely to occur than vacancies. Nonetheless, V_N and V_B can also arise, and they interestingly present opposite effects on the lattice. While V_N tends to create a "contraction", reducing the distance between the first-neighboring B atoms, more expressive deformations are produced by V_B, since it leads to an increase in that distance due to repulsion from the neighboring N atoms (Azevedo et al., 2007).

In respect to MoS_2, the 2D lattice may present a nearly limitless number of defects, as has been demonstrated for GRM (Banhart, Kotakoski, & Krasheninnikov, 2011). However, due to the

additional complexity imposed by the three-dimensional architecture and the binary element system involved, structural defects have been less investigated in MoS_2 (W. Zhou et al., 2013). Thus, only the simplest intrinsic defects will be presented here. Similar to h-BN, these consist basically on different possible vacancies and antisites atoms created during the growth in bottom-up processes, being much less observed in samples obtained by top-down approaches (Banhart et al., 2011). For example, it has been demonstrated both theoretically and experimentally that Mo_{S2} and $S2_{Mo}$ antisite defects have higher formation energies, whereas V_S has the lowest, making it the most easily observable (W. Zhou et al., 2013).

It's also curious that S divacancies (V_{S2}) require almost twice as much energy as single V_S to form, which diverges from GRM, in which divacancies are energetically favored over monovacancies (G. Do Lee et al., 2005). Additionally, it has been observed that, since the neighbor S atoms from a V_{Mo} become loose, it is unusual for a V_{Mo} to occur, more commonly being observed complex vacancies, e.g., V_{MoS3}. However, this can be leveraged for applications where active edge sites are desirable, such as chemical sensing and hydrogen generation (Kumar et al., 2017; Pham et al., 2019; T. Wang et al., 2014). It's worth mentioning that, despite not being the scope of this work, many other dislocations have been predicted for MoS_2 structures, which could be utilized in the future to modify the material's characteristics for particular uses (W. Zhou et al., 2013).

1.3.2 Synthesis Methods

The selection of a proper synthesis method is essential, because it will define not just the level of structural defects, but also the number of layers (*n*), degree of functionalization, and lateral size. When the aspect ratio decreases, which can be due to increased *n* or shorter sheets, inferior properties arise. For example, an eight-layer graphene has a modulus and ultimate strength 30% lower than a monolayer graphene due to the slippage of layers (Falin et al., 2017). A similar trend occurs for TC. When it surpasses 4 layers, TC gets close to bulk graphite (~ 1300 $Wm^{-1}K^{-1}$) (Ghosh et al., 2010).

There are three variations that can be applied for the top-down synthesis of 2DM: (i) liquid phase exfoliation; (ii) chemical exfoliation; (iii) intercalation-assisted exfoliation. Figure 1.4 summarizes the most common approaches for exfoliating 2DM, highlighting each procedure's main advantages and disadvantages.

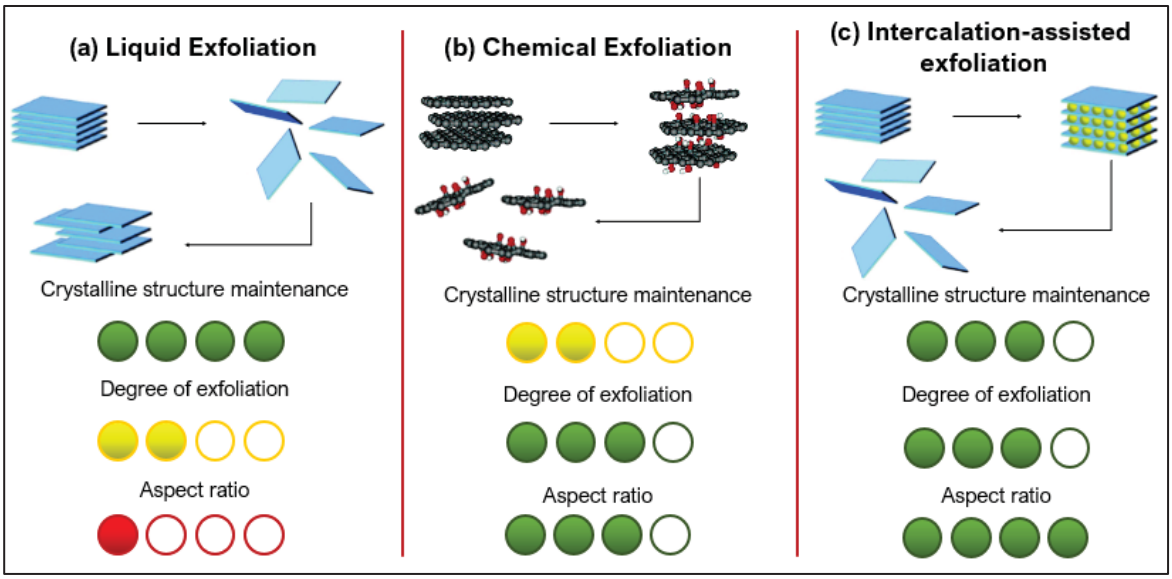

Figure 1.4 – Main procedures adopted to exfoliate 2DM, highlighting their main advantages (green) and disadvantages (red) related to the nanomaterial's features: (a) Direct liquid exfoliation; (b) Chemical exfoliation; (c) Exfoliation assisted by intercalating agents

The top-down exfoliation of bulk crystals in solvents using sonication or high shear is the most straightforward method to create 2DM for composites, providing sufficient mechanical energy to separate the nanosheets. A large variety of 2DM, including graphene (Hernandez et al., 2008; Paton et al., 2014), h-BN (Coleman et al., 2011), and MoS_2 (Coleman et al., 2011; Varrla et al., 2015), have already been successfully produced by this technique. Its main advantage is the maintenance of the crystalline network with few defects. However, in other media, the absence of functional groups makes it more challenging to disperse 2D nanosheets. The most used solvents, usually chosen by the match of their surface tension and the crystal's surface energy, are organic solvents such as dimethylformamide (DMF) or n-methyl-2-pyrrolidone (NMP) (Chhowalla et al., 2013; Jawaid et al., 2016), ionic liquids, or their combinations. The exfoliation in other media is also possible in the presence of surfactants, but such procedure predominantly yields multilayer particles even after prolonged times of sonication and shear,

which is harmful to the sheets' lateral size, i.e., the material's aspect ratio (Hennrich et al., 2007; Khan, O'Neill, Lotya, De, & Coleman, 2010). However, stable dispersions of few-layers MoS_2 were recently obtained through exfoliation in water without any surfactant (Rodriguez et al., 2020). It was proposed that hydrogen atoms provided by H_2O molecules decorated MoS_2 edges during the exfoliation, making the nanosheets dispersion highly stable. Moreover, it was found that due to the optimized geometry of MoS_2 with thiol (S–H) decorated edges, the crystallinity of the material was kept higher than non-functionalized flakes.

The Hummers' method, which involves using strong oxidizing agents like potassium permanganate ($KMnO_4$) and sulfuric acid (H_2SO_4) to produce oxygenated functional groups like epoxide, hydroxylic, and carboxylic groups that increase the lattice spacing in graphite derivatives, can be used to make layer separation easier (Hummers & Offeman, 1958). The obtained groups facilitate the nanosheets' exfoliation, which increases the stability of the material in water and, consequently, the yield of particles with fewer layers and larger sheet lateral sizes (J. E. Kim et al., 2011; Z. Xu & Gao, 2011). However, the crystal lattice structures originally formed by sp^2 hybridized carbons suffer significant changes when there are oxygenated functional groups, leading to much lower EC and TC. This makes chemical or thermal reduction an interesting step before the fabrication of composites that require high conductivity (X. Lin et al., 2012; Stankovich et al., 2007).

A modified Hummers' approach or other chemicals like sodium hydroxide (NaOH) have also been used to exfoliate h-BN and MoS_2 (Jing et al., 2017; X. Li et al., 2013; G. Zhao et al., 2015). In the case of h-BN, the smaller interplanar distance makes its exfoliation much more difficult than that of graphene (N. Wang et al., 2019), promoting preferential functionalization only at the edges (Jing et al., 2017). As a result, some investigations have attempted to maximize exfoliation using a ball mill while urea, furoic acid, or NaOH is included. Although this step increased the exfoliation, the lateral dimensions were significantly reduced due to the high energy applied by the mill. On the other hand, hydroxyl and amine groups at the edges of h-BN have been beneficial for dispersion and interfacial interactions with different solvents and polymeric matrices (Ding, Zhao, & Yu, 2018; D. Lee et al., 2015; Lei et al., 2015).

A third alternative mentioned in the literature is exfoliation assisted by intercalating agents. For example, a pre-step can be used to intercalate acids, such as H_2SO_4, or HNO_3, between the basal planes of the bulk material, after which expanded graphite (EG) is created by thermal expansion (Geng, Wang, & Kim, 2009). As EG has a much greater interplanar distance than the original graphite, exfoliation is already possible with moderate mechanical agitation, which avoids excessive breakage, allowing the production of 2D nanomaterials with a lateral size of up to 50 μm (Geng et al., 2009; J. Li, Sham, Kim, & Marom, 2007). Since there is no expressive functionalization of the basal planes, the formed nanomaterial continues to exhibit expressive EC and TC. Although acids, such as H_2SO_4, and H_3PO_4, have also functioned as efficient intercalating agents for h-BN (Kovtyukhova et al., 2013), allowing exfoliation of monolayers with lateral sizes > 10 μm (Kovtyukhova, Perea-López, Terrones, & Mallouk, 2017), it was noticed that ionic liquids and Li^+ are effective in the intercalation of MoS_2 [168,169].

1.3.3 Preparation Methods

Another key factor to achieve multifunctional characteristics in polymer nanocomposites is strongly related to how the nanofillers are added to the matrix. These nanocomposites are typically manufactured by three processes: (i) in-situ polymerization; (ii) solvent casting; (iii) melt mixing. Figure 1.5 presents the basic principles of each technique along with a summary of their advantages and disadvantages.

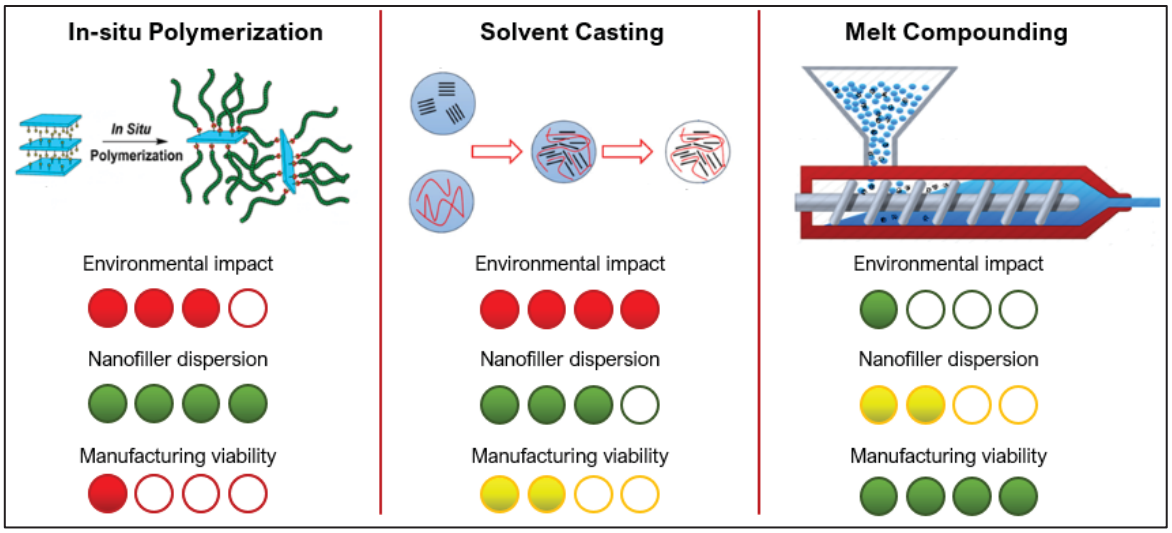

Figure 1.5 – Different processing methods for polymer nanocomposites, highlighting its main advantages (green) and disadvantages (red): (a) in-situ polymerization; (b) solvent casting; (c) melt compounding

In the first method, the nanofiller and the monomer are mixed in a reaction chamber prior to polymerization (Galpaya et al., 2012; O'Neill, Bakirtzis, & Dixon, 2014). The liquid monomer is initially used to incorporate the nanofiller before polymerization is started using a suitable initiator and either radiation or heat (Kuilla et al., 2010; Verdejo, Bernal, Romasanta, & Lopez-Manchado, 2011). Through several chemical reactions, covalent bonds are formed between the nanofiller and the polymer. Since the polymer macromolecules grow in between the filler's layers, this method is known to achieve the highest degree of exfoliation (F. Meng et al., 2017), as well as the lowest percolation thresholds (Papageorgiou, Kinloch, & Young, 2015).

Solvent casting is considered the simplest method for preparation of polymer nanocomposites. In this procedure, the polymer and nanofiller are dissolved or dispersed in a suitable solvent (B. Li and Zhong 2011). The nanocomposite is then produced by precipitating or casting a film with further evaporation of the solvent (Mensah et al. 2018; Madhad and Vasava 2019). Compared to other methods, solvent casting provides a simpler preparation process, however it is unhealthy and environmentally unfriendly, since it usually requires the use of organic, toxic solvents (Fu, Yao, and Yang 2015).

The melt blending technique has been regarded as the most practical, realistic, and economical method for manufacturing nanocomposites (Fu, Yao, and Yang 2015). The polymer is heated to a high temperature, which melts it and blends it with the nanoparticles using high shear and extensional forces. Since the matrix is already polymerized and not solubilized, it presents a greater challenge compared to the other approaches to properly disperse the nanofillers. Nevertheless, this approach is thought to lead to industrial processes that are more compatible, ecologically benign, and cost-effective due to the much higher production rates and the absence of toxic solvents (Madhad et al. 2021; Verdejo et al. 2011; Hussain et al. 2006; Mohan et al. 2018; Muñoz et al. 2018; H. Kim, Abdala, and Macosko 2010).

Due to the aforementioned advantages of the melt blending technique, much research has been devoted to improving, and even tailoring, the morphology of nanocomposites obtained by such process (W. hua Xu et al. 2021; Muñoz et al. 2018; Danda et al. 2020). For example, our research group has recently performed a study based on design of experiments (DOE) to identify what would be the best way to add 2DM into the polymer matrix. Two strategies were investigated, as can be verified in Figure 1.6Figure , and it was observed that coating the polymer powder with exfoliated 2DM prior to melt mixing (solid-solid deposition - SSD) improved the dispersion and amount of nanosized particles, while feeding the 2DM liquid dispersion directly in the extruder (liquid-phase feeding - LPF) promoted a higher aggregation trend (Muñoz et al. 2018).

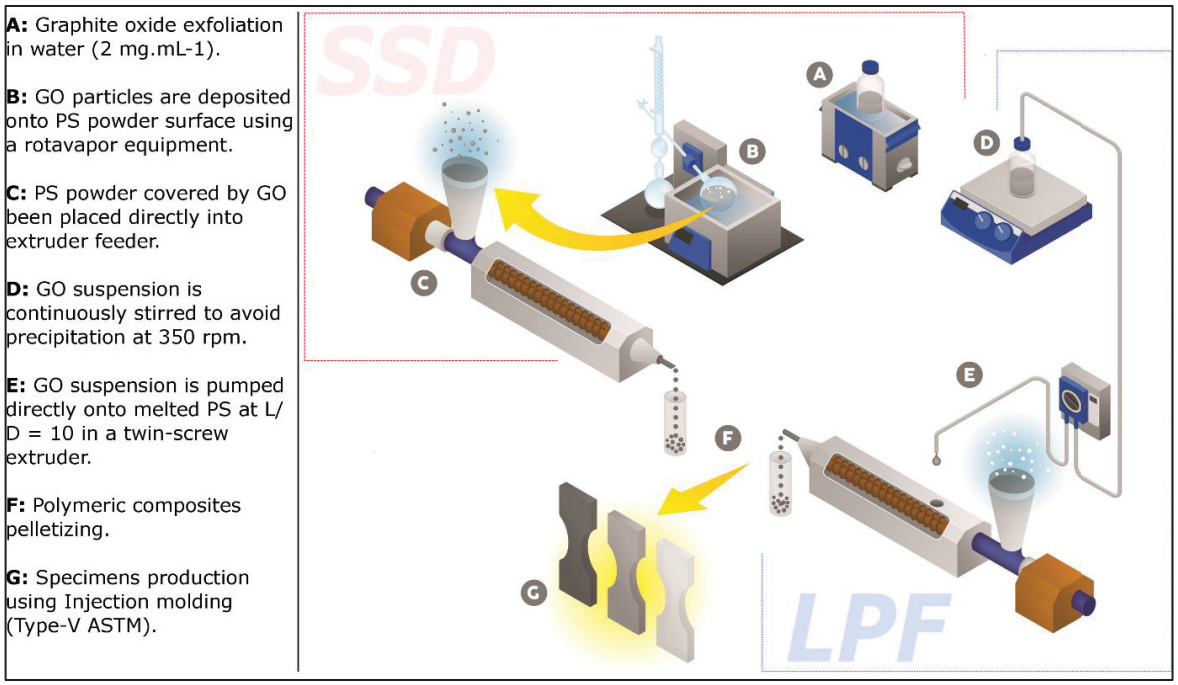

Figure 1.6 – Different strategies developed to insert 2DM into the polymer matrix through melt compounding: SSD is based on the deposition of the exfoliated nanosheets onto the surface of the polymer powder prior to melt mixing; LPF is based on feeding the 2DM liquid suspension directly into the extruder. Reproduced with permission from (Muñoz et al. 2018)

Alternatively, it has recently been proposed the use of a one-step melt mixing method based on the dynamic interplay involving alternating convergent and divergent flows and steam explosion (Xu et al., 2021). This approach is of interest because it does not require chemical agents or complex procedures, since the fast exfoliation of water-infiltrated EG into few-layer graphene nanosheets and synchronous dispersion in melts are made possible by the co-action of the internal force produced by steam explosion and the exterior force received from elongational melts. However, it is important to point out that this strategy is viable only for polyolefins and other non-polar thermoplastics, since they are not sensitive to water during melt processing, while polar matrices, e.g., polyesters, polyamides, and polycarbonates are susceptible to hydrolysis.

1.4 Mechanical Properties

This section will address the main results in the literature regarding the advent of 2DM as mechanical reinforcements for polymer nanocomposites. Special care is taken to detail the fundamental features of 2DM that mainly influence their degree of reinforcement, or lack thereof. These consist basically in the 2DM stacking, presence of structural defects, and sheet lateral size (specific surface area). Then, some strategies and conditions that may improve the efficiency of reinforcement are presented, e.g., functionalization, processing techniques that allow the tailoring of the nanocomposites' final morphology, employment of hybrid 2DM, and even environmental parameters.

1.4.1 Physical Characteristics

1.4.1.1 Number of layers

As previously described, the number of layers is a very significant feature that influences the intrinsic mechanical properties of 2DM. Therefore, the same is valid for their polymer-based nanocomposites, where an increased number of layers can be deleterious. The relationship between the number of layers in 2DM and the mechanical properties of its polymer nanocomposites has been experimentally studied. It was revealed that there is good stress transfer between both the monolayer and bilayer graphene and the polymer matrix. However, tri-layer and multilayer graphene showed less effective stress-transfer, which was credited to the slippage across internal graphene layers. Therefore, as there are more layers added, the nanocomposite's modulus drops (Gong et al. 2012).

It has also already been proven that the agglomeration effect, detrimental for the reinforcement, is induced by the use of high filler contents. For example, 40 wt.% of h-BN led to decreases of ~ 80% and 20% in tensile strength and elastic modulus, respectively, in an epoxy matrix (X.-B. Wang et al. 2014). Since higher filler contents favor the formation of aggregates, one needs

to be very cautious about how much filler is introduced into the polymer so that the mechanical properties are not prejudiced.

This effect has recently been proposed to originate from a “superlubricity state” when the lamellar material is subjected to high shear stresses. It has been demonstrated that it is not precisely stacked layers that slip, since the required shear force for that would be too high, even during melt processing. What actually happens is that when the filler is not sufficiently distributed, different clusters can aggregate in an out-of-register orientation. This effect is different from the precise re-stacking of layers, requiring much lower stresses to promote slippage. Therefore, in such cases, there might be a disaggregation of these smaller clusters (Ferreira, Andrade, & Fechine, 2019; Ferreira, de Lima, & Fechine, 2020), as depicted in Figure 1.7a.

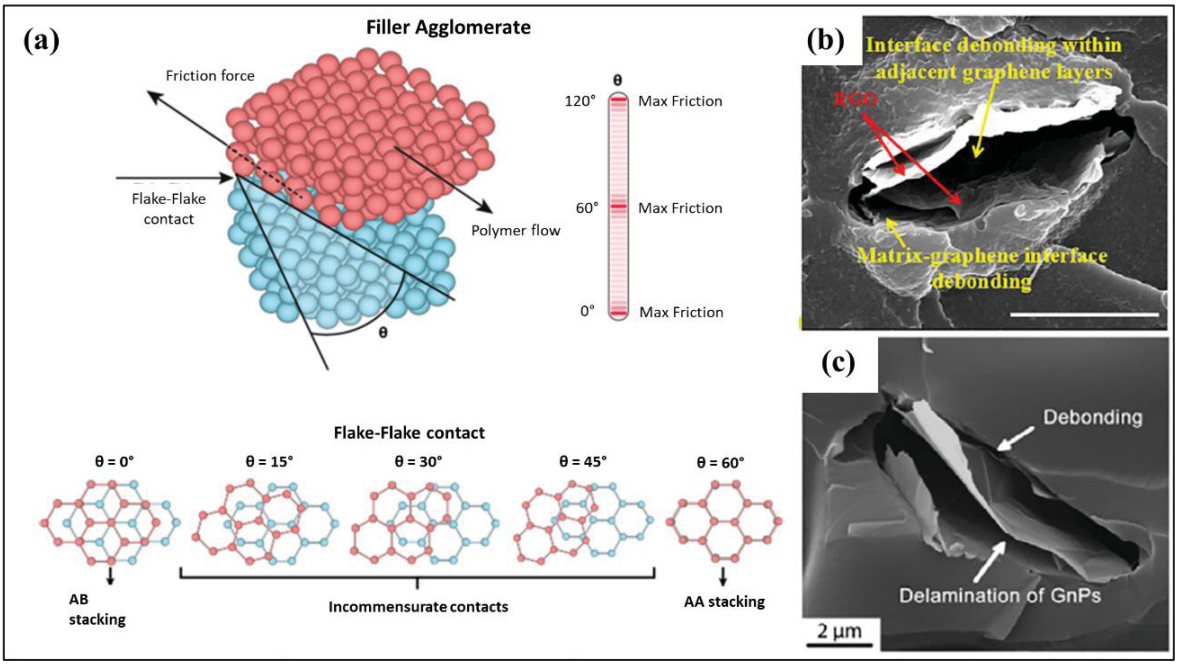

Figure 1.7 – (a) Superlubricity effect of agglomerates; (b) and (c) are SEM images exhibiting toughening mechanisms from the sliding and debonding of GRM flakes on the fractured surface of a 0.07 wt% PC/rGO composite and a 0.54 vol% epoxy/GNP composite, respectively. Scale bar is 5μm in (b). Reproduced with permission from (Ferreira et al., 2019; J. Wang et al., 2017; Wu et al., 2015)

On the other hand, it has also been demonstrated that this effect can actually be beneficial in some situations, e.g., as observed for polycarbonate (PC) and epoxy nanocomposites (Figure 1.7b,c) (J. Wang et al., 2017; Wu et al., 2015). It can clearly be seen in the SEM images from the fractured surfaces that debonding takes place not only at the matrix/GRM interface, but also at flake-flake contacts, causing microcracks around the nanosheets. As a result of this additional mechanism, primarily driven by the sliding of the flakes, the nanocomposite's toughness can be substantially improved (J. Wang et al. 2019; Chandrasekaran et al. 2014), increasing by 46% for PC/0.07 wt% rGO and nearly 900% for epoxy/0.8 vol% GNP, respectively.

1.4.1.2 Presence of Structural Defects

The final mechanical behavior of nanocomposites will be significantly influenced by structural defects, not just because they affect the intrinsic properties of 2DM, but mainly for the reason that the polymer-filler interface will be affected by them. This has been verified by molecular dynamics (MD) simulations based on three different structural defects. It has been observed that, even though interfacial and shear strength were negatively affected by single vacancy (SV) and double vacancy (DV), Stone-Wales (SW) defects improved the mechanical properties of nanocomposites (M. Li et al. 2017). These SW defects are presented in Figure 1.8a, and consist on the rotation of C-C bonds in 90°, which changes four adjacent benzene rings with sp^2 hybridization to pentagons and heptagons in the atomic structure.

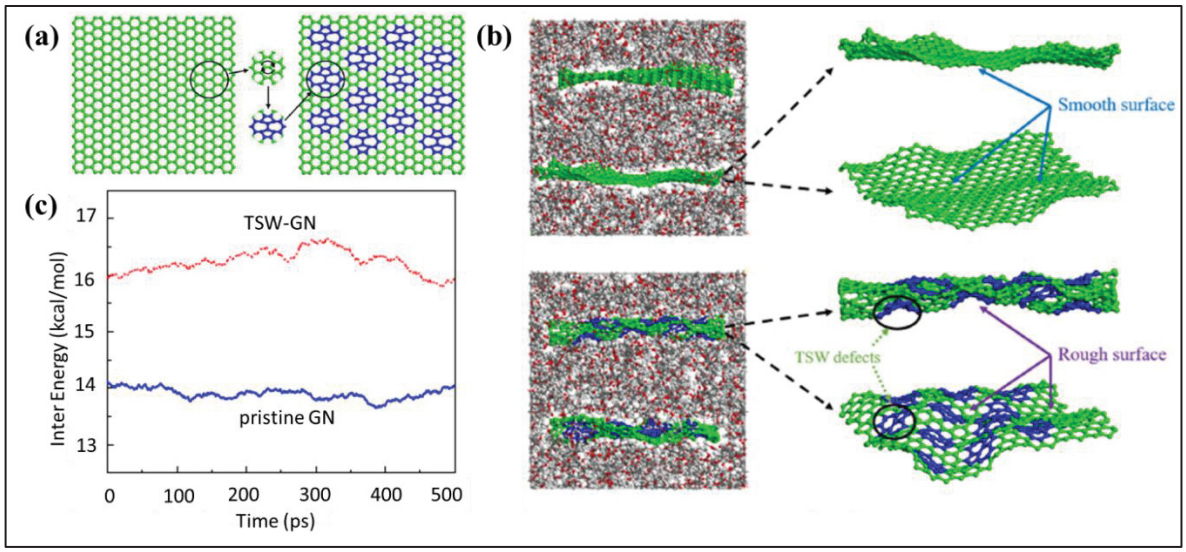

Figure 1.8 – (a) Formation of Stone-Wales defect in the graphene structure; (b) Increased surface roughness generated by SW defects in the graphene structure; (c) Variations in the interaction potential energy between pristine graphene and SW-graphene with PMMA polymer chains during NPT simulations. Adapted with permission from (B. Yang et al. 2021a)

As the presence of SW defects increases the surface roughness of graphene sheets (Figure b), SW-graphene has a stronger adsorption capacity and interaction with polymer molecular chains, which limits their mobility (B. Yang et al. 2021a). Figure 1.8c illustrates this effect by comparing the interaction potential energy of pristine graphene and SW-graphene with polymer chains during isothermal-pressure ensemble (NPT) simulations. It can be seen that, due to the introduction of "ravines" and "pits" on the surface of SW-graphene, it becomes more capable of binding polymer chains.

Similarly, another MD simulation study checked the effect of such defects not just on the interaction energy with polymer macromolecules, but also on the interfacial shear strength and on the pull-out energy. Curiously, it was verified that, even though SW defects indeed promote a higher interaction with polymer chains than DV, the interfacial shear strength and pullout energy are more affected by DV than SW defects. Therefore, it was stated that the interfacial bonding strength must not be the determining factor in the interfacial shear strength of these systems, with the surface roughness, which is more prominent with DV defects, playing a more important role in creating mechanical interlocking between 2DM's surface and the polymer

chains. Nevertheless, it was noticed that, when these nanosheets are functionalized with hydroxyl groups, the opposite is true. That is because these hydroxyl groups become more exposed to the macromolecules when the sheets are not as pleated. Since DV defects create more pronounced deformations on the bidimensional plane, the functional groups become less exposed, which hinders their capability to increase the interfacial shear strength (Xin, Duan, and Mu 2020).

1.4.1.3 Lateral Dimensions

The nanofiller aspect ratio is perhaps one of the most recognized factors that influences the mechanical characteristics of nanocomposites. As it is widely known, 2DM with a larger lateral size are better suited to act as mechanical reinforcement in polymers due to more interaction sites available for stress transfer. This has been demonstrated in the literature by both theoretical and experimental investigations.

MD simulations have been used to investigate the influence of 2DMs' sheet lateral size on their mechanical reinforcing capabilities. A greater number of exposed atoms are available in nanoparticles with larger surface area to volume ratios, which leads to more molecular interactions with polymer chains, i.e., larger interfaces. Consequently, 2DM with larger lateral dimensions act better as mechanical reinforcements, since the stress created at the interface is proportional to the stress generated within the nanomaterial sheets. (Kelly and Macmillan 1986; Rouhi 2016).

These theoretical results, which were obtained for h-BN, are experimentally confirmed in the case of graphene. Indeed, the effect of the size of graphene nanosheets has been evaluated, ranging from 20 nm to 1 μm. It was observed that, as the size of the platelet increased, the mechanical reinforcement was larger, as can be seen in Figure 1.9a (J. Kim et al. 2017). Since larger nanosheets have more friction during pullout from the matrix due to a larger interface, the energy needed to fracture the polymer composite should indeed be higher with increasing sheet size. This is clearly visible in the SEM images of the fractured surfaces (Figure 1.9b). In

contrast to the smooth surface of the neat polymer, the composites exhibit rippling patterns that become denser when the lateral size of the 2DM is increased, which is translated into more energy being dissipated by the material before failure.

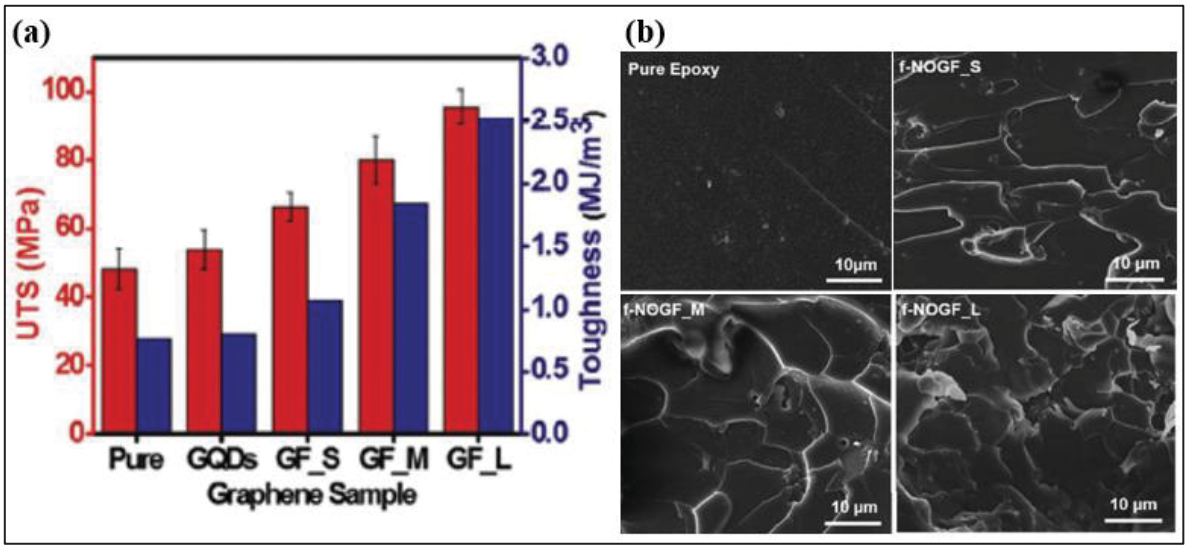

Figure 1.9 – Polymer composites' mechanical properties as a function of GRM lateral sheet size: (a) Ultimate tensile strength and toughness of graphene/epoxy nanocomposite as a function of graphene lateral size (GQDs = graphene quantum dots; GF_S = small graphene sheets; GF_M = medium graphene sheets; GF_L = large graphene sheets); (b) SEM images of the composites' fractured surfaces as a function of GRM lateral size. Adapted with permission from (J. Kim et al. 2017)

A similar behavior was observed in a study of PET/multi-layer graphene oxide (mGO) nanocomposites. It was verified that, when mGO is better dispersed in the polymer matrix, its specific surface area increases. Therefore, there is more interfacial adhesion in the composite as a whole, which enables more dissipation of strain energy when subjected to mechanical stresses (Pinto, Silva, & Fechine, 2020).

1.4.2 Strategies to Improve Reinforcement

1.4.2.1 Functionalization

Some polymer matrices may present some degree of interaction with 2DM without further functionalization, e.g., tensile strength, elongation at break, and toughness were improved by 27%, 94%, and 100%, respectively, by using ultra-low concentrations (0.05 wt%) of MoS_2 in a PS matrix (Rodriguez et al. 2021). When it is considered that these nanocomposites were developed using the straightforward melt compounding approach, these findings are even more astounding. However, this is only due to the good interaction of the nanofiller with some polymers. In such cases, hydrogen bonding is considered a major factor. On the other hand, for polymers that have no available sites for such interactions, a suitable strategy for the improvement of interface is functionalization, which may be covalent or non-covalent.

While covalent functionalization allows the polymer chains to chemically bond to the surface of the nanofiller, non-covalent functionalization only creates sites where stronger physical interactions are possible, e.g., π-π interactions and hydrogen bonds (Sayed-Ahmad Baraza 2019; Hirsch and Hauke 2018; Punetha et al. 2017; Layek and Nandi 2013). For instance, a simultaneous increase in the maximum stress and ductility, resulting in 134% increase in the toughness of PVA, using only 0.5 wt% MoS_2 has been demonstrated after functionalizing it with hydroxyl groups. As a result, hydrogen bonding between the polymer and the nanofiller was boosted, being noticed through significant displacement in the infrared stretching vibrational mode of the PVA hydroxyl groups (νOH) (J. Zhang et al. 2019). A similar approach was adopted for developing MoS_2/Nylon-6 nanocomposites. Lipoic acid covalently attached to the MoS_2 surface offered carboxyl terminal groups as initiators for *in situ* polymerization of ε-caprolactam. Thus, the macromolecular chains grew chemically linked onto the MoS_2 nanosheets. As a result, with the amount of only 0.1 wt%, the tensile modulus and strength increased by 42% and 50%, respectively, compared to only 10% and 14% without functionalization (X. Wang, Kalali, and Wang 2015).

Functionalization is more widely common in GRM/polymer composites, even when dealing with polymers that may present good affinity due to polar groups. This is explained by the greater interest that GRM has attracted. To exemplify this trend, some functionalized-GRM/PET nanocomposites are presented in Table 1.4.

Table 1.4 – Influence of functionalization on GRM/PET based nanocomposites' mechanical properties

Functionalization	Mixture Method	Content (wt%)	Highlights	Ref.
Alkyl-ether groups	Solution blending	0.5	Improvements of ~ 100%, 56%, and 67% in the tensile strength, Young's modulus, and strain at break, respectively.	(Shim et al. 2012)
Pyrene-terminated molecule	Melt mixing	1.0	Impact strength increased by a factor of 9	(Tong et al. 2017)
Trimellitic anhydride	Melt mixing	1.0	Increase of 12.2% in Young's modulus, without significant loss of elongation at break	(Aoyama et al. 2018)
Amine, amide, and magnetite	Melt mixing	0.1	Low degree of functionalization led to increases of ~ 18% in strain at break, 87% in tensile strength, 38% in Young's modulus, and 256% in toughness in respect to neat PET	(Souza et al. 2021)

It is noticeable that the insertion of functional groups can lead to better interactions between 2DM and polymers, as can be observed in Figure 1.10, where the GRM presents a much larger interfacial area with the polymer matrix after functionalization with dodecyl-ether functional groups. This enables the use of very low filler contents. Nevertheless, one has to be cautious about how much the crystalline structure of 2DM, which is responsible for their potential mechanical properties, is affected by functionalization. If the crystalline plane becomes excessively distorted, it may lose some of its advantageous properties (Sun, Li, Zhang, & Yang, 2020; Xin, Duan, & Mu, 2020). It is also worth mentioning that functionalizing 2DM adds

another step in the production ladder, which may take significant time and not be as industrially viable.

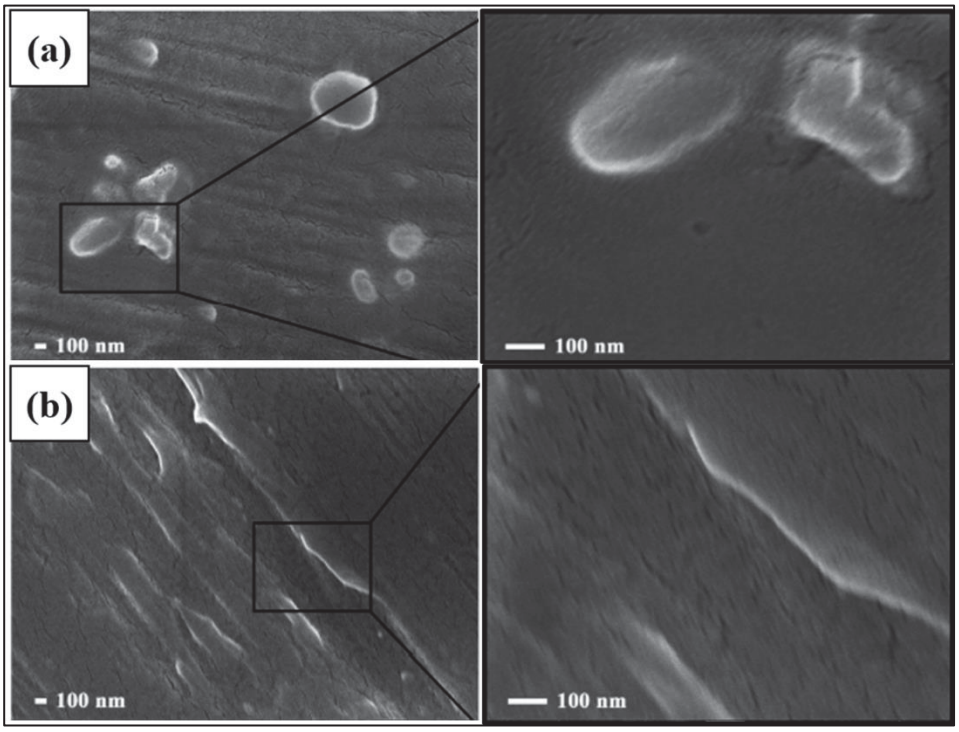

Figure 1.10 - SEM images of 0.1wt% PET/GO nanocomposites obtained by solution blending without (a) and with (b) functionalization of GO sheets by dodecyl-ether groups. Images were acquired with a voltage of 5.0 kV. Reproduced with permission from (Shim et al. 2012)

1.4.2.2 Morphology Tailoring

Even though it would be interesting to assemble interconnected pre-networks to avoid 2DM agglomeration in polymer matrices, for instance, by forming a nanomaterial pre-network based on a metallic foam template, and then infiltrating it with polymer resin (Jia et al., 2014), these techniques are highly complex and not easily adaptable to industrial thermoplastic processes.

However, to optimize the dispersion and orientation of the nanofiller inside the polymer matrix, several processing techniques can be used. For instance, the alignment of 2DM inside the matrix might result from the composites' uniaxial or biaxial drawing and stretching. An

increased ratio of 11 in Young's modulus has been obtained for ultrahigh molecular weight poly(ethylene) (UHMWPE)/h-BN composites, and polyvinyl chloride (PVC)/h-BN composites had their tensile strength increased by 100% after such operations (Tajaddod et al. 2016; Jan et al. 2014). Figure 1.11 presents the increase in Young's modulus acquired in the UHMWPE/h-BN composites after drawing due to the additional exfoliation and dispersion promoted by this process.

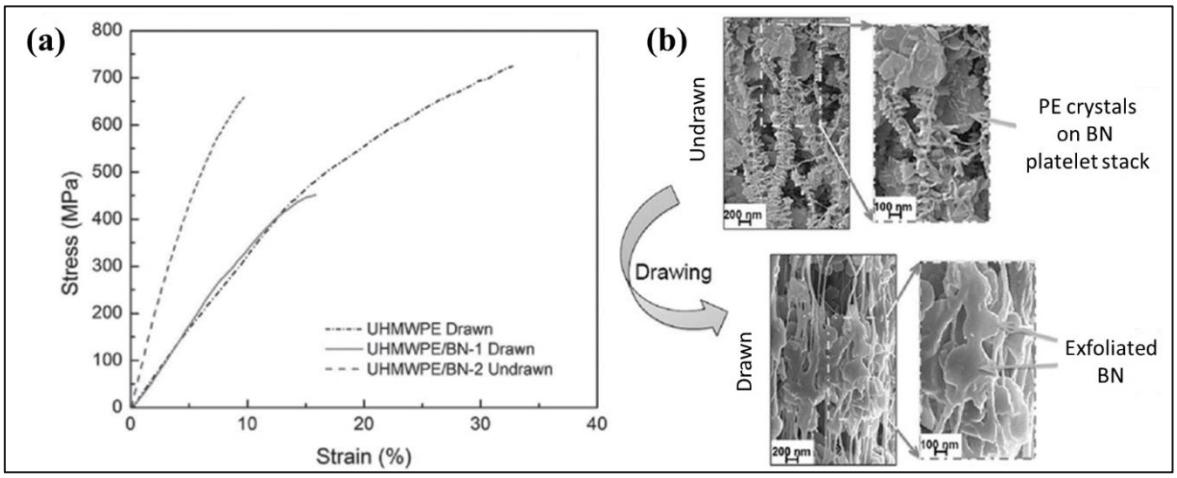

Figure 1.11 – (a) Increase in Young's modulus after drawing of h-BN/UHMWPE nanocomposite; (b) SEM images comparing the UHMWPE/h-BN composites morphology before and after the drawing process, highlighting the enhanced exfoliated nature of the h-BN sheets in the drawn sample. Reproduced with permission from (Tajaddod et al. 2016)

Another interesting approach combines the advantage of functionalization with different processing methods. In this case, noncovalently functionalized 2DM are pre-incorporated into the polymer matrix via solvent mixing to produce masterbatches, and it is subsequently diluted to the final composition by melt blending. The employment of such approach led to an astounding 26.6 fold increase in elongation at break for a PLA/fGO system at only 0.2 wt% without losing its tensile strength (Zhang et al., 2018). Even though these results are indeed impressive, this strategy still requires an additional processing step to produce the masterbatches by solution casting.

An alternative would be substituting some of the regular kneading blocks (KB) by extensional mixing elements (EME) in the mixing zone of an extruder. It has been shown that the increased

elongational flow promoted by these special mixing elements significantly improves the 2DM exfoliation in the matrix during melt blending, which is especially hard to achieve with simple KB (Danda et al. 2020). Consequently, the total interface between the two phases is also increased, which leads to much higher transfer of properties from the polymer matrix to the nanofiller, as can be verified in Figure 1.12 for a TPU/GO nanocomposite at only 0.25 wt%.

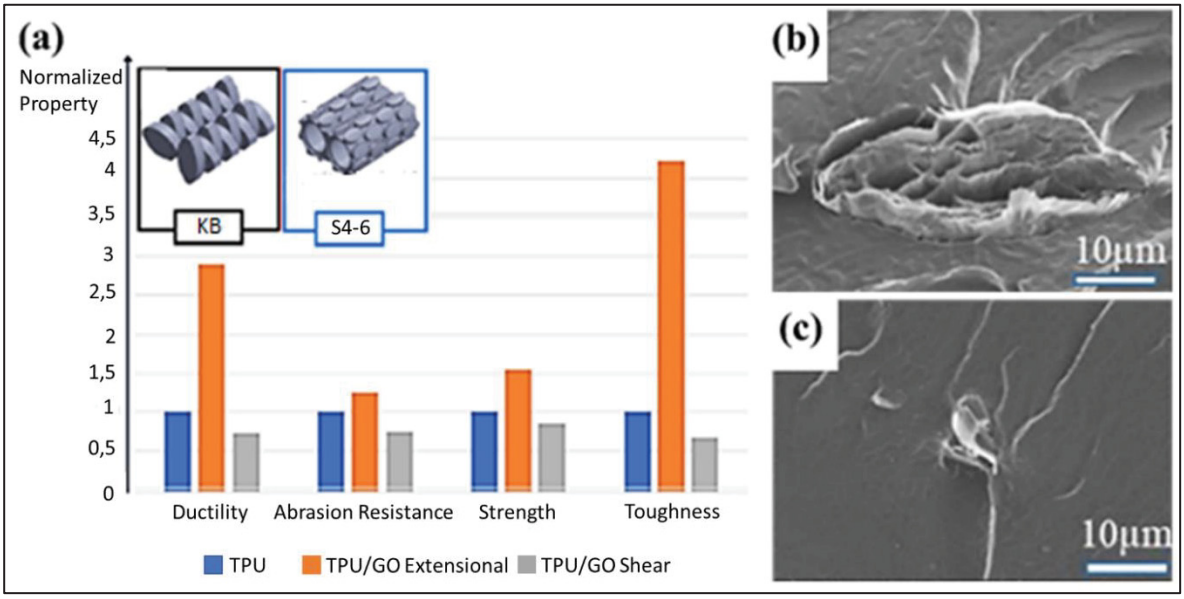

Figure 1.12 – Effect of employing extensional mixing elements during the melt blending of a TPU/GO nanocomposite at 0.25 wt%: (a) Normalized mechanical properties as a function of mixing element. Inset: Extensional mixing elements with different elongational rates; (b) SEM image of the fractured surface of the nanocomposite mixed by kneading blocks, evidencing the presence of large agglomerates; (c) SEM image of the fractured surface of the nanocomposite mixed by extensional mixing elements, evidencing the better level of dispersion. Adapted with permission from (Danda et al. 2020)

1.4.2.3 Hybrid 2DM

A very promising alternative to functionalization and to the employment of more complex processing strategies could be the use of 2DM in the form of hybrids, i.e., combining different

2DM that could lead to synergistic effects in polymer nanocomposites. Table 1.5 presents some examples of studies that investigated such hybrid systems.

Table 1.5 – Effects of 2DM nanohybrids on the mechanical properties of polymer nanocomposites

Polymer matrix	Hybrid filler	Content (wt%)	Highlights	Ref.
Epoxy	GO/h-BN	0.5	Increases of 140% in tensile strength, 177% in ultimate strain, and 32% in elastic modulus	(Ribeiro, Trigueiro, Owuor, et al. 2018)
Polyurethane	GO/h-BN	0.5	Increases of 85% in tensile strength, and 140% in Young's modulus	(Ribeiro et al., 2020)
Polyurethane	h-BN/MoS_2	0.5	Increases of 80% in Young's modulus, and 102% in the elastomer crosslink density	(Ribeiro, Trigueiro, Lopes, et al. 2018)
Epoxy	h-BN/MoS_2	1.0	Increases of 95% in tensile strength, 60% in ultimate strain, and 58% in Young's modulus	(Ribeiro et al. 2019)
GF-reinforced epoxy	rGO/MMT	0.3	Increases of 97% in tensile strength, and 44.5% in flexural strength, along with enhancements in the energy absorption capability	(Kavimani et al. 2021)

It is evident that through this strategy, great mechanical improvements are achieved at very low filler contents. To explain the phenomena of how 2DM nanohybrids act, MD simulations have been performed with a focus on the system stabilization energy. According to the findings, hybrid 2DM can stop exfoliated layers from becoming stacked again, since the force necessary to promote the separation of layers is much lower than with a single 2DM, as can be seen in Figure 1.13. This illustrates how the nanostructures work together to improve dispersion in the composite, proving their synergism.

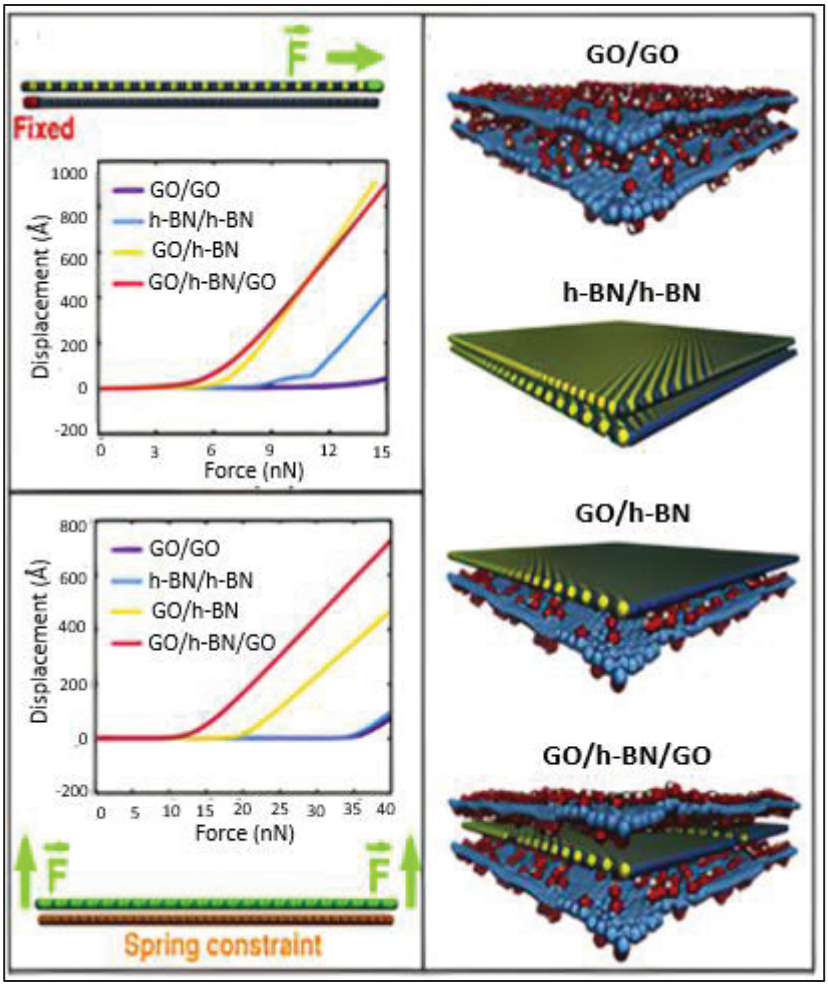

Figure 1.13 - MD simulations of GO/h-BN hybrid stacking structure and how its eases the displacement of nanosheets under shear and normal forces compared to individual fillers. Reproduced with permission from (Ribeiro, Trigueiro, Owuor, et al. 2018)

1.4.3 Environmental Aspects

Although the intrinsic characteristics of 2DM, as well as the morphology in polymer nanocomposites, are extremely important aspects that need to be considered when assessing the mechanical properties of a final product, the environmental conditions are also something to consider. For example, for uses like hydrogen storage tanks in electric vehicle fuel cells, sterilization tanks for space missions, and structural components in the aerospace industry, composites with excellent mechanical performance in low temperatures are necessary (Govindaraj, Fox, Aitchison, & Hameed, 2019). Additionally, hierarchical composites for structural and high velocity impact resistance applications, such as ballistic protection, are also

a promising field for 2DM (Clifton et al. 2020; Valorosi et al. 2020). With that in mind, experimental studies have been conducted to investigate hierarchical polymer nanocomposites that could be applied in these situations.

The inclusion of 2DM has been a promising method for improving the performance of fiber-reinforced polymers, in which the fiber surface is modified to increase its surface area and ensure better adhesion and stress transfer at the interface. For that, a continuous coating process, in which carbon fibers (CF) are directly submersed in a graphene dispersion can be employed (Valorosi et al. 2020; Karger-Kocsis, Mahmood, and Pegoretti 2020; Qin et al. 2015). This method has been effective in enhancing the cryo-mechanical attributes of composites made of short carbon fibers (SCF) and poly(ether-sulfone) (PES). When GO was applied to the SCF surface, the cryogenic mechanical characteristics significantly improved. Figure 1.14 illustrates the difference between the tensile strength improvement for this PES hierarchical nanocomposite at room temperature (RT) and cryogenic temperature (CT). The proportion of matrix adhering to the pulled-out GO-coated fiber is more substantial at CT than at RT, which explains the enhanced cryogenic mechanical properties (Li, Hua, Qu, Xiao, & Fu, 2016). A similar response was achieved for a graphene/epoxy composite. While at RT the percentage increase in tensile strength was only 3.5%, at CT it was 17.1% at only 0.1 wt% (Shen et al., 2012). Due to the discrepancy in the coefficients of thermal expansion (CTE) at such temperatures, the clamping stress created at CT on the 2DM-polymer interface has been identified as the strengthening mechanism (Hussein et al. 2017).

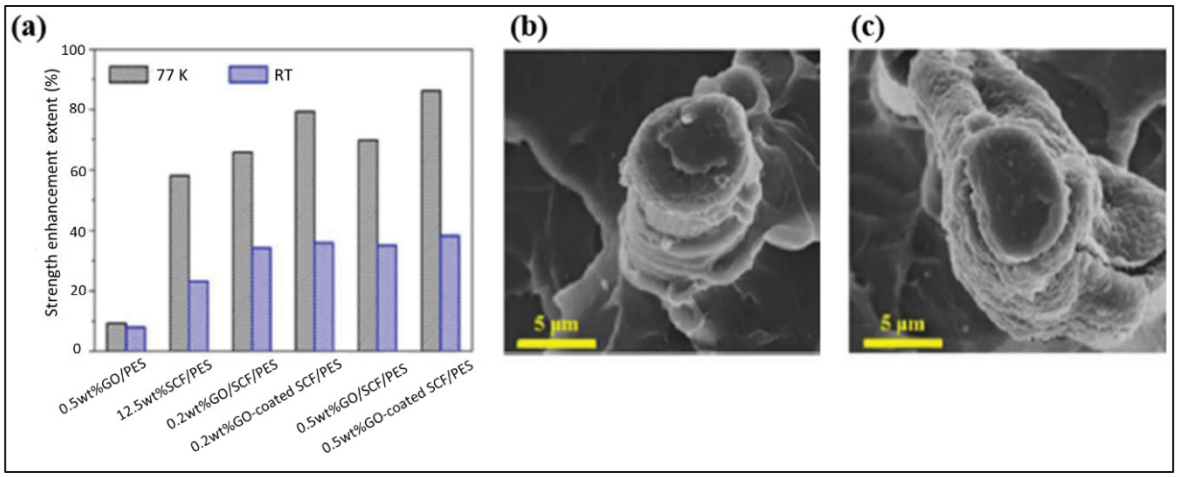

Figure 1.14 – (a) Tensile strength enhancement at 77K and RT for different GO/SCF/PES systems; (b) SEM image of 0.5 wt% GO-coated SCF composite at RT, and (c) at 77 K. Adapted with permission from (Li et al., 2016)

Although it has been shown that the tensile properties of polymers are enhanced in a more expressive manner at low temperatures by the addition of 2DM, this trend is not repeated for impact strength. The cryo-mechanical impact strength of GO/epoxy nanocomposites functionalized by surface-modified silica nanoparticles (APTES) were measured, and the results show that it reaches its maximum value at 0.5 wt% for both CT and RT. However, the increase is 92% at CT, and 154% at RT. This may be attributed to the decreased matrix molecular mobility at CT, which is even lower in the presence of nanofillers (Jiang et al. 2014).

1.5 Thermal Properties

Thermal management is a crucial element for the safety, dependability, and effectiveness of many applications, including textiles, electronics packaging, communications systems, energy storage, medical equipments, vehicle and aerospace components, among others. (Chen, Huang, Sun, & Jiang, 2019; Han et al., 2020; Moore & Shi, 2014; Shanker et al., 2017; Zhang, Deng, & Fu, 2018). However, conventional heat sink materials like metals and ceramics present a significant density and limited flexibility, severely impeding the advancement of technologies (Boden et al. 2014). Fortunately, widespread attention has been given to 2DM/polymer composites because of their improved TC and stability. Three primary reasons are credited for the improved performance: (i) the homogenous distribution of the nanofiller in the composite;

(ii) its excellent structural stability and aspect ratio; (iii) its appropriate interfacial interactions with the matrix (Burger et al., 2016; Cui et al., 2015; Govindaraj, Fox, Aitchison, & Hameed, 2019; Guerra, Wan, & McNally, 2019; Morishita & Okamoto, 2016). Additionally, it is also worth noting that 2DM usually have a nucleating effect on semi-crystalline polymers, which also helps to improve TC, since the crystalline part of a polymer is more organized, decreasing the number of sites for phonon scattering events (Li, Yang, Zou, Liang, & Chen, 2017).

Therefore, this section is separated into two categories. First, the effect of 2DM on the TC of a diverse range of polymers is addressed from the perspective of physical features, i.e., stacking, aspect ratio, and structural defects, as well as from the interfacial thermal resistance point of view. Secondly, the effect of 2DM on the thermal stability of polymers is addressed from the viewpoint of how they block the passage of gaseous products, which is also interesting for packaging purposes. Additionally, how the advent of hybrid 2DM could lead to the development of multifunctional nanocomposites based on low contents of filler by employing a proper filler ratio is also presented.

1.5.1 Thermal Conductivity

Even though structural defects, increased number of layers, and functionalization are deleterious to the intrinsic TC of 2DM, it is important to consider the interfacial thermal conduction (ITC) when dealing with polymer nanocomposites, since most of the heat is actually transported through the polymer-filler interface. Here, a brief summary of the aspects that can influence ITC is presented.

1.5.1.1 Physical Features

Despite the TC mechanism in 2DM being dominated by the lattice thermal vibration, when it is embedded in a polymer matrix, it is surely suppressed by polymer chains. In addition to that, the phonon scattering by the matrix is significant, which makes a multi-layer nanomaterial

more efficient than a monolayer, since the internal layers are not sensitive to the adverse effect of the matrix (Shen et al., 2016; Sun et al., 2021).

In order to prove this effect, MD simulations have been performed. It was observed that as the number of layers increased, ITC actually increased, as depicted in Figure 1.15a. In addition, it was also noticed that large sheets are beneficial to reduce interfacial thermal resistance in composites. Consequently, when monolayer and multilayered graphene nanosheets exhibited the same aspect ratio, the latter consistently outperformed the former in raising the composites' TC. (Shen et al., 2016).

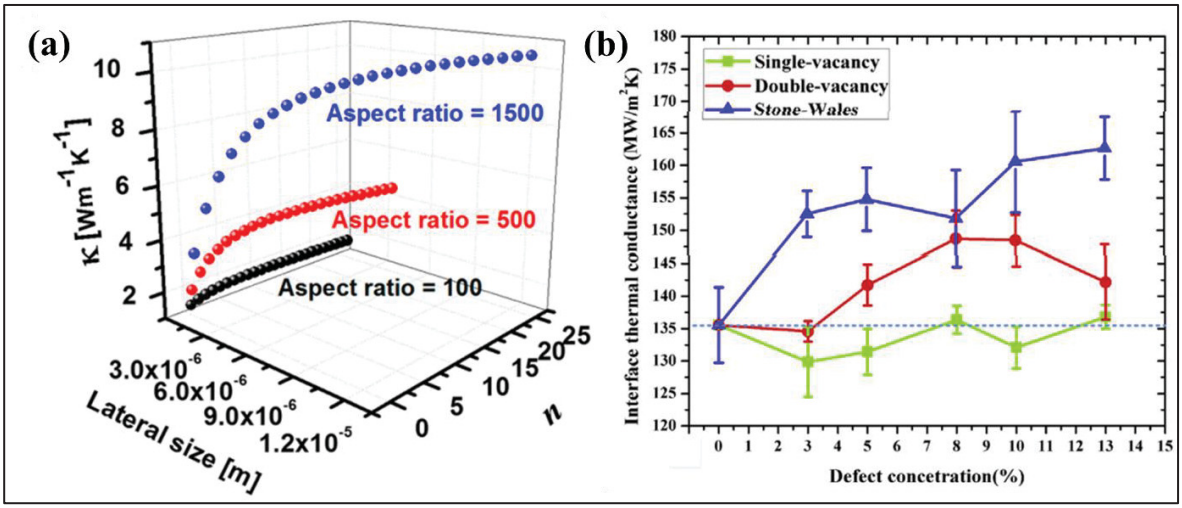

Figure 1.15 – The effect of graphene physical features on the TC of graphene/polymer nanocomposites: (a) TC of graphene/epoxy nanocomposites as a function of graphene's lateral size and number of layers at varying aspect ratios; (b) ITC of graphene/epoxy nanocomposites as a function of concentration and type of structural defect. Reproduced with permission from (Li, Zhou, Zhang, Liao, & Zhou, 2018; Shen et al., 2016)

Similarly to the number of layers, it has already been verified by NEMD simulations and the effective medium theory that some structural defects, e.g., DV, MV, and SW, increase ITC in polymer composites, as presented in Figure 1.15b. The overlapping of vibrational density states among 2DM and polymer, fostered by these defects, is thought to be the cause of the improved ITC. (Li et al., 2018).

1.5.1.2 Functionalization

The ITC of polymer nanocomposites is also significantly influenced by functionalization. RNEMD simulations have demonstrated that functionalization, both non-covalent and covalent, may improve ITC between 2DM and polymer matrix due to stronger interfacial interactions and greater phonon vibrational match, even though it degrades the TC of pristine graphene by orders of magnitude (Bellussi et al. 2021). This effect is presented in Figure 1.16a, and it has been experimentally verified when coupling h-BN to silane agents to improve epoxy's TC, achieving an enhancement of more than 500% at 30 wt% (Hou et al. 2014).

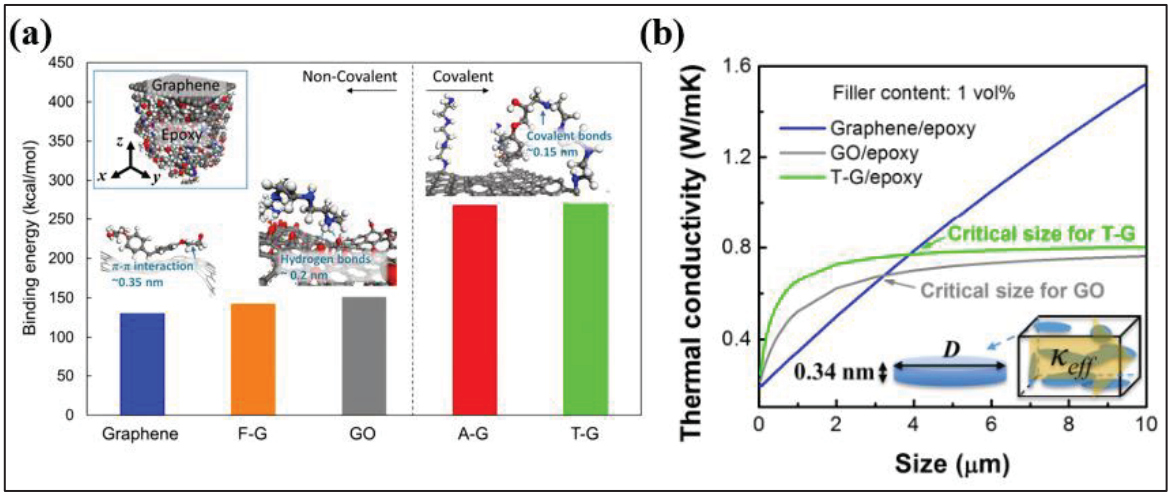

Figure 1.16 – Graphene functionalization's impact on a graphene/polymer nanocomposites' TC: (a) Epoxy-graphene interfacial binding energy with covalent and noncovalent functionalizations; (b) TC of GRM/epoxy nanocomposites as a function of sheet lateral dimension with various functionalizations. (F-G = fluorine-functionalized graphene; GO = graphene oxide; A-G = amine-functionalized graphene; T-G = triethylenetetramine-functionalized graphene). Adapted with permission from (X. Shen, Wang, Wu, Liu, and Kim 2016)

However, there exists a critical lateral size of nanosheets, below which the functionalization can effectively improve the nanocomposite's TC, while above it the size of the sheets is more important, and functional groups become an adversity (Figure 1.16b). When the nanosheets are smaller than the critical value, the conductivity mechanism is dominated by the interface. On the other hand, the intrinsically greater TC of the basal plane predominates once the nanosheets are wider than the critical value, leading to a "filler dominant mechanism." Since

in this scenario the most important aspect is the intrinsic TC of 2DM's pristine surface, functionalization is not advised.

1.5.1.3 Hybrid 2DMs

As mentioned in the case of mechanical properties, the best possible scenario is to achieve a well-structured and interconnected 3D network. This would enable phonons to travel through the composite without having to excessively jump from one phase to another. However, it is still very difficult to achieve such a complex microstructure in a controlled manner, requiring the combination of intricate methodologies. For example, some works have been successful in achieving such structures by utilizing ice-templating associated with external force assisted techniques, such as wet spinning and tape casting (H. Shen et al. 2020; Y. Cui et al. 2018).

Alternatively, the use of 2D nanohybrids could be a more feasible solution to these issues. When compared to single thermally conductive fillers, conductive 2D nanohybrids have better TC in polymer composites. Their synergistic dispersion, which can be observed in Figure 1.17, and the improvement of thermally conductive networks are considered the main causes for that (Ribeiro, Trigueiro, Owuor, et al., 2018; Ribeiro et al., 2020a; Yang et al., 2021).

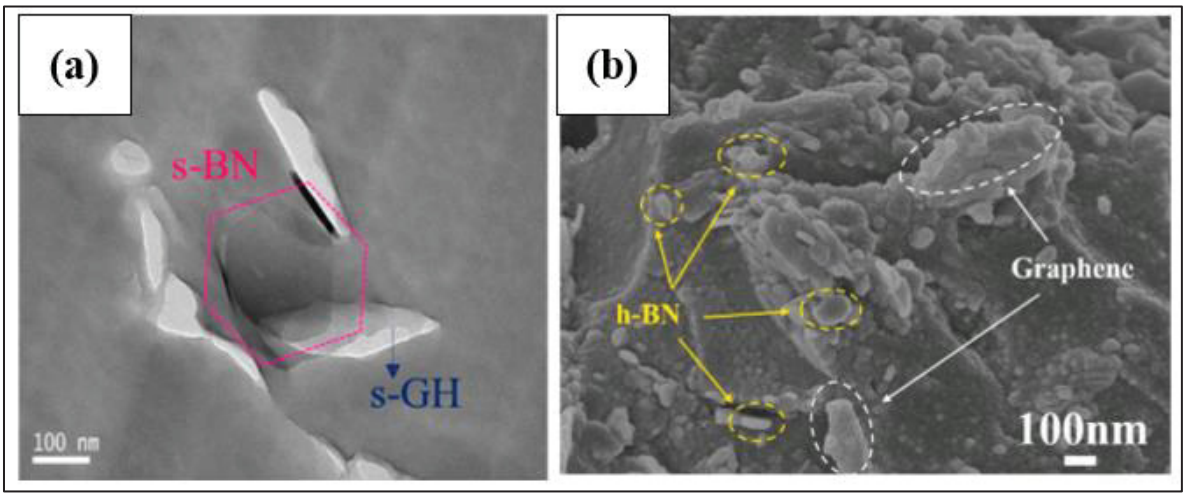

Figure 1.17 – Synergistic dispersion of hybrid 2DM in polymer composites: (a) TEM image of a PS filled with 30 wt% graphene and 1.5 wt% h-BN; (b) SEM image of a styrene acrylic

resin composite filled with 3 wt% graphene and 1 wt% h-BN. Reproduced with permission from (X. Cui et al., 2015; Jia et al., 2021)

Cui et al. (X. Cui et al. 2015) obtained Polystyrene (PS) and Polyamide 6 (PA6) nanocomposites based on a h-BN/graphene hybrid. The experimental results suggested that the TC of the PS and PA composites increases with higher amounts of hBN. For example, additional introduction of 1.5 wt % h-BN increased the TC by 38 and 34% in PS and PA6, respectively, when compared to the same polymers containing 20 wt% graphene. Meanwhile, the mechanical properties of the composites were synchronously enhanced. It was found that h-BN filled the interspaces of the graphene sheets and formed a h-BN/graphene stacked structure, which was helpful for synchronously improving the TC and the mechanical properties.

Huang et al. (Huang et al., 2016) reported an epoxy-based composite with increased TC by using graphene oxide-encapsulated boron nitride (h-BN@GO) hybrids as fillers. The TC of the obtained composites increased with the loading of h-BN@GO hybrids to a maximum of 2.23 W m^{-1} K^{-1} when the loading of h-BN@GO hybrids was 40 wt%, which is double that of composites filled only with h-BN. This increase was attributed to the presence of GO, which improved the compatibility of h-BN with the epoxy system, along with the reduced interfacial thermal resistance. In addition, h-BN@GO/epoxy composites exhibited enhanced dielectric properties, which makes them suitable as excellent electronics packaging materials.

Su et al. (Su et al., 2018) have functionalized graphene oxide (GO) by diethylenetriamine (DETA) to obtain NH_2-functionalized graphene (NfG), which was designed to be immobilized on the surface of large-sized insulating hBN via π-π stacking interaction. Since the NfG sheets were fixed on the surface of h-BN, good dispersion was achieved, enabling it to participate in the cycloaliphatic epoxy (CER-170) resin curing process. Hence, not only significantly enhanced TC (~ 3.409 W $m^{-1}K^{-1}$, in-plane direction) was obtained, but also a very low electrical conductivity, which makes the composite useful for fabricating TIMs.

Esfahani et al. (Seyed Esfahani et al. 2021) inserted hBN and rGO into a polymer blend of PA6/PP by first producing masterbatches of PA6/hBN-rGO and then melt blending it with PP. The hybrid fillers had a synergetic effect on the heat conductive network, forming a more efficient percolating network of h-BN and rGO in the PA6 matrix phase than h-BN alone. The improved TC was partially attributed to a shift in the blend morphology, from matrix-disperse morphology for PP/PA6-hBN to co-continuous morphology in the PP/PA6-hBN-rGO composite.

Another work has also demonstrated that the enhancement in TC of a styrene acrylic resin was even higher (87.14%) by adding 1 wt% graphene-3 wt% h-BN versus 20 wt% h-BN (83.63%) due to the larger surface area of graphene, which increases the interfaces with the polymer and allows h-BN to act as a "bridge" between different graphene sheets, creating a three-dimensional thermal network and greatly increasing the heat dissipation (Jia et al., 2021).

Although nanohybrids show a higher potential than individual fillers, it is noticed that the contents studied are still relatively high, i.e., > 1 wt%. In spite of that, it has already been demonstrated that the advent of nanohybrids opens up the possibility of utilizing even lower contents.

Ribeiro et al. (Ribeiro, Trigueiro, Owuor, et al., 2018; Ribeiro et al., 2020b) studied the effect of GO/h-BN hybrids in the TC of epoxy and polyurethane (PU) resins. An increase of 125% was observed in the TC for the hybrid GO/h-BN epoxy composite with just 0.5 wt% (Ribeiro, Trigueiro, Owuor, et al. 2018). As for the PU system containing 0.5 wt% of the hybrid GO/h-BN mixture, an impressive increase of ~1450% was observed when compared to the neat polymer (Ribeiro et al., 2020b). To explain this phenomena, the authors performed MD simulations with a focus on the system stabilization energy. The results showed that the hybrid GO/h-BN combination can prevent the re-stacking process of exfoliated layers, demonstrating the synergism between these nanostructures with the final effect of better dispersion in the composite material.

Despite most of the research on 2D nanohybrids having been devoted to GRM/h-BN systems, there are several other possible systems that have been recently explored. Ribeiro et al. (Ribeiro, Trigueiro, Lopes, et al. 2018) have produced nanocomposites based on MoS_2, h-BN and hybrid MoS_2/h-BN nanofillers with different wt% in elastomeric PU as polymer matrix. The hybrid MoS_2/h-BN nanofiller at just 0.5 wt% increased the elastomer crosslink density up to 102%, indicating strong interactions between the hybrid nanofiller and PU. However, the most important synergistic effect was the increase of 752% in TC with respect to the neat polymer. In another study, the same nanohybrid was incorporated to an epoxy matrix and the same characterizations were conducted. The hybrid 2D mixture imparted efficient reinforcement to the epoxy, leading to increases of 203% in TC at 1.0 wt% when compared to the pure polymer (Ribeiro et al. 2019). Therefore, it was stated that hybrid composites based on 2D MoS_2/h-BN nanofillers with multifunctional attributes can be applied in advanced polymeric materials that require high mechanical and thermal performance.

Some other interesting results in the literature are related to the incorporation of h-BN/MoS_2 nanohybrid into different ester-based biodegradable insulating lubricants. Although not much effect was observed at RT, the hybrid filler increased the lubricants' TC by 20-32% at 323K with loadings as low as 0.25 wt% (Taha-Tijerina et al. 2020). The phenomenon behind these nanofluids' TC increasing in a more sensitive manner at higher temperatures is the increased Brownian motions. It is worth mentioning that this behavior is industrially desirable, because there is a reasonable number of applications that actually occur at harsh operational conditions such as at elevated temperatures (Govindaraj, Fox, Aitchison, & Hameed, 2019). Table 1.6 summarizes the works mentioned above.

Table 1.6 – Literature review on hybrid 2DM used as nanofillers to improve polymers' TC

Polymer matrix	Hybrid filler	Content (wt%)	Highlights	Ref.
PS	h-BN/graphene	20.0 – graphene 1.5 – h-BN	Increase of 38% in TC compared to the composite filled only with graphene	(X. Cui et al. 2015)
PA6	h-BN/graphene	20.0 – graphene 1.5 – h-BN	Increase of 34% in TC compared to the composite filled only with graphene	(X. Cui et al. 2015)
PA6/PP blend	h-BN/rGO	27.0 – h-BN 4.7 – rGO	Increase of 254% in TC compared to the composite filled only with h-BN	(Seyed Esfahani et al. 2021)
Epoxy	h-BN@GO	40.0	Increase of 100% in TC compared to the composite filled only with h-BN	(Huang et al., 2016)
Epoxy	NfG@h-BN	30.0	Significantly enhanced TC (~ 3.409 W $m^{-1}K^{-1}$, in-plane direction	(Su et al., 2018)
Styrene acrylic resin	Graphene/h-BN	1.0 - graphene 3.0 - h-BN	Enhancement in TC was even higher (87.14%) than with 20 wt% h-BN (83.63%)	(Jia et al., 2021)
Epoxy	GO/h-BN	0.5 (Ratio 1 : 1)	Increase of 125% in TC when compared to neat polymer	(Ribeiro, Trigueiro, Owuor, et al. 2018)
PU	GO/h-BN	0.5 (Ratio 1 : 1)	Increase of 1450% in TC when compared to neat polymer	(Ribeiro et al., 2020b)
PU	MoS_2/h-BN	0.5 (Ratio 1 : 1)	Increase of 752% in TC when compared to neat polymer	(Ribeiro, Trigueiro, Lopes, et al. 2018)
Epoxy	MoS_2/h-BN	1.0 (Ratio 1 : 1)	Increase of 203% in TC when compared to neat polymer	(Ribeiro et al. 2019)
Ester-based biodegradable insulating lubricants	MoS_2/h-BN	0.25 (Ratio 1 : 1)	Higher increases in TC at 323K, reaching values 20 – 32% higher than for the neat lubricants	(Taha-Tijerina et al. 2020)

While some of the previous works have established the filler ratio as 1 : 1, RNEMD simulations have been performed to verify what would be the optimal filler ratio in a PDMS/MoS_2/h-BN hybrid nanocomposite. In this study, it has been observed that, since the nanofillers are inorganic materials, their interfacial contact with polymer matrices is poor, resulting in a relatively high interfacial thermal resistance and the appearance of voids, which are detrimental for TC. Additionally, when the filling percentage is too high, the fillers are easily aggregated, which in turn increases the volume of these voids. However, it was noticed that the addition of a second nanoplatelet structure appreciably improves the dispersion, significantly reducing the volume fraction of holes (ϕ) in the composite (Wang et al., 2021). Therefore, it was observed that ratios closer to 1 : 1 are in fact the optimal condition for polymeric composites based on 2D nanohybrids, as is presented in Figure 1.18.

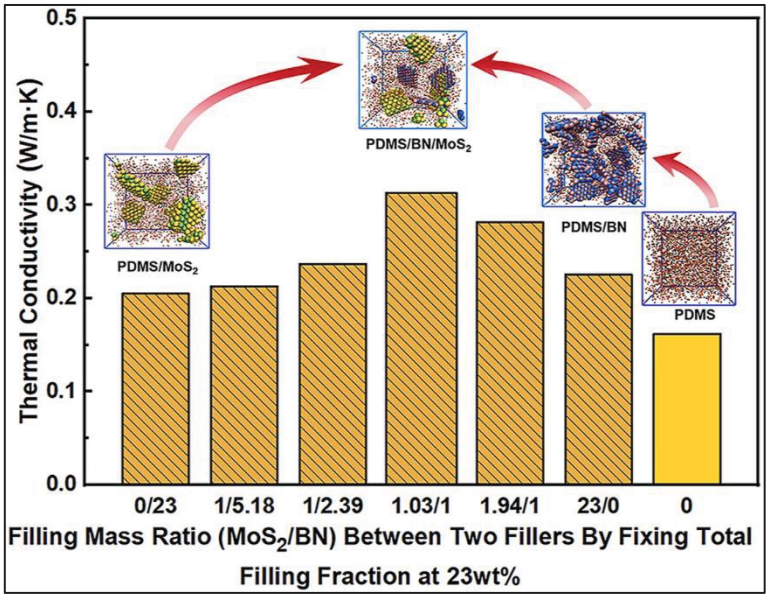

Figure 1.18 – Conductivity as a function of filler mass ratio between MoS_2 and h-BN for a PDMS-based nanocomposite. Reproduced with permission from (Wang et al., 2021)

Although 2D nanohybrids show higher promise than individual fillers, it is noticed that there is still a significant number of publications that studied relatively high contents. In spite of that, it has already been demonstrated that the advent of 2D nanohybrids opens up the possibility of utilizing lower contents. This is crucial because excessive filler contents typically result in degraded mechanical capabilities, high density, and challenging processing (Chen et al., 2016).

Additionally, it could compromise these materials' applicability in areas that demand both outstanding mechanical and thermal properties, e.g., aerospace materials and thermal energy storage systems (Pasupathi et al. 2020; He et al. 2020; Kadhim et al. 2021; Zakaria et al. 2020).

1.5.2 Thermal Stability

Besides being great choices for improving TC of polymer composites, 2DM also possess high thermal stability, which might be interesting for some applications where high temperatures might be present. The increase in the thermal stability of polymers is possible due to a barrier effect promoted by 2DM. Therefore, the tortuous path for the gases diffusion is significantly increased, inhibiting the emission of degraded gas molecules and preventing the supply of oxygen from the surface. In addition, the formation of a charred layer that also acts as a physical barrier can be promoted, slowing down heat and mass transfer during the burning. Such effect is especially desired for flame retardant and smoke suppression materials for fire safety (Zhou, Liu, Zeng, Hu, & Gui, 2015; Zhou, Tang, Gao, & Guo, 2018).

Taking advantage of that, polystyrene (PS) was encapsulated into MoS_2 core-shell structures for regulating thermal and fire safety properties. To achieve a high-performance nanocomposite, a non-trivial production method was adopted, combining latex technology and layer-by-layer assembly. The degradation temperature of the PS@MoS_2 was increased by around 50°C when compared to neat PS. Besides, the nanocomposite showed lower generation of gaseous products and lower heat release rate, allowing to be inferred that 2DM can enhance thermal stability, smoke suppression, and reduce fire hazards during combustion of polymer composites (Zhou et al., 2018).

Thermal stabilization of other polymers by 2DM has also been reported. For instance, 0.5 wt% of functionalized MoS_2 highly dispersed in nylon-6 showed an increment of ~ 36°C in $T_{-5\%}$ compared to pure nylon-6 (Wang, Kalali, & Wang, 2015). Similarly, increases of 21°C in $T_{-50\%}$ and of 32°C in $T_{-5\%}$ were reported for PVA (J. Zhang et al. 2019) and PE (H. Zhang et al., 2017) nanocomposites, respectively.

Although most works that studied 2DM nanohybrids have focused mostly on TC, it has also been verified that these hybrids can enhance the thermal stability and retard the flammability of such products. For instance, the limiting oxygen index (LOI) of an epoxy/MMT composite increases by up to 26.32% with the introduction of 0.4 wt% rGO (Kavimani et al. 2021). This means that the incorporation of hybrid 2DM shows significant promise for improving the flame-retardant behaviour of polymer composites.

The same thermal stabilization mechanism provided by 2DM to most polymers is of great interest for packaging applications. Increasing the length and the tortuosity of the diffusion path of gases and moisture through the material significantly increases its service life. As can be seen in Figure 1.19, a multifunctional PVA/MoS_2 nanocomposite showed outstanding barrier properties for helium compared to pure PVA. With only 1.0 wt%, the permeability decreased by 99%, without a significant change in the material transparency (J. Zhang et al. 2019).

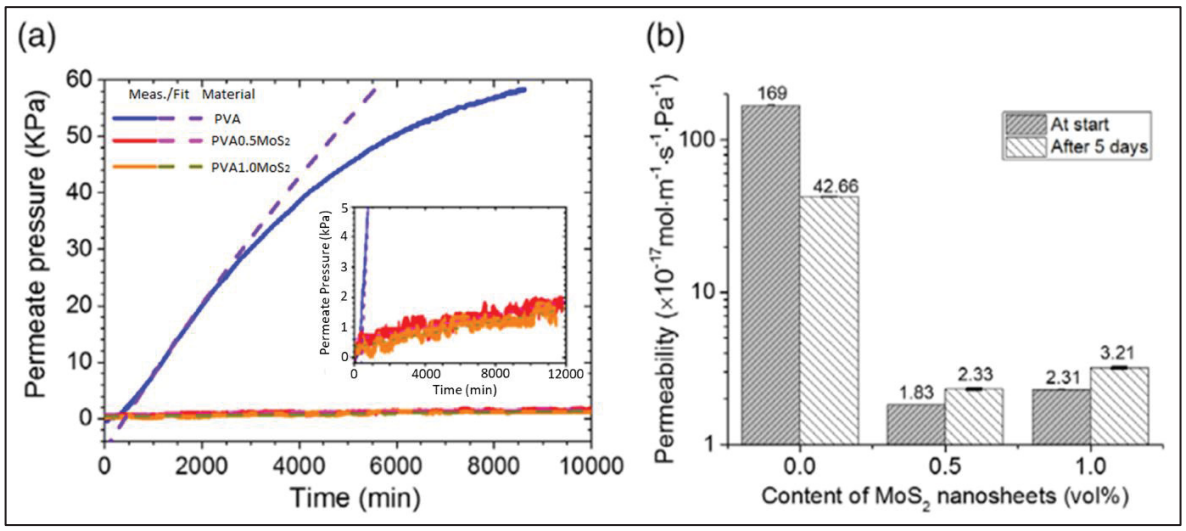

Figure 1.19 - PVA/MoS_2 nanocomposites' gas barrier characteristics. (a) Permeate pressure changes as a function of time for helium. (b) Helium permeability comparison between films made of polymer and nanocomposite (at start and after 5 days of testing). Reproduced with permission from (J. Zhang et al. 2019)

Similarly, film coextrusion was utilized to produce multilayered composites based on high-density polyethylene (HDPE), a conventional thermoplastic employed in the packaging industry, and an industrial grade graphene. The experimental results showed that the permeability could be reduced by 43% at only 0.5 wt%. This excellent performance was related to the filler's aspect ratio and exceptional dispersion efficiency. Nevertheless, due to a worsening dispersion within the composite, barrier and mechanical characteristics deteriorated as the graphene percentage rose (Ferreira Junior et al. 2022).

1.6 Electrical Properties

Many processes can be responsible for EC in polymer nanocomposites. However, the most crucial ones are ohmic conduction, which results from the direct contact of conductive nanofillers, and tunnelling conduction, which happens when electrons can travel through a thin insulating barrier. Therefore, even though electrons may “tunnel” from one nanosheet to another, passing through a thin layer of polymer in between, the most effective way to improve EC is through interconnecting the fillers, i.e., enhancing the ohmic conduction. With this uninterrupted path along which free electrons can be transported, a polymer that was originally insulating can become highly conductive. This phenomenon is widely defined in the literature as achieving the system’s percolation threshold (McNally and Pötschke 2011).

Differently from the other properties, where all 2DM have a very similar behavior towards the improvement of polymers’ properties, the electrical properties significantly vary depending on which 2DM is employed. Therefore, this section will be divided into three sub-sections, one for each addressed 2DM. First, GRM-based nanocomposites will be discussed, highlighting what aspects are important when aiming at improving EC of polymers. Then, even though MoS_2-based composites are less studied, its 1T allotropic form presents great potential. On that account, these promising applications will also be addressed. Finally, although h-BN is an insulating material, there are some emerging electrical applications that actually value this

feature. Consequently, another sub-section regarding h-BN-based composites towards high breakdown strength materials is presented.

1.6.1 Graphene-Related Materials

One of the promising fields for GRM/polymer nanocomposites due to graphene's unusual EC is electromagnetic interference (EMI) shielding (Godoy et al. 2021). It has already been shown that graphene's shielding effectiveness (SE) per unit of thickness is substantially greater than that of a Au sheet. (7.73 dB nm^{-1} vs. 1.04 dB nm^{-1}) (Hong et al. 2012). One example is the SEBS/GnP/CNT composites that have been produced by melt compounding, and their EMI SE measured in the X-band microwave frequency range (8.2–12.4 GHz). It was observed that at 5 wt% GnP and 10wt% CNT, synergistic effects were created when compared to single-component nanocomposites, leading to an EC 17 orders of magnitude greater than the neat polymer, and reaching an optimal value of 36.47 dB (reduction of 99.98% of the incident radiation) (Kuester et al. 2017). However, defects are very detrimental to EMI SE. In addition, other traits, such as aspect ratio, functionalization, and content will also affect the nanocomposites electrical properties. It has been recently demonstrated that small size GnP (~ 13 μm) may present higher EMI SE, i.e., 27 dB (reduction of 99.8% of the incident radiation), than large size GnP (~ 38 μm) at 25 wt% content in polyester composites (Madinehei et al. 2021). This behavior is due to lower anisotropic effects created during the molding of the composite, which in turn leads to a larger absorption coefficient, as can be seen in Figure 1.20.

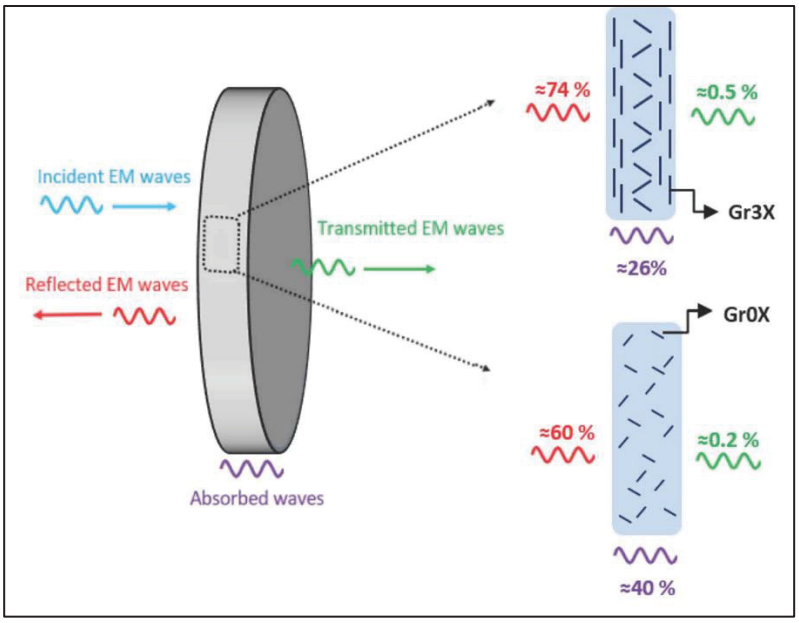

Figure 1.20 – Comparison between EMI SE of large size GnP (Gr3X) and small size GnP (Gr0X) in a polyester nanocomposite. Reproduced with permission from (Madinehei et al. 2021)

However, at lower contents, graphene's ability to improve EC of polymer matrices is very limited, requiring the use of high surface area sheets. One example is the study of Ravindran et al. (Ravindran et al. 2018), in which additions of 0.1 to 5.0 wt% GNP kept the EC of an epoxy matrix in the order of 10^{-9} to 10^{-8} S m^{-1}, and only after additions of 10 and 20 wt% the EC was increased to 10^{-7} and 10^{-6} S m^{-1}, respectively. These characteristics are associated with the dependency of the electron hopping across two adjacent graphene sheets on alternate current (AC).

Additionally, chemical functionalization usually decreases the composites capacity to conduct electricity due to the introduction of new defects and bonds, which changes the energy band state of electrons (Sun et al., 2021). In spite of that, if functionalization is performed only at the edges, it can be beneficial. A composite of PA6 filled with an edge-selectively functionalized graphene (EFG) has been synthesized via in situ ring-opening polymerization of ε-caprolactam without creating defects on its basal plane. Even when compared to graphite, ball-milled graphene, and commercial grade graphene-reinforced nanocomposites, the resulting nanocomposite showed improved EC. This behavior was attributed not just to the

lack of defects on EFG's basal plane, but also to the greater interfacial interactions between the functional groups on the filler edges and the polymer macromolecules, which led to an enhanced electron tunnelling effect (Cho et al. 2020).

Since EC of polymer nanocomposites depends mainly on the fillers interconnected path through which free electrons can be transported, i.e., the percolation threshold, constructing a pre-network could theoretically assist in enhancing EC (Chen, Xu, Ma, Ren, & Cheng, 2013; Román-Manso et al., 2016; Zhang et al., 2017; Zhao et al., 2018). That is usually done by a complex technique prior to mixing the filler with the polymer matrix. For example, a "multilayer graphene web" (MGW) has been synthesized through deposition of CVD graphene on a multilayer compressed Ni foam and then embedded in an epoxy matrix (Shen et al., 2016). In comparison to comparable epoxy nanocomposites, this resulted in an EC that was orders of magnitude greater.

Another example is an aerogel pre-network of GO that was thermally reduced with hydrazine vapor (TRGA) and then annealed at 1000°C, in order to reduce the number of structural defects (Xu et al., 2018). Afterwards, flexible PDMS was injected into the TRGA pre-network. The EC of this TRGA/PDMS nanocomposite was raised to 66 S m^{-1}, which is about 8 orders of magnitude greater than that of random distribution at only ~ 2 wt%. This same TRGA/PDMS nanocomposite exhibited an EMI SE of 54.26 dB (thickness of 2mm) within 8 – 12 GHz (X-band) at ~ 3 wt%. These examples evidence the importance of constructing interconnected filler networks to significantly enhance the electrical performance of polymer nanocomposites, enabling them to achieve properties that would characterize industrially interesting alternatives. The main issue is that this is more easily accomplished by very intricate techniques, which are hardly compatible to the current industrial landscape.

Alternatively, a straightforward process of melt-mixing by twin-screw extrusion, to produce a hybrid blend nanocomposite based on LLDPE/EMA reinforced by FWCNT and FLG, has been reported. The co-continuity of the polymer blend changed after the nanofillers were added, presumably due to their migration from the EMA (hydrophilic) phase to the LLDPE

(hydrophobic) phase. Due to the preference for percolation in the blends including FWCNT and FLG/FWCNT, these systems had greater EC (Nunes et al. 2021). Similarly, other works have also produced LLDPE/EVA/graphene composites by melt compounding (Helal et al., 2019; Kurusu, Helal, Moghimian, David, & Demarquette, 2018). In such cases, it was possible to significantly reduce the percolation threshold to 0.5 vol%. This was done by applying an annealing process after compounding, which leads to a phase separation and morphology coarsening in the blend. As a consequence, the graphene nanosheets migrate to the interface, more easily forming the interconnected path necessary for EC. The nanosheets' migration promoted by the microstructural refinement during annealing is defined as double percolation threshold (Mir et al. 2016; Bose et al. 2009; Göldel, Kasaliwal, and Pötschke 2009; Pötschke, Kretzschmar, and Janke 2007; Pötschke, Bhattacharyya, and Janke 2004; Strugova et al. 2021; Strugova, David, and Demarquette 2022).

This double percolation threshold obtained by thermal annealing has also been observed for LLDPE/PP/graphene and HDPE/PLA/graphene nanocomposites, reaching values as low as < 0.1vol% (Mun et al. 2019). In this cases, the graphene migrates towards the interface when a (PP + graphene) or (PLA + graphene) masterbatch is blended with either LLDPE or HDPE. It has been observed that the annealing promotes a coarsening in the blend co-continuous morphology and, since graphene has stronger attraction to the PE phase, it tends to relocate from its original matrix, i.e., PP and PLA. However, the energy barrier needed to move the nanosheets from the interface to the bulk PE may prevent it from escaping the interface (Bai, Sharma, Cheng, & Macosko, 2018). This is supported by the fact that 2DM, particularly for very incompatible blends, are quite stable when orientated in a parallel direction to the blend interface (Göldel et al. 2011). Figure 1.21a presents an illustration of this co-continuous morphology with the 2DM preferentially located at the interfaces along with a TEM image of the (PLA/graphene) + HDPE composite. This controlled morphology leads to the formation of interconnected networks, which are confirmed by rheological measurements (Figure 1.21Figure b), and allows the achievement of ultra-low percolation thresholds, as can be seen in Figure 1.21c.

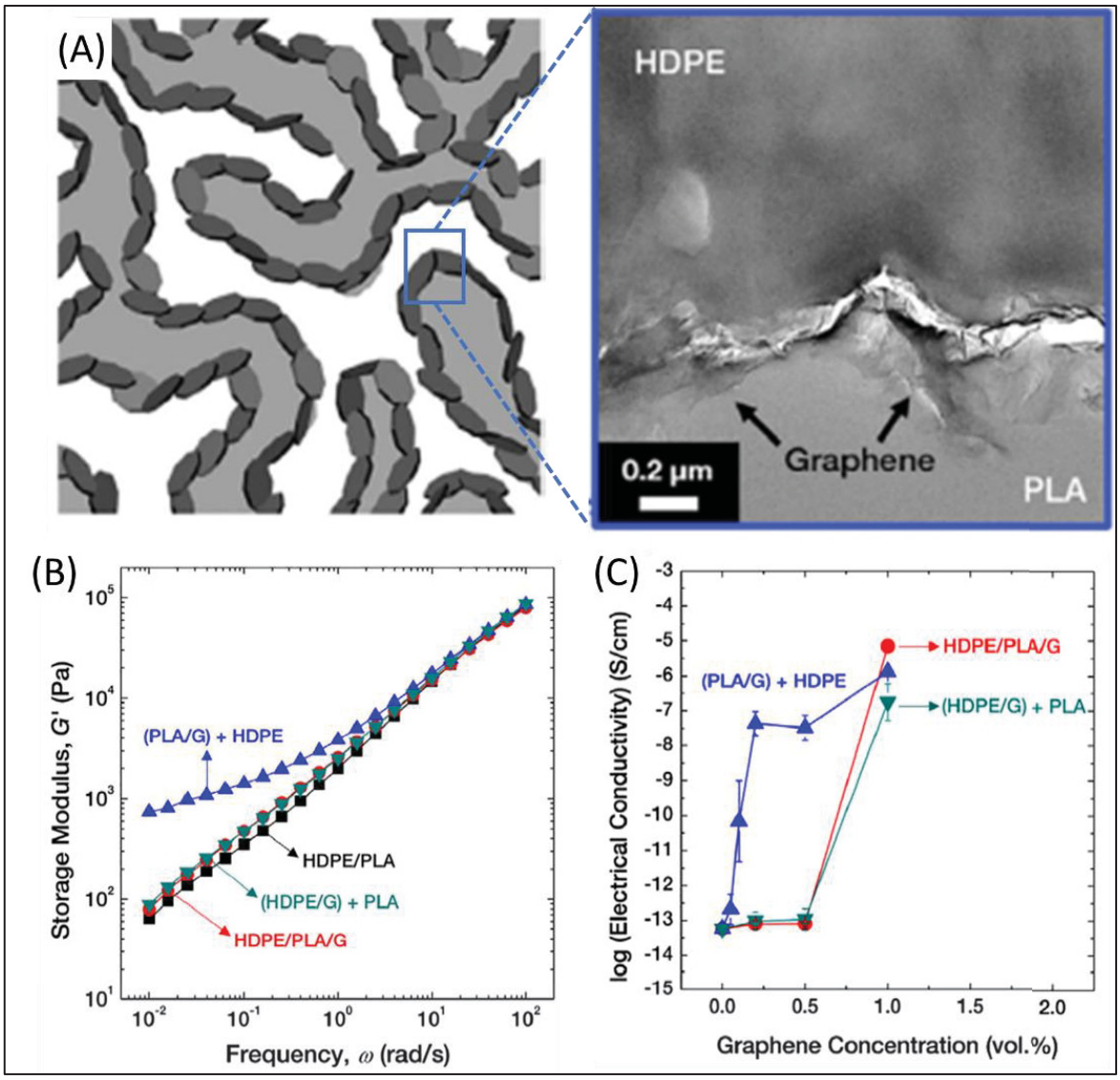

Figure 1.21 – (a) Schematic illustration of the preferential 2DM localization at the interfaces in co-continuous polymer blends (left), and TEM image of the morphology of (PLA/graphene) + HDPE nanocomposites at 0.2 vol% (right); (b) Storage modulus as a function of frequency for the (PLA/graphene) + HDPE nanocomposites at 0.2 vol%; (c) Electrical conductivity as a function of graphene content, exhibiting the ultralow percolation threshold for the composites produced from the (PLA + graphene) masterbatch. Adapted with permission from (Mun et al. 2019)

1.6.2 Molybdenum Disulfide

As previously stated, molybdenite, the natural occurring form of MoS_2, shows low EC, but its chemical exfoliation yields highly electrically conductive 1T-MoS_2 monolayers. The EC of

1T-MoS_2 is reported in the range of 0.1 - 1.0 S m^{-1} (Acerce, Voiry, and Chhowalla 2015). Thus, this nanomaterial is a valuable filler candidate for conductive polymer nanocomposites.

The most common technique employed in the preparation of such nanocomposites has been established as the solution blending approach. For that, solutions of the polymers previously dissolved in a solvent, are simply mixed with chemically exfoliated MoS_2. The restacking of the MoS_2 layers results in sandwiched compounds (Rabin Bissessur, Gallant, and Brüning 2003). Polymer-intercalated MoS_2 compounds from poly[oxymethylene-(oxyethylene)] (POMOE) (Rabin Bissessur, Gallant, and Brüning 2003), polyanilines (PAni) (Rabin Bissessur and White 2006) and polypyrrole (PPy) (R Bissessur and Liu 2006) have successfully been developed through this method. Using a different approach, polythiophene (PTP) monomers were inserted into Li-intercalated MoS_2 lamellae, and were subsequently polymerized. The resulting nanocomposite was found to have an electrical conductivity in the order of 10^{-2} S cm^{-1} at RT (Lin, Ding, Xu, Chen, & Chen, 2009). Such polymers are known to be conductive due to their conjugated structures, and are of great interest for applications such as cathodes in lithium batteries, and the addition of MoS_2 could lead to gains of an order of magnitude in their EC (Rabin Bissessur, Gallant, and Brüning 2003).

Other applications for these conductive MoS_2 nanocomposites are hydrogen evolution electrocatalysis (T. Wang et al. 2014) and supercapacitors (Zhao, Ang, Liu, & Lu, 2017). As an example, a PAni/MoS_2 nanocomposite obtained through an electrostatic attraction-induced self-assembly process exhibited improved rate capability and cycling stability for electrochemical processes. The enhanced performance was attributable to the higher charge carrier transport and structural stability of the developed nanocomposite (Zhao et al., 2017).

1.6.3 Hexagonal-Boron Nitride

Highly dielectric polymers have shown promising reliability and higher voltage breakdown strength for applications in power electronics (Tanaka, Montanari, and Mulhaupt 2004). However, when subjected to high temperatures, these materials have underwhelming

performances (Johnson et al. 2004). Hence, the use of h-BN/polymer nanocomposites could address such issues. For example, the dielectric loss at low frequencies of epoxy decreases significantly at 150°C after adding 1 – 5 wt% h-BN, as can be seen in Figure 1.22a (Tang et al. 2019).

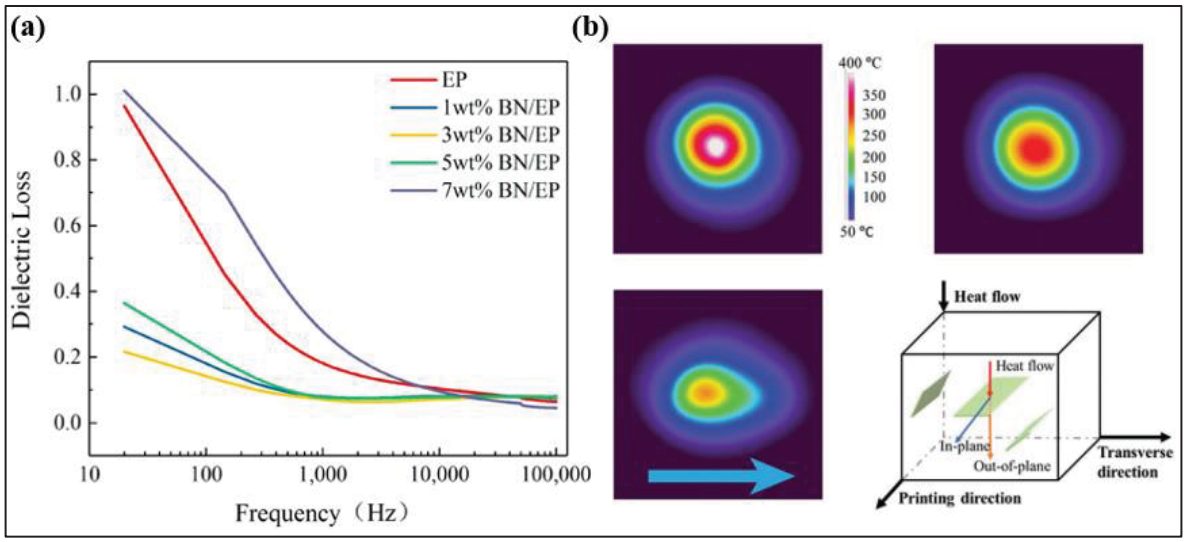

Figure 1.22 – (a) Frequency dependence of dielectric loss of EP/h-BN nanocomposites with different contents of h-BN. (EP = epoxy); (b) IR images of the temperature distribution of CPE (upper left), CPE/r-h-BN (upper right), and CPE/a-h-BN (lower left) at laser source power of 100 μW; schematic illustration of the battery heat dissipation when heated by a laser power source (lower right). (CPE = composite polymer electrolyte; r-h-BN = randomly distributed h-BN; a-h-BN = aligned h-BN). Adapted with permission from (Cheng et al., 2021; Tang et al., 2019)

Many applications, such as TIMs and microwave electronic packaging, require characteristics like strong electrical resistivity and dielectric breakdown strength. Since h-BN has a high bandgap, its incorporation in polymers should not increase their electrical resistivities, as has been shown by some works in literature (Wang et al., 2014).

Even though other 2DM, like graphene, MXene, and MoS_2 have demonstrated that they are good fits for Li batteries as cathode, anode, and catalysts (Liu, Ullah, Kuo, & Cai, 2019), they are not compatible with other applications, such as battery electrolytes and packaging because of their elevated EC. This is due to possible short circuiting that would lead to battery failure. In these cases, h-BN has a great advantage due to its intrinsic electronic insulation.

Additionally, the superior TC of h-BN is of great interest, since it allows greater dissipation of the heat generated during the battery's operation, avoiding the formation of hot-spots and thermal run-away events (Cheng et al., 2021). Figure 1.22b exhibits such behaviour

1.7 Outlook

With the continuous development of polymer composites and their processing methods, the importance of 2DM nanocomposites has become increasingly prominent. In addition to gains in the properties mentioned throughout this manuscript, other enhancements have already been reported, e.g., photoprotection, modification of surface energy, which can lead to some degree of biocompatibility, gas barrier, and processing aid due to superlubricity effects (Y. D. C. de Oliveira, Amurin, Valim, Fechine, & Andrade, 2019; Ferreira, Andrade, & Fechine, 2019; Medeiros et al., 2020; C. F. P. Oliveira et al., 2019; Pinto et al., 2020; Rodriguez, Kessler, Dubey, Rosa, & Fechine, 2017).

Nevertheless, there remain significant obstacles to be addressed before these composite materials may be steadily employed in multifunctional engineering applications. Firstly, it is noticed that, even though great results have already been achieved with low contents in respect to the enhancement of mechanical properties, other features, e.g., TC and EC, still usually require the use of high filler contents or complex processing techniques to achieve desirable results. This is most likely caused by the stronger relationship between the mechanical properties of polymer composites and the interfacial quality between the polymer matrix and 2DM, which may be achieved through relatively straightforward functionalization procedures. On the other hand, TC and EC are more intrinsically dependent on the formation of a filler interconnected path, i.e., reaching the percolation threshold, which is not easily achieved, even for 2DM. Secondly, although most academic research does not tackle such issues, there are large performance differences and unstable quality of the produced composites, even when using the same processing routes and fillers, which is the biggest bottleneck that needs to be solved for their large-scale employment.

It has been seen that the use of hybrid fillers, i.e., combining different 2DM in the same composite is a promising way to at least mitigate some of these challenges due to synergistic effects and improved dispersion. However, it is paramount to take into account the different intrinsic properties of each 2DM, which will naturally affect the final properties of the composite. Additionally, research of such systems is still in its early stages, requiring a deeper understanding of the combined effects promoted by these hybrid 2DM.

Finally, as the demand for new 2DM technologies in emerging multifunctional applications continues to grow, research should focus on innovating key 2DM technologies, e.g., accelerating the breakthroughs in the preparation of stable high-quality 2DM and their dispersion in polymer matrices. Notwithstanding, the formulation of technical standards and specifications for the application of 2DM in these high-tech fields should be emphasized by the collaboration of enterprises and scientific research institutes.

ACKNOWLEDGEMENTS

The authors would like to acknowledge Fundação de Apoio à Pesquisa do Estado de São Paulo (FAPESP) for the grants 2020/11496-0 and 2021/07858-7, the Natural Sciences and Engineering Research Council of Canada (NSERC), the Conselho Nacional de Desenvolvimento Científico e Tecnológico (CNPq) for the grant 140241/2019-1, the Coordenação de Aperfeiçoamento de Pessoal de Nível Superior (CAPES) for the grant PRINT 88887.310339/2018-00, the Mackenzie Research Fund (MackPesquisa, Project number 181009), and the European Commission, within the framework of the H2020-MSCA-RISE-2016-734164 Graphene 3D project.

CHAPTER 2

EXPLORING THE RELATIONSHIP BETWEEN INTERFACIAL ADHESION, MOLECULAR DYNAMICS, AND THE BRILL TRANSITION IN FULLY BIO-BASED POLYAMIDE 1010 NANOCOMPOSITES REINFORCED BY TWO-DIMENSIONAL MATERIALS

Gabriel M. Pinto[1,2,3], Aelton B. Santos[4], Emna Helal[1], Hélio Ribeiro[2], Eric David[1], Cristiano F. Woellner[4], Nicole R. Demarquette[1], Guilhermino J. M. Fechine[2,3]

1 Department of Mechanical Engineering, École de Technologie Supérieure, Montréal, QC, Canada
2 Engineering School, Mackenzie Presbyterian University, São Paulo, SP, Brazil
3 Mackenzie Institute of Research in Graphene and Nanotechnologies – MackGraphe, Mackenzie Presbyterian Institute, São Paulo, SP, Brazil
4 Physics Department, Federal University of Parana – UFPR, Curitiba, PR, Brazil

Paper published in *Polymer*, 2023
DOI: https://doi.org/10.1016/j.polymer.2023.126482

ABSTRACT

One of the greatest goals of modern polymer science can be considered the production of high-performance polymer nanocomposites from renewable sources due to the growing interest in environmental and sustainability issues. Within that scope, a good strategy is to pair the processability of thermoplastic materials with the outstanding characteristics of 2D nanomaterials. However, the final performance of the produced nanocomposite is mainly attributed to the interphase, i.e., the volume fraction of the bulk polymer that has its molecular dynamics affected by interactions with the surface of the filler. Therefore, we aim to investigate how different 2D nanomaterials, i.e., graphene oxide (GO), hexagonal-boron nitride (h-BN), and molybdenum disulfide (MoS_2) affect the molecular dynamics of a fully bio-based polyamide 1010 (PA 1010) by a new correlation between experimental results from differential scanning calorimetry, broadband dielectric spectroscopy, and dynamic mechanical analysis. For that, nanocomposites based on single and hybrid-fillers were produced through melt mixing. It was observed that, although all nanofillers seem to hinder the molecular relaxation of the polymer chains, GO and h-BN were more effective than MoS_2. This remained true when the fillers were applied individually and in the hybrid form. This effect has been attributed to the following aspects: (I) higher enthalpy related to the melting of the polyamide crystals after the Brill transition, which indicates lower thermal motion being gained before the transition takes place; (II) higher activation energy of the glass transition, which was estimated from the fitting of the dielectric spectra to the Havriliak-Negami function and then to the Vogel-Fulcher-Tammann model; (III) lower values of the "adhesion factor", which is calculated from the decrease in intensity of the mechanical tan(δ) in the nanocomposites with respect to the neat polymer, indicating higher adhesion for the composites filled with GO and h-BN. To confirm

the trends observed experimentally for each nanomaterial, molecular dynamics simulations, which enabled the investigation of the adhesion force as a function of nanosheet displacement, were also carried out. The simulations corroborated with the experimental observations, in which h-BN leads to a more intense force of separation, followed by GO, and lastly by MoS_2. Since the level of interfacial interactions is what mainly dictates the performance of polymer nanocomposites, it is suggested that GO, and especially h-BN, might present greater promise for novel bionanocomposites based on PA 1010.

Keywords: Polymer nanocomposites; Interfacial adhesion; Molecular dynamics; Bio-based polyamide, 2D nanomaterials

2.1 Introduction

One of the greatest goals of modern polymer science can be considered the production of conventional polymers from renewable sources due to the growing interest in environmental and sustainability issues. An advantage of this new class of materials is the reduction of the carbon footprint associated to them (Kiziltas et al., 2021; Kyulavska et al., 2017). Among the currently known biopolymers, biopolyamides derived from castor oil, e.g., polyamide 1010 (PA 1010), are characterized as one of the most interesting (Kuciel, Kuźniar, and Liber-Kneć 2012; Keridou et al. 2020). This polyamide grade is a commercially produced engineering polymer, with high strength, elasticity, toughness and abrasion resistance (W. Li et al., 2008; Zhang et al., 2005; Zhishen et al., 1993). This has led to its employment in many fields, ranging from sports equipment, textiles, and as a coating material, to the automotive and electronics industries (Rusu et al., 2011). On top of that, it is possible to further fine-tune its characteristics for particular applications by developing nanocomposites through the addition of nanofillers (Kiziltas et al., 2021; Zeng et al., 2006). Figure 2.1 presents the atomic structure of a PA 1010 macromolecule.

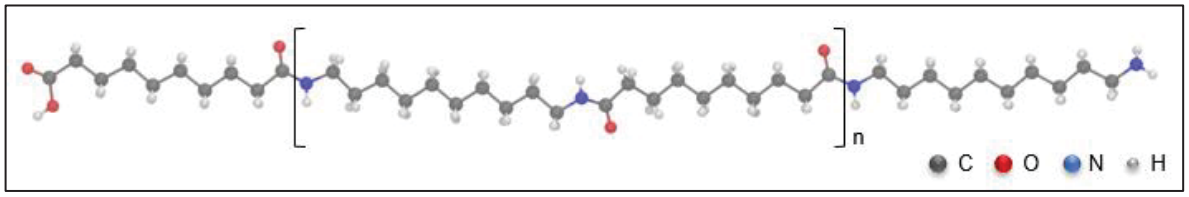

Figure 2.1 – Atomic structure of PA 1010

In order to create composites with much better macroscopic characteristics, the main advantage is to pair the processability of thermoplastics with the outstanding material characteristics of nanomaterials (Pinto et al., 2023). The fundamental idea behind this strategy is the great interfacial area that arises when at least one of the fillers' characteristic sizes is scaled down to the nanometer range, which amplifies filler-polymer interactions. Since polymer chains that are in the interphase, as this intermediary region between the filler surface and the bulk polymer is commonly called, are the main contributors to the composite's macroscopic properties, nanocomposites present greater promise than conventional composites (Cheng, Carroll, Bocharova, et al., 2017; Huang et al., 2022; Sattar, 2021; Wang et al., 2022; Xiao et al., 2023).

Therefore, understanding how the interactions between polymers and nanofillers affect the interfacial arrangement and molecular dynamics (MD) is crucial for technological advancement. However, the factors governing such conformations, dynamics, and confinement effects throughout the interfacial area have proved difficult to identify and understand (Sattar 2021). Nevertheless, differential scanning calorimetry (DSC), broadband dielectric spectroscopy (BDS), and dynamic mechanical analysis (DMA) have been widely employed to experimentally investigate interfacial interactions of nanomaterials with polymer chains in nanocomposites (Carroll et al., 2017; Cheng, Carroll, Lu, et al., 2017; Cheng et al., 2016; Helal et al., 2015, 2017; Holt et al., 2014; Klonos et al., 2019; Xiao et al., 2023).

BDS is a useful tool to evaluate the molecular dynamics of polymer materials in a broad frequency range with very high accuracy (Carroll et al., 2017; Cheng, Carroll, Lu, et al., 2017; Cheng et al., 2016; Czaderna-Lekka & Kozanecki, 2021; Gálvez et al., 2023; Helal et al., 2015, 2017; Holt et al., 2014; Klonos et al., 2019; Soccio et al., 2017; Xiao et al., 2023). This is done by the measurement of the relative complex dielectric permittivity of the material, which is its response to an applied electrical field, either by polarization or conduction mechanisms. When dealing with nanocomposites, the technique is able to detect the slower segmental relaxation of the macromolecules in the vicinity of nanofillers, which is intrinsically related to the adhesion between the different phases (Carroll et al., 2017; Kremer & Schönhals, 2003).

DMA is a great tool to couple with BDS, since much the same as the dielectric relaxation in response to an applied electric field, relaxation processes also occur in polymer materials under external mechanical stimuli. These processes are easily identified in the evaluation of the storage modulus, loss modulus and damping factor [tan(δ)] of a polymeric material. Since the addition of nanofillers tend to reduce the mobility of the macromolecules around them, DMA is able to detect the lower molecular mobility in nanocomposites through changes in the intensity of tan(δ) during such relaxations, or even in the shift of the temperature at which the process takes place (Correa et al., 2007; Helal et al., 2015, 2017; Jyoti et al., 2016; Rittigstein et al., 2007).

Additionally, it is known that even-even polyamides present a Brill transition when heated, which might be studied through DSC. This transition consists on the polymorphic transformation of the monoclinic α crystals into pseudo-hexagonal γ crystals. Depending on the length of its aliphatic chains, this transition can occur either before or at the melting temperature, which is the case for PA 1010 (Lotz 2021). Since these two crystalline phases are very similar, there is a thermodynamical competition between the thermal motion (melting) and the packing tendency (Brill transition) of polymer chains in the crystalline structure, leading to a complex melting behavior (Tashiro & Yoshioka, 2004; X. Yang et al., 2001; Zhishen et al., 1993). However, one can take advantage of this transition, which usually appears as a double melting peak due to the exothermic event right in the middle of melting, to gain insights on filler-polymer interactions. It is assumed that in systems with better chemical affinity, a reduction of the macromolecules' mobility due to filler-polymer interactions may shift the balance of the competition between the thermal motion and the packing tendency to an increased number of α crystals participating in the transition to γ crystals, which would change the shape of the melting peaks.

In addition to the aforementioned experimental techniques, MD simulations have also demonstrated great promise for predicting the interfacial properties and degree of interactions in polymer nanocomposites (Asadian & Shelesh-Nezhad, 2020; Chen et al., 2021; Fechine et al., 2015; Hagita & Morita, 2019; Krishna et al., 2021; H. Li et al., 2021; Lu et al., 2021;

Rastegar & Montazeri, 2022; Ries et al., 2021; H. Sun et al., 1994; R. Sun et al., 2020; Wadkin-Snaith et al., 2023; B. Yang et al., 2021; Zhou et al., 2022). For instance, Ries et al. (Ries et al. 2021) investigated a composite of silica-reinforced polystyrene, for which, even though an exponential saturation profile for Young's modulus and yield stress inside the interphase was found, the polymer's hardening coefficient and Poisson's ratio remained basically unchanged. In a similar manner, Rastegar et al. (Rastegar and Montazeri 2022) simulated a composite of polylactic acid (PLA) filled by pristine and surface-treated boron nitride nanosheets, and the findings demonstrated that functionalizing the sheets with chemical hydroxyl functional groups and grafting PLA chains onto them can contribute to the enhancement of PLA toughness. On the other hand, Lu et al. (Lu et al., 2021) revealed a softening effect at the interface due to the very low stiffness of slip along graphene plane. Additionally, they suggested that the interphase stiffening is outweighed by this interfacial softening. The effect of structural defects on the nanomaterial's plane on the glass transition (T_g) of a polymer matrix has also been simulated for a PMMA/graphene nanocomposite (B. Yang et al., 2021), and it has been shown that the introduction of some defects can actually increase the T_g of the polymer matrix due to changes in the polymer's density distribution, mean square displacements, and free volume. Although most studies focus on the mechanical characteristics of nanocomposites' interfaces, MD simulations can also be used to assess other properties. For example, Chen et al. (Chen et al., 2021) looked at the effect of size and chemical interconnectivity of graphene nanosheets on the thermal conductivity of a graphene-reinforced PA 6 nanocomposite. It has been determined that the thermal conductivity is considerably improved for large, covalently bonded graphene sheets because less heat is lost through the polymer matrix, being carried along the graphene architecture.

For these modeling and simulation processes, the large-scale atomic/molecular massively parallel simulator (LAMMPS) (Plimpton 1995) is frequently utilized. LAMMPS allows to simulate the behavior of atoms and molecules in various materials by using force fields to describe the interactions between particles. Thus, it can provide insights into the structural, thermodynamic, and dynamic properties of materials. To do that, Newton's laws are used to simulate the motion of atoms and molecules. The software also uses integration algorithms to

numerically solve the equations of motion, which allows the calculation of particle positions and velocities at successive time steps based on their current state. In order to set the conditions for the simulations, different ensemble methods are supported, such as the isothermal-isobaric (NPT) ensemble, which can be used to produce a system with an appropriate density and low residual stresses, and the canonical ensemble (NVT), which is commonly used for further analysis of atomic data and calculation of properties.

With that in mind, this paper endeavors to establish a compelling correlation between results-derived coefficients from the distinct experimental techniques, as well as associate such results with the adhesion force predicted by MD simulations of each nanomaterial's interface with PA 1010. The main objective is to examine the interfacial strength of graphene oxide (GO), hexagonal-boron nitride (h-BN), and molybdenum disulfide (MoS_2), i.e., prominent two-dimensional nanomaterials, with PA 1010 macromolecules, specifically by assessing the consequential changes in the molecular dynamics of the polymer. By doing so, this research aims to shed new light on the intricate interplay between these nanomaterials and the polymer, unraveling novel insights into their interfacial interactions. Figure 2.2 exhibits a 3D view of these two-dimensional materials' structure.

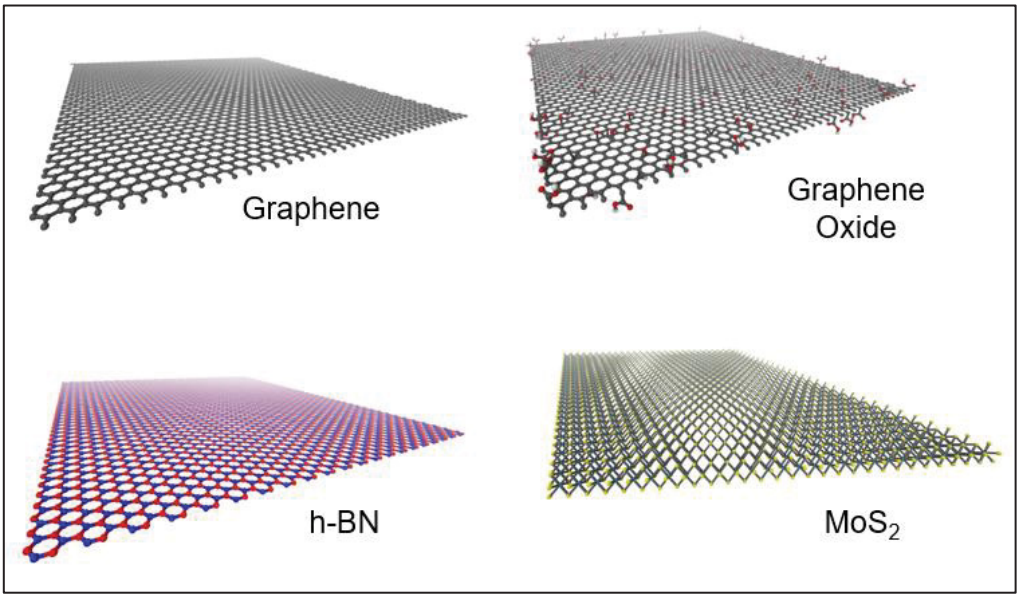

Figure 2.2 – 3D view of the studied nanomaterials' structure

2.2 Materials and Methods

2.2.1 Materials

The polymer matrix used is the Grilamid XE 4181 natural. It is an extrusion grade, unreinforced, high viscosity, plasticized, high impact resistant PA 1010 from EMS Grivory. As for the nanofillers, systems based on GO, h-BN, MoS_2, as well as their hybrids, i.e., GO@h-BN, GO@MoS_2, and h-BN@MoS_2 were investigated. The GO used was synthesized in-house, presenting a C : O ratio of ~ 1, less than 5 layers, good structural quality, and lateral size ≤ 2.5μm (Andrade et al. 2021). The bulk h-BN was purchased from Sigma-Aldrich and has purity of ~ 100% and relative density of 2.29 g/cm^3. The bulk MoS_2 was purchased from Merck and has a purity of ~ 100% and density of 5.06 g/cm^3. The morphologies of such nanoparticles are presented in Figure A I-1 and the range of their dimensions, i.e., thickness, width, aspect ratio, and number of layers is presented in Table 2.1. For the calculation of number of layers, it was assumed that each layer of GO, h-BN, and MoS_2 has a thickness of 0.70, 0.34, and 0.65 nm, respectively.

Table 2.1 – Range of thickness, lateral size, number of layers, and aspect ratio of the nanomaterials after exfoliation

	Thickness (nm)	**Lateral size (μm)**	**Number of layers**	**Aspect ratio**
GO	1.0 – 2.0	1.50 – 2.00	1 – 3	~ 750 – 2,000
h-BN	2.0 – 3.0	0.02 – 0.40	6 – 9	~ 7 - 200
MoS_2	1.3 – 6.0	0.14 – 1.30	2 – 9	~ 23 – 1,000

2.2.2 Methods

2.2.2.1 Preparation of the Nanocomposites

Before mixing the nanomaterials with the polymer, the nanofillers were properly exfoliated in adequate solvents since it has been shown that it improves their dispersibility in the melt mixing step of the polymer nanocomposites preparation (Muñoz et al., 2018; Pinto et al., 2020). On the basis of achieving similar exfoliation yields of previous works, different exfoliation protocols have been followed for each nanomaterial (Andrade et al., 2021; Kalupgian, 2021; Marciano de Oliveira Cremonezzi et al., 2022). Table 2.2 Table presents the procedures discriminating the solvent, type of sonication and time employed.

Table 2.2 – Exfoliation protocol for each 2D material used

Material	Solvent	Exfoliation type	Exfoliation time (min)
Graphene oxide	Water	Ultrasonic bath	30
Hexagonal-boron nitride	Water / Isopropanol with a ratio of 7 : 3 in volume	Tip sonication	240
Molybdenum disulfide	Ethanol	Ultrasonic bath	180

The reason for the much lower exfoliation time employed for GO is that this material was already freeze-dried, which means it had already been exfoliated after its synthesis. Thus, only a mild exfoliation was applied from our part to disperse it in the proper solvent.

After exfoliating the nanomaterials, they were mixed in the polymer matrix through melt compounding, assisted by the" solid-solid deposition" methodology. This step was developed by our research group and it is used to pre-deposit the nanomaterials on the surface of the polymer powder before feeding the mixture to a twin-screw extruder (Muñoz et al. 2018). For the solid-solid deposition, a Buchi B-100 roto-evaporator with heating bath was used, operating at 50 °C and 80 mBar. As for the extrusion process, a Process 11 twin-screw extruder (ThermoScientific), with L/D = 40 and 11 mm in screw diameter was employed. Figure 2.3

illustrates the extruding parameters employed, and Table 2.3 presents the filler contents studied for each system.

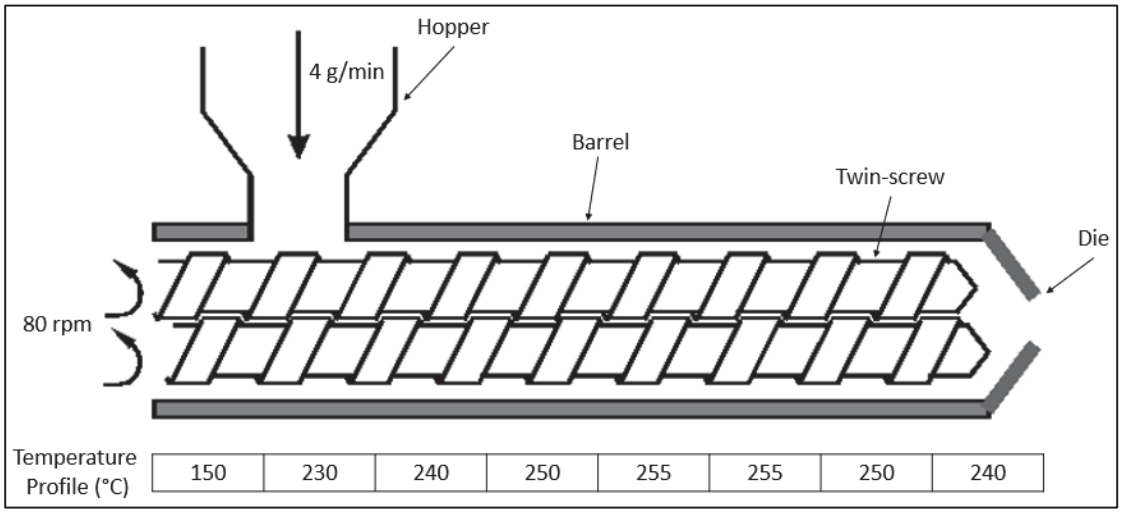

Figure 2.3 - Parameters used in the extrusion for processing the nanocomposites

Table 2.3 - Compositions of produced nanocomposites

Acronym	GO wt%	hBN wt%	MoS_2 wt%	Total wt%
GO	0.10	-	-	0.10
	0.30	-	-	0.30
	0.50	-	-	0.50
h-BN	-	0.10	-	0.10
	-	0.30	-	0.30
	-	0.50	-	0.50
MoS_2	-	-	0.10	0.10
	-	-	0.30	0.30
	-	-	0.50	0.50
GO@h-BN	0.05	0.05	-	0.10
	0.15	0.15	-	0.30
	0.25	0.25	-	0.50
h-BN@MoS_2	-	0.05	0.05	0.10
	-	0.15	0.15	0.30
	-	0.25	0.25	0.50
MoS_2@GO	0.05	-	0.05	0.10
	0.15	-	0.15	0.30
	0.25	-	0.25	0.50

After processing the nanocomposites, the extrudates were pelletized and then molded into disc samples (1 mm x 25 mm) by injection molding for the BDS measurements. The injection molding machine used was a Haake Minijet Pro (Thermo-Scientific) with barrel temperature of 255 °C, mold temperature of 100 °C, injection pressure of 600 bar for 30 s, and post pressure of 400 bar for an additional 20 s. In addition to injection molding, rectangular samples (1.5 mm × 8.5 mm × 40 mm) for DMA analyses were also produced by compression molding at 220 °C. For compression molding these samples, the pellets were first pre-heated in the mold at the specified temperature for 180 s to soften the material. Then, a small pressure of 0.8 MPa was applied for 120 s, and then increased to 5.0 MPa for an additional 180 s. After the molding step, the samples were cooled down by the hot-press circulating water system until 150 °C was reached, and then they were left to cool back to room temperature on the top of the bench.

Before all processes in which the polymer was molten, i.e., extrusion, injection molding, and compression molding, the pellets were properly dried in a vacuum oven at 80 °C for at least 12 h to avoid possible degradation by excess moisture. This drying procedure is important for this polymer matrix because polyamides are known to present high hydrophilicity, being sensitive to hydrolysis when processed in the molten state.

2.2.2.2 Characterizations

DSC scans were performed on a DSC-60PLUS (Shimadzu) equipment. Pellets of ~ 5 mg were used as samples. Two heating scans were performed in a N_2 atmosphere to exclude the thermal history of the samples. The first heating scan was carried out from room temperature up to 230 °C at a heating rate of 10 °C min^{-1}. The material was then allowed to recrystallize by cooling it back to room temperature with a cooling rate of 10 °C min^{-1}. Afterwards, a second heating cycle was conducted at 10 °C min^{-1} up to 230 °C for acquisition of the melting data. To investigate the Brill transition, the fraction of enthalpy related to the melting step after such transition takes place was estimated by dividing the enthalpy of the second melting peak by the overall melting enthalpy ($\Delta H_B/\Delta H_m$).

The relative complex dielectric permittivity was measured through BDS using a frequency-domain broadband dielectric spectrometer. Disc specimens of 25 mm diameter were coated with a 10 nm layer of gold on both sides to improve the contact with the plated brass electrodes of the equipment. Measurements swept through a frequency range from 1×10^{-2} Hz to 3×10^{5} Hz under an excitation voltage of 3 V. Isothermal measurements were consecutively performed at different temperatures by increasing it from 30 °C to 120 °C with 10 °C steps. In order to model dipolar polarization mechanisms, the Havriliak-Negami (HN) function has been established as appropriate for fitting the dielectric relaxation spectra of polymers, thanks to its four adjustable parameters (Kremer & Schönhals, 2003). Equation 2.1 is a general equation allowing to take into account N different relaxation processes expressed by the summation of HN functions, as well as the contribution of charge carriers fluctuation expressed by the power law term.

$$\hat{\varepsilon}(\omega) = b(i\omega)^{n-1} + \sum_{k=1}^{N}\left[\frac{\Delta\varepsilon_k}{(1+(i\omega\tau_k)^{\alpha_k})^{\beta_k}} + \varepsilon_{\infty k}\right] \quad (2.1)$$

Where, ω is the angular frequency, n is an exponential factor between 0 and 1, characterizing the nature of the charge hopping process (n = 0 corresponds to pure electronic conduction with $b = \sigma_0/\varepsilon_0$), τ_k and $\Delta\varepsilon_k$ are respectively the relaxation time and the dielectric strength related to relaxation process k, $\varepsilon_{\infty k}$ is the residual dielectric constant at much higher frequencies than the one of the relaxation process, α_k is a width parameter, characteristic of the slope at the low frequency side of the relaxation peak, β_k is an asymmetry parameter, where $-\alpha_k\beta_k$ determines the slope at the high frequency side of the relaxation peak, and N is the number of relaxation mechanisms observed in the studied range of frequencies and temperatures.

After fitting a dielectric spectrum to Equation 1, it is possible to obtain the relaxation time (τ) associated to a specific process. The same procedure was done for the various temperatures, which enables the creation of an Arrhenius plot of $\ln(\tau)$ as a function of 1/T. With these Arrhenius plots, it was possible to gain insights on the morphology of the nanocomposites by analyzing the effect of the nanoparticles on the relaxation times of a specific transition as a function of temperature.

Additionally, by fitting the curves of ln(τ) as a function of 1/T to Equation 2.2, defined as the Vogel-Fulcher-Tammann (VFT) equation, it is possible to estimate the activation energy (E_a) of the polymer's relaxation process, and how the nanofillers affect it. Similarly to the effect on τ, if the nanoparticles are well dispersed and present good interfacial adhesion, it is expected that E_a would increase in respect to the neat polymer due to the confinement of macromolecules. Here, we have employed the VFT function for fitting the data, because it has been shown that it usually provides better fits for the α process (glass transition) of polymers (Gao & Jian, 2020; Liu et al., 2020).

$$\tau(T) = \tau_0 \exp\left(\frac{E_a}{k_B(T-T_v)}\right) \quad (2.2)$$

Where E_a is a constant related to the activation energy of the relaxation process, τ_0 is the relaxation time at infinite temperature, k_B is the Boltzmann's constant, and T_v is the Vogel-Fulcher temperature. Aside from these calculations, it is also possible to infer on the nanocomposites' morphology by observing the shape of the relaxation peaks. It has been widely proposed in the literature that the peaks can change in shape and even a new peak, related to a "secondary" glass transition from the restricted chains at the interphase, may appear (Carroll et al., 2017; Cheng et al., 2016, 2017; Helal et al., 2017; Holt et al., 2014; Klonos et al., 2019).

DMA was performed in an Anton Paar MCR 501 rheometer in torsion mode through the use of the equipment's solid rectangular fixture (SRF). The amplitude strain was exponentially increased from 0.01 to 0.1% along the test duration in order to improve the signal quality after the glass transition of the material. Even though the strain was varied during the scans, it is important to note that the whole range applied was within the linear viscoelastic regime (LVR) of the material, which was previously determined through amplitude sweeps. The frequency was kept constant at 1.0 Hz and the normal force at 1.0 N to avoid possible sagging of the sample. Since the glass transition of PA 1010 is slightly above room temperature, the samples

were measured within a temperature range of 30 °C to 70 °C. After acquiring the damping factor data, the “adhesion coefficient” was calculated according to Equation 2.3.

$$A = \frac{1}{(1-\emptyset_f)} \frac{\tan \delta_c}{\tan \delta_m} - 1 \tag{2.3}$$

Where A is the adhesion factor, $\emptyset_f$ is the filler volume fraction, $\tan \delta_c$ is the damping factor of the composite, and $\tan \delta_m$ is the damping factor of the neat polymer. At high levels of interface adhesion, the macromolecular mobility near the filler surface tends to be less than that in the bulk matrix, which lowers tan(δ) and hence, A. Thus, a low value of A denotes a high level of adhesion, or contact between the phases.

This adhesion coefficient was first introduced by Kubát, Rigdahl, and Welander (Kubát et al., 1990), with the aim to investigate the effect of filler surface treatments on the interfacial interactions of high-density polyethylene (HDPE) filled by glass spheres. Later, the same parameter was employed by Correa, Razzino, and Hage Jr. (Correa, Razzino, and Hage 2007) in an attempt to investigate the coupling efficiency of malleated polypropylene (PP-MAH) with varying MAH contents in PP–wood composites, and more recently, Jyoti et al. (Jyoti et al. 2016) used it to evaluate the interfacial interactions between acrylonitrile butadiene styrene (ABS) and multi-wall carbon nanotubes (MWCNT). Even though this parameter has not been widely applied in the literature, we strongly believe that it can be valuable when determining the intensity of filler-polymer interactions. Therefore, we aim to explore it for the first time for polymer nanocomposites filled by two-dimensional nanomaterials.

2.2.2.3 Molecular Dynamics Simulations

The protocol used to perform MD simulations was followed according to a previous research (Fechine et al. 2015), and it is dissected in the next paragraphs.

GOPY, a free open-source python tool (Muraru et al., 2020), was utilized to create a single layer of GO. GOPY, as stated in (Muraru, Burns, and Ionita 2020), is a "free and open-source

Python tool specifically written to automate the generation of 2D graphene-based molecular models such as pristine graphene and several graphene derivatives".

In order to generate the h-BN sheet, VMD (Visual Molecular Dynamics), a software used for visualizing, analyzing and even modelling molecular systems, was employed. For that, its available nanotube builder was utilized, which has as one of its capabilities the creation of both C-C and B-N sheets (Humphrey et al., 1996).

For the creation of MoS_2, VESTA was employed (Momma and Izumi 2011), another visualization software capable of building crystal morphologies through the introduction of lattice parameters. Here, the lattice parameters were obtained from the Materials Project App [351], and all pair coefficients of the MoS_2 structure were extracted from the research conducted in [352] and manually integrated into the Packmol package (Martinez et al., 2009).

In this way, all data files were created using said Packmol package, a tool capable of creating initial configurations for MD simulations. We mainly take advantage of its automated aspect for the conversion of the previously created files into LAMMPS data files containing both the position of all atoms and their interaction coefficients. To ensure complete coverage of the XY plane in the simulations, all sheets were created with an approximate area of 100 Å × 90 Å, as is presented in Figure 2.4.

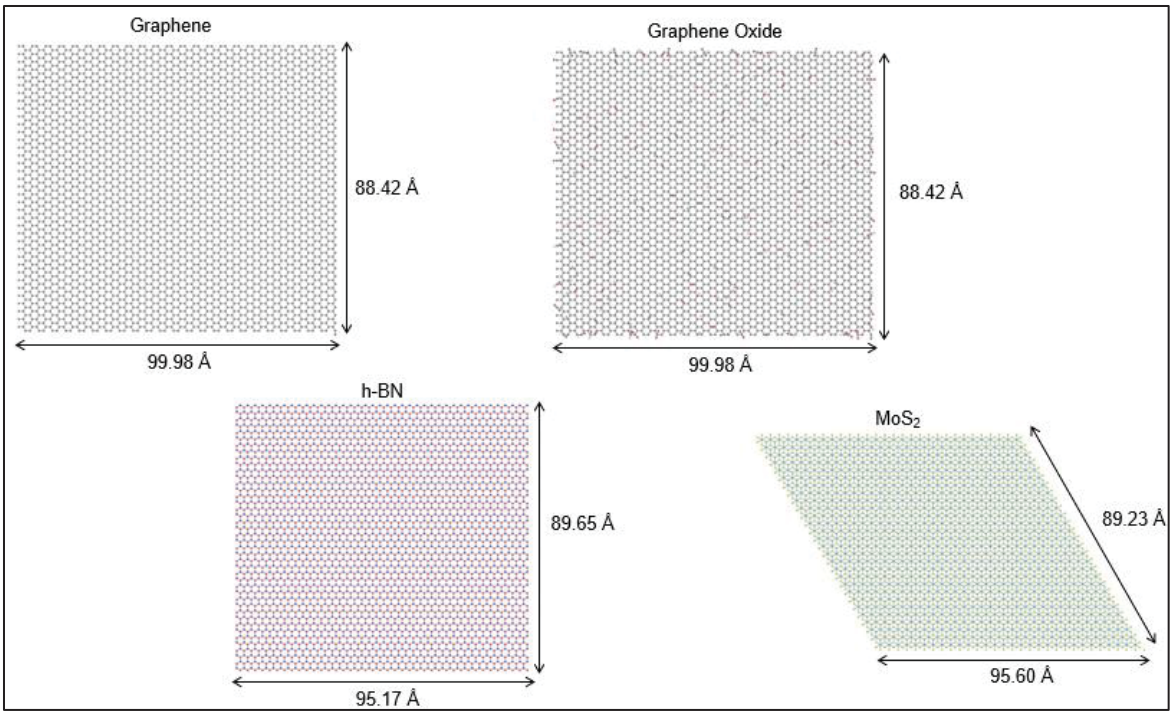

Figure 2.4 – Dimensional parameters set for of each nanosheet in the simulations

For the construction of PA 1010, the polymer builder (Choi et al. 2021) provided by CHARMM-GUI (Jo et al., 2008) was employed, and the polymer was created considering 100 repeating units. The chains' end-groups were specified according to the end-groups of PA 1010's monomers, i.e., sebacic acid and decamethylenediamine. Therefore, a carboxylic acid was applied at one end, and an amine group at the other, as can be verified in Figure 2.1. The initial relaxation of the polymer was performed using Biovia's Materials Studio (BIOVIA 2023). To prepare the initial files and format them for LAMMPS, Packmol (Martinez et al. 2009) was employed for all structures.

The Dreiding potential was chosen for all atom interactions, mainly due to its availability and general accuracy. Dreiding is a non-reactive potential, which means that bond creation and destruction is not permitted. The guiding principle behind Dreiding is to employ general force constants and geometry parameters based on simple hybridization considerations. This approach ensures that all bond distances are derived from atomic radii, and that there is a

singular force constant for each bond, angle, and inversion, along with six distinct values for torsional barriers (Mayo et al., 1990).

The simulations were conducted using LAMMPS under periodic boundary conditions in all directions. A timestep of 1 fs was used. The process began with a previously relaxed polymer system inside a simulation box of 100 Å × 90 Å × 54 Å. The system was initially heated to 211 ºC for approximately 1 ns. Subsequently, one of the sheets was introduced at a distance of 60 Å from the upper surface of the polymer and the macromolecules almost immediately move towards the sheet. To accommodate this distance, the box length was adjusted to 170 Å. Once the sheet was added, a pressure of 350 kPa was applied in the negative Z direction. This was achieved by exerting a force of 5.0×10^{-5} across the entire sheet. The simulation was then continued until the polymer made contact with a bottom wall, created 60 Å away from the center of the box in the negative Z direction. Upon contact, the system was cooled back down to room temperature. Upon reaching room temperature, the atoms in direct contact with the created bottom wall were excluded from further calculations. This process aimed to prevent the polymer from excessively moving towards the upper region of the simulation box. Subsequently, the 2D sheet was moved back to its initial position at a speed of 1.2×10^{-4} Å/fs. During this displacement, the interaction force between the sheet and the polymer, as well as the distance between their centers of mass, were calculated. Detailed illustrations of each step of the simulation can be seen in Figure 2.5.

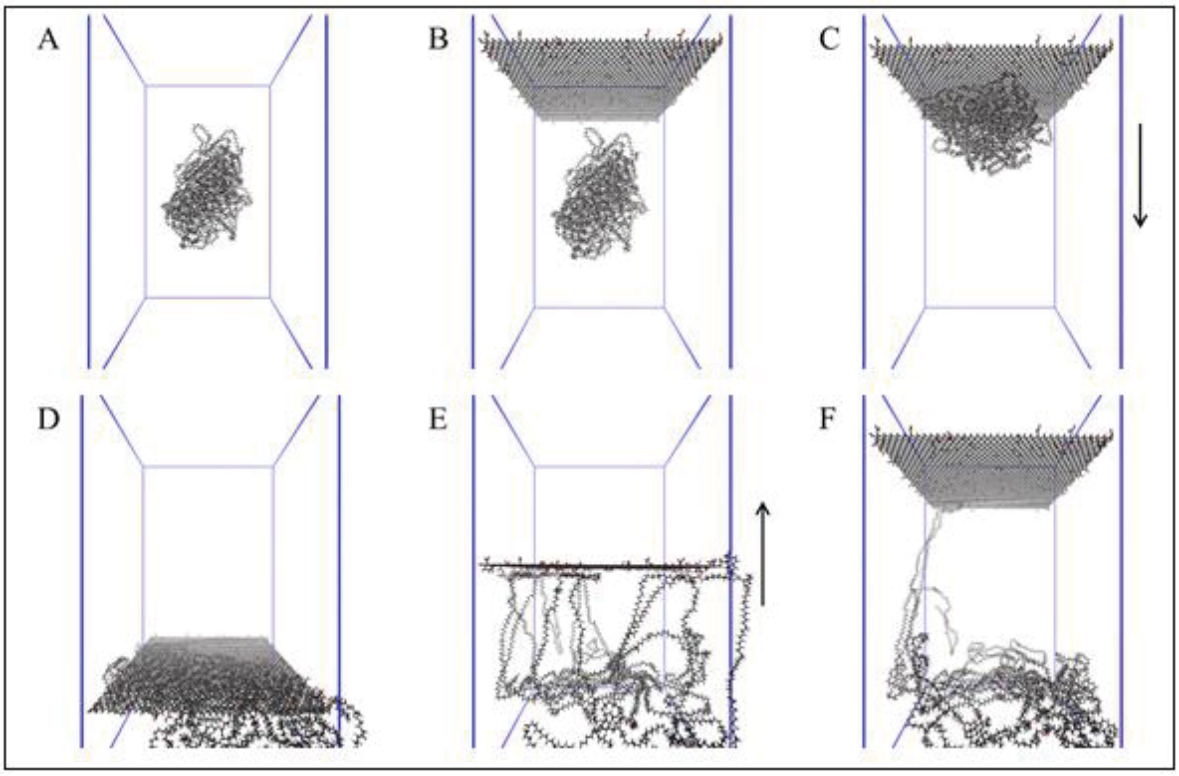

Figure 2.5 - Multiple stages of the simulation: (a) relaxed PA1010 macromolecules after initial heating; (b) the 2D sheet is introduced at a distance from the center of the simulation box; (c) the sheet is moved towards the bottom of the box; (d) the atoms of the polymer touch the bottom wall and are frozen in place after the system is cooled back down to room temperature; (e) the sheet is moved back up to its initial position; (f) final stage after the separation of the polymer chains from the 2D sheet

2.3 Results and Discussion

2.3.1 Differential Scanning Calorimetry

The DSC curves, from which the melting behavior of all the systems under study can be observed are presented in Figure 2.6. It is noticed that the melting behavior of PA 1010 is complex, with two melting events being observed. As has been mentioned in the Introduction section, it is known that even-even polyamides present a Brill transition when heated, and depending on the length of their aliphatic chains, this transition can occur either before or at the melting temperature, which is the case for PA 1010 (Lotz 2021).

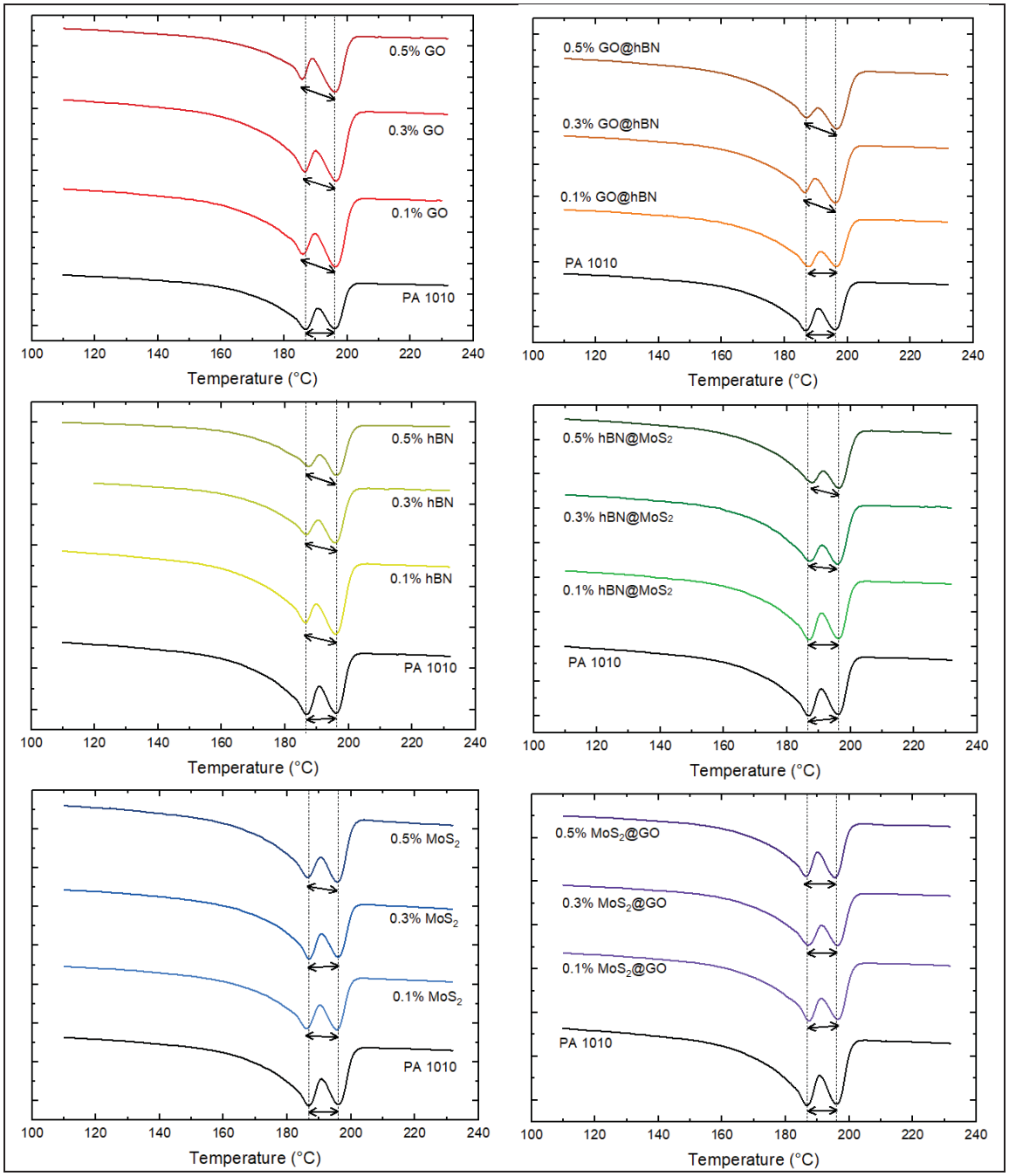

Figure 2.6 – DSC heating scans (10°C/min) of the various PA 1010 nanocomposites studied as a function of filler content (exo up)

Interestingly, there is a general trend of increasing the enthalpy of the high-temperature melting peak with respect to the overall enthalpy for all of the systems under study, but it was much stronger for the composites containing h-BN, and especially GO, as is evidenced by the $\Delta H_B/\Delta H_m$ ratio presented in Figure 2.7.

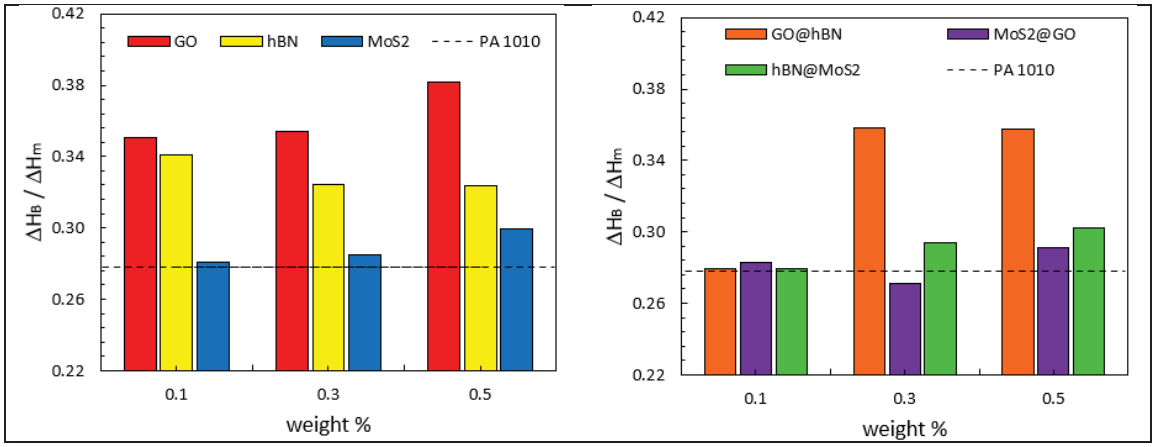

Figure 2.7 - Fraction of enthalpy related to the melting after the Brill transition

It is believed that the increase of $\Delta H_B/\Delta H_m$ could be explained by a reduction of the macromolecules' mobility due to filler-polymer interactions. In turn, this could lead to an increased number of α crystals turning into γ crystals during the Brill transition. As $\Delta H_B/\Delta H_m$ was dependent on the nanomaterial, different degrees of filler-polymer interactions can be inferred from it. GO presented the largest increase, which could be explained by the presence of oxygenated groups on its surface and its much larger aspect ratio. These oxygen containing groups can create hydrogen bonds with the amide segments in PA 1010 (Huang et al., 2022; Wang et al., 2019), hindering the molecular mobility gained during melting and, therefore, increasing the fraction of macromolecules that participate in the Brill transition. On top of that, its larger aspect ratio may be more efficient in creating physical hindrances for the mobility of polymer chains, favoring the molecules packing tendency in the competition with the thermal motion.

Despite exhibiting the lowest aspect ratio due to its small lateral dimensions, h-BN also promoted a significant increase in $\Delta H_B/\Delta H_m$, although lower than GO. This may be due to h-BN's lip-lip bonds, which promote some ionic character to the material and has already been demonstrated to increase its interactions with polymers (Chen et al., 2015). In addition, the lower aspect ratio may have assisted in h-BN's dispersion within the molten polymer during mixing, which would also increase the overall number of interfaces in the composite. Thus, it is likely that this increased affinity and dispersion led to a similar behavior of reduced

molecular mobility during melting, assisting in the crystalline polymorphic transformation during the Brill transition.

Although MoS_2 had the lowest effect on $\Delta H_B/\Delta H_m$, it was also increased when compared to neat PA 1010, probably due to its reasonable aspect ratio that may also have promoted some physical impediments to the motion of the macromolecules. However, since it was much less apparent than the other fillers, it is suggested that its interactions with PA 1010 might not be as strong.

2.3.2 Broadband Dielectric Spectroscopy

The real (ε') and imaginary (ε") parts of the dielectric permittivity as a function of frequency and temperature for neat PA 1010 are presented in Figure 2.8. ε' and ε" are also known as dielectric constant and dielectric loss, respectively. For the sake of space, the curves for the composite systems are presented in Annex I of this thesis, from Figure A I-2 to Figure A I-7.

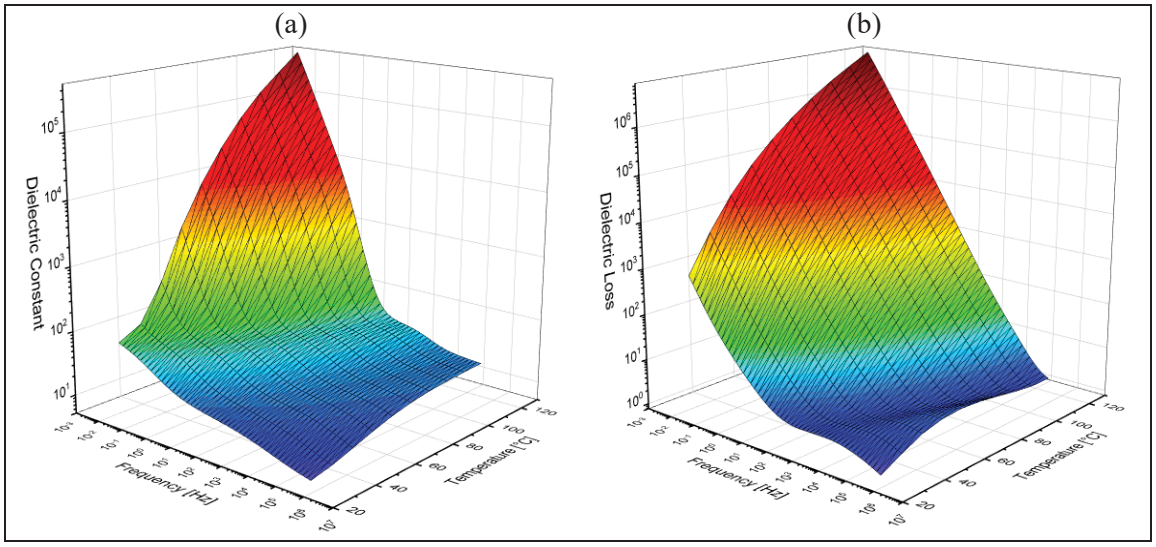

Figure 2.8 – ε' (a) and ε" (b) measured by BDS as a function of frequency and temperature for neat PA 1010

Even though the relaxation processes should be more visible in the ε" curves, this is not the case here since the contribution of charge carriers to the dielectric losses dominates at low

frequencies and high temperatures. Indeed, experimental values of ε", unlike the theoretical expression obtained by the Fourier Transforms of the dielectric response function, are affected not just by polarization mechanisms related to molecular relaxations, but also by conduction mechanisms. Therefore, the latter can "mask" the first (Steeman and Van Turnhout 1997; Steeman and Maurer 1992). As frequency decreases and temperature increases, the material enters its DC regime, where conduction mechanisms prevail due to the greater molecular mobility presented by the material, which eases the transport of charge carriers (McCall & Anderson, 1960; Pathmanathan et al., 1992; Steeman & Maurer, 1992; Steeman & Van Turnhout, 1997). Hence, only one relaxation can be observed at high frequencies and low temperatures in the ε" curves from the measured data.

Nevertheless, although ε' is less sensitive than ε" to the molecular relaxations, it is in theory independent of pure conduction mechanisms. Thus, it is possible to see in the ε' curves that the material actually presents more relaxation mechanisms at lower frequencies that are not visible in the ε" curves. Fortunately, ε" can also be estimated from ε' data according to a Kramers-Kronig transform and, since ε' is independent of conductivity, the ε" curves obtained from this mathematical relation should also be free of conduction contributions (Steeman and Van Turnhout 1997; Steeman and Maurer 1992). Equation 2.4 presents the Kramers-Kronig transform used to estimate ε" from ε' data. After applying this equation, the transformed ε" curves presented in Figure 2.9 were acquired. As for the measured data, the transformed ε" curves of the composites are presented in Figure A I-8.

$$\varepsilon''(\omega, T) \cong -\frac{\pi}{2}\frac{\partial \varepsilon'(\omega,T)}{\partial \ln(\omega)} \tag{2.4}$$

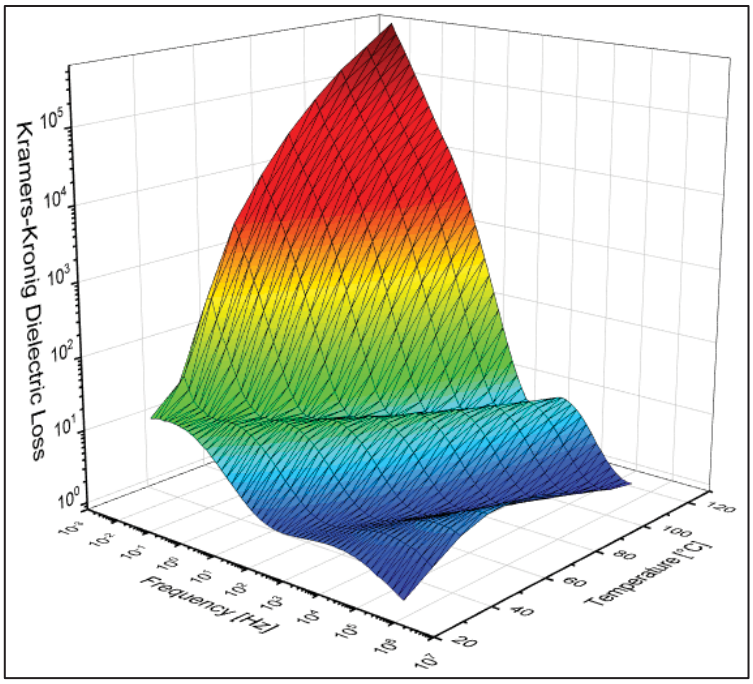

Figure 2.9 – Dielectric loss of PA 1010 calculated from the dielectric constant data using the Kramers-Kronig transform

With these transformed ε" curves, all the relaxation processes that the material goes through within the frequency and temperature range investigated become evident. There are generally three molecular motion-related polarization mechanisms that are seen in polyamides. The local motion of chain segments, primarily CH_2 segments situated between the interchain hydrogen bonds, is assumed to be the cause of a weak polarization mechanism that emerges at lower temperatures (-150 to -100°C). A second process appears close to -50 °C, which is related to the rotation motion of the amide bonds and water molecules that may be attached to them. Then, a strong relaxation, which corresponds to the glass-rubber transition of the amorphous phase, emerges at higher temperatures, i.e., 40 to 70°C depending on the kind of polyamide. These three relaxation processes are often conventionally called by γ, β, and α processes, respectively (Steeman and Maurer 1992).

In addition to these three primary molecular relaxations, polyamides may also exhibit an interfacial polarization process, also known as Maxwell-Wagner-Sillars (MWS) polarization, which is intrinsically related to the accumulation of electrical charges at the boundaries

between a more and a less conductive phase. This process usually appears at low frequencies, in the region where the polymer becomes electrically conductive (DC regime) above the α transition temperature, emerging as a sharp increase in the dielectric constant (Baird et al., 1971; McCall & Anderson, 1960). Indeed, unlike DC conductivity, which is produced by charge carriers that can flow freely to the electrodes during the test, other carriers might become trapped at the boundary between crystalline and amorphous phases, not reaching the electrodes. Since this phenomenon involves distances that are considerable in molecular terms, a space charge and subsequent polarization are slowly built-up, which manifest as a low-frequency loss mechanism (McCall and Anderson 1960).

Therefore, going from high to low frequencies, the three relaxation mechanisms that can be seen in Figure 2.9 could likely be ascribed to the β, α and MWS polarizations, respectively. Due to the increased dynamics at higher temperatures, the polarization processes shift towards higher frequencies, with the β process practically disappearing above 100 °C, the α process shifting from 3×10^{-1} Hz at 30 °C to 4×10^{3} Hz at 120 °C, and the MWS process emerging at 40 °C and increasing in intensity up to 120 °C. As has been described earlier, by fitting the measured data to the HN function, it was possible to estimate the relaxation times of the α process for every studied nanocomposite as a function of temperature. Figure 2.10 exhibits the Arrhenius plots of ln(τ) as a function of 1/T for all the systems.

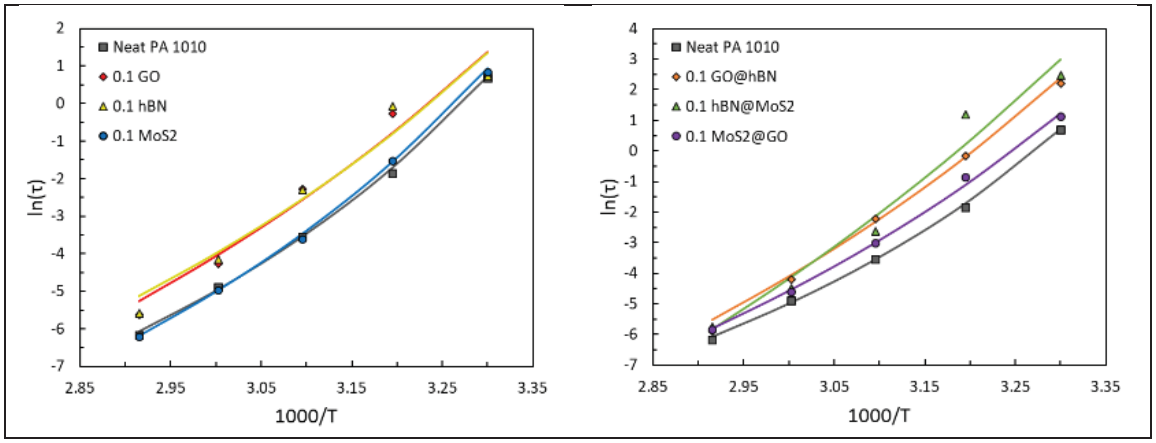

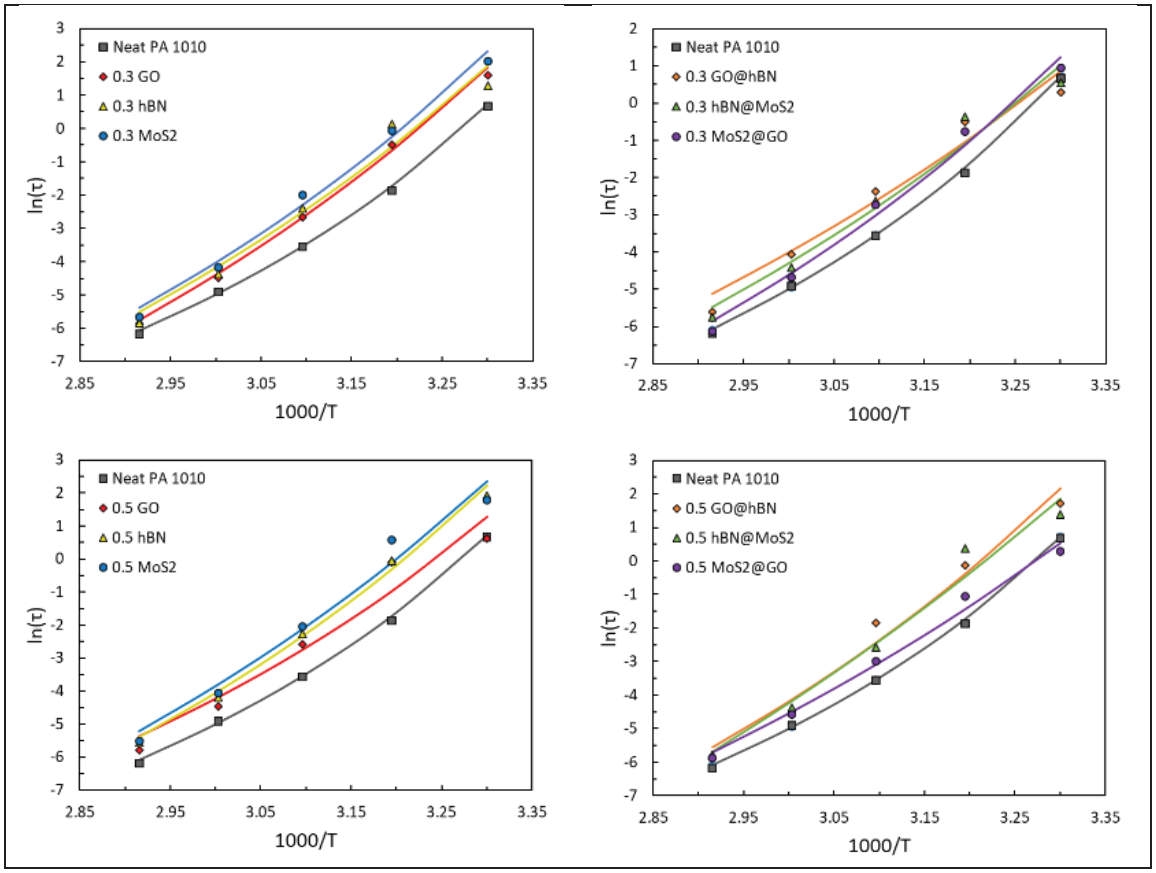

Figure 2.10 - Arrhenius plots of ln(τ) as a function of 1/T calculated from fitting the dielectric loss curves to the HN function

In the case of proper dispersion and interfacial interactions, the nanocomposites should present longer relaxation times than the neat polymer due to hampered chain dynamics (Helal et al., 2017). Although no clear trend is observed as a function of nanomaterial or content, it is perceptible that all nanocomposites presented higher relaxation times with respect to neat PA 1010 in the temperature range analyzed. This corroborates to the premise that the nanofillers are indeed restricting the mobility of the polymer chains.

In order to confirm that, the Arrhenius plots were fitted to the VFT equation, which enabled the calculation of the corresponding E_a needed for the relaxation process to take place. Figure 2.11 presents E_a as a function of nanomaterial and content.

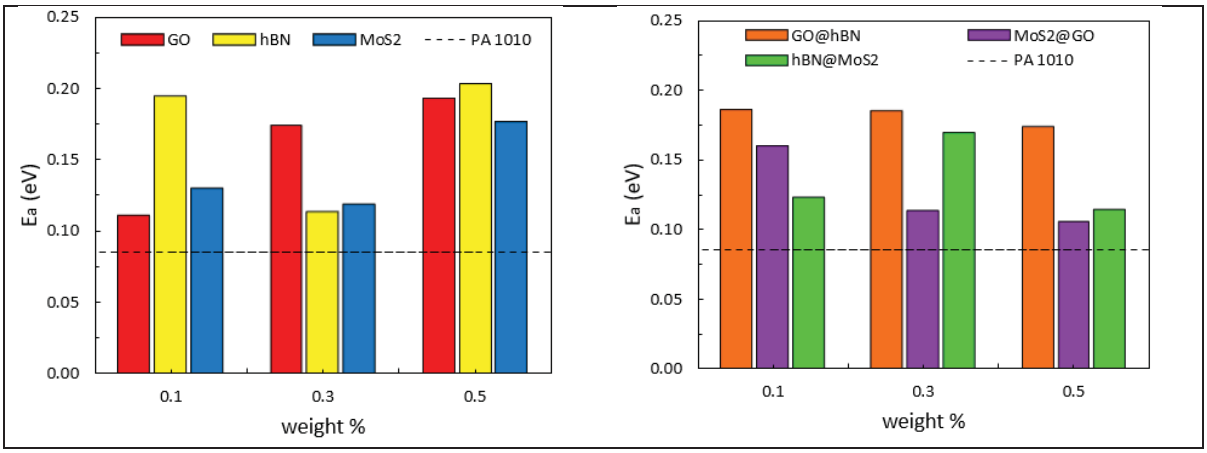

Figure 2.11 – E_a calculated from fitting the Arrhenius curves to the VFT equation as a function of nanofiller and content

In a similar manner to the relaxation times, no clear conclusions can be drawn as a function of nanomaterial. Also, although E_a was increased for all contents, the range studied in this work does not seem to be wide enough to present a notable effect on the degree in which E_a is increased. Nevertheless, some trends could be inferred based on the calculated values. Even though all nanomaterials promoted similar levels of hindrance to the macromolecular dynamics of PA 1010 during the α transition, E_a of GO and h-BN filled systems were slightly higher than MoS_2's. This corroborates with the better degree of dispersion and higher adhesion presented by GO and h-BN, as suggested by the DSC results. This trend is maintained for the hybrid fillers, in which h-BN@MoS_2 and MoS_2@GO composites exhibited E_a values closer to MoS_2 composites, while GO@h-BN composites exhibited higher E_a through the whole content interval.

In addition to the identification of relaxation times and E_a, one can also get insights on the filler-polymer interfacial contacts by analyzing changes in the shape of ε" during MWS polarization. With that in mind, Figure-A I-9 presents the superposition of the Kramers-Kronig ε" at 120 °C for all the systems investigated. This temperature was selected because of the highest molecular dynamics presented, which eases the identification of any effects promoted by the nanofillers.

The shape of the dielectric loss curves in the MWS polarization region was clearly affected by the addition of the nanomaterials, which is further evidence of morphological changes and interfacial contacts. These changes emerge as a more pronounced shoulder during this polarization process and can be associated to additional interfacial effects that were not present in the neat polymer. However, all nanomaterials affected this process in the same order of magnitude when added individually.

While the single-filler composites exhibited a more intense MWS polarization than neat PA 1010 for basically all the contents, the hybrid systems didn't affect this process as much. Nonetheless, it can be observed that the higher affinity of GO with PA led to some meaningful changes in the composites filled by 0.3 wt% MoS_2@GO and 0.5 wt% GO@h-BN. Despite of that, the trends observed in the nanocomposites' interfacial polarization lead one to believe that the nanosheets may have formed more interfaces with PA 1010 when applied separately than in hybrids.

2.3.3 Dynamic Mechanical Analysis

Tan(δ) is a very useful parameter to investigate the molecular dynamics effects of nanofillers in a polymer nanocomposite. That is because it is calculated by the ratio between the loss and storage modulus, which means it is intrinsically related to how much mobility is gained by the macromolecules during thermal transitions such as in the glass transition (T_g). If there is proper dispersion and a strong contact between the phases, the mobility of polymer chains around the nanofiller is reduced. Thus, it would be expected that the intensity of the peak in tan(δ) during T_g decreases in the nanocomposites. Hence, Figure 2.12 presents tan(δ) as a function of temperature for every nanocomposite under study.

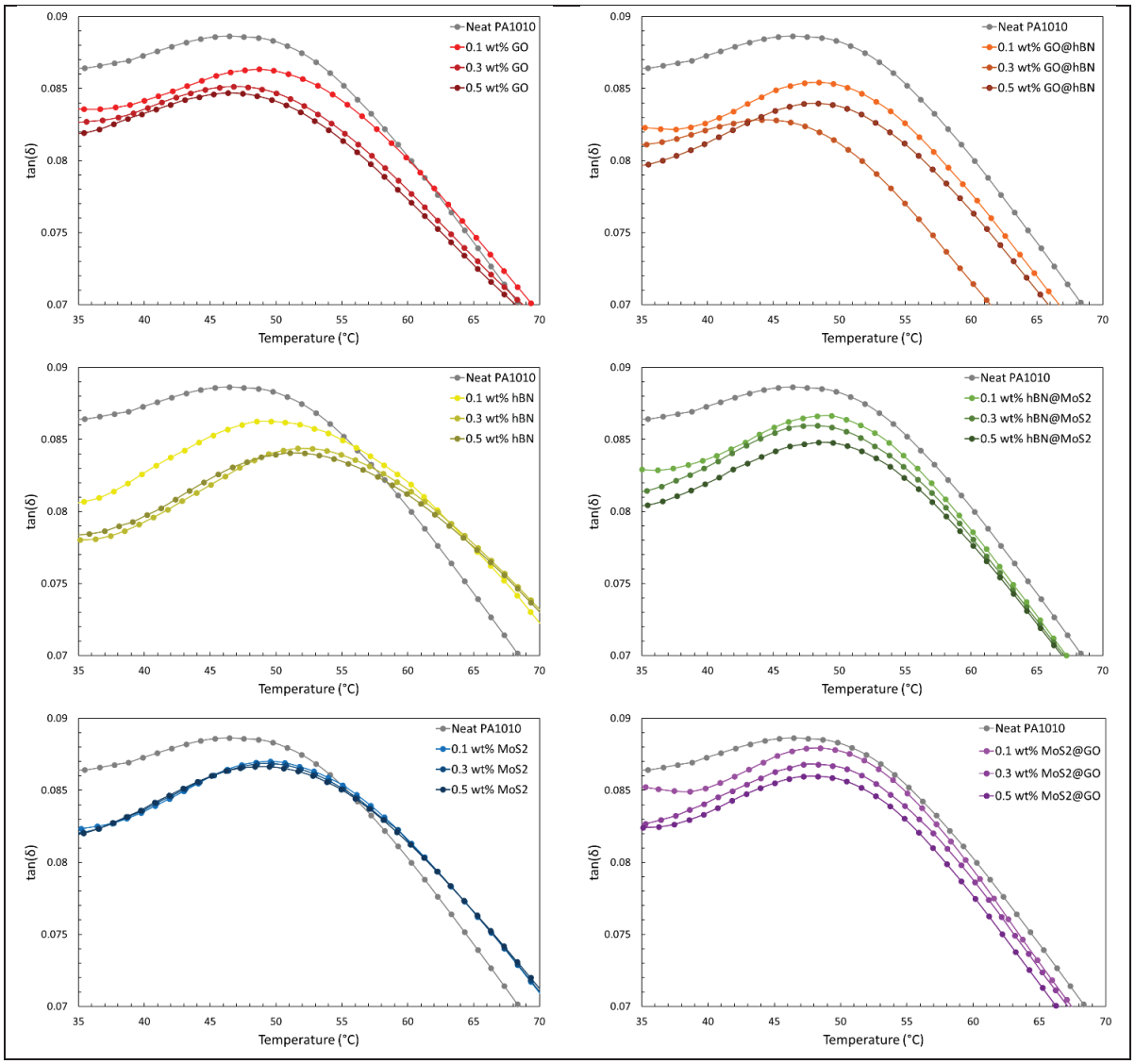

Figure 2.12 – tan(δ) as a function of temperature for all nanocomposites studied

It is noticeable that all nanocomposites presented a lower intensity of tan(δ) than pure PA 1010 during the glass transition. This is in agreement with the observed in the BDS analysis, and it suggests that all nanomaterials promote molecular hindrances to the mobility of polymer chains during this relaxation process. It is also noticed that, with the exception of MoS_2 systems, all composites exhibited a further decrease in the intensity of tan(δ) as the content increased. This is probably related to the greater restriction of movement promoted by the greater number of nanosheets in the more concentrated nanocomposites.

Moreover, despite the subtle differences, the systems with GO and h-BN presented greater reductions in the intensity of tan(δ) compared to the ones with MoS_2. This may be associated with the former's stronger affinity for PA 1010, GO's larger aspect ratio, and the likely better dispersion of hBN within the matrix, as suggested earlier. This trend is supported by the hybrid systems, in which the intensities of tan(δ) for GO@h-BN composites were lower than for the other two, again corroborating with the higher E_a calculated from the BDS results for this specific hybrid system. Nevertheless, in order to confirm these trends, we have calculated the "adhesion factor" (A) at T_g for all the systems, as can be verified in Figure 2.13. It's important to highlight here that at high levels of interfacial adhesion, the macromolecular mobility near the filler surface tends to be less than that in the bulk matrix, which lowers tan(δ) and hence, A. Thus, the more negative A is, the higher level of adhesion the composite exhibits.

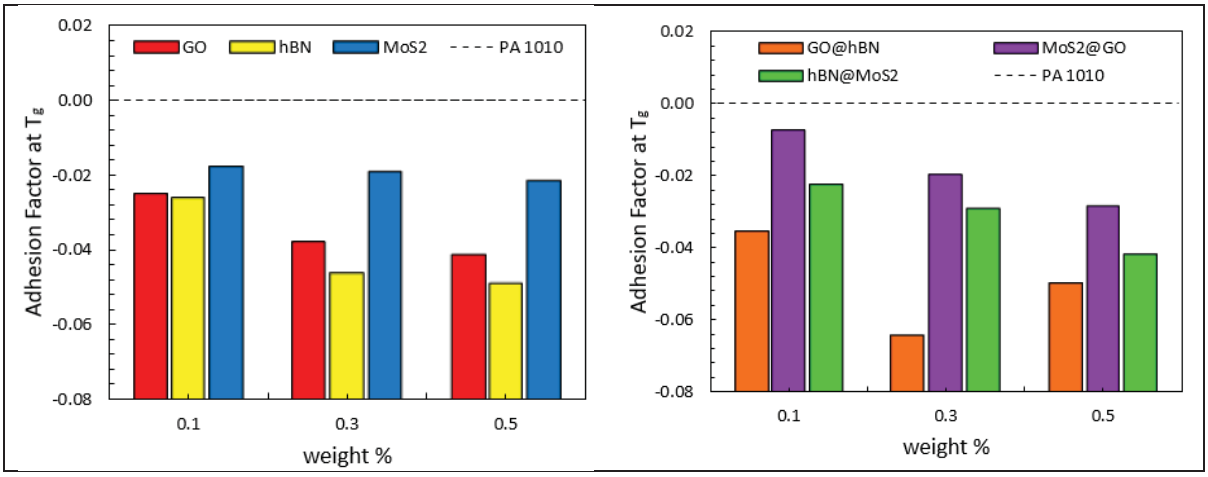

Figure 2.13 – A at T_g for all the nanocomposites under study as a function of content

Clearly, GO and h-BN composites exhibit lower values of A at T_g compared to the MoS_2 composites. Moreover, the former also demonstrate a higher sensitivity to content, confirming that they form a greater number of interfaces with PA 1010 due to superior chemical affinity and finer dispersion. As for the hybrid fillers, one can notice that the GO@h-BN system presented the lowest A for all three contents, corroborating the hypothesis of greater interactions for these nanomaterials. Nevertheless, the other two combinations also presented A values below zero, which indicates that there is also some level of interfacial adhesion with the polymer chains.

Since T_g is the temperature at which the macromolecules gain their mobility, the investigation of A at this specific temperature might give the strongest insights of interfacial interactions between polymer and fillers. However, one can extrapolate its calculation for the whole temperature range, as is presented in Figure A I-10 Curiously, although A starts at lower values for the single-filler composites, it is evident that it significantly increases above T_g, surpassing the "zero threshold" at higher temperatures. Although this occurs more strongly for h-BN and MoS_2, this behavior is sustained even in the GO composites. On the opposite direction from the suggested by the MWS relaxation analysis, the increase of A as a function of temperature may be a sign that the single-fillers' adhesion to PA 1010 decreases with temperature (Kubát, Rigdahl, and Welander 1990; Correa, Razzino, and Hage 2007). Although this trend seems not to agree very well with the observed in the MWS polarization, it is important to note that the interfacial mechanism is actually different. In the case of MWS polarization, more carriers can be trapped at the interfaces at higher temperature, while in the case of T_g, it is expected that the macromolecules can be less constrained by the presence of nanoparticles at high temperatures. Thus, for more consistent comparison of trends, one should consider the α relaxation from BDS, as is presented in the following section.

Nevertheless, we see that A tends to stabilize at lower values for the hybrid-fillers even at elevated temperatures, which could mean that the nanomaterials may better withhold the adhesion to the polymer matrix above T_g when added together.

2.3.4 Combined Effects on the Molecular Dynamics

As was mentioned at the beginning of this work, each of the employed techniques is useful in providing some characteristics about the filler-polymer interactions, however, it is when their individual results are correlated that a clear picture of how each nanomaterial affects the polymer dynamics is obtained. Within that scope, Figure 2.14 presents the averages of $\Delta H_B/\Delta H_m$ and A at T_g for each nanocomposite, as a function of the E_a calculated from the BDS data.

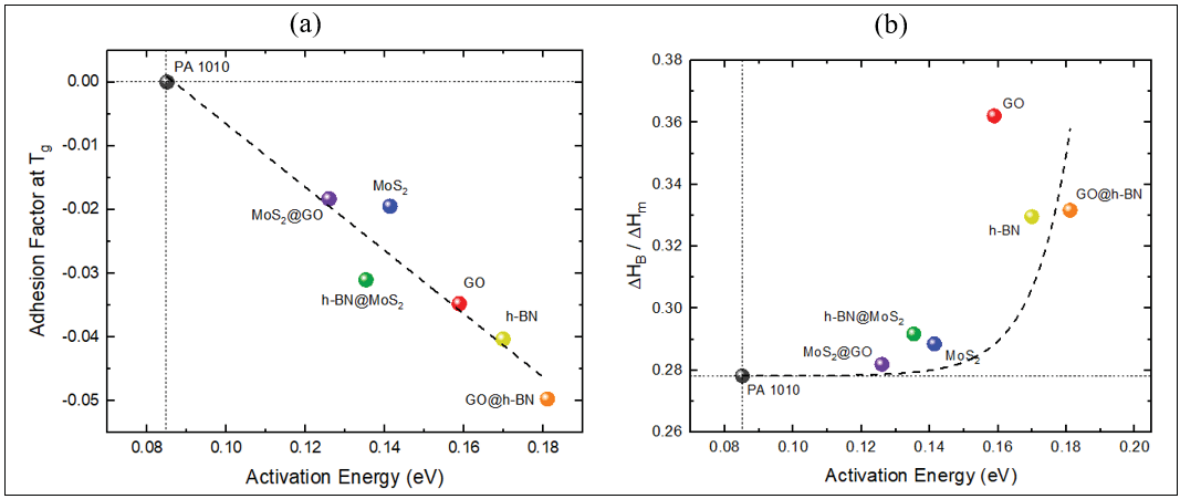

Figure 2.14 – Averages of A at T_g (a), and $\Delta H_B/\Delta H_m$ (b) as a function of the calculated E_a for all the nanocomposite systems

It is astounding the good fit that each of these parameters present when plotted against each other, especially the linear dependency between E_a of the α transition (glass transition) and A at T_g. It is noticed that the lower the adhesion factor presented by the nanocomposites, e.g., in the systems with GO and h-BN, the higher the E_a, which confirms that these nanomaterials tend to disperse better and present enhanced interfacial contact with PA 1010, thus restricting its molecular mobility. Interestingly, there seems to be a synergistic effect in the GO@h-BN hybrids, in which the greater aspect ratio of GO, and the favorable dispersibility of h-BN work together to increase even further the adhesion with the macromolecules, and therefore, the glass transition E_a. On the contrary, the hybrids with MoS_2 seem to decrease the more beneficial effect of the second filler, be it GO or h-BN. This corroborates with the probable lower interactions that MoS_2 have with PA macromolecules.

In a similar manner to A at T_g , as E_a increases, $\Delta H_B/\Delta H_m$ increases in a semi-exponential manner. This is also a positive sign of the raised hypothesis, in which the greater adhesion provided by the larger aspect ratio of GO, the easier dispersion of h-BN, and their favorable chemical affinity to PA 1010 lead to lower thermal motion during the melting process. Therefore, the number of macromolecules that participate in the Brill transition is increased.

One can go even further and correlate all three coefficients in the same chart, as is presented in the colormaps of Figure 2.15. When the colormaps are analyzed, the previous relationships become even more apparent. As A becomes lower (more adhesion), and $\Delta H_B/\Delta H_m$ increases (lower thermal motion – increased number of chains taking part in the Brill transition), E_a increases from the violet region (neat PA 1010) to the dark red region (composites containing GO and/or h-BN), evidencing the role that such bidimensional nanomaterials have on the reduced molecular dynamics of PA 1010. Since polymer chains that are in this interphase, i.e., in this region where the molecular dynamics are affected by interfacial interactions with the filler's surface, are the main contributors to the composite's macroscopic properties, it is expected that these systems with GO and/or h-BN would present the most promise for producing high-performance PA 1010 nanocomposites based on 2D nanomaterials.

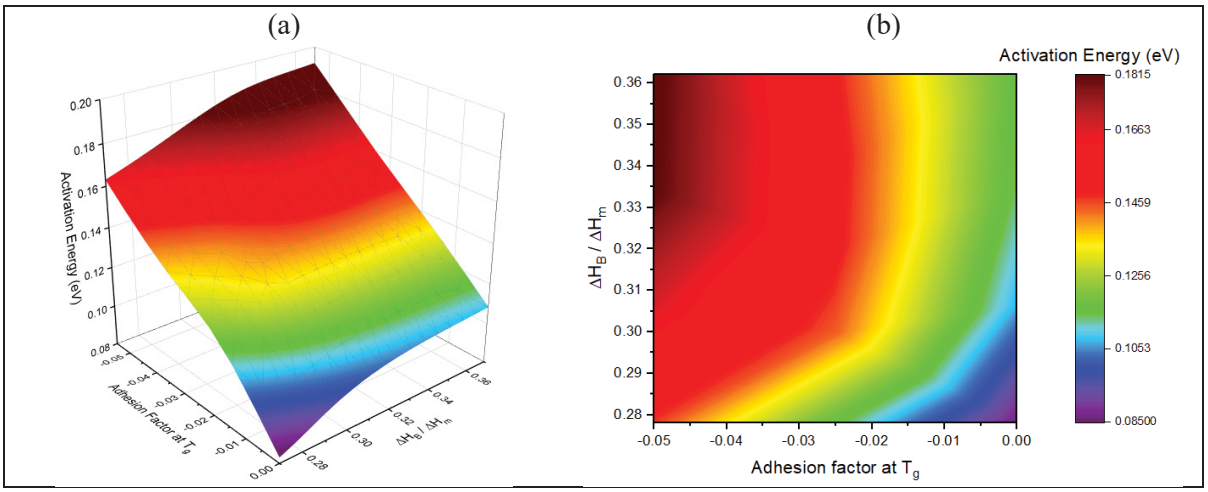

Figure 2.15 – 3D (a) and 2D (b) colormaps correlating the averages of A at T_g, $\Delta H_B/\Delta H_m$, and the α transition E_a

2.3.5 Adhesion Force from MD Simulations

In order to confirm the different levels of interaction that each of the studied nanomaterials present to PA 1010, we have also performed MD simulations to investigate the force necessary to separate a single sheet of each nanomaterial from adhered PA 1010 macromolecules. This force is directly related to how strongly the polymer chains adhere to the surface of the nanosheets and can be correlated with the experimental results from this work.

Even though h-BN and MoS_2 should have a known chemical configuration, GO can present varied degrees of oxidation through its oxygenated groups, such as hydroxyl, carboxyl, and epoxide groups. Therefore, we have first simulated only graphitic systems to identify the influence of the level of oxidation on the adhesion force between PA 1010 and GO. Figure 2.16 a presents the force curves as a function of the sheet displacement in the simulation box when retracting it from the macromolecules.

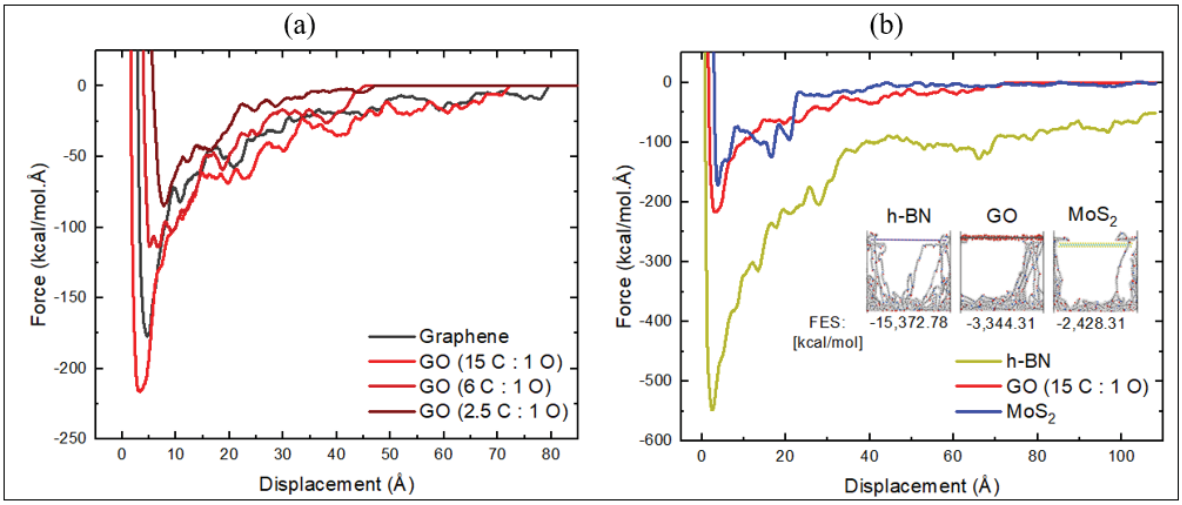

Figure 2.16 – Adhesion force as a function of the separation between the sheets and the polymer for the graphitic structures (a), and the nanomaterials used in the experimental part of this work (b)

Curiously, although a small degree of oxidation seems to improve the adhesion force of a graphene structure to PA 1010, it is evident that lower C : O ratios decrease the peak force of separation, as well as the distance where there is no more interaction with the polymer chains, which was ca. 72 Å for a C : O ratio of 15 : 1, and ca. 48 Å for C : O ratios of 6 : 1 and 2.5 : 1. A possible reason for the lower adhesion of the more oxidized GOs with PA 1010 could be that the distance between the functional groups on the sheet become shorter. This might lead to interactions between the different groups on the sheet itself, reducing the available interaction sites for the polymer.

Although the GO used in this work has an initial C : O ratio closer to the simulated 2.5 : 1 (Andrade et al. 2021), it is very likely that it undergoes some reduction during melt processing due to the elevated temperatures needed to melt the polymer. Therefore, it is fair to assume that the final C : O ratio is increased when the sheets are embedded in the polyamide. Additionally, since our experimental results suggest a strong adhesion for the GO system, the lower C : O ratio was considered for the comparison with the other fillers, i.e., h-BN and MoS_2.

Figure 2.16b exhibits the adhesion force as a function of sheet displacement for the three nanomaterials employed in this work. h-BN clearly presented the deepest force peak and largest absolute free energy of separation (FES – area under the curve), indications of greater interfacial strength with PA 1010. Although GO has a less intense peak force than h-BN, it clearly presents a deeper peak and more gradual decrease in the adhesion force with sheet displacement than MoS_2, which also indicates fairly better attraction of the macromolecules to the sheet's surface. In a different manner, MoS_2 exhibits the lowest peak force and FES, corroborating with its lower interactions with PA 1010. Notably, there is a significant drop in the adhesion force for the MoS_2 system at ca. 23 Å of displacement, and at ca. 43 Å it reaches a plateau of zero force.

An important aspect that needs to be addressed is the edge effect on the h-BN and MoS_2 simulations, in which the sheets were not able to cover the whole box area. This effect allowed some chains to slip to the top of the sheet when the components were moved to the bottom of the simulation box. Consequently, when the sheet was moved back up, these chains were dragged as well, as is presented in the inset of Figure 2.16b. Even though this drag is not directly linked to the adhesion, it could contribute to the force curve to some extent. However, this effect was more intense in the MoS_2 simulation, and it still presented the lowest adhesion. Thus, while it may have contributed to the greater force obtained by the h-BN simulation, it is not believed to have played a major role.

Nevertheless, it's interesting how the simulation results agree with the experimental coefficients, i.e., E_a and A, calculated from BDS and DMA data, respectively. The relationship between the calculated FES with both experimental coefficients is presented in Figure 2.17.

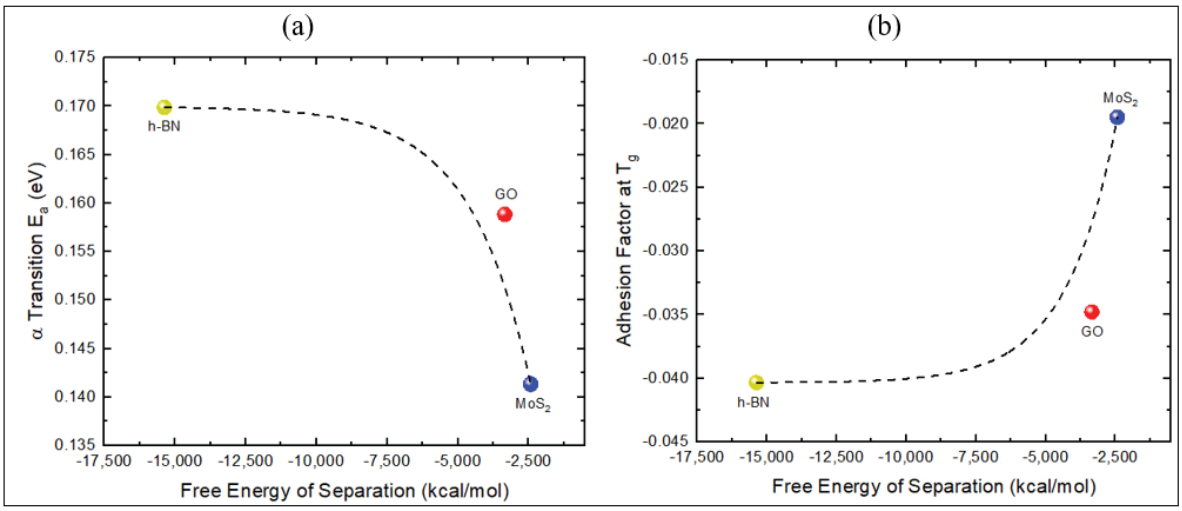

Figure 2.17 – Experimental coefficients as a function of FES for the GO, h-BN and MoS_2 systems: (a) Activation energy of the α transition from BDS analysis; (b) Adhesion factor from DMA

It's evident the exponential decay of the α transition E_a, as well as the exponential growth of A as the absolute value of FES decreases. This confirms the raised hypothesis that the stronger the adhesion between polymer and nanosheet, represented by more negative values of FES, the higher the activation energy required for the macromolecules to gain mobility in the glass transition (higher E_a), and the more negative the adhesion factor estimated by DMA (better adhesion). However, an important detail that needs to be highlighted in this section is that all of the nanosheets were simulated considering the same aspect ratio, i.e., monolayers with no changes in lateral dimensions. This may also help to explain the underestimated GO response in the simulations. It has been seen that, in reality, the GO used in this work has a much larger aspect ratio than the other nanomaterials. Therefore, although h-BN may exhibit stronger intrinsic adhesion to polyamide macromolecules, as observed in the force curves, the higher aspect ratio of GO in the real composites likely contributed in improving its experimental coefficients.

2.4 Conclusions

We have, for the first time, experimentally investigated the effect of different bidimensional nanomaterials, i.e., GO, h-BN, and MoS_2 on the molecular dynamics of bio-based PA 1010. This was achieved by correlating results from differential scanning calorimetry, broadband dielectric spectroscopy, and dynamic mechanical analysis. For that, nanocomposites based on single and hybrid-fillers were produced through melt mixing the polyamide matrix with the nanomaterials in a twin-screw extruder, and further molding samples by injection and compression molding.

It was observed that, even though all of the nanomaterials affect the Brill transition of PA 1010, GO and h-BN seem to further increase the number of macromolecules that participate in it, enlarging the enthalpy of the second melting event due to lower thermal motion being gained by the macromolecules before the Brill transition.

This trend is corroborated by the calculated E_a of the polymer glass transition through fitting of the dielectric loss curves. It was estimated that the nanocomposites presented longer relaxation times, and therefore, higher E_a than the neat polymer. Although all three nanofillers seem to slow down the macromolecules' relaxation process, the composites with GO and h-BN exhibited higher E_a, which suggests their stronger interactions with PA 1010.

Curiously, it was noticed that even though the high aspect ratio of GO may have assisted in providing steric hindrance to the polymer chains, the small aspect ratio of h-BN may have cooperated for its dispersion during melt mixing, which also enabled an increased number of interfacial contacts with the macromolecules. The level of such interactions was confirmed by the A coefficient, calculated from the DMA damping factor, and corroborated by the adhesion force as a function of sheet displacement from MD simulations. The composites with h-BN presented not just lower values of A, but also a larger absolute FES, which agrees well with the estimated E_a from BDS fitting.

The relationship between these coefficients was highlighted by plotting them as a function of one another. While A exhibited a clear linear correlation with E_a, $\Delta H_B/\Delta H_m$ presented an exponential trend. It was also observed an exponential decay of E_a, as well as an exponential growth of A, as the absolute FES decreases.

Ultimately, since the level of interfacial interactions, which lead to molecular hindrance, is what mainly dictates the performance of polymer nanocomposites, it is suggested that the systems reinforced by GO and h-BN might present greater promise for novel bionanocomposites based on PA 1010.

ACKOWLEDGEMENTS

The authors would like to acknowledge FAPESP – Fundação de Amparo à Pesquisa do Estado de São Paulo (Process 2020/11496-0 and 2021/07858-7), CNPq – Conselho Nacional de Desenvolvimento Científico e Tecnológico (Process 130466/2022-0), NSERC – Natural Sciences and Engineering Research Council of Canada (RGPIN-2018-03888), and Coordination of Superior Level Staff Improvement (CAPES), Brazil - Finance Code 001 [PrInt 88887.310339/2018–00] for funding this work.

CHAPTER 3

EFFECT OF ENVIRONMENTAL TEMPERATURE AND SEMI-CRYSTALLINE ORDER ON THE TOUGHENING OF POLYAMIDE 1010 BY 2D NANOMATERIALS

Gabriel M. Pinto[1,2,3], Emna Helal[1], Hélio Ribeiro[2], Eric David[1], Nicole R. Demarquette[1], Guilhermino J. M. Fechine[2,3]

1 Department of Mechanical Engineering, École de Technologie Supérieure, Montréal, QC, Canada
2 Engineering School, Mackenzie Presbyterian University, São Paulo, SP, Brazil
3 Mackenzie Institute of Research in Graphene and Nanotechnologies – MackGraphe, Mackenzie Presbyterian Institute, São Paulo, SP, Brazil

Paper published in *Polymer Composites*, 2024
DOI: http://doi.org/10.1002/pc.29019

ABSTRACT

By incorporating nanomaterials into polymer matrices, nanocomposites can be produced with enhanced properties, combining the ease of processing thermoplastics with the superior physical characteristics of nanoparticles. In this study, fully bio-based polyamide 1010 was used as the polymer matrix, with graphene oxide (GO), hexagonal-boron nitride (h-BN), and molybdenum disulfide (MoS_2), both individually and in hybrids, serving as fillers. The tensile behavior of these nanocomposites was evaluated at room temperature and -40 °C, along with their morphology and microstructure. Results showed that the nanomaterials slightly shifted the polymer's crystallization temperature upward, indicating a small nucleating effect, but also hindered the development of crystalline domains, reducing the crystallization kinetics. Despite no change in the final crystalline form, nanocomposites with h-BN and MoS_2 showed lower microstructural order as evidenced by XRD. Regarding tensile behavior, GO provided the greatest toughening at room temperature due to its larger lateral dimensions and good chemical affinity with the matrix. However, at low temperatures, h-BN-based nanocomposites maintained the toughening effect better than GO-based ones. This can be attributed to the lower order of the semi-crystalline structure promoted by h-BN, allowing greater energy dissipation. Hybrid fillers did not exhibit synergistic effects, with one nanomaterial hampering the effect of the other. SEM analysis indicated that the fracture mechanisms of the nanocomposites remained unchanged from the neat polymer, which makes them interesting options for applications that require desirable mechanical properties at a wide temperature range.

Keywords: Polyamide 1010; Nanocomposites; Mechanical properties; Microstructural analysis

3.1 Introduction

Due to the growing concern in environmental and sustainability issues, one of the main objectives that drives current polymer research might be regarded as the manufacture of traditional polymers from renewable sources, with their decreased carbon footprint representing a great benefit (Kyulavska, Toncheva-Moncheva, and Rydz 2017; Kiziltas et al. 2021).

Biopolyamides based on castor oil, such as polyamide 1010 (PA 1010), are considered to be among the most intriguing biopolymers currently available (Kuciel, Kuźniar, and Liber-Kneć 2012). Commercial grades of this engineering polymer offer great strength, elasticity, toughness, and abrasion resistance (Li et al., 2008; Zhang et al., 2005; Zhishen et al., 1993). This has led to its use in a variety of industries, including automotive, electronics, athletic supplies, fabrics, and coatings (Rusu et al. 2011).

Although polyamides are in the family of engineering polymers, they are rarely applied by themselves, with the automotive industry using them mainly as matrices in composites reinforced with glass or carbon fibers (Chauhan et al., 2022; Kuciel et al., 2016). This has led to a great interest in the literature to look for filler alternatives, as the conventional glass and carbon fibers are not environmentally friendly. For instance, Quiles-Carrillo et al. (Quiles-Carrillo et al., 2021) have recently produced a fully bio-based composite of PA 1010 filled by 20 wt% coconut fibers. Even though this could provide a solution for a by-product of the coconut industry in the form of fiber, significant losses in the mechanical behavior of the neat polymer were observed even after adding compatibilizers to the composite. The composite compatibilized by epoxidized linseed oil, which presented the best recovery of properties, still exhibited reductions of ca. 43%, 97%, and 82% in tensile strength, elongation at break, and impact strength, respectively, when compared to the neat PA 1010. The same research group has also produced composites based on fully bio-based PA1010 reinforced with 15 wt% waste derived slate fibers (Quiles-Carrillo et al., 2019). In a similar manner to the previous case, the

fibers had to be compatibilized before being added to PA 1010 and, even though the tensile modulus reached a 3-fold increase, the ductility of the material was reduced by ca. 98%.

Conversely, creating nanocomposites through the addition of nanomaterials makes it possible to further adjust the properties of polyamides for specific purposes at lower filler contents, which brings a lightweighting advantage (Baniasadi et al., 2021; Chen et al., 2018; Chiu & Huang, 2012; Guerreiro et al., 2021; Huang et al., 2022; Japić et al., 2022; Kang et al., 2020; Korkees et al., 2021; Lee et al., 2022; Lu et al., 2020; Mousavi et al., 2020; Petrény & Mészáros, 2020; Sarac et al., 2019; Xiang et al., 2018, 2019; Zang et al., 2015). The key benefit is to combine the ease of processing thermoplastic materials with the exceptional physical characteristics of nanoparticles to produce composites with superior macroscopic attributes (Pinto et al., 2023). A few examples of papers exploring the mechanical performance of nanocomposites based on bio-based polyamides are presented in Table 3.1.

Table 3.1 – Literature review of the percentual changes in the main mechanical properties of bio-based PA nanocomposites reinforced by 2D nanomaterials. The values are with respect to the polymer matrix presented in the first column, be it pure or in a blend

Polymer	wt%	Tensile strength	Elongation at break	Flexural strength	Impact strength	Ref.
PA 1010/PTA (90:10)	0.03 (GNP)	+67%	–50%	+18%	+73%	(Kausar, 2017b)
PA 1010/PU (80:20)	5.00 (GNP)	+140%	–47%	+15%	+77%	(Kausar, 2017a)
PA 1010/FPA (80:20)	5.00 (GNP)	+46%	–70%	+29%	+29%	(Kausar, 2018)
PA 1010/PEA (80:20)	5.00 (PANI-Graphene)	+73%	–48%	+27%	+59%	(Kausar, 2019)
PA 1010	6.00 (OMMT) + 7.00 ($CaCO_3$)	+50%	*	+41%	–27%	(Yin and Hu 2015)
PA 1010	5.00 (OMMT) + 6.00 ($CaCO_3$)	+40%	–93%	+37%	–35%	(Yin et al., 2017)

PA 610	8.00 (GNP)	–12%	*	+10%	–44%	(Kiziltas et al. 2021)
PA 610	30.00 (HNT)	–10%	–96%	*	–77%	(Marset et al. 2020)

PTA: polythioamide; PU: polyurethane; FPA: fluorinated polyamide; GNP: graphene nanoplatelets; PANI-Graphene: polyaniline modified graphene; OMMT: organic montmorillonite; $CaCO_3$: calcium carbonate. * indicates the property was not reported.

It can be seen that the great majority of research applies relatively high contents of nanofiller. Additionally, even though the tensile and flexural strengths, as well as the impact strength for some of the systems tend to increase, the final composites exhibit much lower ultimate strains, which is the determining factor to release energy under loading. Therefore, it is also expected that the intrinsic flexibility of the thermoplastic matrix to be highly compromised in such conditions, which would make the application of these nanocomposites impracticable for some developing fields, e.g., in flexible electronics and wearable devices.

As one of the main contributors to a poor mechanical performance is usually an inadequate dispersion of the nanofillers within the matrix, an interesting approach to deal with that is to combine different fillers in the form of hybrids. This approach could also enable the use of much lower filler contents. The main idea is that hybrid 2D materials can prevent the restacking of exfoliated layers, as it has been shown by molecular dynamics simulations that the force required to induce layer separation is significantly less compared to when a single 2D material is used (Ribeiro, Trigueiro, Owuor, et al. 2018). Ribeiro et al. (Ribeiro et al., 2020; Ribeiro, Trigueiro, Owuor, et al., 2018) studied the effect of adding graphene oxide/hexagonal-boron nitride (GO/h-BN) on the mechanical properties of epoxy and polyurethane (PU) resins. Increases of 140% in tensile strength, 177% in ultimate strain, and 32% in elastic modulus were observed for the epoxy composite with just 0.5 wt% of hybrid GO/h-BN (Ribeiro, Trigueiro, Owuor, et al. 2018). As for the PU system, the tensile strength and Young's modulus showed increases of up to 85% and 140%, respectively, for the same filler content (Ribeiro et al., 2020). Hybrids of hexagonal-boron nitride/molybdenum disulfide (h-BN/MoS_2) have also been investigated in these matrices. While the PU composite with 0.5 wt% increased the Young's modulus by 80% due to a significant increase in the elastomer crosslink density (Ribeiro, Trigueiro, Lopes, et al., 2018), the epoxy composite with 1.0 wt% h-BN/MoS_2

presented increases of 95% in tensile strength, 60% in ultimate strain, and 58% in Young's modulus (Ribeiro et al., 2019). One can notice that the previous research that studied 2D hybrids in polymer nanocomposites was done for thermosets, where the fillers chemically bond to the matrix in the curing stage. Although there might be a few investigations of 2D hybrid nanomaterials in thermoplastics, as the one from Cui et al. (Cui et al., 2015), the contents employed are still extremely high (> 20 wt%), which inevitably compromises the processability, flexibility, and ductility of thermoplastic materials. Therefore, the literature still lacks thorough studies of nanohybrids as fillers for thermoplastic matrices, especially at low contents.

Another aspect that is commonly overlooked when investigating polymer nanocomposites is how environmental factors, e.g., the environmental temperature, affect the properties of the material. However, composites with sustained mechanical performance at low temperatures are required for usage in emerging applications, e.g., in hydrogen storage tanks of electric vehicle fuel cells, sterilization containers, and structural parts in aerospace applications (Govindaraj et al., 2019).

Therefore, this work aims to expand on the use of different 2D nanomaterials, i.e., GO, h-BN, and MoS_2, individually and in hybrids, as fillers for polymer nanocomposites. Due to the growing concern in environmental and sustainability issues, a fully bio-based PA 1010 was selected as polymer matrix, and due to the growing number of applications that require maintenance of adequate mechanical properties at a wider temperature range, we have investigated the tensile behavior of the produced nanocomposites not just at room temperature, but also at -40 °C in order to simulate a more extreme environment. A morphological and microstructural investigation was also performed through X-ray diffraction (XRD), differential scanning calorimetry (DSC), and scanning electron microscopy (SEM) to evaluate the effect of the nanomaterials, as well as how these characteristics affect the mechanical performance of the nanocomposites at the different conditions explored. Additionally, viscometric analysis was conducted to follow the molecular weight of the polymer as a function of processing and filler.

3.2 Materials and Methods

3.2.1 Materials

Grilamid XE 4181 natural is the particular grade of polymer matrix that is utilized in this work. It is an extrusion grade PA 1010 from EMS Grivory that exhibits high viscosity and impact resistance, is unreinforced, and plasticized. Composites incorporating GO, h-BN, and MoS_2, as well as their hybrid forms (GO/h-BN, MoS_2/GO, and h-BN/MoS_2), were studied. The GO was synthesized by Andrade et al. (Andrade et al., 2021) and is characterized by high structural quality, a carbon to oxygen ratio of approximately 1, a maximum of five layers, and a lateral dimension not exceeding 2.5 μm. The h-BN was sourced from Sigma-Aldrich, featuring a relative density of 2.29 g/cm³ and 100% purity. Merck supplied the bulk MoS_2, which also has 100% purity and a density of 5.06 g/cm³. The morphology of these nanoparticles is detailed in a recent study (Pinto et al., 2023), where GO exhibits the highest aspect ratio and the fewest layers. Although h-BN also has low thickness, its nanosheets have very short lateral dimensions, which restricts its aspect ratio. MoS_2 has a wide range of thicknesses and number of layers, but since its sheets are larger in their bulk form, it achieves a higher aspect ratio compared to h-BN.

3.2.2 Methods

3.2.2.1 Nanocomposites' Preparation

The nanofillers were appropriately exfoliated in suitable solvents prior to incorporating them into the polymer. It has been demonstrated that this exfoliation process enhances the sheets' dispersibility in the following melt blending step (Muñoz et al., 2018; Pinto et al., 2020). Alternative exfoliation strategies have been used for each nanomaterial in order to achieve equivalent exfoliation yields to those of prior works (Andrade et al., 2021; Kalupgian, 2021; Marciano de Oliveira Cremonezzi et al., 2022). All dispersions were produced with a concentration of 1 g/l. GO was exfoliated in water for 30 min in an ultrasonic bath. Although

MoS_2 was also exfoliated in an ultrasonic bath, the solvent used was ethanol and the procedure took 180 min. Unlike the previous two materials, h-BN was exfoliated using a tip sonicator in a water and isopropanol solution at a 7:3 volume ratio for 240 minutes. In contrast, GO required a significantly shorter exfoliation time because it was already freeze-dried post-synthesis. Consequently, only a mild exfoliation to disperse it in the appropriate solvent was applied.

To incorporate the nanomaterials into the polymer matrix, we employed the "solid-solid deposition" method. This technique, developed by our research team, involves pre-depositing the nanomaterials onto the polymer particles' surfaces before feeding the mixture into a twin-screw extruder (Muñoz et al., 2018). For this procedure, a Buchi B-100 roto-evaporator with a heating bath was utilized, operating at 50 °C and 80 mBar. The extrusion process was conducted using a Process 11 twin-screw extruder (ThermoScientific) with an L/D ratio of 40 and a screw diameter of 11 mm. The settings included a feeding rate of 4 g/min, a screw speed of 80 rpm, and a temperature profile of 150/230/240/250/255/255/250/240 °C from hopper to die. Table 3.2 lists the filler contents examined.

Table 3.2 – Concentration of nanomaterial used in each nanocomposite

Acronym	GO wt%	h-BN wt%	MoS_2 wt%	Total wt%
GO	0.10	-	-	0.10
	0.30	-	-	0.30
	0.50	-	-	0.50
h-BN	-	0.10	-	0.10
	-	0.30	-	0.30
	-	0.50	-	0.50
MoS_2	-	-	0.10	0.10
	-	-	0.30	0.30
	-	-	0.50	0.50
GO/h-BN	0.05	0.05	-	0.10
	0.15	0.15	-	0.30
	0.25	0.25	-	0.50
h-BN/MoS_2	-	0.05	0.05	0.10
	-	0.15	0.15	0.30
	-	0.25	0.25	0.50
MoS_2/GO	0.05	-	0.05	0.10
	0.15	-	0.15	0.30
	0.25	-	0.25	0.50

After the extrusion process, the filaments were pelletized and subsequently injection molded into tensile test specimens (type V - ASTM D 638) and disc samples (1 mm thick and 25 mm in diameter). This molding was performed using a Haake Minijet Pro (Thermo-Scientific) injection molding machine. The barrel was heated to 255 °C, while the mold was maintained at 100 °C. An injection pressure of 600 bar was applied for 30 seconds, followed by a holding pressure of 400 bar for another 20 seconds. Given the high hydrophilicity of polyamides and their tendency to undergo hydrolysis when processed in the molten state, the pellets were dried in a vacuum oven at 80 °C for a minimum of 12 hours before any melt processing.

3.2.2.2 Characterizations

DSC scans were conducted using a DSC-60PLUS (Shimadzu) device. Samples consisted of pellets weighing approximately 5 mg each. An initial heating scan was performed, raising the temperature from room temperature to 230 °C at a rate of 10 °C min^{-1} to eliminate the sample's thermal history. The material was then cooled back to room temperature at the same rate of 10 °C min^{-1} to collect crystallization data. While the crystallization temperature (T_{mc}) was acquired directly from the measured data, the crystallization kinetics, represented by the time to achieve "half-crystallinity" ($t_{1/2}$), were estimated based on Equation 3.1.

$$t_{1/2} = \frac{|T_{mc} - T_{on}|}{X} \tag{3.1}$$

Where:
$t_{1/2}$ - Time for half-crystallinity;
T_{mc} -Temperature at the peak of crystallization;
T_{on} – Temperature of the onset of crystallization;
X - Cooling rate.

To investigate the microstructure achieved after injection molding, X-ray diffraction (XRD) was performed on injection molded discs in a Rigaku MiniFlex II diffractometer with K_{Cu}^{α} radiation (λ = 1.42 Å). The scan was performed from 3° to 30° with a rate of 2° min^{-1}. The crystallinity (X_c) of the injection molded samples was then estimated based on the

deconvolution of the crystalline peaks, as can be seen in Figure A II-1 of the Annex II. The crystalline lamellae thickness was estimated by the Scherrer equation, as shown in Equation 3.2.

$$L_{(hkl)} = \frac{0{,}9\lambda}{B\cos\theta} \tag{3.2}$$

Where:

$L_{(hkl)}$ = crystalline lamella thickness;

λ = X-ray wavelength;

B = Full width at half maximum (rad) of the diffraction peak;

θ = Diffraction angle.

Tensile tests were conducted at a crosshead speed of 10 mm/min, according to ASTM D638. For these tests, a MTS Alliance RF-200 testing machine mounted with a 1 kN load cell and pneumatic grips was used. In addition to the tests at room temperature, tests at -40 °C were carried out inside an environmental chamber that can be coupled to the MTS machine. The tests at low temperatures are made possible via an input of liquid nitrogen, and the controlling part of the chamber is made possible by an Eurotherm controller. The description of the assembly and operation of the chamber is given in more detail in the Supporting Information, and the assembly can be seen in Figure A II-2. For these tests, all samples were placed inside the chamber prior to testing in order to acclimate them to the temperature, and the tests were started only after thermal equilibrium was achieved.

The values of tensile strength and strain at break were acquired directly from the measured data, the Young's modulus was calculated based on the slope of the stress × strain curve in the elastic regime, and the energy released by the material during the test, i.e., its toughness, by integrating the whole area under the stress × strain curve. At least ten specimens were tested at room temperature for each composition. For the tests at -40 °C, as the composites presented a lower variability in their tensile behavior, the number of samples tested per composition was reduced to at least five specimens.

Thermogravimetric analysis (TGA) was performed from 30 °C to 600 °C with a 10 °C/min ramp in a Diamond TG/DTA analyzer from Perkin Elmer Instruments. This analysis was employed to investigate if the nanofillers addition might have increased the water absorption of PA 1010 by analyzing the weight loss as a function of temperature in samples of neat PA 1010, GO composites, and h-BN composites.

To monitor the molecular weight of PA 1010, falling-ball viscometry tests were carried out in triplicates. For that, polymer samples were solubilized in a solution of 90% formic acid at a concentration of 0.005 g/cm^3, according to ASTM D2857. For complete solubilization, the solutions were kept heated at ca. 50 °C under magnetic stirring until they were transferred to the viscometer, in which the tests were conducted at 30 °C. The molecular weight was then calculated through the Mark-Houwink equation, according to Equation 3.3.

$$\eta = KM^a \tag{3.3}$$

Where η is the intrinsic viscosity, K is the Mark-Houwink constant, M is the molecular weight, and a is the Mark-Houwink exponent. K and a were considered 22.6 × 10^{-3} mL/g and 0.82, respectively, which are values commonly employed for the polyamide/formic acid pair (Oh et al., 2019, 2020). To estimate the intrinsic viscosity, the Billmeyer equation (Billmeyer, 1949) was applied, as is presented in Equation 3.4.

$$\eta = \frac{0.25[\eta_r - 1 + 3\ln(\eta_r)]}{C} \tag{3.4}$$

Where η_r is the relative viscosity, calculated by the ratio between the ball falling time in the polymer solution and in the neat solvent, and C is the solution concentration.

Scanning Electron Microscopy (SEM) was used to examine the fractured surfaces of cryo-fractured specimens. The analyses were carried out using a Hitachi TM3000 microscope at an

operating voltage of 15 keV. Before examination, the surfaces were coated with a gold layer using a Bal-tec metallizer at 22 mA for 150 seconds.

3.3 Results and Discussion

This section begins by exploring the microstructure of PA 1010 and how each of the studied nanomaterials affect the evolution of said microstructure. Then, the tensile properties of the nanocomposites are presented, both at room temperature and at -40 °C, constantly discussing the possible reasons behind each of the observed behaviors. The complete characterization of the used nanoparticles can be seen in the works of Andrade et al (Andrade et al., 2021), Cremonezzi et al. (Marciano de Oliveira Cremonezzi et al., 2022), and Soares et al. (Soares et al., 2023).

3.3.1 Microstructural Analysis

The microstructural analysis of the nanocomposites will be presented in this section. Firstly, the effect of the nanomaterials on PA 1010's crystallization behavior will be explored by DSC, and then the formed microstructure will be analyzed through XRD diffractograms.

3.3.1.1 Crystallization Kinetics

The DSC cooling curves, from which the crystallization process of the polymer can be visualized, are presented in Figure 3.1. It can be seen from the cooling curves that PA 1010 exhibits a non-ordinary crystallization behavior. It is noticed that it has a first crystallization peak located at 173°C, however, a very broad and low-intensity second exothermal event at lower temperatures can also be seen. Even-even polyamides are known to present crystalline polymorphism, i.e., different crystalline phases can be formed depending on thermal history. The most stable crystalline phase is called α phase, exhibiting a monoclinic/triclinic structure with two prominent *hkl* reflections at 3.7 and 4.4 Å. However, the amide-aliphatic segments can present twisted conformations, leading to structures that are intrinsically or dynamically

more disordered. For example, the Brill structure, also known as γ phase, is formed at high temperatures and is described as a pseudo-hexagonal phase with generation of gauche bonds in the aliphatic parts. Therefore, because of its pseudo-hexagonal structure, it is characterized by a single reflection with a distance of ~ 4.2 Å (Lotz, 2021). Thus, the complex crystallization behavior observed in the DSC scans can be assigned to the further ordering of the initially formed pseudo-hexagonal γ crystals at higher temperatures into the more packed monoclinic α structure at lower temperatures (Ramesh, 1999). The assignment of each event is graphically presented in Figure A II-3 of Annex II.

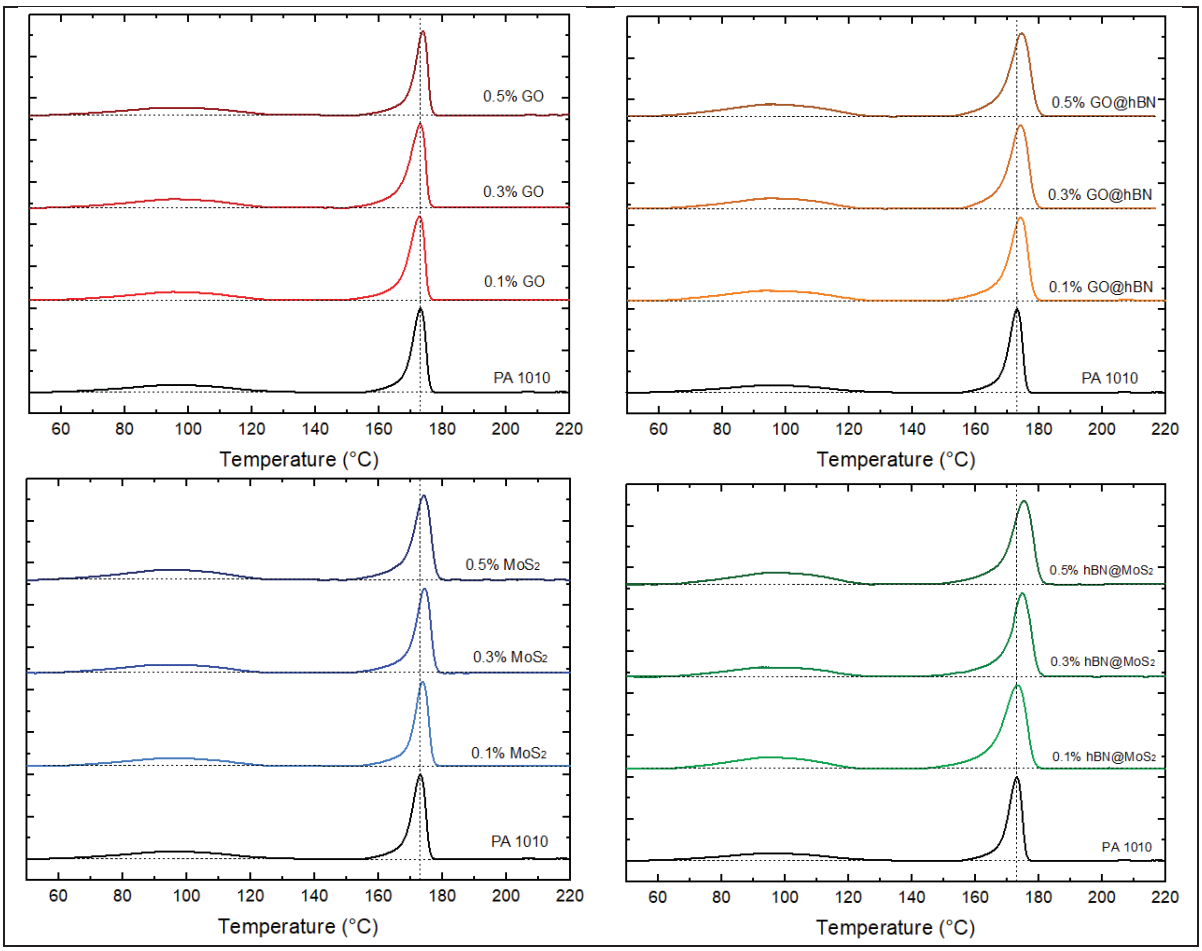

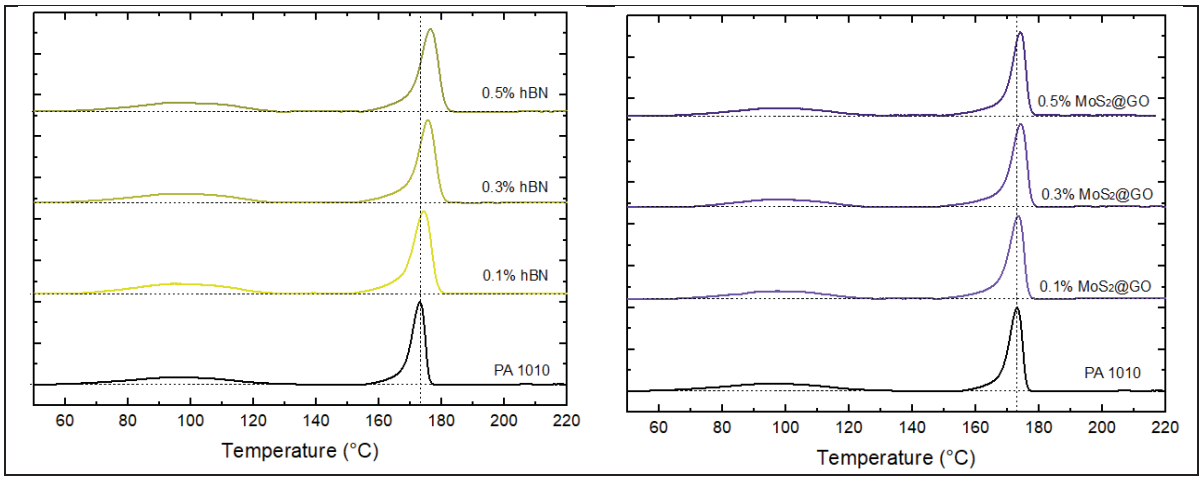

Figure 3.1 – DSC cooling curves (10 °C/min) of the various PA 1010 nanocomposites studied (exo up)

Although a small nucleating effect can be seen in some of the nanocomposites, as is evidenced by a slight shift of T_{mc} to higher temperatures, all samples still presented the low temperature exothermic halo, which suggests that all studied composites go through the $\gamma \rightarrow \alpha$ transition. Additionally, it is interesting that all nanomaterials, both individually and in hybrids, reduced the crystallization kinetics of PA 1010, leading to longer $t_{1/2}$, as can be seen in Figure 3.2. It is known that the crystallization process of thermoplastic materials occurs in two stages, nucleation and growth. While nanomaterials may favor the heterogeneous formation of nuclei, which is observed by the high-temperature shift of T_{mc}, they may impose physical hindrances to the growth of said crystals, which leads to the longer $t_{1/2}$ observed (Jimenez et al., 2020; Michell & Müller, 2016; Vanroy et al., 2013; Wurm et al., 2010; Xu et al., 2005).

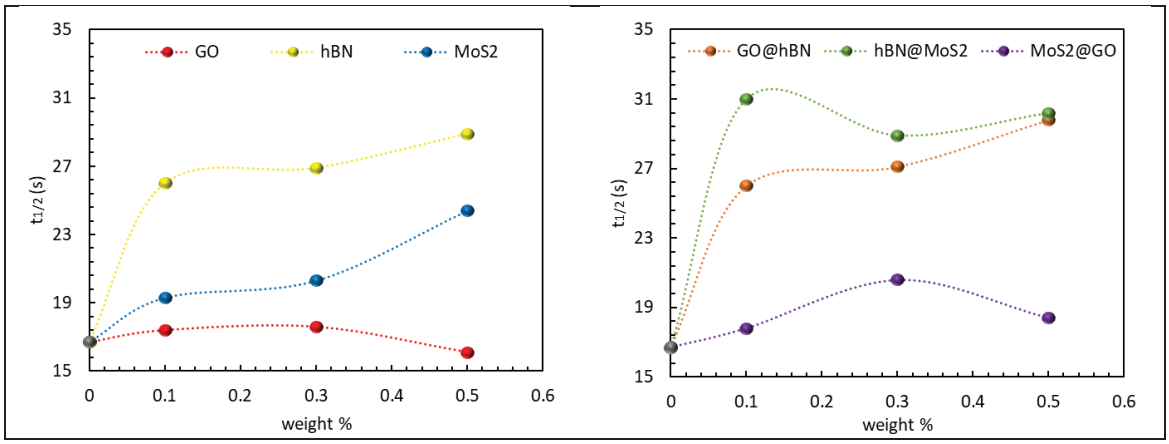

Figure 3.2 – Time for half crystallization calculated from the data acquired in the cooling curves of DSC tests

The results presented here show that the crystallization kinetics of PA 1010 was decreased upon addition of nanofillers for all the systems studied. However, the effect was different depending on the filler. While GO did not seem to affect the dynamics significantly, MoS_2, and especially h-BN, led to more significant changes. While MoS_2 increased $t_{1/2}$ of neat PA 1010 by ca. 46% at 0.5 wt%, h-BN presented a much more impactful effect, increasing it by ca. 56% already at 0.1 wt%, and reaching a maximum 73% higher than PA 1010 at 0.5 wt%. These trends were corroborated by the hybrid composites, in which the highest $t_{1/2}$ was achieved by the h-BN/MoS_2 composite at 0.1 wt%, delaying the dynamics by ca. 86%. Due to the lower effect of GO, the GO/h-BN hybrids a more gradual increase of $t_{1/2}$ as a function of content, reaching an increase of when compared to neat PA 1010 78% only at 0.5 wt%. Additionally, although the MoS_2/GO hybrid also delayed the crystallization kinetics of PA 1010, its effect was much lower than the hybrids with h-BN, which agrees well with the results from the single-filler nanocomposites. Since $t_{1/2}$ is inversely proportional to crystallization kinetics, it would be expected that the composites with longer $t_{1/2}$ would reach the lowest X_c and/or microstructural order after molding processes, as will be demonstrated by the XRD of the injection molded samples.

3.3.1.2 Microstructural Order

The diffractograms obtained for every nanocomposite are presented in Figure 3.3. Two main diffraction peaks can be observed for PA 1010. These peaks are related to the (100) and (010) diffraction planes of the monoclinic α crystalline structure, and they appear at 20.4° and 24.0°, respectively (Yang et al., 2001; Yoshioka & Tashiro, 2003). The appearance of only these two diffraction peaks for PA 1010 supports the crystallization data from DSC, in which all the samples go through the low-temperature transition from γ → α microstructure.

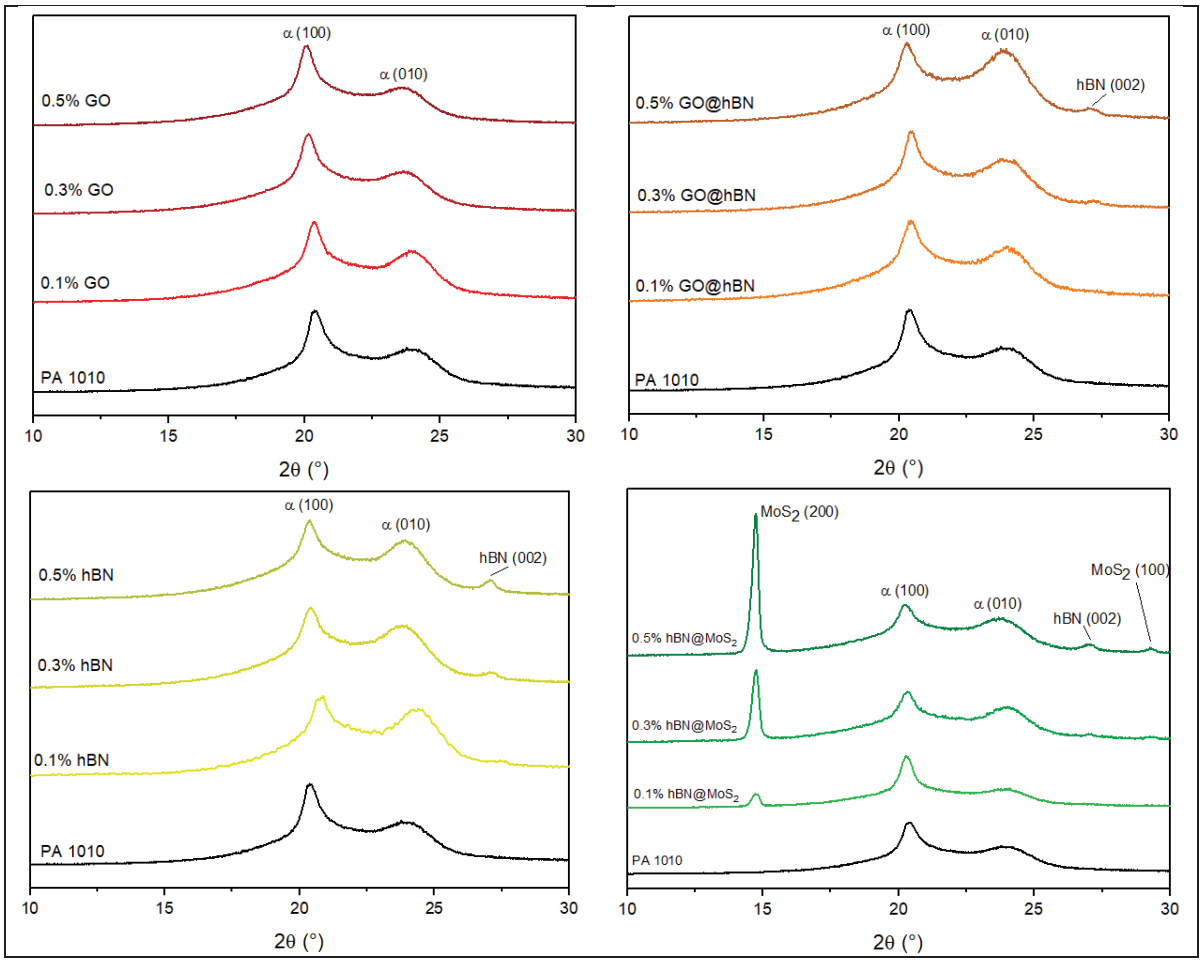

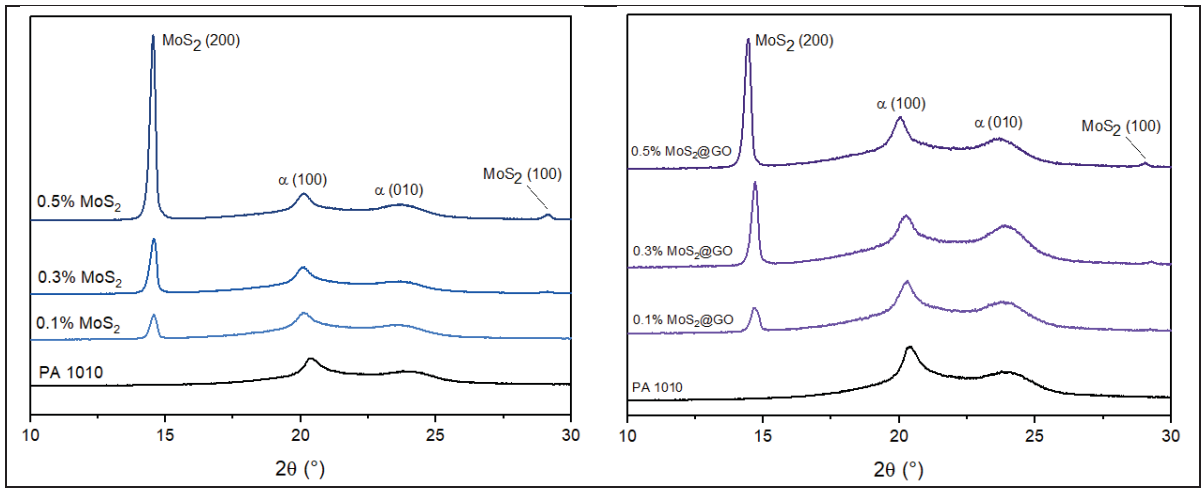

Figure 3.3 – XRD diffractograms of the studied nanocomposites

In the case of h-BN and MoS2 nanocomposites, diffraction peaks corresponding to the ones of the particles can also be observed (Bhimanapati et al., 2014; Ye et al., 2014). It's worth pointing out that the intensity of these peaks increases with content, which suggests a higher number of agglomerates as content increases. Nevertheless, the intensity of the (002) diffraction peak from h-BN, which appears at 27.0°, is still very low even at 0.5 wt%. However, the (200) diffraction peak from MoS2, which appears at 14.6°, increases in a much more sensitive manner with content. This suggests that MoS_2 formed bigger agglomerates. In the case of GO, no peaks were observed independently of content, which might indicate its better dispersion within PA 1010. Interestingly, the ratio between the intensities of the (010) and (100) diffraction peaks of the α crystals also changed as a function of filler. This indicates that, although the nanomaterials didn't change the polymer's crystalline phase, they certainly affected its organization. Figure 3.41 presents the ratio between the intensity of the α crystals' peaks ($I_{(010)}/I_{(100)}$) and the X_c estimated from the deconvolution of the crystalline peaks.

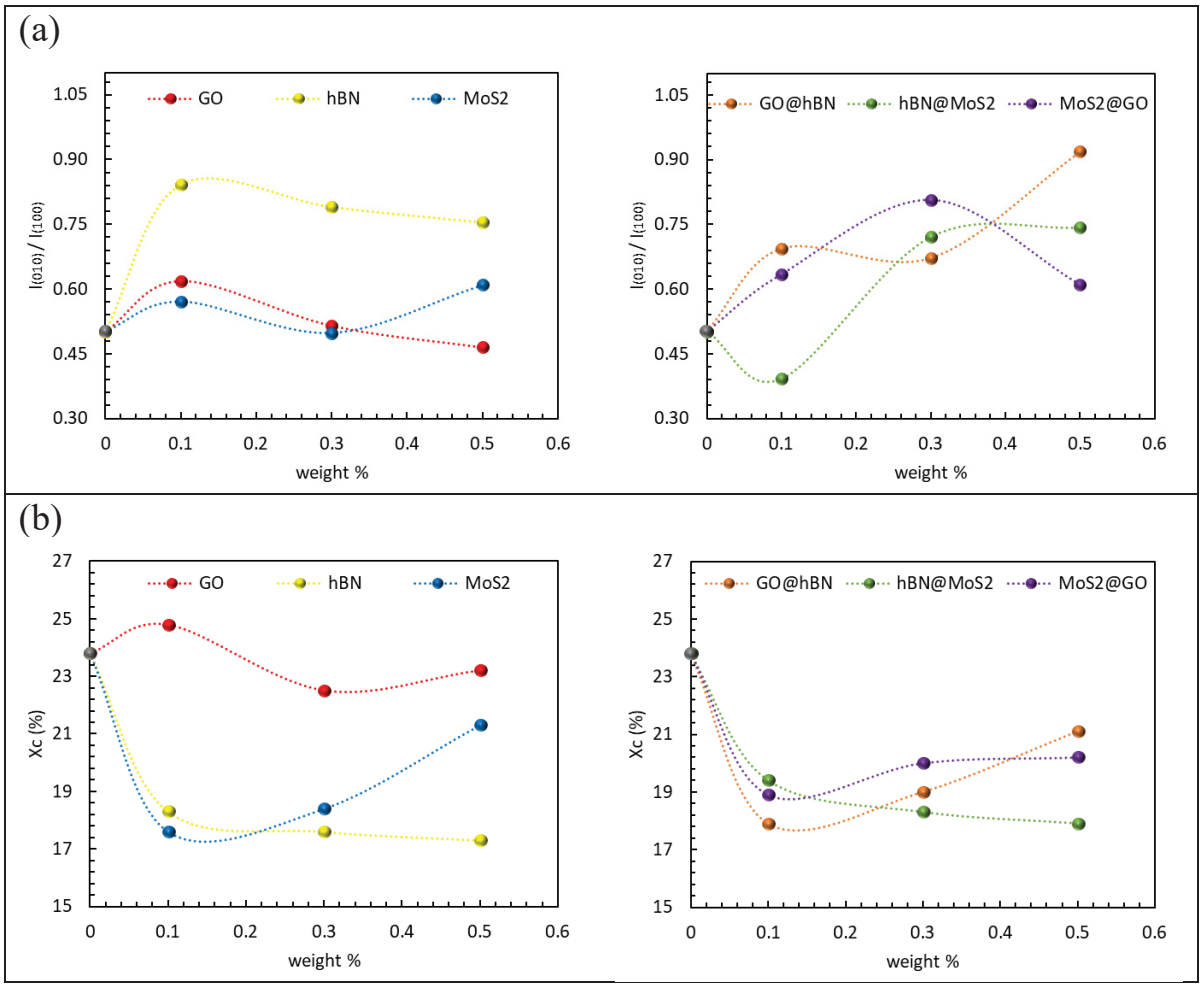

Figure 3.42 – Morphological changes promoted in the semi-crystalline microstructure of PA 1010 by the addition of different 2D materials: (a) $I_{(010)}/I_{(100)}$; (b) X_c

It can be seen that $I_{(010)}/I_{(100)}$ increases more steeply with content when h-BN or its hybrids are added to PA 1010 than when GO, MoS_2, or their hybrid is added. Since the (010) direction corresponds to the intersheet spacing between adjacent hydrogen bond sheets in the unit cell, and the (100) direction corresponds to the hydrogen bonds intrasheet distance, the (010) plane is less packed than the (100) (Yoshioka & Tashiro, 2003). Thus, an increase in $I_{(010)}/I_{(100)}$ can be correlated to a lower packing degree of the α crystals, which is further evidenced by the reduction of X_c in the composites. Figure A II-4 in the Annex II illustrates the α crystalline structure of PA 1010 based on the direction of hydrogen bonds for more clarity. Another factor that agrees with such observation is the increasing trend that $L_{(010)}$ exhibits with respect to $L_{(100)}$, which suggests that the lamellae growth is favored in the direction of the less dense

crystalline plane. The lamellae thickness is presented in Figure A II-5. The less ordered microcrystalline structure, as well as the lower overall X_c, might significantly contribute to the mechanical response under tensile loads, as will be presented in the next section. Regarding the dynamics behind the semi-crystalline organization of the polymer chains, it is interesting to correlate the data obtained from the deconvolution of the XRD peaks with the crystallization kinetics calculated from the DSC data in a colormap, as is presented in Figure 3.5.

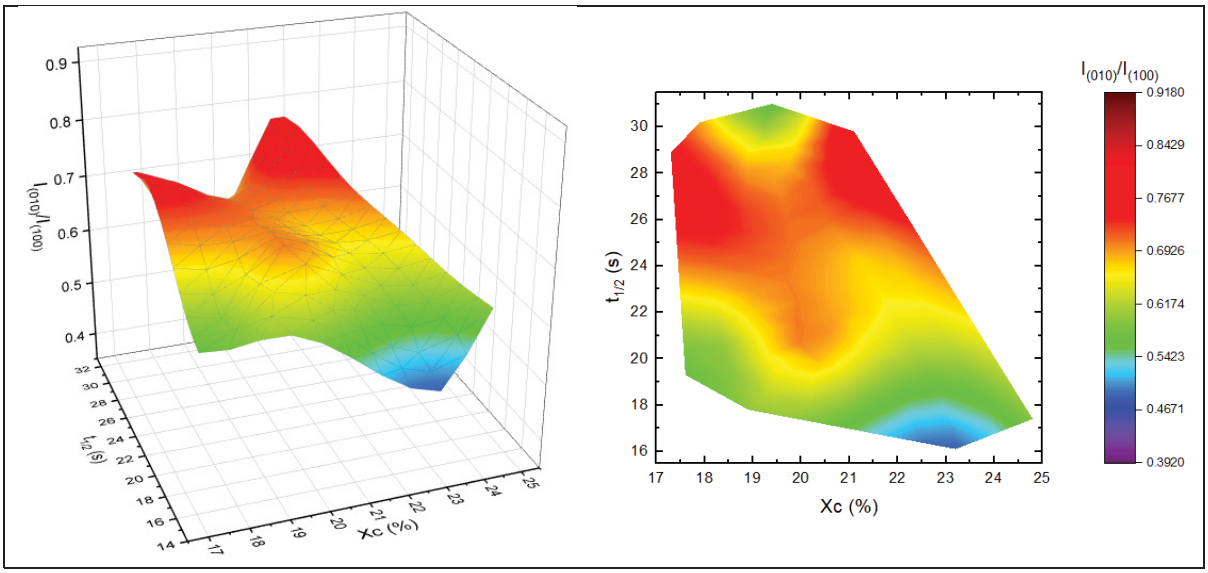

Figure 3.5 – Correlation of morphological changes promoted by the 2D materials on the semi-crystalline structure of PA 1010 with the crystallization kinetics by plotting $I_{(010)}/I_{(100)}$ as a function of X_c and $t_{1/2}$

A very high correlation between crystallization kinetics, represented by $t_{1/2}$, crystalline development, represented by X_c, and crystalline ordering, represented by $I_{(010)}/I_{(100)}$, is observed. The samples that had their crystallization kinetics retarded the most by the addition of nanoparticles are the ones that developed the lowest X_c, and whose semi-crystalline structure became less ordered. Based on these results, $I_{(010)}/I_{(100)}$ could be used as a proxy for the effects of different fillers on the crystallization dynamics of PA 1010 composites.

3.3.2 Mechanical Properties

This section will present the tensile behavior of the developed nanocomposites, both at room temperature and at -40 °C, which simulates an extreme environmental condition. The results are correlated with, and explained by the different physical aspects of the nanomaterials, their level of interactions with the polymer's macromolecules, and the polymer's overall microstructure, molecular weight, and morphology.

3.3.2.1 Room Temperature

The tensile properties of the composites at room temperature are presented in Figure 3.6. Curiously, all composites presented an unconventional mechanical response, in which the modulus was reduced, the tensile strength was either unchanged or slightly reduced, and the energy dissipated during stretching was enhanced, leading to much higher ultimate strains and toughness compared to neat PA 1010. Nevertheless, it is evident that the degree in which the properties changed depends on the employed nanomaterial.

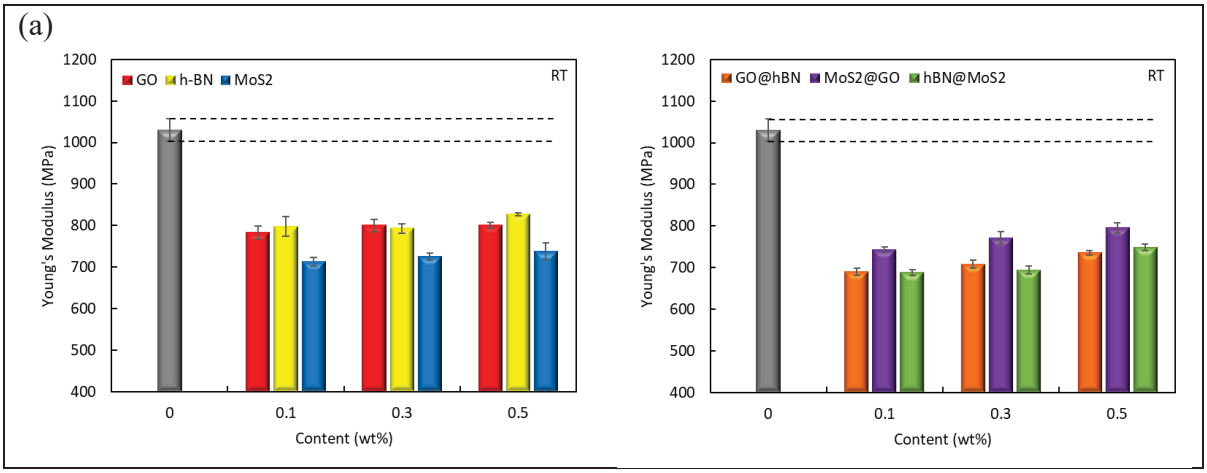

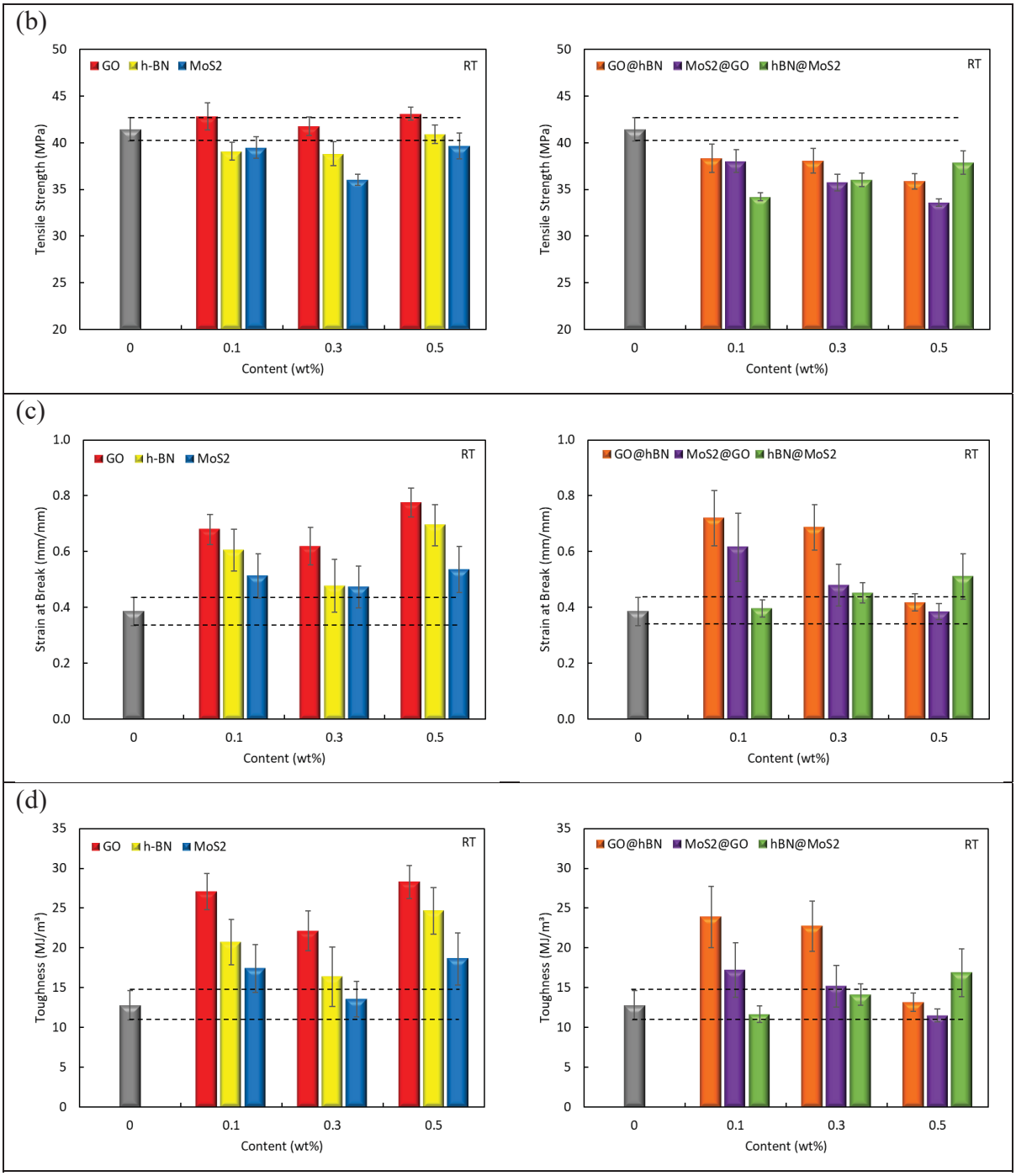

Figure 3.6 – Mechanical properties acquired from tensile tests at room temperature: (a) Young's modulus; (b) Tensile strength; (c) Strain at break; (d) Toughness. RT: room temperature

The addition of GO clearly led to a more expressive enhancement in the toughness of PA 1010, increasing it by 112%, 73%, and 121% at 0.1, 0.3, and 0.5 wt%, respectively. However, it is

worth pointing out that the content didn't seem to affect the toughening degree in a very expressive manner, since there is no significant difference for the value obtained at 0.1 wt% compared to the one at 0.5 wt%. Even though the other 2D materials had milder effects, their composites still presented enhanced ability to release strain energy, reaching toughness values 93% and 46% higher than neat PA 1010 for h-BN and MoS_2 composites at 0.5 wt%, respectively.

Based on the level of interactions that these nanomaterials can develop with PA chains, as well as their physical characteristics, this trend would be expected to some degree. In fact, the increase of toughness in nanocomposites based on different PA grades reinforced by graphene-related materials has already been reported in the literature, with the main explanation being a change in the crystal form, from the monoclinic α phase to the pseudo-hexagonal γ phase. Since the γ phase is less packed than the α phase, with the amide groups tilted out of the hydrogen bond sheet in the unit cell structure, the polymer becomes capable to dissipate more energy under mechanical loads. In addition, hydrogen bonds between the nanosheets' functional groups and the amide segment of PA chains has also been identified as a major contributor (Huang et al., 2022; Wang et al., 2019). It is assumed that there is a delay in the rupture of hydrogen bonds due to interactions between the oxygen-containing groups of GO and the amide groups of PA chains. Hence, the material would be able to elongate and dissipate more energy before fracturing (Rafiq et al., 2010; Yuan et al., 2013). Nonetheless, recent MD simulations have suggested that this increased energy absorption in polymer nanocomposites is optimized for nanosheets with a limited number of functional groups. That is explained by the improved interactions with the polymer macromolecules, but in such a way that they are not overly interlocked, which would prevent the release of the stored energy (B.R. & Ghosh, 2023; Pinto et al., 2023; Rastegar & Montazeri, 2022).

Nevertheless, no change in the crystalline phase was observed in this work, as has been clarified by XRD analysis. On top of that, even though the nanomaterials' addition seems to have decreased the long-range order of the polymer semi-crystalline structure to some extent, GO was the nanomaterial that promoted the least microstructural changes. Therefore, the

toughening observed in this work cannot be solely explained by this effect. It is believed that, (I) as GO is expected to have a good chemical affinity with PA 1010 due to its oxygenated groups, (II) it exhibits the largest aspect ratio among the three nanosheets, and (III) it seemed to reach the best dispersion within the polymer, there are more sites for energy dissipation from matrix to filler in the GO composites.

Notwithstanding, although h-BN exhibits the smallest lateral size among the three nanofillers, its partial ionic bonding character (lip-lip bonds) can also improve its interactions with polymers (Chen et al., 2015). Actually, it has been recently proposed that h-BN might promote even stronger interactions to PA 1010 than GO (Pinto et al., 2023). This may actually help to explain the slower crystallization dynamics presented by the composites filled with h-BN, which led to the most affected semi-crystalline microstructure. Although the strong affinity, and the less ordered microstructure definitely contributed to the enhancement of toughness, it is evident that the larger aspect ratio, as well as the likely better dispersion of GO were the main contributors to increase the polymer's capability to dissipate energy under tensile loads at room temperature.

Lastly, even though some research has already stated that MoS_2 can also promote hydrogen bonds to polymers (Rodriguez et al., 2021), it does not possess either oxygenated functional groups or h-BN's lip-lip bonds, which could limit its degree of interactions with PA 1010. On top of the lower intrinsic attraction to the polymer matrix, it has also been observed that MoS_2 formed larger agglomerates than the other nanofillers by the higher intensity of its diffraction peaks. These agglomerates decrease the overall interfacial area available for energy dissipation from the matrix to the nanosheets, which may also have contributed to its lower toughening character.

Interestingly, the toughening aspect was only partially transferred to the hybrid fillers. It is noticeable that the GO/h-BN system sustained the behavior up to 0.3 wt%, reaching an optimal value 86% higher than neat PA 1010 at 0.1 wt%. As for the MoS_2/GO and h-BN/MoS_2 systems, although there were significant increases of 60% in the ultimate strain for 0.1 wt% MoS_2/GO,

and 32% for 0.5 wt% h-BN/MoS_2, when the toughness is analyzed, these same samples reached increases of just 35% and 32%, respectively. Nevertheless, even though the hybrid fillers didn't present synergistic effects as proposed in the literature for other matrices, the GO/h-BN composites reached better properties than the MoS_2/GO and h-BN/MoS_2 ones, which reinforces the hypothesis that GO exhibits the strongest toughening effect on PA 1010, followed by h-BN, and then by MoS_2. In addition, as was discussed for the single-filler composites, the number of agglomerates present in each system can also contribute to the observed results. As was presented earlier by XRD analysis, MoS_2 was still more agglomerated than GO and h-BN in the hybrids, which could lead to lower filler-polymer interfacial area and, therefore, lower toughening mechanisms.

Notably, the combination of nanomaterials in the same composite seems to have hindered the potential of the individual fillers, as all hybrids exhibited either intermediary or even lower performance than its respective counterparts when added individually. As a secondary filler is added, it may reduce the overall area available for interactions between the first filler and the polymer chains, therefore, limiting the energy transfer from one phase to the other. This is especially important for the hybrids that contain MoS2, as its lower forces of interaction to PA 1010 may lead to the proposed effect in a more pronounced manner, which agrees with the observed results (Pinto et al., 2023). The hybrid composites containing both GO and h-BN maintained their toughening characteristics up to 0.3 wt%, likely due to the stronger interfacial attraction forces exhibited by these nanomaterials compared to MoS2. However, as the filler content increased to 0.5 wt%, the propensity for agglomeration likely became dominant, leading to a reduction in the toughening effect.

Although the composites were able to release much more energy than neat PA 1010, the Young's modulus and tensile strength were either decreased or unchanged. Since water molecules act as plasticizer agents in polyamides, the first hypothesis for such unconventional behavior would be that the nanomaterials might have increased the water absorption of PA 1010. In order to test this idea, TGA analyses were conducted on neat PA 1010, as well as on the composites filled by 0.3 wt% GO and h-BN. The TGA and DTG curves are presented in

Figure A II-6Figure , and it can be seen that, although the h-BN composite seems to have its thermal degradation shifted to slightly lower temperatures, the weight loss of each process is the same as in the neat sample. Additionally, no significant difference was observed between the neat sample and the GO composite. Therefore, it is believed that the nanomaterials did not meaningfully increase the water absorption of PA 1010 to the point that this could explain the tensile response of the composites. Similarly to the plasticizing effect that water can have on polyamides, a reduction of molecular weight could also lead to a decrease of stiffness. Therefore, the molecular weight of the unprocessed PA 1010, extruded PA 1010, and of the composites filled with 0.5 wt% fillers was calculated from viscometry data, as is presented in Table 3.3.

Table 3.3 -Viscosity and molecular weight data calculated from viscometry analysis for neat PA 1010 and 0.5 wt% nanocomposites

Material	**η_r**	**η (dL/g)**	**M (kg/mol)**
unprocessed PA 1010	1.58 ± 0.02	0.97 ± 0.03	26.99 ± 1.17
extruded PA 1010	1.58 ± 0.02	0.98 ± 0.03	27.36 ± 0.90
PA 1010 + 0.5wt% GO	1.56 ± 0.02	0.95 ± 0.03	26.09 ± 1.08
PA 1010 + 0.5wt% h-BN	1.52 ± 0.02	0.88 ± 0.03	23.99 ± 0.92
PA 1010 + 0.5wt% MoS_2	1.54 ± 0.01	0.92 ± 0.02	25.30 ± 0.50
PA 1010 + 0.5wt% GO/h-BN	1.54 ± 0.01	0.92 ± 0.01	25.21 ± 0.42
PA 1010 + 0.5wt% h-BN/MoS_2	1.57 ± 0.02	0.96 ± 0.02	26.71 ± 0.78
PA 1010 + 0.5wt% MoS_2/GO	1.55 ± 0.01	0.94 ± 0.01	25.88 ± 0.29

The first important aspect to highlight from the viscometry data is that the extruded PA 1010 basically presented an identical molecular weight to the unprocessed polymer. This indicates that the extrusion parameters were well selected and that there is no significant degradation during processing. Regarding the molecular weights estimated for the nanocomposites, even though there are a few variations between each filler system, the nanocomposites seem to exhibit slightly lower molecular weights than neat PA 1010. However, these changes are either insignificant when the error is taken into account or too small for being responsible for the observed effect on the polymer's stiffness.

Another known factor that affects the stiffness of thermoplastic materials is their semi-crystalline structure and overall X_c. It is known that the crystalline phase in thermoplastics is responsible for its stiffness, while the amorphous part is responsible for dissipating energy. Therefore, the lower X_c and less ordered microstructure exhibited by most nanocomposites must have contributed to the decrease of the Young's modulus. However, as remarked earlier, GO didn't notably change the X_c of PA 1010. Thus, these morphological changes cannot be the only reason behind this phenomenon. An interesting reason that might have corroborated is the possible lubricity effect that these 2D materials can exhibit (Ferreira et al., 2019, 2020; Wang et al., 2017, 2019; Wu et al., 2015). In this case, since the nanosheets' content is extremely low, there would be enough room and mobility for the flakes to slide over one another and in between the polymer chains under loading, resulting in the reduction of Young's modulus. This softening effect has recently been proven through atomistic simulations, which have demonstrated that for tensile directions between 6° and 86° with respect to the nanosheet's plane, this interfacial "slippage" prevails over the stiffened chains at the proximity of the nanosheets (Lu et al., 2021).

3.3.2.2 Low Temperature

The tensile properties of the nanocomposites at -40 °C are presented in Figure 3.7. Interestingly, it is still possible to observe the lubricity effect of the nanofillers at -40 °C, which maintained lower values of Young's modulus when compared to the neat polymer. However, this effect occurred in a less intense manner than at room temperature, possibly due to the lower molecular mobility at lower temperatures.

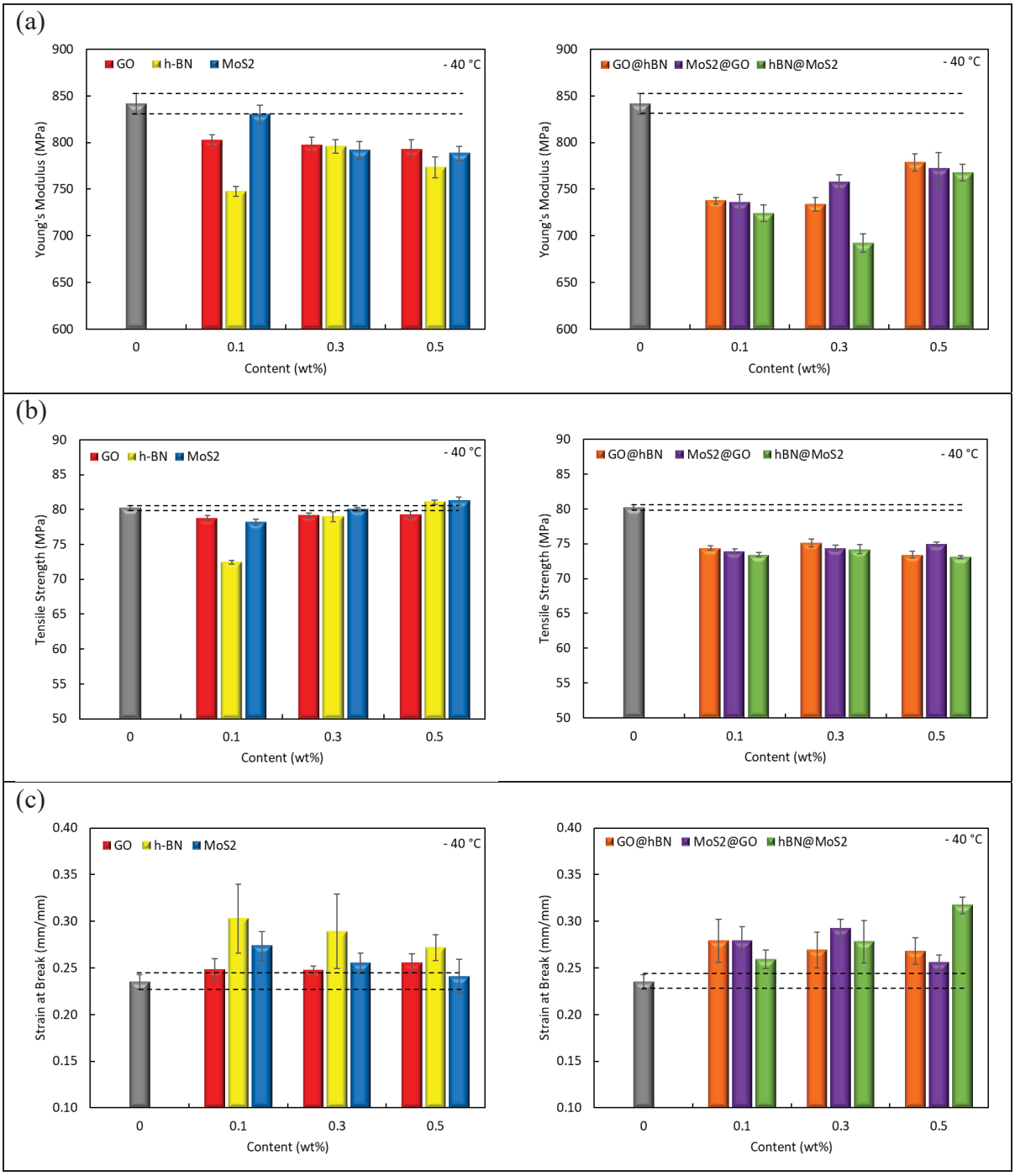
(a)
GO
h-BN
MoS2
- 40 °C
Young's Modulus (MPa)
900
850
800
750
700
650
600
0
0.1
0.3
0.5
Content (wt%)
GO@hBN
MoS2@GO
hBN@MoS2
- 40 °C
Young's Modulus (MPa)
Content (wt%)
(b)
GO
h-BN
MoS2
- 40 °C
Tensile Strength (MPa)
90
85
80
75
70
65
60
55
50
Content (wt%)
GO@hBN
MoS2@GO
hBN@MoS2
- 40 °C
Tensile Strength (MPa)
Content (wt%)
(c)
GO
h-BN
MoS2
- 40 °C
Strain at Break (mm/mm)
0.40
0.35
0.30
0.25
0.20
0.15
0.10
Content (wt%)
GO@hBN
MoS2@GO
hBN@MoS2
- 40 °C
Strain at Break (mm/mm)
Content (wt%)

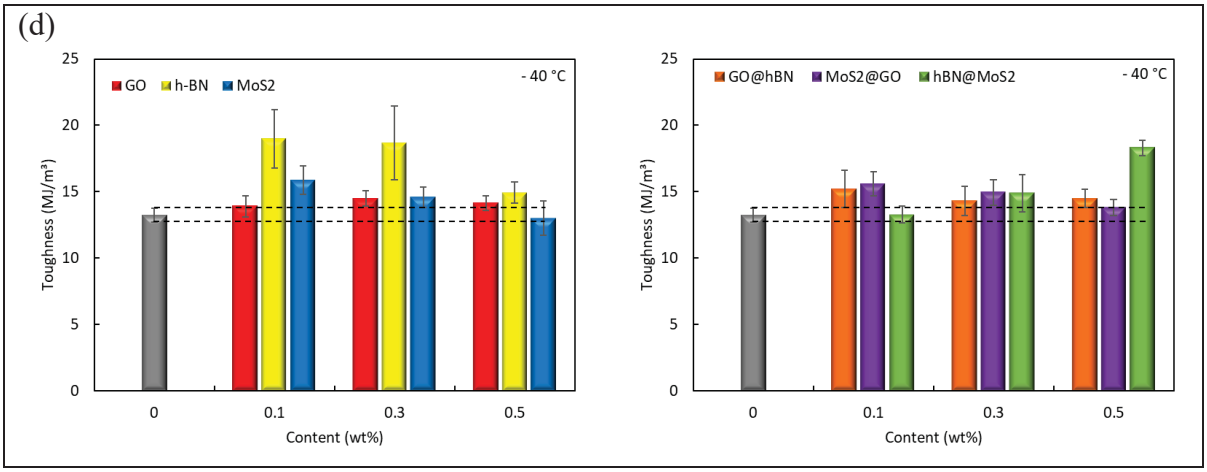

Figure 3.7 – Mechanical properties acquired from tensile tests at –40 °C: (a) Young's modulus; (b) Tensile strength; (c) Strain at break; (d) Toughness

The tensile strength and strain at break are also in good agreement with what would be expected from the tests at low temperature. The tensile strength basically presented a two-fold increase, and the strain at break decreased by ca. 38% for neat PA 1010 when compared to the tests at room temperature. This agrees well with the lower molecular mobility that the polymer chains should exhibit at lower temperatures. Nevertheless, it is interesting that some of the trends that were observed at room temperature were changed in the low temperature tests. Even though the tensile strength remained only slightly lower than the neat polymer's for most composites, one can notice that the astounding increase of strain at break, which led to the toughening of the composites filled with GO at room temperature, is greatly suppressed at -40 °C. On the other hand, it is curious that h-BN and MoS_2 were able to maintain the toughening character to a certain degree, enhancing the toughness of PA 1010 by 44% and 20% at 0.1 wt%, respectively. In a similar manner, the GO/h-BN hybrid also seems to lose some of its toughening characteristics, probably due to the same effect observed in the GO composites. However, h-BN/MoS_2 at 0.5 wt% was the hybrid filler that toughened the polymer the most at -40 °C, increasing the energy dissipation by 38%.

Based on these results, it is proposed that the main factor leading to the toughening at such low temperatures is the lower long-range organization of the polymer chains, while the chemical affinity, and the nanomaterial's physical characteristics must play a much reduced role. The

relationship between the mean values of X_c, $t_{1/2}$, and toughness for each filler system at -40 °C is presented in Figure 3.8.

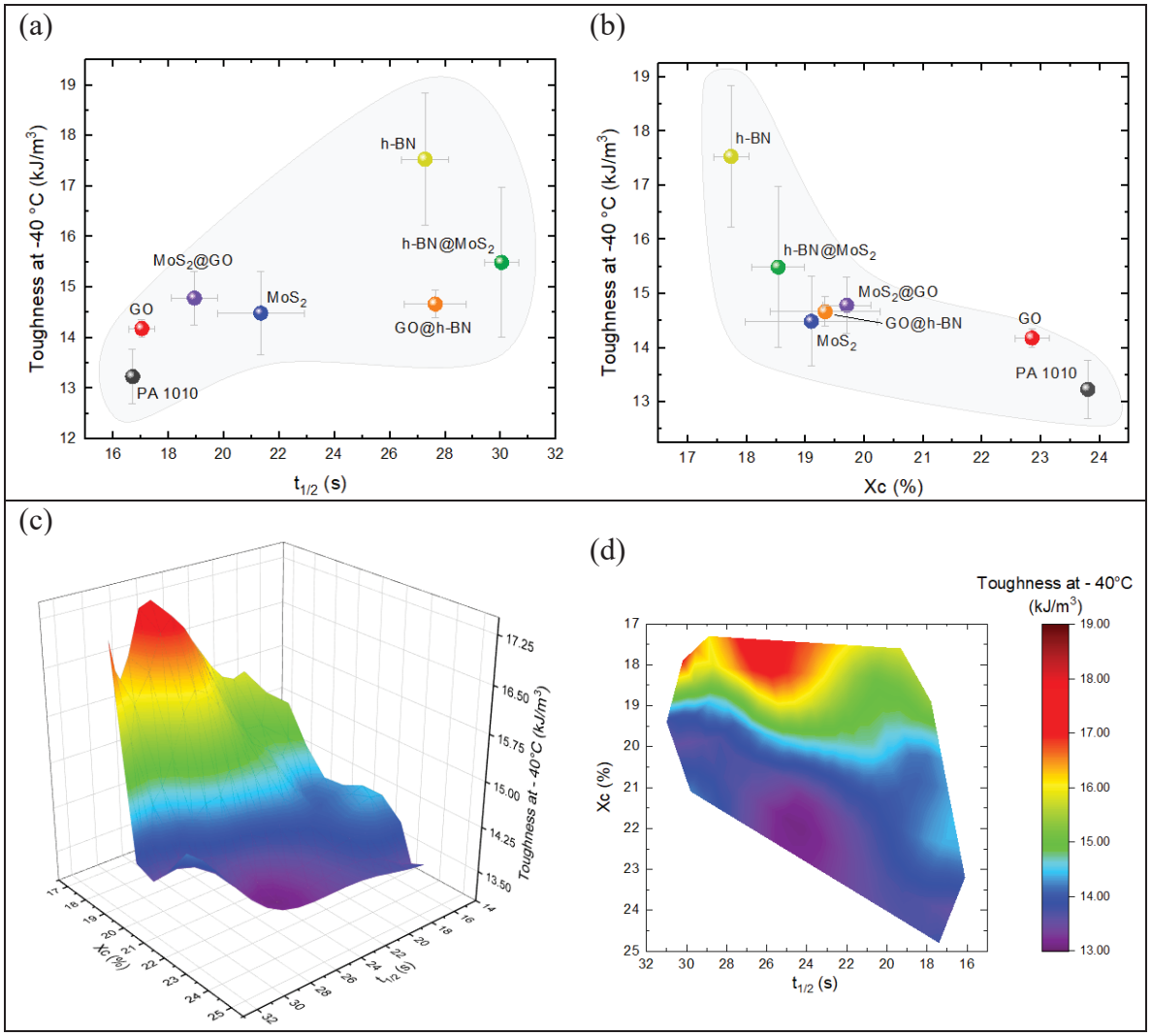

Figure 3.8 – Relationship between the toughness at -40 °C with: (a) crystallization kinetics; (b) crystallinity; (c) 3D colormap as a function of both crystallization kinetics and crystallinity; (d) 2D colormap as a function of both crystallization kinetics and crystallinity

It becomes evident that the nanocomposites that had their crystallization kinetics hampered the most, i.e., the ones that faced the greatest decrease in their crystalline fractions, were able to dissipate the most energy at -40 °C. Additionally, in an environment with such reduced molecular mobility, it is expected that the nanosheets with larger aspect ratio might hinder the motion of the polymer chains even further, which could explain the suppressed effect of GO,

both individually and in the hybrids. Actually, since h-BN has the shortest nanosheets, it is also reasonable to assume that this mechanical interlocking at low temperatures occurs the least in its composites, suppressing less the toughening effect. In order to verify the morphology and fracture mechanisms of the nanocomposites, Figure 3.9 exhibits SEM images of cryo-fractured surfaces for neat PA 1010 and the composites at 0.5 wt%. As there was not a significant difference between the fracture morphology of the nanocomposites as a function of nanoparticle content, micrographs of the other compositions can be seen in Figure of Annex II.

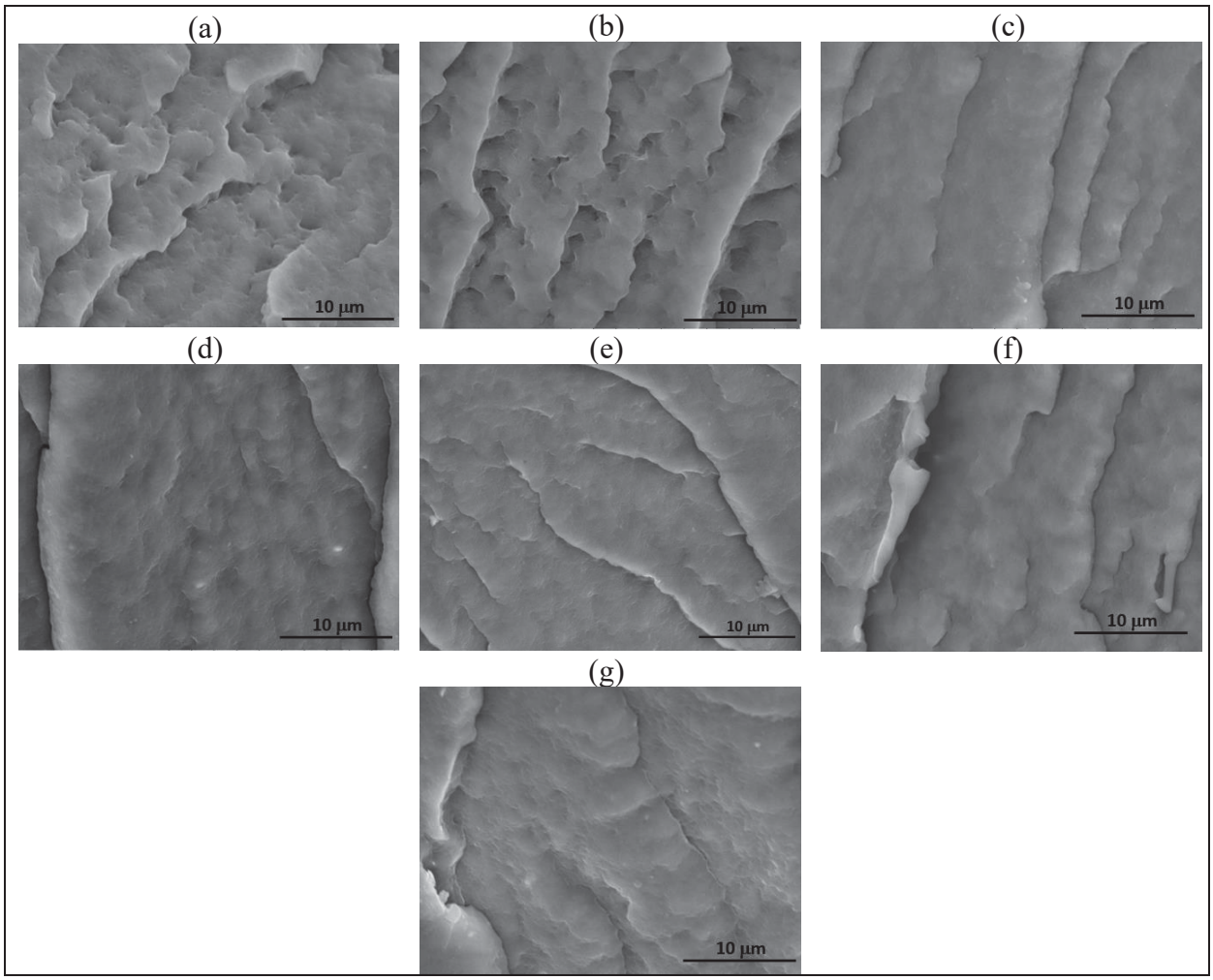

Figure 3.9 – SEM images of cryo-fractured surfaces for PA 1010 (a), GO composite at 0.5 wt% (b), h-BN composite at 0.5 wt% (c), MoS_2 composite at 0.5 wt% (d), GO/h-BN composite at 0.5 wt% (e), MoS_2/GO composite at 0.5 wt% (f), h-BN/MoS_2 composite at 0.5 wt% (g)

One can see from the SEM images the morphological aspects that provide crucial insights into the mechanical behavior of all investigated compositions. Independent of filler and content, all images exhibit a very similar morphology and fracture aspect to neat PA 1010, where a rough surface full of grooves and dimples can be observed through the whole fracture area. The surface roughness, evident by the presence of dimples and grooves, highlight the material's ability to absorb energy through localized plastic deformation. Additionally, no interfaces and voids from debonding can be seen in the SEM images, which may suggest that the nanosheets are fully embedded within the matrix. Therefore, although the nanocomposites were toughened by the nanomaterials' incorporation, no significant changes in the fracture mechanisms were observed.

3.4 Conclusions

The tensile properties of PA 1010 nanocomposites filled by GO, h-BN, and MoS_2, both individually and in hybrid form, have been investigated under different environmental conditions. We have demonstrated for the first time what is the effect of low environmental temperatures on the tensile response of such nanocomposites. It has been observed that at extremely low contents, i.e., less than 0.5 wt%, the bidimensional nanomaterials provide an unconventional type of reinforcement, in which these fillers reduce the Young's modulus of PA 1010, but significantly enhance its ductility, and hence, its toughness. This behavior has been attributed to three factors: (I) physical characteristics and chemical compatibility between the nanosheets and polymer matrix.; (II) The lubricating character that such bidimensional nanostructures exhibit when employed at such low contents; (III) The decrease in the overall crystallinity of the polymer, as well as in the order of such crystalline regions. Additionally, even though the combination of different nanomaterials has shown promise in previous works due to their synergistic contributions in the dispersion within the polymer matrix, no such effect was observed in this work, and the second filler seems to hamper the effects of the first one.

Curiously, it was observed that some of these factors become less significant at lower temperatures, where the difference in aspect ratio, chemical affinity, and the lubricity aspect

contribute much less to the tensile behavior of the nanocomposites. This leaves the changes in the polymer microstructure as the main contributors to the toughness enhancement at low environmental temperature. Since h-BN promoted the biggest reduction of X_c, as well as in the order of the crystalline domains, it is proposed that it should be the nanomaterial of choice to be employed in PA nanocomposites that will be exposed to low temperatures in their applications. On the other hand, for materials that will not experience such conditions, GO seems to be the better option, since it was more effective in toughening PA 1010 at room temperature. Ultimately, this work evidences the importance of considering external factors, e.g., the temperature to which the material will be exposed during its application, when designing polymer nanocomposites and selecting the most adequate nanomaterial to be used as filler.

ACKOWLEDGEMENTS

The authors would like to acknowledge FAPESP – Fundação de Amparo à Pesquisa do Estado de São Paulo (Process 2020/11496-0 and 2021/07858-7), CNPq - Brazilian National Council for Scientific and Technological Development (process 314093/2021-4), CAPES - Coordination of Superior Level Staff Improvement (PrInt grant 88887.310339/2018–00), and NSERC – Natural Sciences and Engineering Research Council of Canada (RGPIN-2018-03888) for funding this work. We would also like to acknowledge Serge Plamondon, technology application technician at ÉTS, for assisting with the development of the environmental chamber where the mechanical tests at -40°C were conducted.

CHAPTER 4

BALANCING THERMAL CONDUCTIVITY, DIELECTRIC, AND TRIBOLOGICAL PROPERTIES IN POLYAMIDE 1010 WITH 2D NANOMATERIALS

Gabriel M. Pinto[1,2,3], Lucas Staffa[4], Emna Helal[1], Carolina Hahn[5], Lúcia Vieira[5], Hélio Ribeiro[2], Eric David[1], Nicole R. Demarquette[1], Guilhermino J. M. Fechine[2,3]

1 Department of Mechanical Engineering, École de Technologie Supérieure, Montréal, QC, Canada
2 Engineering School, Mackenzie Presbyterian University, São Paulo, SP, Brazil
3 Mackenzie Institute of Research in Graphene and Nanotechnologies – MackGraphe, Mackenzie Presbyterian Institute, São Paulo, SP, Brazil
4 Department of Materials Engineering (DEMa), Federal University of São Carlos (UFSCar), São Carlos, SP, Brazil
5 Research and Development Institute (IP&D), University of Paraiba Valley (Univap), São José dos Campos, SP, Brazil

Paper accepted for publication in *Journal of Applied Polymer Science*, September 2024

ABSTRACT

Low electrical conductivity and good heat dissipation are crucial for electronic packaging materials. Additionally, friction is critical for the lifespan and energy efficiency of components. To address these requirements, polymer nanocomposites based on bio-based polyamide 1010 and ultra-low contents of 2D nanomaterials were produced by melt-blending. Graphene oxide, hexagonal boron nitride, and molybdenum disulfide were selected for their two-dimensional structure and electrical insulation, providing high thermal conductivity while preserving the polymer's dielectric nature. Hybrid nanocomposites were also produced to explore potential synergistic effects. Results showed all compositions maintained the polymer's intrinsic dielectric properties. Although the friction coefficient increased slightly compared to neat polyamide, all nanocomposites stayed within the low-friction range required for low-friction materials. Thermal conductivity improved by 5-10% compared to unfilled polyamide, with hybrid systems performing slightly better, indicating a minor synergistic effect. Despite these enhancements being modest compared to the literature, achieving high thermal conductivity usually requires over 20 wt%, which is detrimental to mechanical performance. In this study, at most 0.5 wt% was used, with composites being obtained directly through melt-blending. This highlights their potential as low-content additives for thermal interface materials without compromising other essential properties.

4.1 Introduction

To meet the demands of fast signal transmission and high energy density devices, electronic packaging materials must possess low electrical conductivity and high heat dissipation capabilities (Evans et al., 2021). However, even though polymers are naturally good electrical insulators, they exhibit poor intrinsic thermal conductivity ranging from 0.1 to 0.4 W/mK, which makes them inadequate for efficient thermal management, and limits their use in such applications (Guo et al., 2020; C. Huang et al., 2018). To address this, researchers are attempting to develop polymer composites with thermally conductive particles that maintain dielectric properties. The primary challenge lies in balancing thermal conductivity and dielectric behavior in these composites. This difficulty arises from the high interfacial thermal resistance (ITR) between the polymer matrix and the fillers, requiring a substantial amount of filler to achieve adequate thermal conductivity. Unfortunately, this complicates processing and compromises the polymers' inherent mechanical flexibility and electrical insulation, as most thermally conductive fillers are also electrically conductive. (Han & Fina, 2011; R. Li et al., 2022; S. Li et al., 2016; Xiao & Du, 2016)

Although heat can be transported by phonons and electrons, maintaining electrical insulation requires phonons to be the primary conduction mechanism. Unlike electrons, phonons convey heat solely through molecular vibrations, without exhibiting tunneling effects. Therefore, enhancing a material's thermal conductivity imposes increasing the phonon mean free path. However, numerous sources of phonon scattering exist in heterogeneous materials such as polymer composites. The primary source is boundary scattering, which is intrinsically linked to ITR, as vibrational mismatches and voids created by low wettability at the filler-polymer interfaces result in significant phonon scattering (Mehra et al., 2018; Pandey & Singh, 2021).

Ideally, constructing a 3D thermally conductive network would resolve this issue, allowing phonons to travel "freely" through the material without jumping between different phases. However, this approach is currently feasible only for thermosets, as it involves infiltrating a preconstructed 3D filler network with a low-viscosity resin and then curing it. Consequently,

ITR becomes particularly significant for thermoplastic composites, where fillers hardly form a continuous path (R. Li et al., 2022; Pandey & Singh, 2021; Ren et al., 2020).

Thus, the main practices for reducing ITR in thermoplastic composites are incorporating fillers with high aspect ratios and combining different fillers with high thermal conductivities. For example, Cui et al. (Cui et al., 2015) developed polystyrene (PS) and polyamide 6 (PA 6) nanocomposites using a hexagonal boron nitride (h-BN)/graphene hybrid. Their experimental results indicated that the thermal conductivity of the composites increased with the addition of h-BN as a secondary filler. Compared to composites containing 20 wt% graphene, introducing an additional 1.5 wt% of h-BN boosted thermal conductivity by up to 38% in PS, and 34% in PA 6. This enhancement was attributed to h-BN filling the interspaces between graphene sheets, forming an h-BN/graphene stacked structure that significantly improved thermal conductivity. Similarly, a polymer blend of PA 6 and polypropylene (PP) was enhanced by incorporating h-BN and reduced graphene oxide (rGO) [246]. The authors initially produced masterbatches of PA 6/(h-BN+rGO) and then melt-blended these masterbatches with PP. The hybrid fillers created a synergistic effect, forming a more efficient percolating network than h-BN alone. The improved thermal conductivity was partly due to a change in the blend's morphology, transitioning from a matrix-dispersed morphology in PP/(PA 6/h-BN) to a co-continuous morphology in PP/(PA 6/h-BN+rGO).

In addition to thermal conductivity and dielectric behavior, friction plays a crucial role in determining the lifetime and energy efficiency of components. Thus, investigating materials' tribological character has sparked increased interest from the scientific community (Marian et al., 2022; Ronchi et al., 2023). Solid lubricants are considered promising fillers for enhancing the tribological properties of polymer composites across various applications. Among them, 2D nanomaterials such as graphene derivatives, h-BN, and transition metal dichalcogenides (TMDs), such as tungsten selenide (WSe_2), molybdenum selenide ($MoSe_2$), tungsten sulfide (WS_2), and molybdenum disulfide (MoS_2) have garnered significant attention. This interest stems from their exceptional two-dimensional layered structure, where Van der Waals forces between adjacent atomic layers result in low shear resistance and self-lubricating properties

(Lahiri et al., 2014; H. Li et al., 2017; L. Liu et al., 2019; Y. Liu et al., 2020; Sun & Du, 2019; Uzoma et al., 2020). Additionally, the large specific surface area of these nanomaterials can lead to extremely high aspect ratios, and thus, to their excellent heat conduction. In fact, heat dissipation has also been identified as a major factor in reducing the friction coefficient (COF) in polymer nanocomposites (Qiu et al., 2018; Senturk & Palabiyik, 2023).

Castor oil-based polyamides, such as polyamide 1010 (PA 1010), stand out as some of the most attractive biopolymers on the market. This engineering polymer is available in tough, flexible, and abrasion-resistant forms, making it suitable for various industries, including electronics, sports equipment, automotive, textiles, and coatings. Its benefits extend beyond its ecological nature, also exhibiting lower density and water absorption than conventional polyamides. Therefore, PA 1010 effectively bridges the gap between long-chain high-performance polyamides such as PA 12 and shorter-chain conventional polyamides such as PA 6 and PA 66 (Kuciel et al., 2016; W. Li et al., 2008; McKeen, 2012; Rusu et al., 2011; Zhang et al., 2005; Zhishen et al., 1993).

Accordingly, we intend to explore the effects of graphene oxide (GO), which is a chemical derivative of graphene due to the addition of oxygenated groups on its basal plane, h-BN, and MoS_2 on the tribological, thermal conductivity, and dielectric behavior of PA 1010. The selection of GO instead of graphene was made due to the greater chemical affinity that the oxygenated groups promote to the amide groups in PA 1010, the much lower electrical conductivity that GO exhibits after the oxidation process, and the increasing interlayer spacing created by such groups, which eases its dispersion and reduces the shear resistance, possibly providing lower friction (Chouhan et al., 2020; H. Huang et al., 2022; Wang et al., 2019). However, unlike most of the previous works in the literature, we are adding extremely low contents of these nanomaterials to the PA 1010 matrix, i.e., up to 0.5 wt%. This is one to two orders of magnitude less than what is usually employed when investigating the same properties (R. Li et al., 2022; Ronchi et al., 2023). The low concentrations are not to prejudice the desirable toughness and flexibility of the thermoplastic matrix, as it has been seen that at such contents these fillers can significantly enhance the polymer's ability to dissipate mechanical

energy (Pinto et al., 2024). In addition, we are also exploring the use of the mentioned nanomaterials as hybrids, i.e., adding two of them in the same composite, to investigate if they exhibit any synergism under such conditions.

4.2 Material and Methods

4.2.1 Materials

The polymer matrix used in this work is the PA 1010 commercialized as Grilamid XE 4181 natural. It is an extrusion grade, unreinforced, high viscosity, plasticized, high impact resistant PA 1010. As for the nanofillers, systems based on GO, h-BN, MoS_2, and their hybrids, i.e., GO/h-BN, GO/MoS_2, and h-BN/MoS_2 will be studied. The GO used was synthesized in-house, presenting a C: O ratio of ~ 1, thickness between 1-5 layers with good structural quality, and lateral size ≤ 2.5μm (Andrade et al., 2021). The h-BN was purchased from Sigma-Aldrich and has a purity of ~ 100% and a relative density of 2.29 g/cm^3. The MoS_2 was purchased from Merck and has a purity of ~ 100% and a density of 5.06 g/cm^3.

4.2.2 Methods

4.2.2.1 Preparation of the Nanocomposites

Before mixing the nanomaterials with the polymer, the nanofillers were thoroughly exfoliated in appropriate solvents to enhance their dispersibility during the melt mixing of polymer nanocomposites. This exfoliation process has been shown to significantly improve the distribution of the nanosheets (Muñoz et al., 2018; Pinto et al., 2020). Different exfoliation methods were employed for each nanomaterial to achieve yields comparable to those reported in previous studies, with all dispersions prepared at a concentration of 1 g/l (Andrade et al., 2021; Kalupgian, 2021; Marciano de Oliveira Cremonezzi et al., 2022). GO was exfoliated in water using an ultrasonic bath for 30 minutes. In contrast, MoS_2 was exfoliated in ethanol for 180 minutes. h-BN underwent exfoliation using a tip sonicator in a 7:3 water-isopropanol

solution for 240 minutes. The shorter exfoliation time for GO was due to its freeze-dried state post-synthesis, requiring only mild exfoliation to disperse it effectively in the solvent.

After exfoliating the nanosheets, they were deposited on the surface of the polymer powder by the" solid-solid deposition" methodology. It has been shown that this process, makes the clusters smaller and better distributed in the matrix after compounding (Muñoz et al., 2018). After further drying, the mixtures were melt-blended in a twin-screw extruder. Figure 4.1 exemplifies the methodology and the parameters used in the extrusion process.

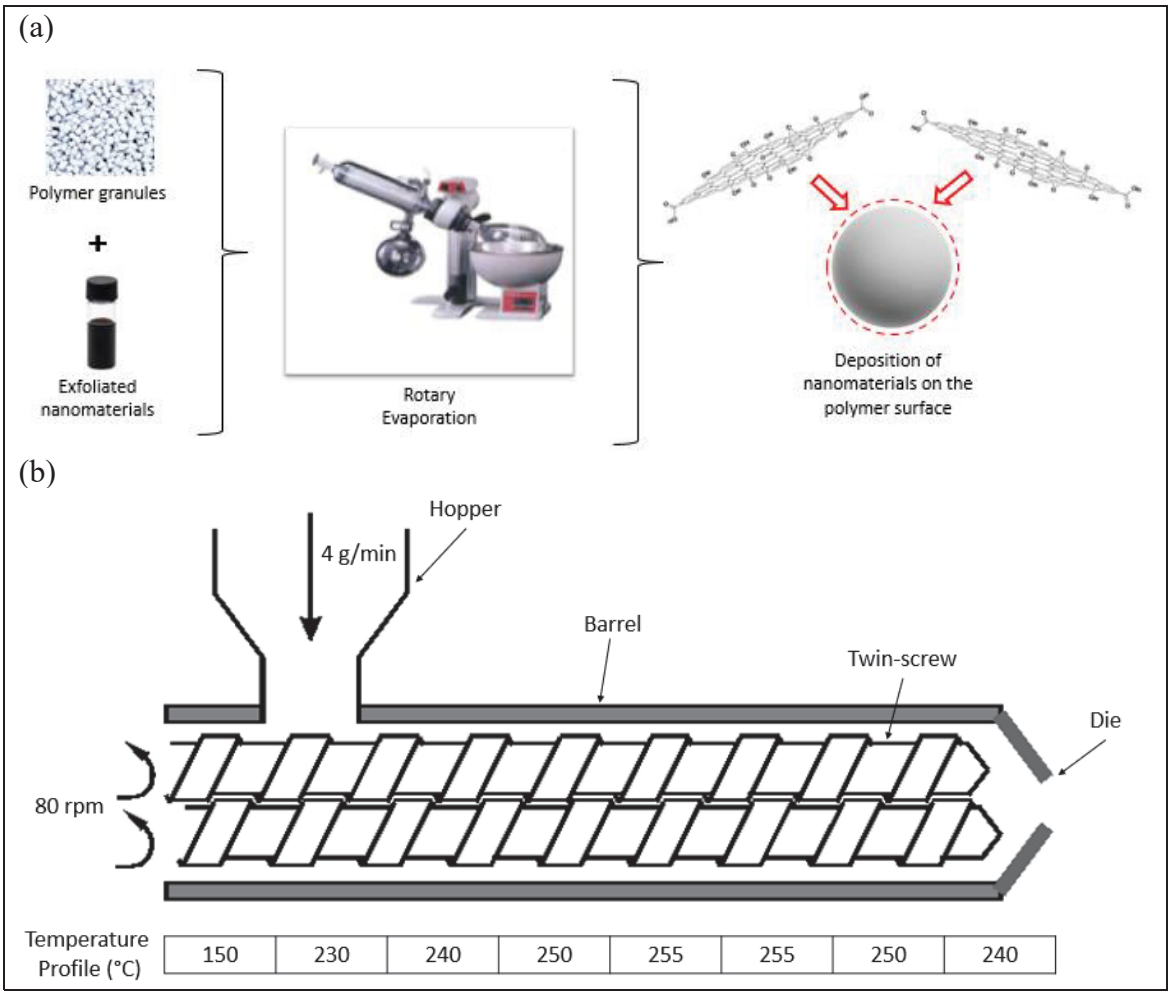

Figure 4.1 - Experimental procedure adopted for the production of PA 1010-based nanocomposites: (a) Solid-solid deposition for pre-deposition of nanomaterials on the surface of polymer powder; (b) Parameters used in extrusion for melt-blending the nanocomposites

A Buchi B-100 roto-evaporator with a heating bath operating at 50 °C and 80 mBar was used for the solid-solid deposition. As for the extrusion process, a Process 11 twin-screw extruder (ThermoScientific), with L/D = 40 and 11 mm in screw diameter was employed. Three filler contents were produced for each system, i.e., 0.1, 0.3, and 0.5 wt%. The ratio was established as 1:1 for the hybrid nanocomposites, maintaining the final content the same as in the single-filler composites. The choice of this ratio was made based on the literature, which indicates that it considerably lowers the volume fraction of voids in the final composite by improving the nanomaterials' dispersion (Wang et al., 2021).

After extruding the nanocomposites, the strands were pelletized and then injection-molded into disc samples with 1 mm in thickness by 25 mm in diameter. The injection molding machine used was a Haake Minijet Pro (Thermo-Scientific) operating at 255 °C, with an injection pressure of 600 bar, post-pressure of 400 bar, and a mold temperature of 100 °C.

The pellets were adequately dried in a vacuum oven at 80 °C for at least 12 hours before any process in the melt to prevent potential degradation by excessive moisture. This drying step is necessary because polyamides exhibit high hydrophilicity and are susceptible to hydrolysis when processed in the melt.

4.2.2.2 Characterizations

This paper will not deal with the characterization of the nanomaterials, as it has already been presented in the literature in previous works (Andrade et al., 2021; Kalupgian, 2021; Marciano de Oliveira Cremonezzi et al., 2022), and summarized in (Pinto et al., 2023). Nevertheless, a brief discussion regarding their morphology is presented at the beginning of the "Results and Discussion" section.

The electrical properties of the nanocomposites were measured through broadband dielectric spectroscopy (BDS). The equipment used was a Novocontrol broadband spectrometer. Disc specimens of 25 mm diameter and 1 mm thickness were coated with a 10 nm layer of gold on

both sides to improve contact with the equipment's plated brass electrodes. Isothermal measurements were conducted through a frequency range from 1 x 10^{-2} Hz to 3 x 10^{5} Hz under an excitation voltage of 3 V. Measurements were consecutively performed at different temperatures by increasing it from 30 °C to 120 °C with 10 °C steps.

Thermal conductivity measurements were carried out in the disc samples using the modified transient plane source method (MTPS). The tests were conducted in a Trident equipment from C-Therm Technologies Ltd. In this device, a heated guard ring is fitted around a one-sided interfacial heater/sensor. A brief electrical current is simultaneously applied to the heater/sensor and guard ring, which creates a heat pulse on the sample surface in contact with the device. To prevent lateral heat losses, and to ensure a one-dimensional heat flow from the heater to the sample, the guard ring provides physical insulation around the heater/sensor assembly. The brief current pulse slightly raises the sensor temperature. How quickly the temperature rises is proportional to the thermal losses caused by the sample conducting heat away from the interface. This increase in temperature leads to a change in the sensor voltage as a function of time, which is then used to create a response curve and directly determine the material's thermal conductivity.

The tribological tests were conducted in reciprocating mode, where wear tests involved linear sliding of samples to characterize friction behavior in a sphere-on-plate contact geometry under a normal load. Tests were performed at room temperature using a Bruker Ultra Micro UMT 2 tribometer, following ASTM G119 protocol. The tribometer software recorded average values for COF, with all samples being tested against a 316L stainless steel sphere, which was purchased from Ceraltec Cerâmica Técnica Ltda, SP, Brazil. The metallic sphere that served as a counterface had a diameter of 4 mm and purity of 99%. The tests were conducted with a sliding speed of 20 mm/s, normal force of 15 N, and frequency of 0.5 Hz over a 1 mm track. Each test was performed twice for reliability, with the sphere being replaced between tests. The wear profile of the materials was measured using a VEECO mechanical contact profilometer, model Dektak 150 Ltd, USA.

The nanocomposites' morphology was observed via Scanning Transmission Electron Microscopy (STEM). A FEI Magellan 400 L microscope was operated at 30 kV and 25 pA for the acquisition of bright-field images. For the preparation of samples, injection molded tensile test specimens were cryo-fractured, and their cross sections were trimmed using a glass knife on an RMC Ultra MT-7000 microtome at room temperature. After that, the trimmed specimens were sectioned with a feed of 50 nm at 1 mm/s using a Reichert Ultracuts FC S. The sample and diamond knife temperatures used were -80 °C and -75 °C, respectively.

4.3 Results and Discussion

As mentioned earlier, this paper does not show the characterizations of the nanomaterials, as it has already been presented in the literature in previous works (Andrade et al., 2021; Kalupgian, 2021; Marciano de Oliveira Cremonezzi et al., 2022), and summarized in (Pinto et al., 2023). However, the physical features of the nanosheets after exfoliation are presented in Table 4.1.

Table 4.1 - Physical characteristics of the produced nanomaterials after exfoliation

Nanomaterial	**GO**	**h-BN**	**MoS_2**
Thickness (nm)	1.0 – 2.0	2.0 – 3.0	1.3 – 6.0
Lateral size (μm)	1.50 – 2.00	0.02 – 0.40	0.14 – 1.30
Number of layers	1 – 3	6 – 9	2 – 9
Aspect ratio	~ 750 – 2000	~ 7 - 200	~ 23 - 1000

Although all nanomaterials were successfully exfoliated, reaching less than 10 layers in their respective suspensions, GO maintained a much larger sheet width, which led to an expressive aspect ratio. On the other hand, MoS_2 exhibited a much wider range of lateral sizes. Thus, its aspect ratios were not as high as GO. As for h-BN, SEM images have shown that its particles already exhibit very short lateral sizes from the bulk, which naturally led to smaller aspect ratios.

The following subsections will focus on the functional properties of the nanocomposites, i.e., the dielectric behavior, tribological characteristics, and the thermal conductivity. After these properties are discussed, the morphology of the nanosheets within the nanocomposites is also presented in STEM images.

4.3.2 Dielectric Behavior

As mentioned earlier, polymer dielectrics must keep their electrical insulation in a range of temperatures to avoid current leakage in electronic applications (Pleşa et al., 2016). Therefore, the determination of the electrical conductivity becomes crucial for these materials. Figure 4.2 presents the map of the real part of the complex conductivity (σ') for neat PA 1010, measured by frequency sweeps in BDS at different temperatures. The real part of the complex conductivity is related to the direct current (DC) conductivity and the dielectric losses (ε") by Equation 4.1.

$$\sigma'(\omega) = \omega\varepsilon_0\varepsilon''_{tot} = \sigma_{DC} + \omega\varepsilon_o\varepsilon''_{rel} \quad (4.1)$$

Where ε''_{tot} is the total dielectric loss as measured experimentally, including losses due to the direct current conductivity (σ_{DC}), and ε''_{rel} is related to the relaxation losses, both dipolar and interfacial.

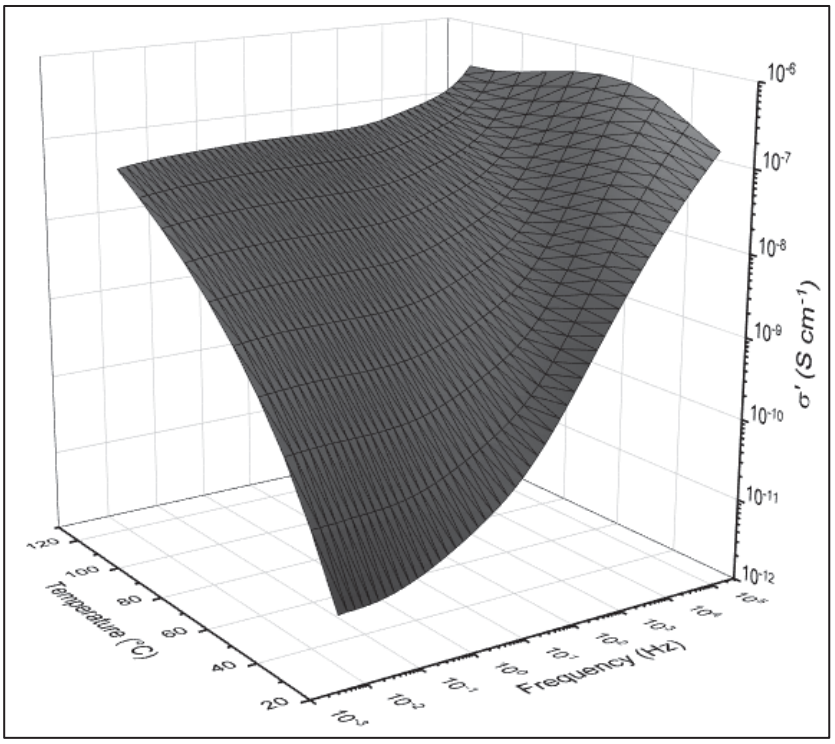

Figure 4.2 – Real part of electrical conductivity (σ') for neat PA 1010 as a function of frequency and temperature

As can be observed, σ' exhibits a frequency dependency, in which it decreases with the frequency to eventually reach a plateau when σ_{DC} becomes much larger than $\omega\varepsilon_o\varepsilon''_{rel}$. This indicates that the material has entered its regime of direct current conductivity, and the value of electrical conductivity (σ_{DC}) can be acquired in that region, usually taken at the lowest frequency. It is noticeable that, as the temperature rises, σ_{DC} increases by several orders of magnitude and, accordingly, the plateau extends towards higher frequencies. This is due to the greater molecular mobility presented by the material at elevated temperatures, which eases the transport of charge carriers (McCall & Anderson, 1960; Pathmanathan et al., 1992; Steeman & Maurer, 1992; Steeman & Van Turnhout, 1997). Hence, Figure 4.3 presents the measured σ_{DC} for all the studied nanocomposites as a function of filler content and temperature.

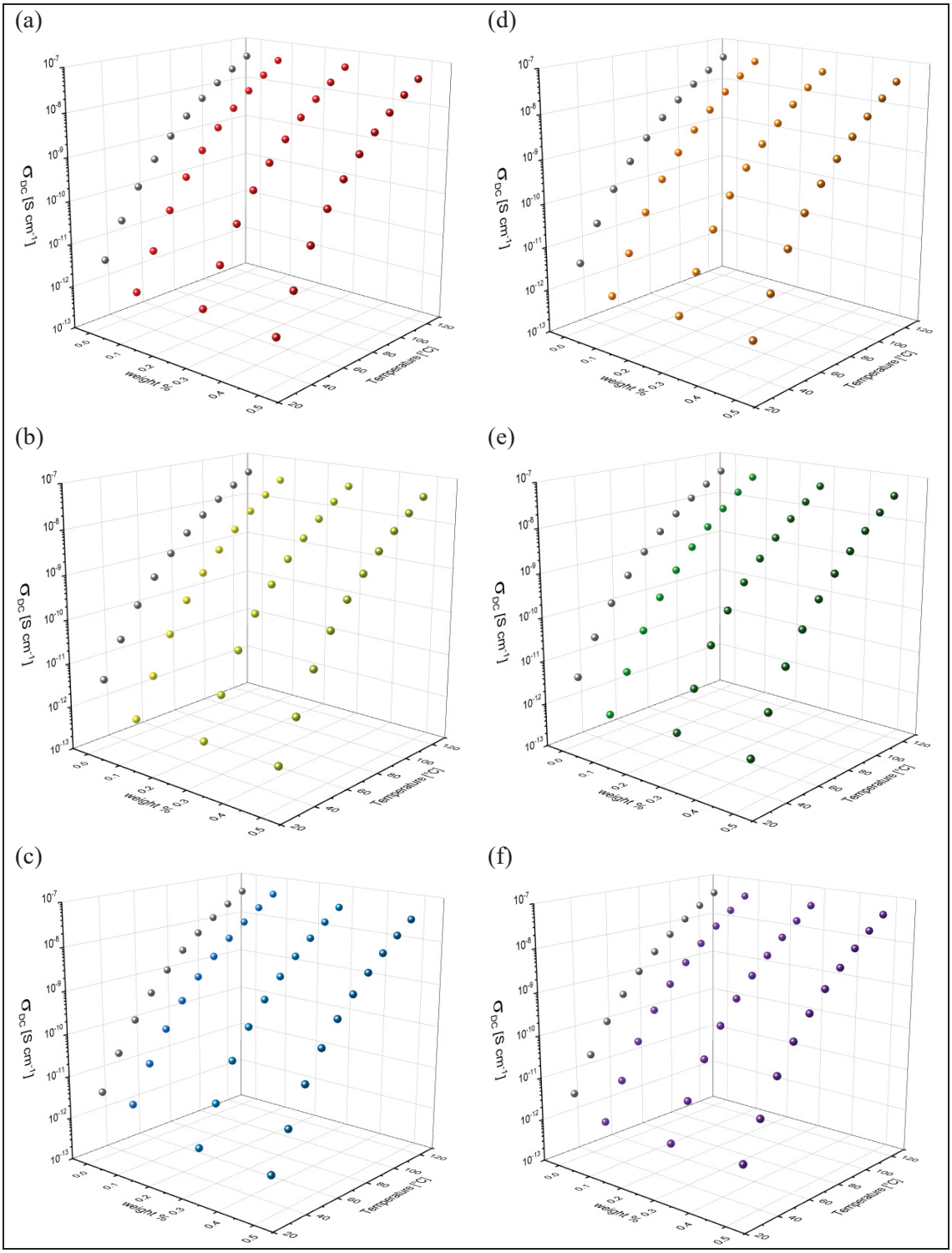

Figure 4.3 – σ_{DC} obtained from σ' at 0.01 Hz of all the studied nanocomposites as a function of wt% (left axis) and temperature (right axis): (a) GO; (b) h-BN; (c) MoS_2; (d) GO/h-BN; (e) h-BN/MoS_2; (f) MoS_2/GO

It can be seen that σ_{DC} increases with temperature for all nanocomposites in a similar manner. However, all of them exhibited lower σ_{DC} than neat PA 1010 at low temperatures, enhancing its insulating behavior. Since none of the 2D materials used are highly electrically conductive, this trend was already expected to some extent.

On the other hand, the nanocomposites had a slightly more sensitive increase in σ_{DC} than neat PA 1010 as a function of temperature. A possible explanation for this behavior would be that the nanosheets act as hindrances for the movement of charge carriers at low temperatures, where the dynamics are low. However, as the temperature increases, the dynamics are accelerated, and charge carriers can be more easily transported through filler-polymer interfaces. This hypothesis is reinforced by the heightened interfacial polarization presented by the nanocomposites, as was presented in our earlier publication (Pinto et al., 2023). Nevertheless, the composites' σ_{DC} didn't meaningfully surpass that of PA 1010 even at the highest temperature, maintaining their suitability for electronics packaging applications.

The composites filled with GO and MoS_2 probably exhibited slightly higher σ_{DC} than neat PA 1010 above 100 °C due to remaining π bonds in the GO plane and the semi-conductive character of MoS_2, respectively. Even though the π bonds are affected by oxidation during the synthesis of GO, some of these bonds are expected to remain in the structure. Since these are the bonds responsible for the impressive electrical conductivity of graphene, it is understandable that the GO nanocomposites exhibited this trend (Yang et al., 2014).

The effect of the second nanomaterial in the hybrid systems can also be identified. While MoS_2/GO hybrids presented slightly higher σ_{DC} than neat PA 1010 above 100 °C, probably due to the reasons mentioned above, all GO/h-BN and h-BN/MoS_2 systems presented lower σ_{DC} than the neat polymer even at the highest temperature. This can be attributed to h-BN's partially ionic nature and insulating character, which may hinder the transport of charge carriers through the interfaces even when the molecular dynamics are heightened at higher temperatures (B. Yu et al., 2022).

4.3.2 Tribological Behavior

Figure 4.4 shows the COF evolution as a function of time for all the samples. It is curious that independent of nanomaterial and content employed, all nanocomposites reached higher COFs than neat PA 1010. Although this was unexpected, as 2D materials should act as solid lubricants, other works in the literature have also reported increased COF after addition of nanoparticles (Pan et al., 2014; Randhawa & Patel, 2020; J. Yu et al., 2018).

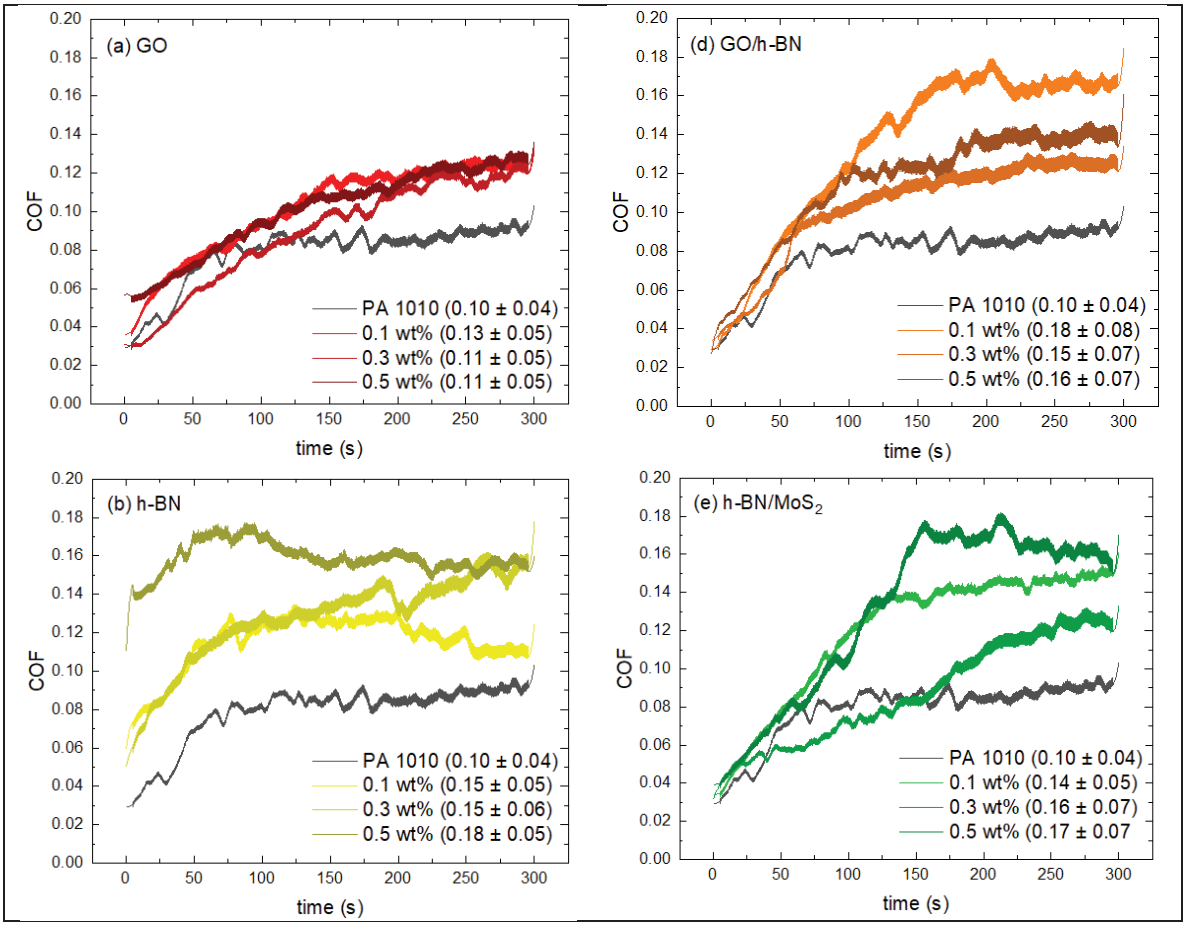

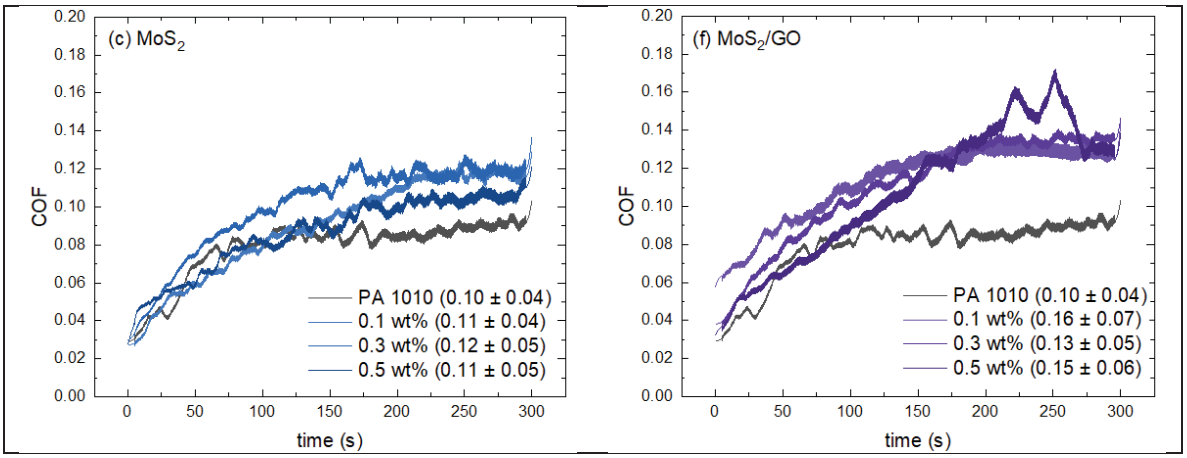

Figure 4.4 – Evolution of all the studied nanocomposites' COF as a function of time: (a) GO; (b) h-BN; (c) MoS_2; (d) GO/h-BN; (e) h-BN/MoS_2; (f) MoS_2/GO

The COF of GO-based nanocomposites showed a consistent behavior over time with a slight increase compared to neat PA 1010, but it remained within the low-friction range with an average not higher than 0.13. The MoS_2-based nanocomposites also presented an average COF near that of neat PA 1010, i.e., 0.10. In a slightly different behavior from the previous two nanomaterials, the hBN-based nanocomposites exhibited higher COFs, between 0.15 and 0.18, over the testing period. However, although the mean value was higher than that of the other nanocomposites and neat PA1010's, they also presented low friction characteristics. Regarding the hybrids, it is visible the effect of h-BN, as all GO/h-BN and h-BN/MoS_2 nanocomposites presented COFs closer to those of h-BN nanocomposites, i.e., in the range of 0.14 to 0.18. As for the MoS_2/GO hybrid, it can be seen that its nanocomposites exhibited slightly higher COFs than its single-filler counterparts, which may suggest that one nanomaterial might slightly hinder the lubrication promoted by the other. Nevertheless, all hybrid nanocomposites maintained low COF values, which makes them excellent choices for tribological applications.

Although it was not possible to calculate the wear rate of the studied samples, as only a small concavity was formed with no real detachment of material, in addition to the COF, examining the wear profile of the frictioned surfaces is also of considerable interest. Thus, Figure 4.5 shows the wear depth of all samples after the friction test in reciprocating sliding mode. The wear was analyzed using a profiler tip in contact with the sample surface along the width of the track.

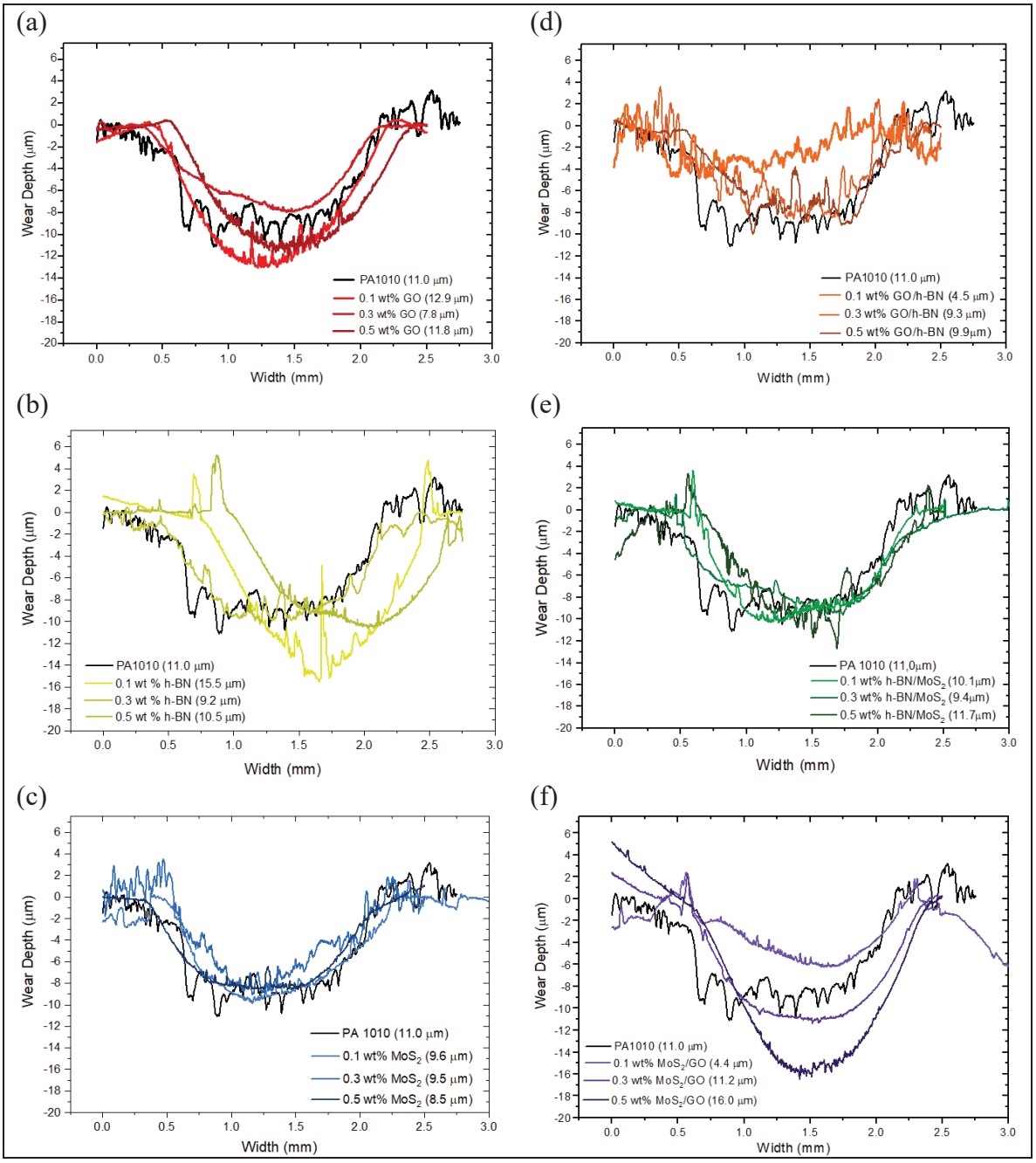

Figure 4.5 - Profilometry of the nanocomposites' friction surface: (a) GO; (b) h-BN; (c) MoS2; (d) GO/h-BN; (e) h-BN/MoS_2; (f) MoS_2/GO

Notably, the overall wear depth of most composites does not exhibit significant changes when compared to neat PA 1010. A noteworthy characteristic of the composites' wear profiles is their markedly smoother shape compared to that of the PA 1010 surface. This characteristic is

particularly significant for applications where a component undergoes continuous friction. A smoother surface reduces the generation and accumulation of debris at the contact interface, thereby minimizing the risk of potential malfunctions by mechanical wear.

4.3.3 Thermal Conductivity

The thermal conductivity of the studied nanocomposites is presented in Figure 4.6. Although all compositions presented slight increases compared to the unfilled PA 1010, there were only minor differences among the nanocomposites as a function of 2D material and content employed.

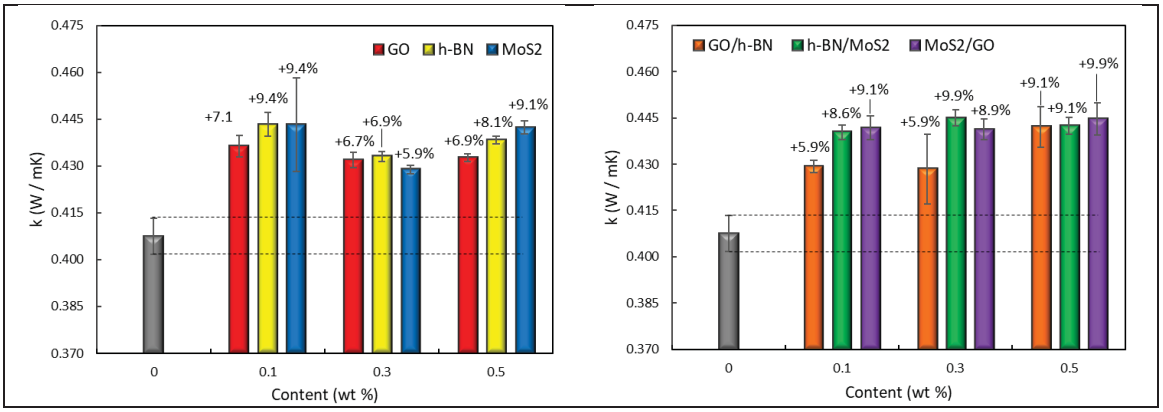

Figure 4.6 –Thermal conductivity of the single-filler nanocomposites (left) and hybrid-filler nanocomposites (right)

The first possible reason behind the observed results might be related to the ITR, which dictates the thermal conductivity in thermoplastic nanocomposites, especially at such low contents where no conductive networks develop, and the nanoparticles are mostly scattered throughout the matrix (Li et al., 2022; Pandey & Singh, 2021; Ren et al., 2020). Notably, the composites filled by h-BN reached thermal conductivities similar to those of the other systems even with h-BN exhibiting much shorter nanosheets. This evidences the greater affinity that h-BN exhibits to PA 1010, as it leads to a better vibrational match at the interface and, therefore, to a lower ITR. A lower ITR allows the phonons to travel through the filler-polymer interfaces more easily, reducing the boundary scattering. Similarly, although the intrinsic thermal conductivity of each nanomaterial is different, it is believed that these discrepancies would

only play a major role above the percolation threshold, where the phonons would be able to travel through interconnected sheets without jumping between filler and matrix (Lin et al., 2020; R. Wang et al., 2018). Figure 4.7 illustrates the situations explained above, evidencing the importance of the intrinsic conductivity of 2D materials for percolated systems, and ITR for systems with scattered particles.

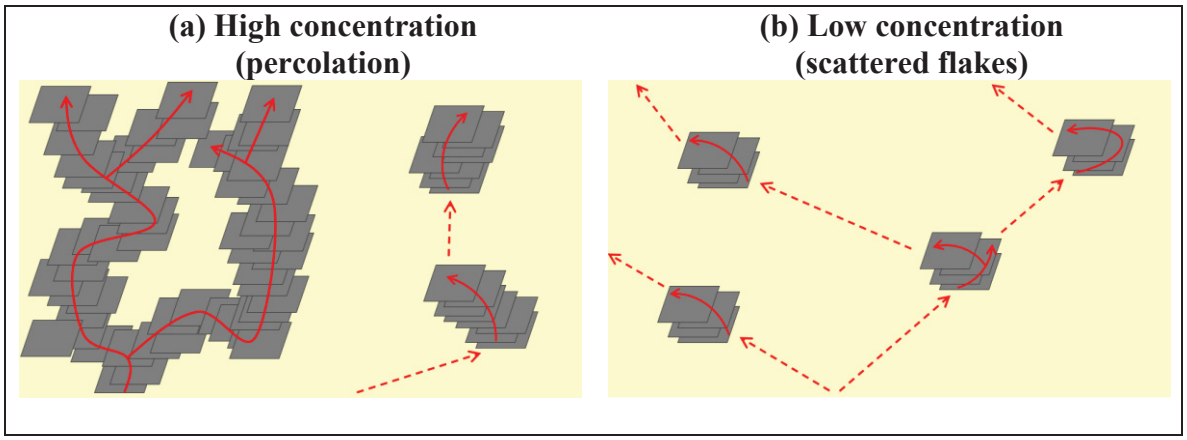

Figure 4.7 – Illustration of possible morphologies presented by nanocomposites under different concentrations: (a) percolated nanocomposite with high content of 2D material; (b) nanocomposite with low content of 2D material. Red arrows indicate possible paths for phonon transport

Since the percolation threshold for conductivity mechanisms is expected to occur only at much higher contents than the ones used in this work (Li et al., 2022; R. Wang et al., 2018), it is likely that any divergence in the intrinsic characteristics of the nanomaterials did not play a large effect on the ultimate performance of the nanocomposites.

Regarding the hybrid systems, the degree of enhancement in thermal conductivity is in general marginally higher than that achieved by the single-filler nanocomposites. This indicates that only a small synergism effect was experimentally observed, as one nanomaterial might interact with the other. This could lead to a minor improvement in the dispersion of the particles, allowing for a larger volume of polymer to be filled by the nanosheets (Ribeiro et al., 2018; Y. Wang et al., 2021). In this scenario, there would be more regions where the phonons could travel through the interface, and the thermal conductivity could be slightly improved.

It's important to highlight that while the improvements achieved may not be as dramatic as those seen in other PA nanocomposites produced through more complex methods or with significantly higher filler contents (Kee et al., 2023; Łątka et al., 2021; Lin et al., 2020; Ren et al., 2020; R. Wang et al., 2018; Zhang et al., 2021), these results are still highly valuable from an industrial perspective. This is because a reasonable enhancement in thermal conductivity could still be achieved by adding very low amounts of 2D materials directly in the extrusion process. Moreover, since this improvement was relatively independent of the added nanomaterial, the most suitable options can be selected based on other criteria relevant to specific applications.

4.3.4 Scanning Transmission Electron Microscopy

Figure 4.8 presents the bright-field STEM images of the single-filler composites and the GO/h-BN hybrid composite at 0.5 wt%. As depicted in Figure 4.8(a,b), GO retains a larger lateral sheet size, thereby increasing its interfacial area with the polymer matrix. In contrast, Figure 4.8(c,d) illustrates the morphology of h-BN, which exhibits a much smaller aspect ratio, appearing as small particles. Notably, this morphology is consistent with the characteristics of the h-BN powder before its incorporation into the polymer. As shown in Figure 4.8(e,f), MoS_2 displays a behavior similar to GO, wherein its sheets maintain a wide aspect when dispersed within the matrix.

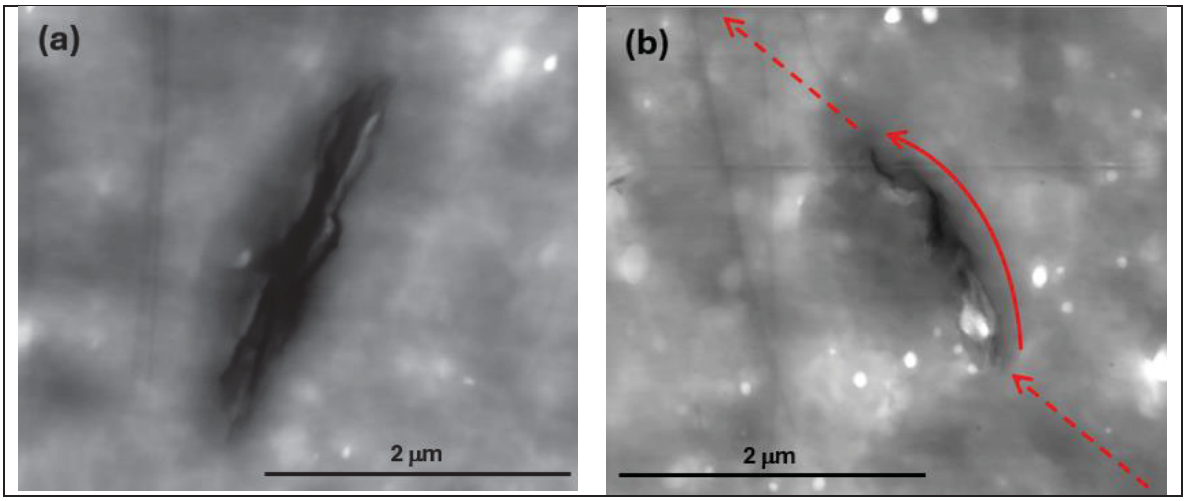

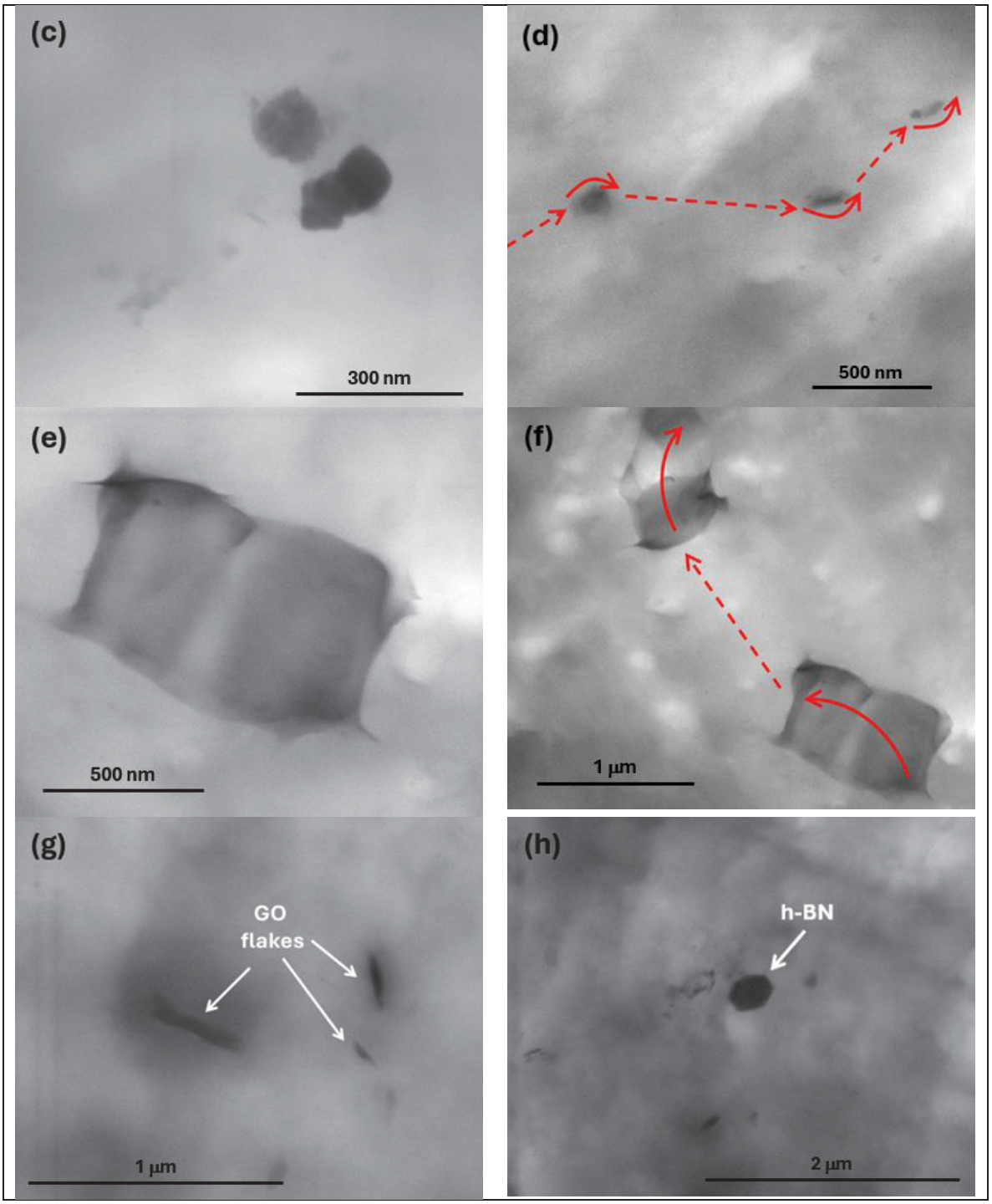

Figure 4.8 – STEM images of PA 1010 nanocomposites at 0.5 wt% for GO (a,b), h-BN (c,d), MoS_2 (e,f), and GO/h-BN (g,h). The red arrows indicate possible phonon pathways, with the dashed lines representing lower conductivity in the polymer, and the full lines representing higher conductivity in the nanomaterials

Regarding the hybrid composite, the micrographs shown in Figure 4.8 (g,h) indicate that, although the nanomaterials appear to remain well dispersed, there is no observed synergism between the different particles, which is consistent with the hypothesis proposed earlier.

Figure 4.8 (b), (d), and (f) also illustrate potential heat conduction pathways in the GO, h-BN, and MoS_2 samples, respectively. No continuous path is formed for phonon transport exclusively along the nanomaterials, which confirms the proposed "scattered flakes" morphology. This observation also elucidates why there was no substantial difference in thermal conductivity among the systems investigated. In all cases, phonons predominantly travel through the polymer matrix, with only short segments exhibiting enhanced conductivity.

4.4 Conclusions

Polymer nanocomposites based on PA 1010 and ultra-low contents of 2D nanomaterials were produced through melt-blending. This approach addresses the growing environmental concerns associated with the sourcing of polymer materials, given that PA 1010 is synthesized from renewable sources, and also showcases the potential of these materials for advanced multifunctional applications. The findings reveal that all the nanomaterials used successfully preserved the dielectric properties of the polymer matrix across a wide temperature range. This is crucial for the packaging of electronic devices, as it prevents current leakages. Furthermore, although COF increased slightly with the addition of nanomaterials, all nanocomposites remained within the acceptable range for solid lubricants. This characteristic makes them suitable for moving parts, thereby enhancing the lifespan and energy efficiency of components. Notably, the major findings stem from thermal conductivity measurements. The nanocomposites displayed thermal conductivities 5 to 10% higher than the neat polymer, even at the ultra-low contents utilized. This improvement is particularly significant for the mentioned applications, as electronic devices and moving parts generate substantial heat that must be dissipated to prevent malfunctions and potential failures. Therefore, this approach should be further explored.

ACKNOWLEDGEMENTS

The authors would like to acknowledge FAPESP – Fundação de Amparo à Pesquisa do Estado de São Paulo (Process 2020/11496-0 and 2021/07858-7), CNPq - Conselho Nacional de Desenvolvimento Científico e Tecnológico (Process 314093/2021-4), NSERC – Natural Sciences and Engineering Research Council of Canada (RGPIN-2018-03888), Mackenzie Research Fund - Mack-Pesquisa (Project #231015, MACK – 0012510), and Coordination of Superior Level Staff Improvement (CAPES), Brazil - Finance Code 001 [PrInt 88887.310339/2018–00] for funding this work. The authors would also like to acknowledge the Laboratory of Structural Characterization, Department of Materials Engineering, Federal University of São Carlos, for use of its general facilities.

CONCLUSION

In this thesis, the influence of two-dimensional nanomaterials (GO, h-BN, and MoS_2) on the molecular dynamics, tensile properties, and multifunctional performance of bio-based PA 1010 nanocomposites was comprehensively investigated. Utilizing differential scanning calorimetry, broadband dielectric spectroscopy, and dynamic mechanical analysis, it was revealed that GO and h-BN present strong molecular interactions with PA 1010, leading to increased enthalpy during the Brill transition and higher glass transition activation energy (E_a). Microstructural analyses showed that h-BN and MoS_2 affected the semi-crystalline order of PA 1010, reducing both the overall crystallinity and the order of the crystalline domains. Tensile tests across different environmental conditions demonstrated that while the nanofillers reduce PA 1010's Young's modulus at the low contents employed, they substantially enhance ductility and toughness, with GO being the most effective at room temperature and h-BN at low temperatures. Additionally, the nanocomposites maintained the dielectric and tribological properties of PA 1010 while increasing its thermal conductivity.

In summary, this thesis presents a novel methodology to assess the interaction between 2D nanomaterials and PA 1010 by establishing a relationship between the Brill transition and the reduced molecular mobility induced by the incorporation of the nanomaterials. The findings also demonstrate that low contents of 2D nanosheets can effectively enhance the tensile toughness of the PA 1010 matrix, not only at ambient conditions but also under a low-temperature environment. While physical interactions with the fillers drive this toughening effect at room temperature, the study identifies a distinct shift at lower temperatures, where these interactions are suppressed, and toughening becomes microstructure dependent. Specifically, the largest reduction in the semi-crystalline order observed in the h-BN composites indicates a transition from filler-driven to microstructure-dominated mechanisms of toughness. Furthermore, this work establishes that the incorporation of minimal filler content does not compromise critical polymer properties, including dielectric and tribological behaviors, while simultaneously achieving improved thermal conductivity. These insights demystify the conventional reliance on high filler loadings to attain desired functional

enhancements, underscoring the effectiveness of low-content nanofillers in producing high-performance polymer nanocomposites.

RECOMMENDATIONS

The following recommendations aim to provide a roadmap for future research to build upon the findings of this study and further advance the understanding and application of the polymer nanocomposites develop in this thesis.

- To explore a broader spectrum of filler compositions to determine the percolation threshold for thermal conductivity. Additionally, identifying the minimum filler content that still effectively enhances the toughness of the polyamide matrix is of great industrial interest;

- To include tensile testing at temperatures lower than -40°C to determine the extent to which microstructural changes influence the toughening of the polyamide matrix. Moreover, performing tensile tests at intermediate temperatures between room temperature and -40°C would be of interest to identify the temperature at which the nanofillers' influence is outweighed by the microstructural effects;

- To study hybrid composites incorporating fillers of varying geometries, such as 0D, 1D, and 2D structures. This approach may facilitate enhanced interactions between fillers. Furthermore, investigating hierarchical systems by combining nanofillers with fillers of different scales, such as micrometric fibers (e.g., glass or carbon fibers), could bring the studied composites closer to industrial applications;

- Conducting thermal conductivity tests at higher temperatures, as existing literature suggests that the effects of nanofillers are amplified at elevated temperatures due to increased molecular and phonon mobility.

ANNEX I

SUPPORTING INFORMATION

Exploring the Relationship Between Interfacial Adhesion, Molecular Dynamics, and the Brill Transition in Fully Bio-Based Polyamide 1010 Nanocomposites Reinforced by Two-Dimensional Materials

Gabriel M. Pinto[1,2,3], Aelton B. Santos[4], Emna Helal[1], Hélio Ribeiro[2], Eric David[1], Cristiano F. Woellner[4], Nicole R. Demarquette[1], Guilhermino J. M. Fechine[2,3]

1 Department of Mechanical Engineering, École de Technologie Supérieure, Montréal, QC, Canada
2 Engineering School, Mackenzie Presbyterian University, São Paulo, SP, Brazil
3 Mackenzie Institute of Research in Graphene and Nanotechnologies – MackGraphe, Mackenzie Presbyterian Institute, São Paulo, SP, Brazil
4 Physics Department, Federal University of Parana – UFPR, Curitiba, PR, Brazil

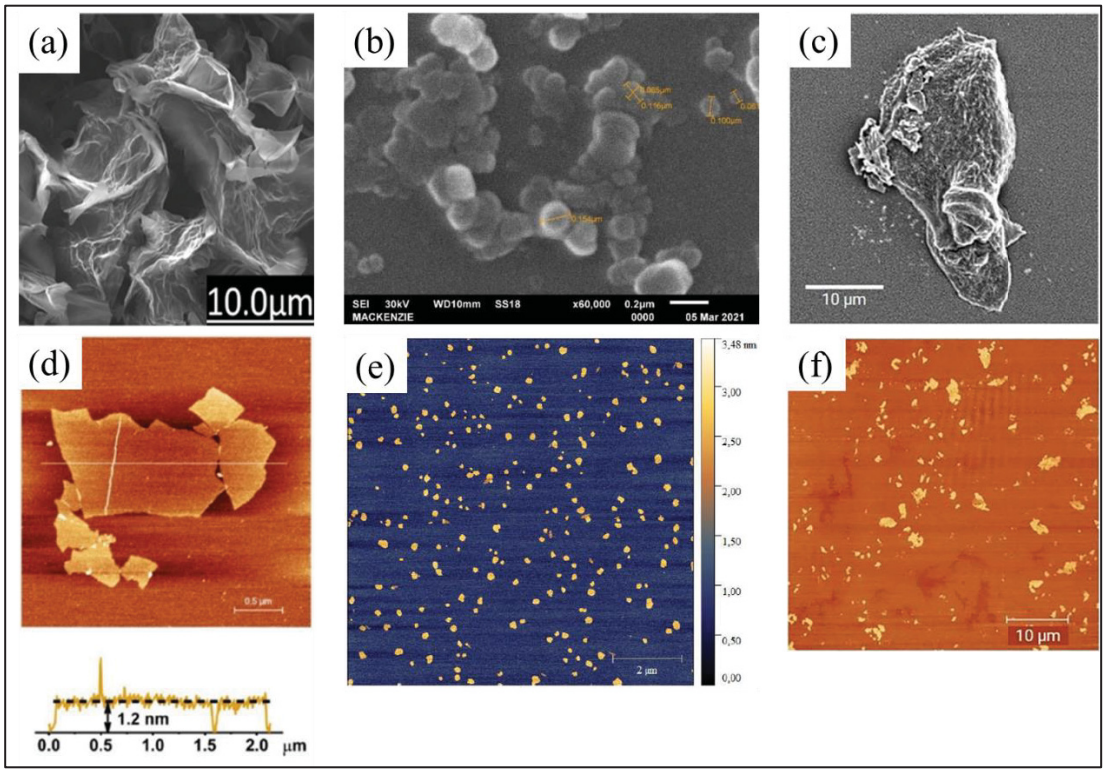

Figure A I-1 – SEM (a – c) and AFM (d – f) images of the exfoliated GO (a,d), h-BN (b,e), and MoS_2 (c,f). (a,d) are reproduced from (Andrade et al., 2021). Copyright © 2021 MDPI.

(b,e) are reproduced from (Kalupgian, 2021). (c,f) are reproduced from (Marciano de Oliveira Cremonezzi et al., 2022). Copyright © 2022 Elsevier

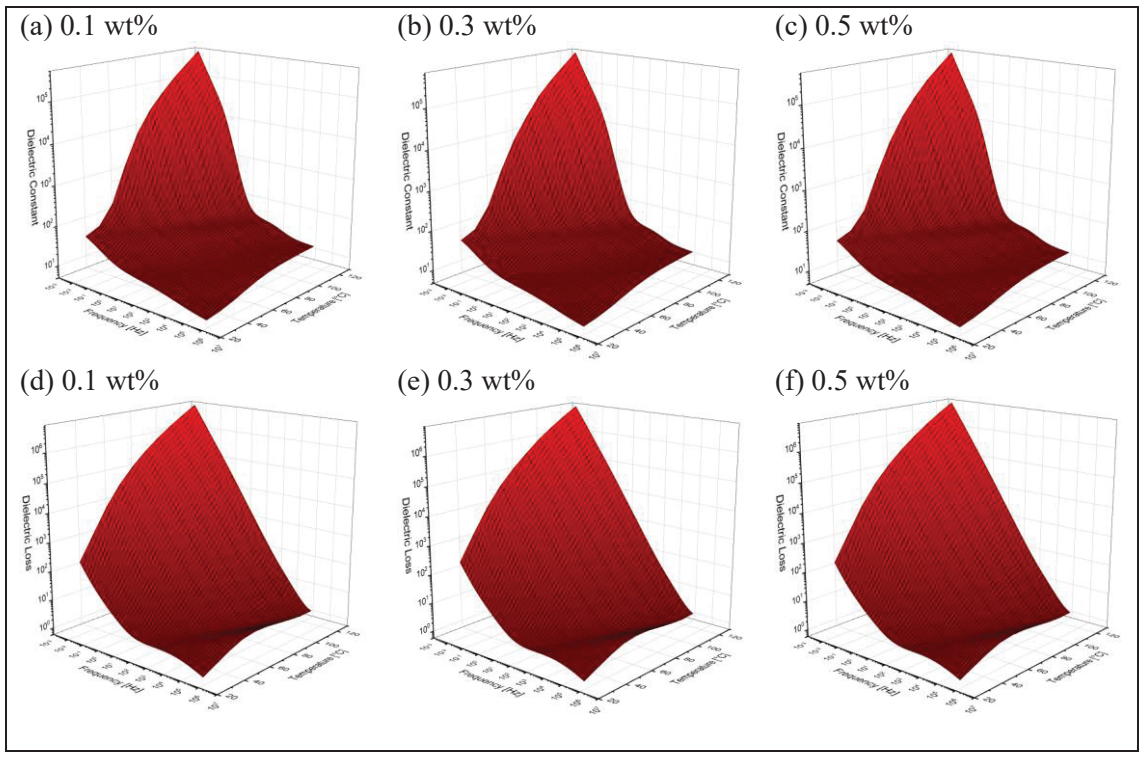

Figure A I-2 – Measured dielectric constant (a-c) and dielectric loss (d-f) of the GO nanocomposites

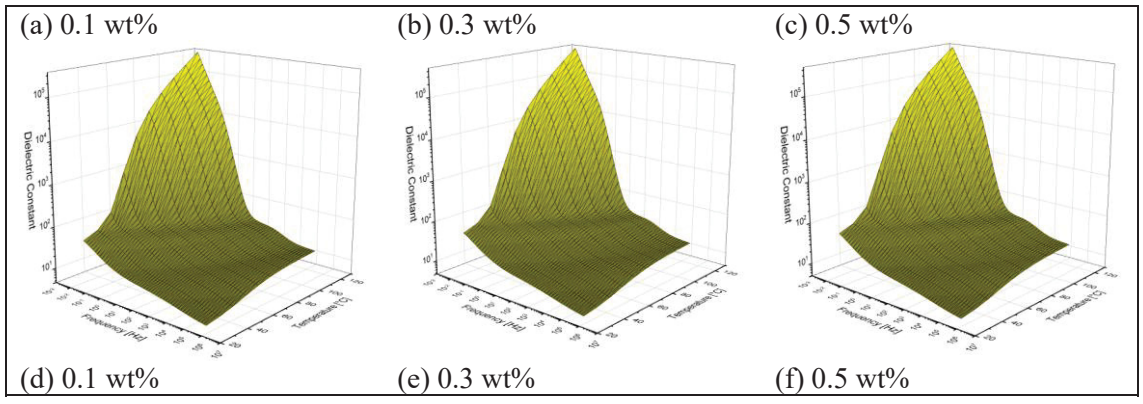

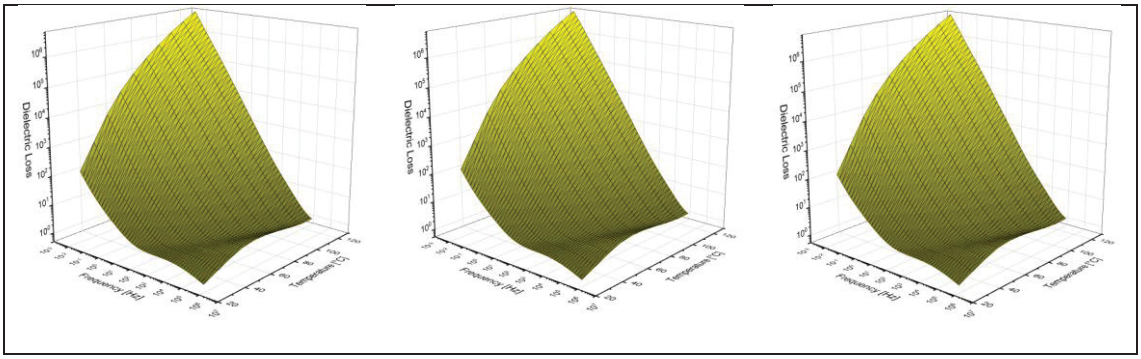

Figure A I-3 – Measured dielectric constant (a-c) and dielectric loss (d-f) of the h-BN nanocomposites

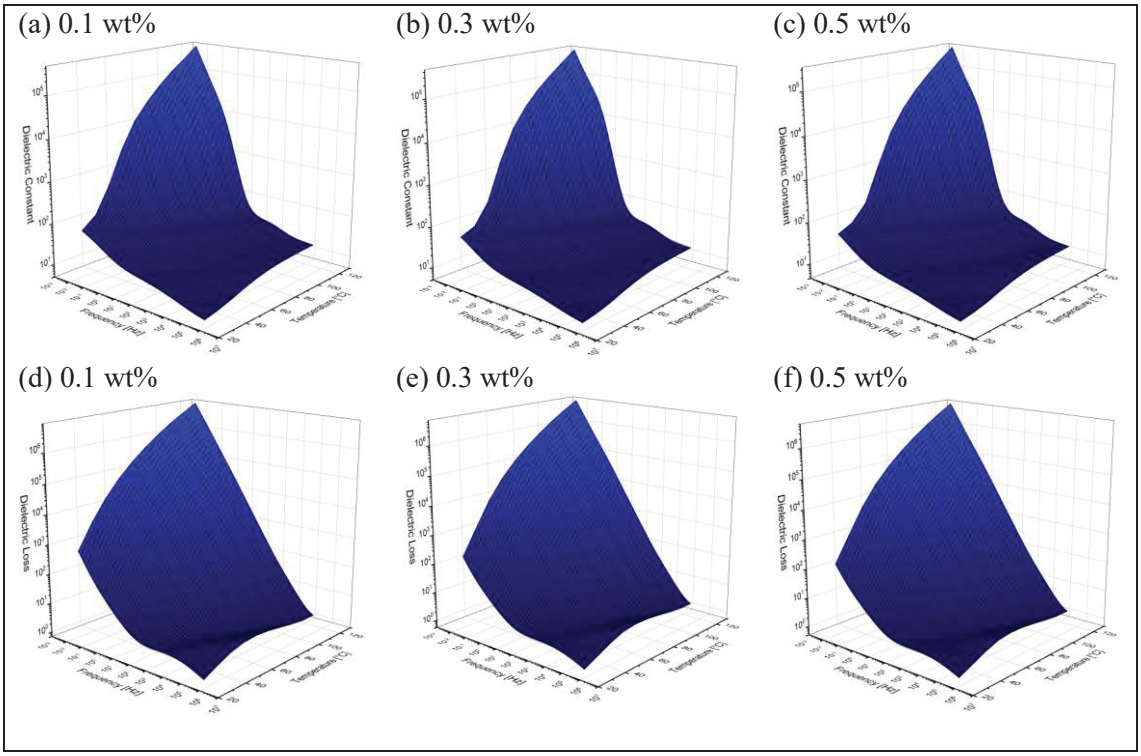

Figure A I-4 – Measured dielectric constant (a-c) and dielectric loss (d-f) of the MoS_2 nanocomposites

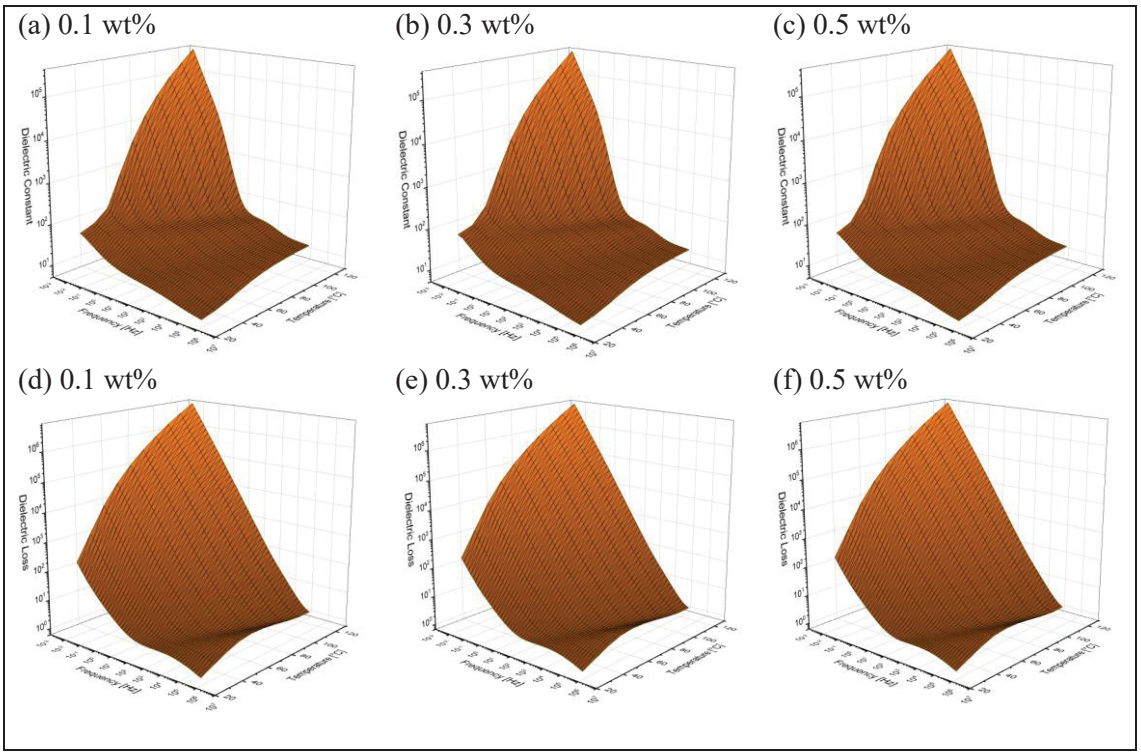

Figure A I-5 – Measured dielectric constant (a-c) and dielectric loss (d-f) of the GO@h-BN nanocomposites

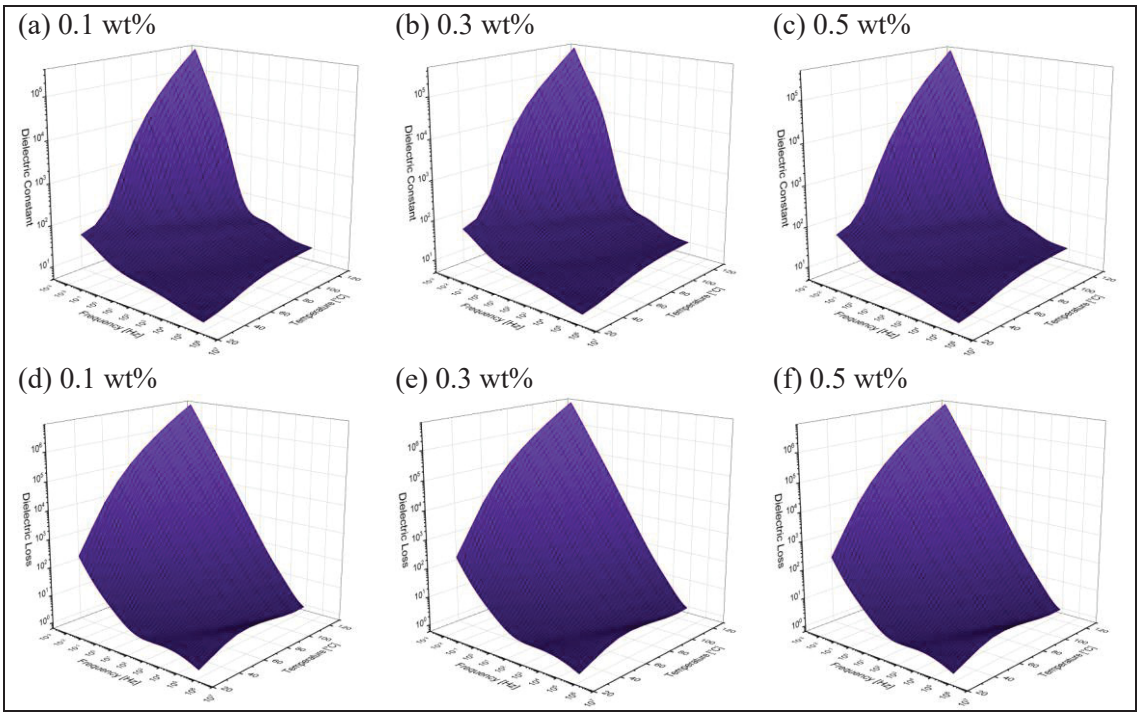

Figure A I-6 – Measured dielectric constant (a-c) and dielectric loss (d-f) of the MoS_2@GO nanocomposites

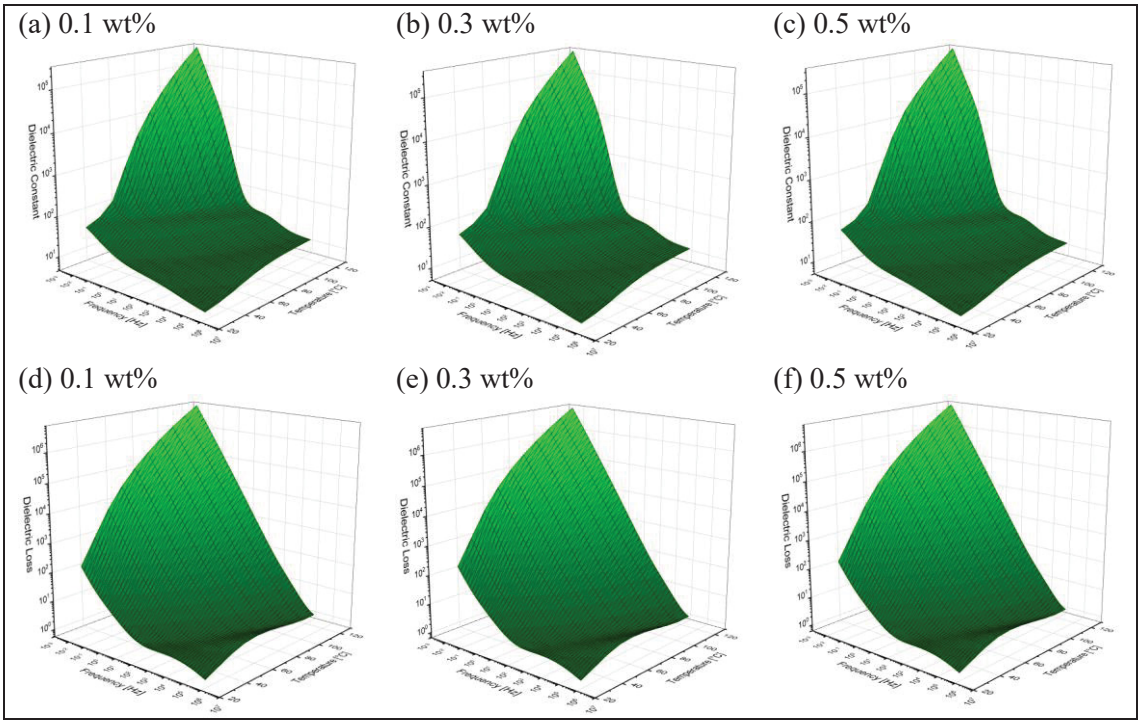

Figure A I-7 – Measured dielectric constant (a-c) and dielectric loss (d-f) of the h-BN@MoS_2 nanocomposites

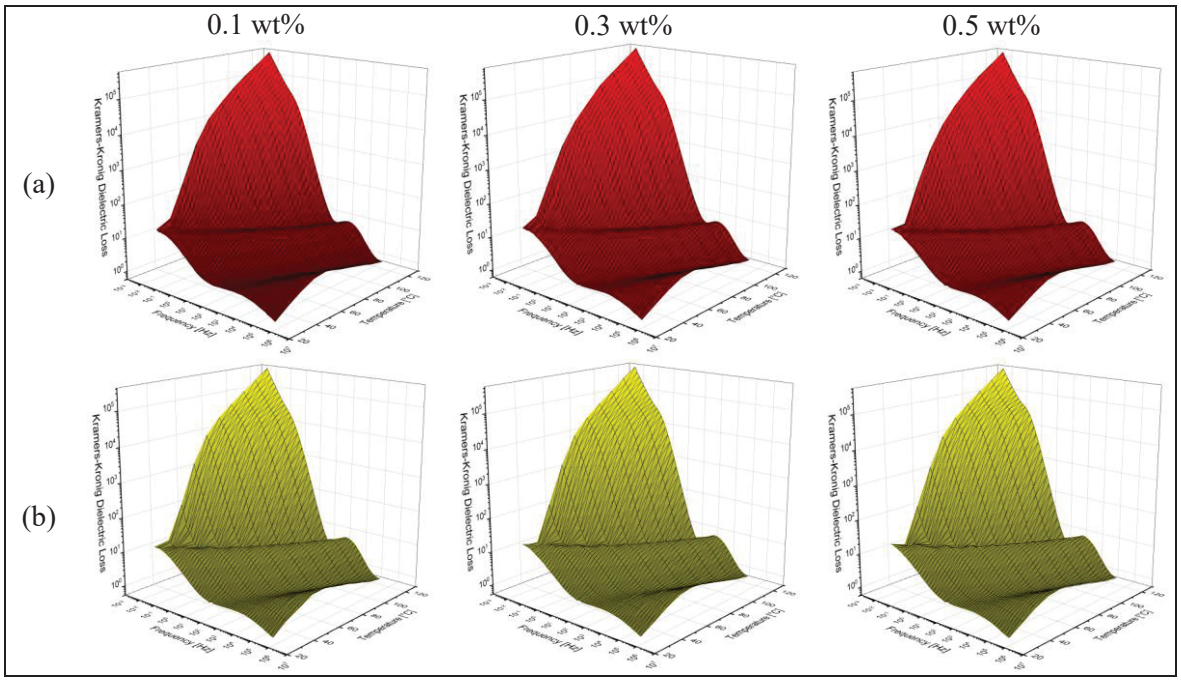

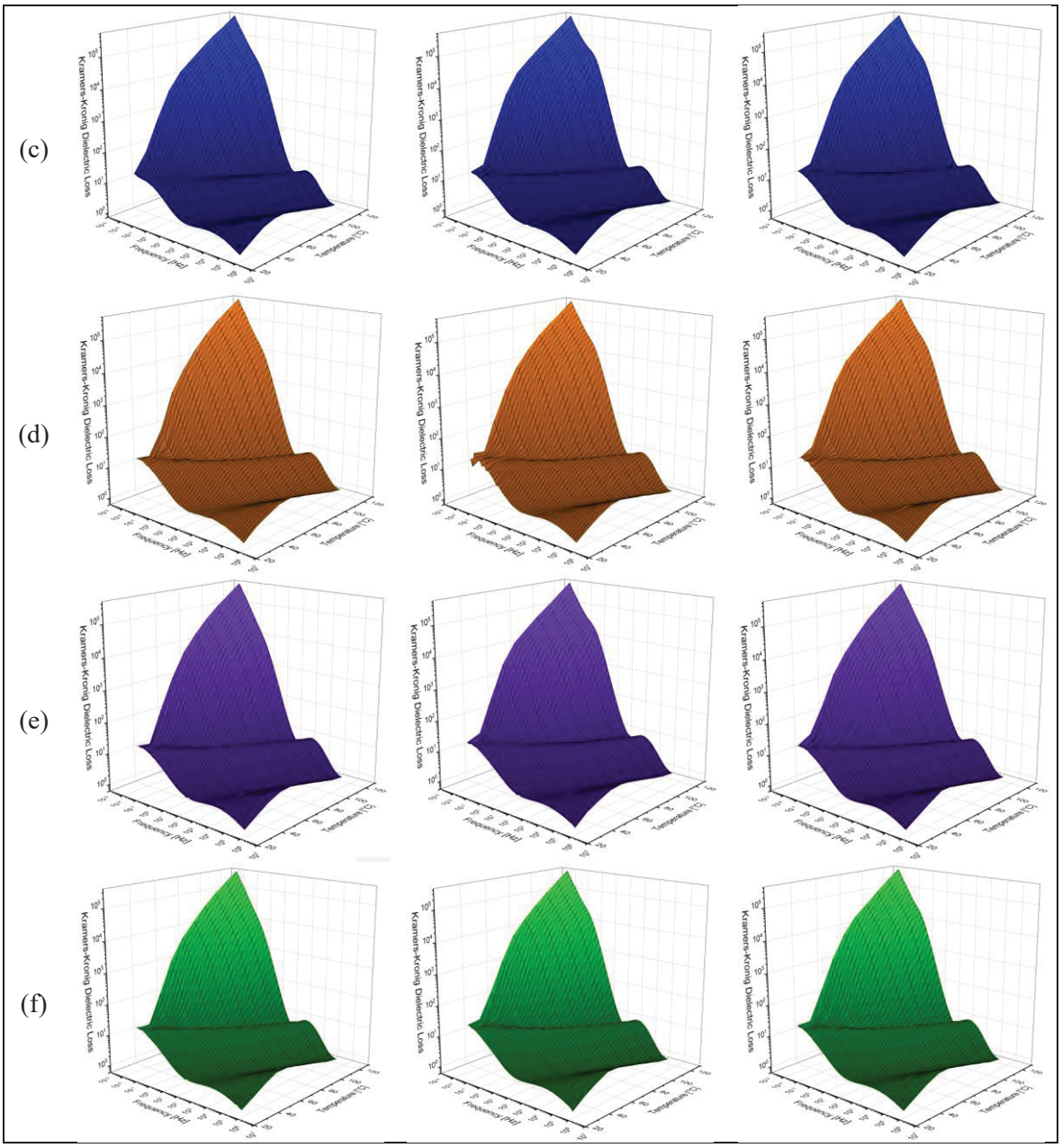

Figure A I-8 – Dielectric loss of the nanocomposites calculated from the Kramers-Kronig relationship: (a) GO; (b) h-BN; (c) MoS_2; (d) GO@h-BN; (e) MoS_2@h-BN; (f) h-BN@MoS_2

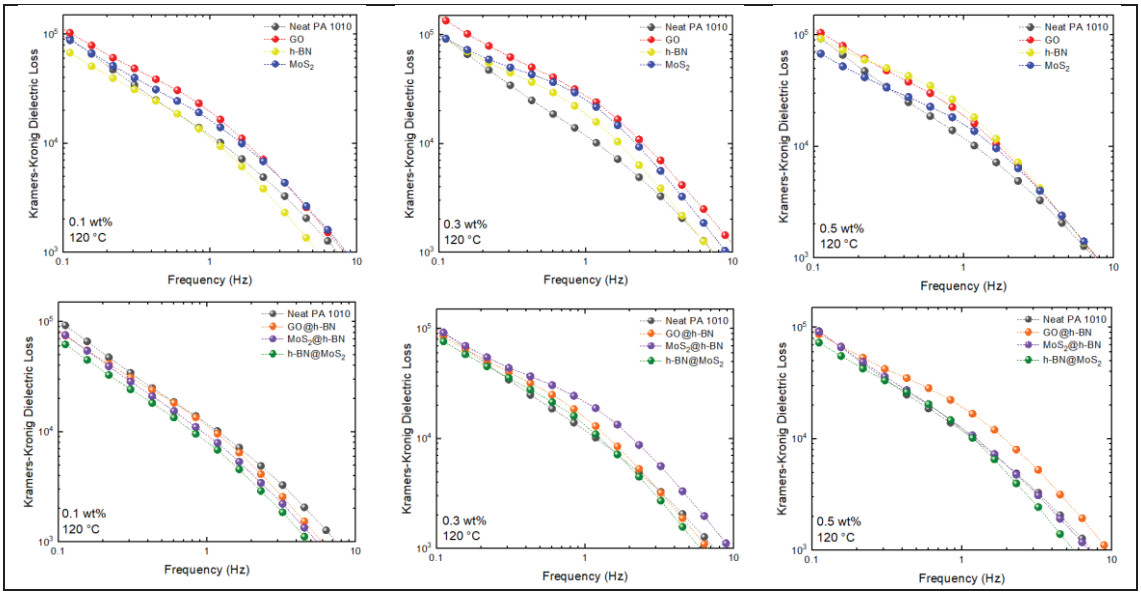

Figure A I-9 – MWS polarization of the single-filler composites (top), and hybrid-filler composites (bottom), at 120 °C observed in the Kramers-Kronig transformed dielectric loss curves

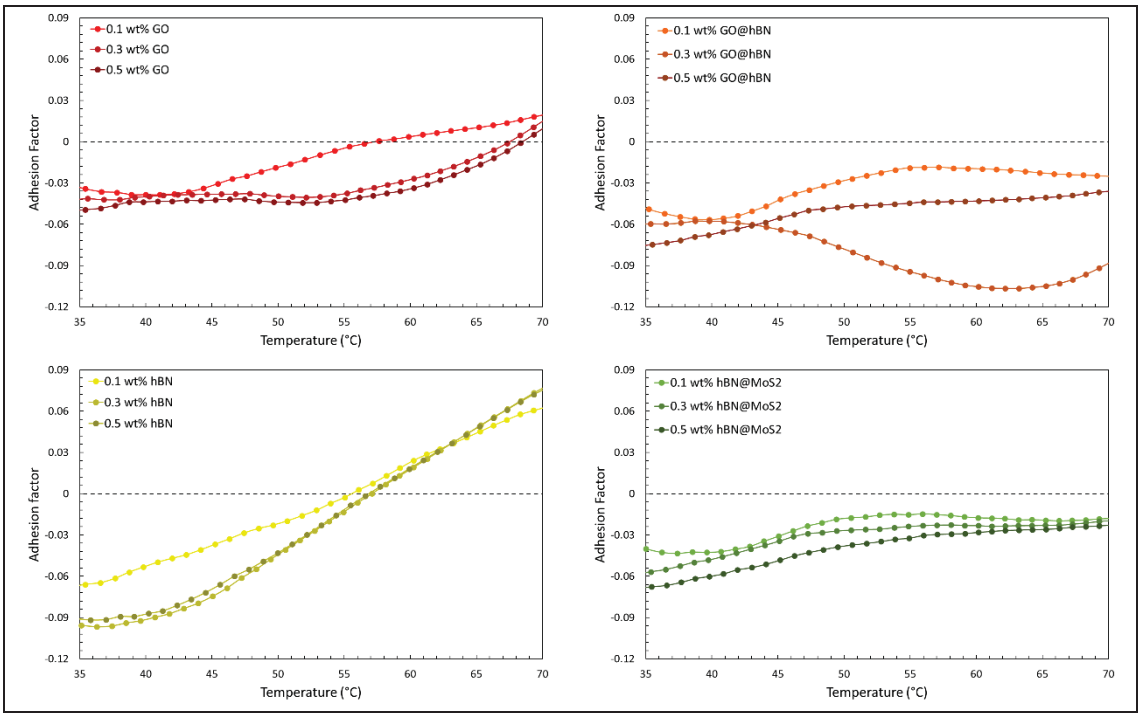

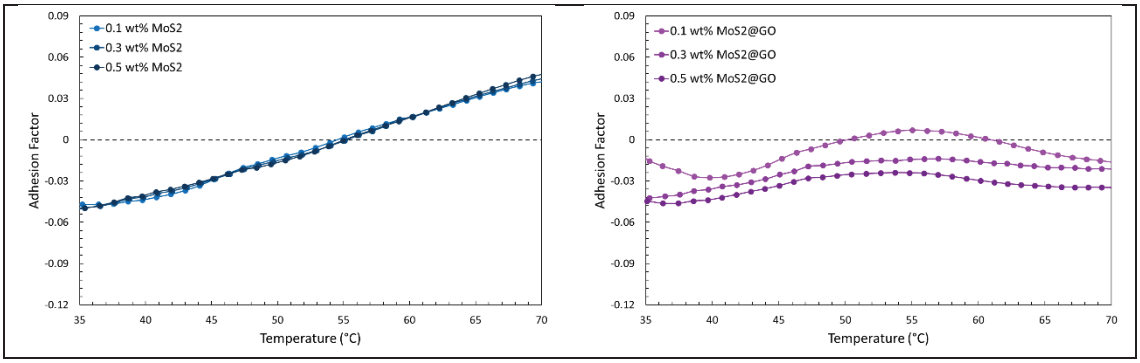

Figure A I-10 – Adhesion factor as a function of temperature for all the studied nanocomposites

ANNEX II

SUPPORTING INFORMATION

Effect of Environmental Temperature on the Toughening of Polyamide 1010 by 2D Nanomaterials

Gabriel M. Pinto[1,2,3], Emna Helal[1], Hélio Ribeiro[2], Eric David[1], Nicole R. Demarquette[1], Guilhermino J. M. Fechine[2,3]

1 Department of Mechanical Engineering, École de Technologie Supérieure, Montréal, QC, Canada
2 Engineering School, Mackenzie Presbyterian University, São Paulo, SP, Brazil
3 Mackenzie Institute of Research in Graphene and Nanotechnologies – MackGraphe, Mackenzie Presbyterian Institute, São Paulo, SP, Brazil

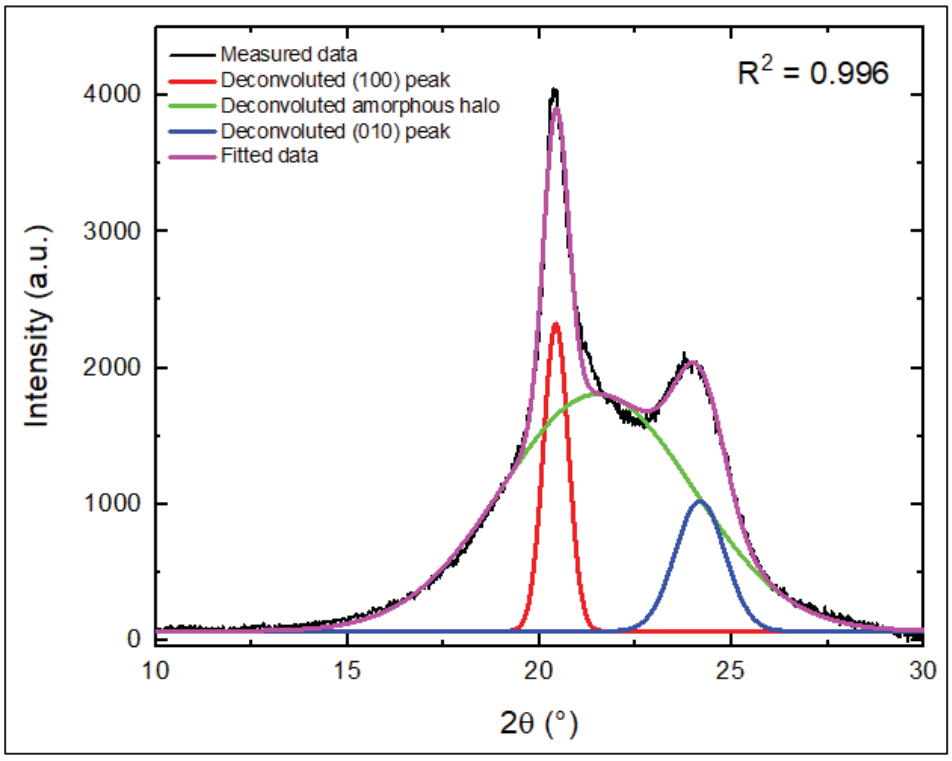

Figure A II-1 – Deconvolution of diffraction peaks for neat PA 1010

Description of environmental chamber's assembly:

The temperature setpoint of the environmental chamber used for the tensile tests at -40 °C is manually adjusted and the controller manages the ramping and regulating. The assembly was

set up by placing the chamber on the bedframe of the MTS Alliance RF-200 machine, making sure it was leveled and centered. Then, cold resistant extensions were placed on the machine to insulate the loadcell and frame from extreme cold. The mechanical grips, which are also cold resistant, are then attached at the ends of those extensions. To allow the liquid nitrogen input, an insulated hose is attached to a 240 L Dewar at one end, and the other end is connected to a port on the back of the chamber. This port is connected to a solenoid valve. After this setup, the liquid valve on the Dewar can be opened, and let the liquid nitrogen starts to flow. Since the setpoint is adjusted on the controller, it automatically manages the opening and closing of the valve to inject the right amount of nitrogen to the system. The controller works in conjuncture with the heating element of the chamber to manage the perfect temperature setpoint. From room temperature, it would take about 5 to 10 min to stabilize the temperature at -40 °C. Figure A II-2 presents a picture of the chamber assembly.

Figure A II-2 – Assembly of the environmental chamber coupled to the Alliance RF/200 MTS universal testing machine used for the ambience of the tensile tests at -40 °C

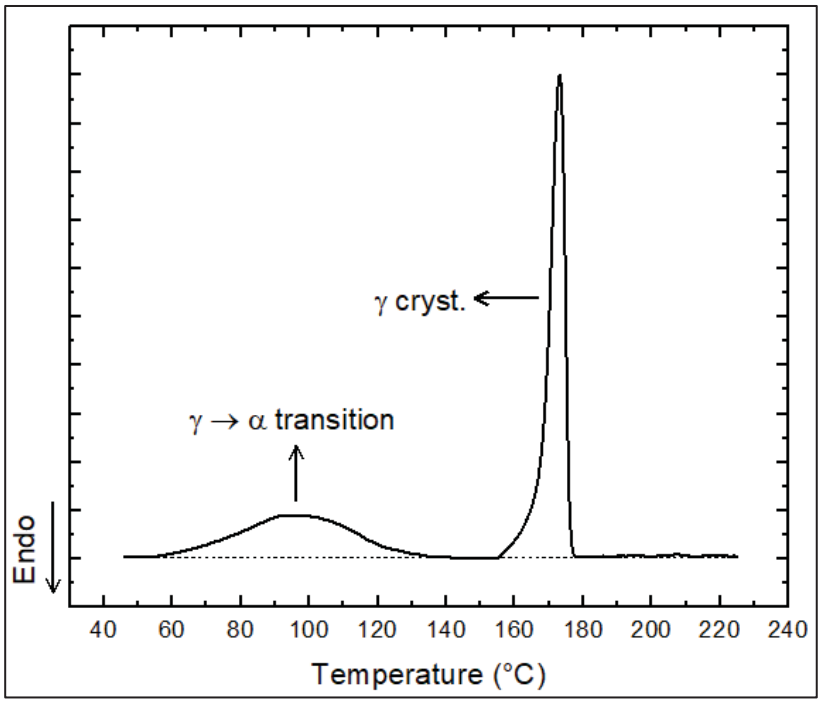

Figure A II-3 – DSC cooling curve of neat PA 1010 with assignments to each exothermic event

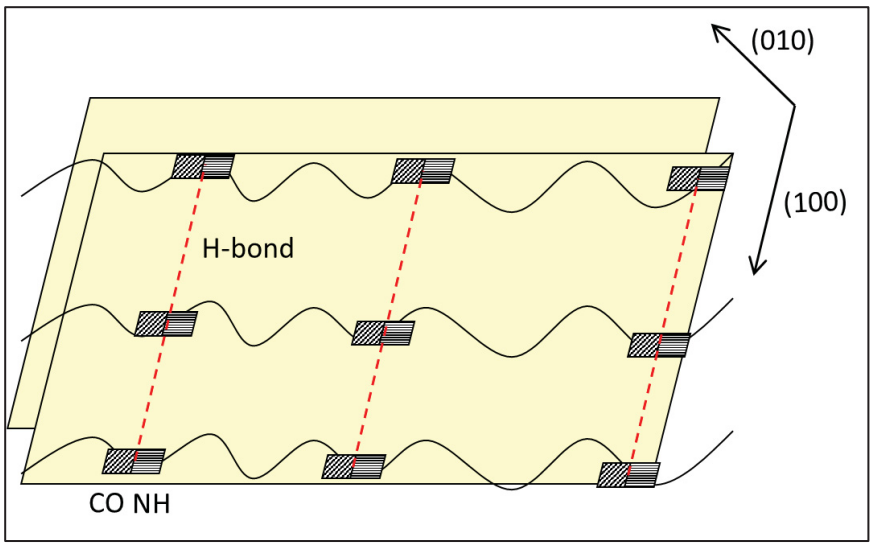

Figure A II-4 - Illustration of PA 1010's α crystal structure as a function of the hydrogen bonds' orientation, highlighting the intrasheet orientation of the (100) plane, and the intersheet orientation of the (010) plane

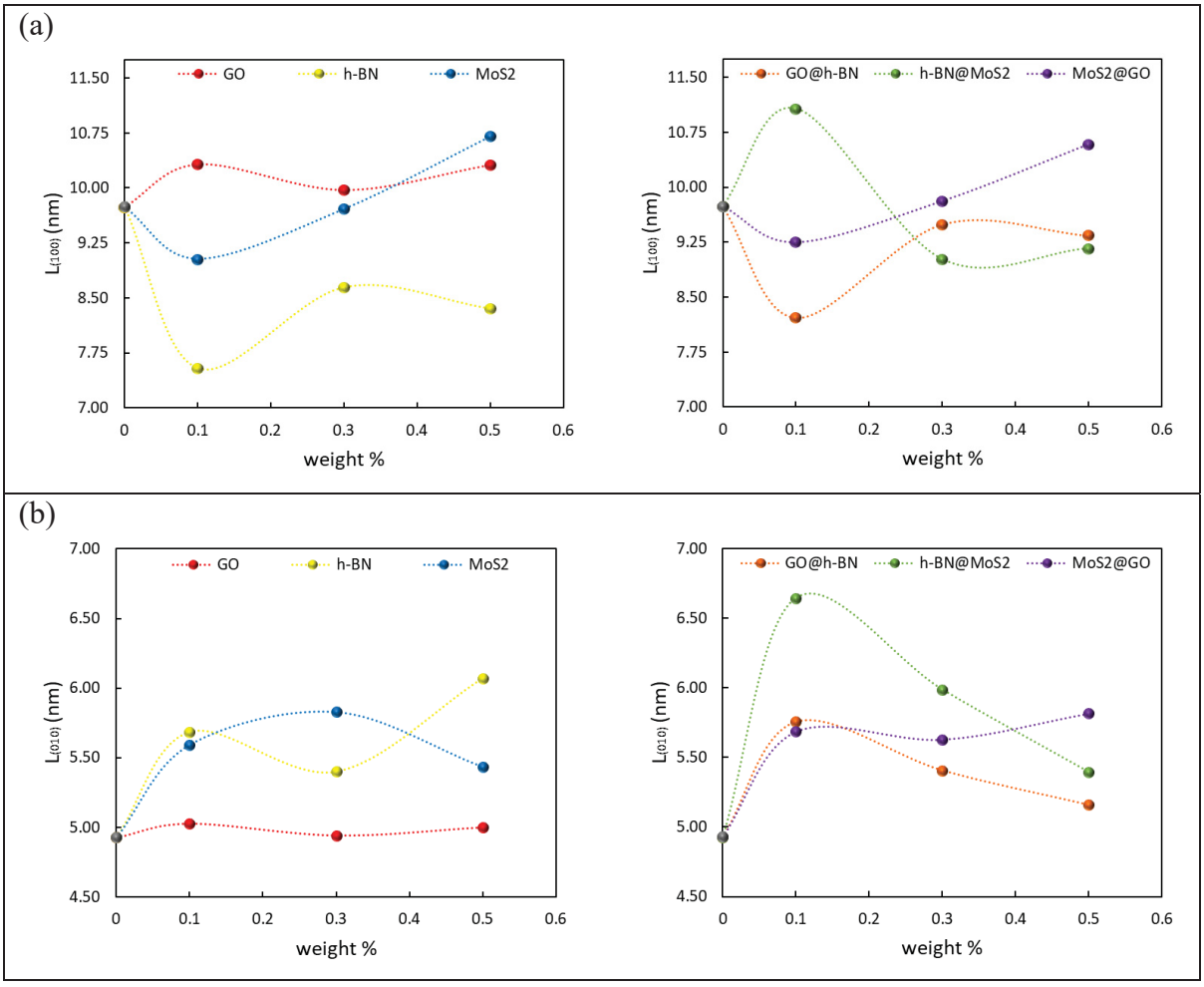

Figure A II-5 – Changes in the crystalline lamella thickness of the (100) (a), and (010) (b) diffraction peaks of the α crystalline structure of PA 1010 by the addition of different 2D materials

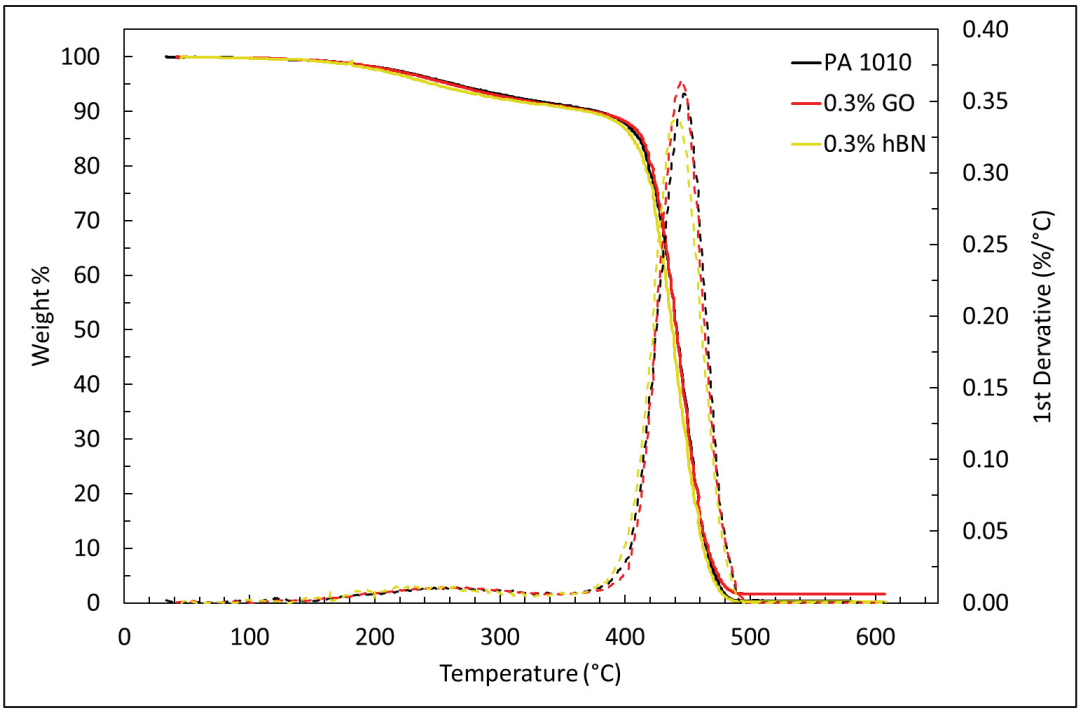

Figure A II-6 – TGA and DTG curves of neat PA 1010, 0.3 wt% GO composite, and 0.3 wt% h-BN composite

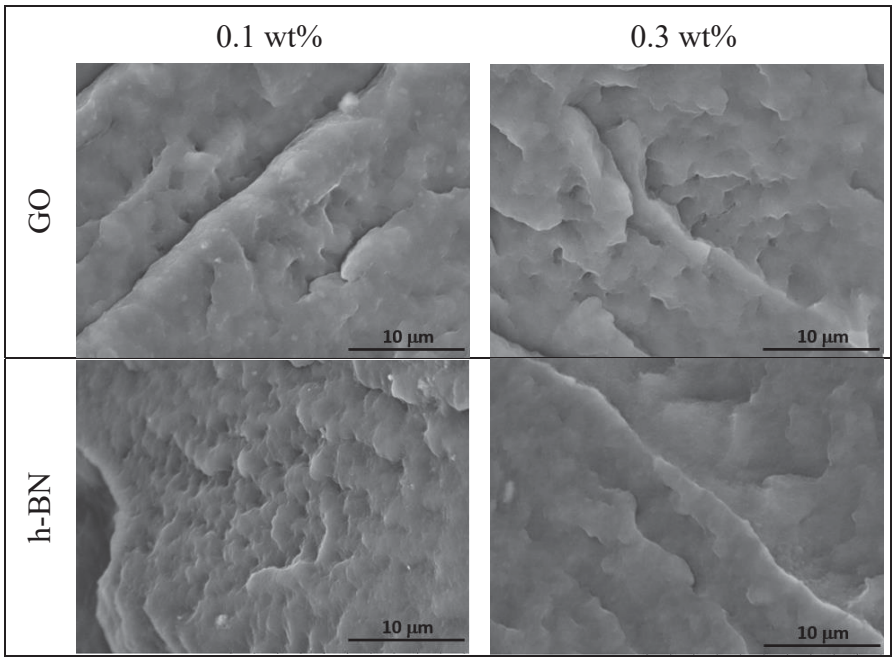

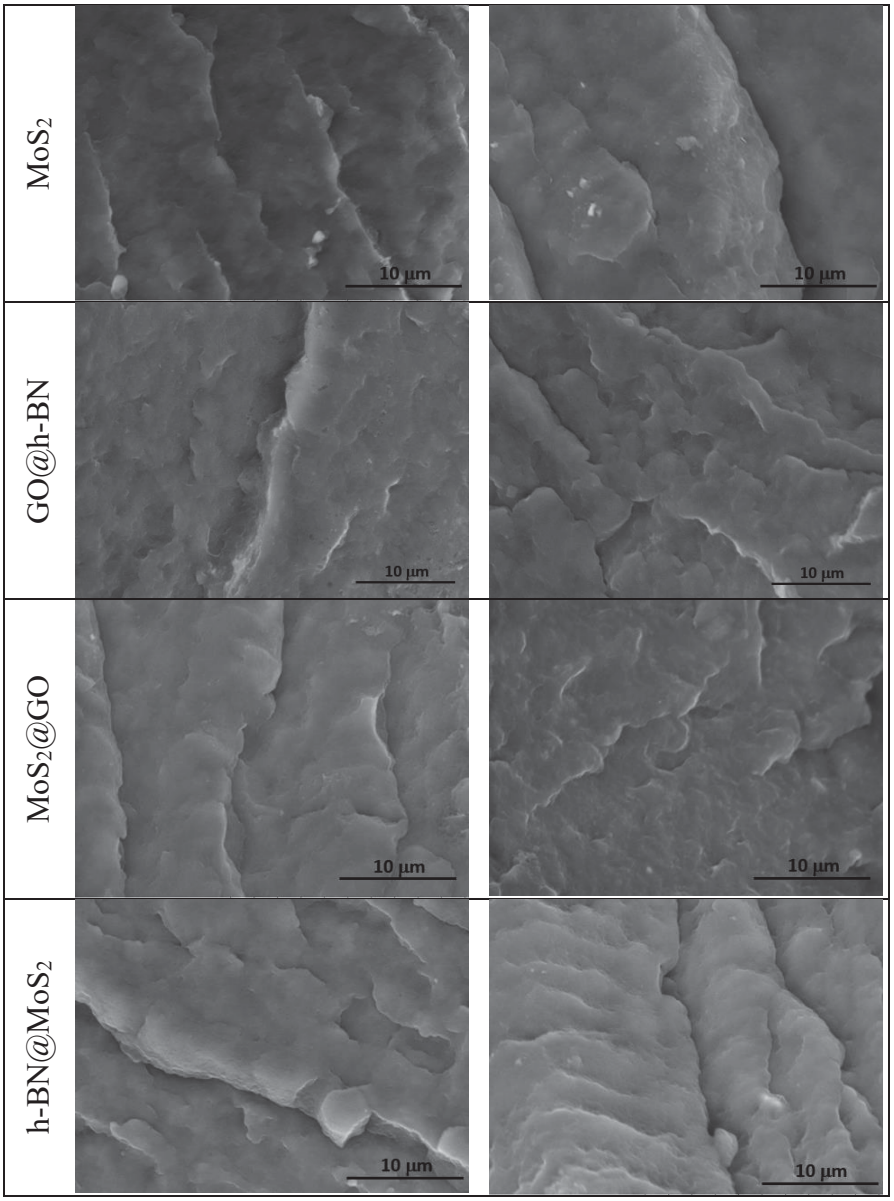

Figure A II-7 – SEM images of cryo-fractured surfaces for the nanocomposites reinforced by 0.1 and 0.3 wt% nanoparticles

APPENDIX
VITA

EDUCATION

- *Doctor of Philosophy in Mechanical Engineering* - École de Technologie Supérieure (ÉTS). Supervisor: Prof. Nicole R. Demarquette, Co-supervisor: Prof. Eric David. From January 2022 to November 2024. Montréal, QC – Canada.
- *Doctor of Philosophy in Materials Engineering and Nanotechnology* – Mackenzie Presbyterian University. Supervisor: Prof. Guilhermino J.M. Fechine, Co-supervisor: Prof. Hélio Ribeiro. From August 2020 to September 2024. São Paulo, SP – Brazil.
- *Master of Science in Materials Engineering and Nanotechnology* - Mackenzie Presbyterian University. Supervisor: Prof. Guilhermino J.M. Fechine. From February 2018 to July 2020. São Paulo, SP – Brazil.
- *Bachelor in Materials Engineering* – The University Center of FEI. From February 2013 to December 2017. São Bernardo do Campo, SP – Brazil.

AWARDS AND SCHOLARSHIPS

- RRECQ Research Grant - École de Technologie Supérieure (ÉTS), Montreal, QC – Canada, 2023.
- Conference travel award – Society of Plastics Engineers (SPE), Montréal, QC – Canada, 2023.
- Conference travel award – École de Technologie Supérieure (ÉTS), Montreal, QC – Canada, 2023.
- NSERC Research Grant - École de Technologie Supérieure (ÉTS), Montreal, QC – Canada, 2022.
- FAPESP BEPE Fellowship (Ph.D.) - Mackenzie Presbyterian University, São Paulo, SP – Brazil, 2022.
- FAPESP Ph.D. Fellowship - Mackenzie Presbyterian University, São Paulo, SP – Brazil, 2021.

- FAPESP BEPE Fellowship (M.Sc.) - Mackenzie Presbyterian University, São Paulo, SP – Brazil, 2019.
- FAPESP M.Sc. Fellowship - Mackenzie Presbyterian University, São Paulo, SP – Brazil, 2019.
- Certificate of Merit - Regional Chemistry Council - IV Region, São Paulo, SP – Brazil, 2018.
- Institute of Engineering Award - Institute of Engineering, São Paulo, SP – Brazil, 2018.
- Fábio Décourt Homem de Melo Award - Brazilian Metallurgy Association (ABM), São Paulo, SP – Brazil, 2018.
- Certificate of Merit - Regional Council of Engineering and Agronomy – SP, São Paulo, SP – Brazil, 2018.
- Academic Prominence - The University Center of FEI, São Bernardo do Campo, SP – Brazil, 2016.
- Best Student of the Materials Engineering Department - The University Center of FEI, São Bernardo do Campo, SP – Brazil, 2015.

JOURNAL PUBLICATIONS

- Pinto, G.M., Staffa, L., Helal, E., Hahn, C., Vieira, L., Ribeiro, H., David, E., Demarquette, N.R., Fechine, G.J.M. 2D Nanomaterials Balance Thermal, Dielectric, and Tribological Behavior in Polyamide 1010. Journal of Applied Polymer Science (Accepted).
- Pinto, G.M., Helal, E., Ribeiro, H., David, E., Demarquette, N.R., Fechine, G.J.M., 2024. Effect of Environmental Temperature and Semi-Crystalline Order on the Toughening of Polyamide 1010 by 2D Nanomaterials. Polymer Composites (In Press).
- Silva, B.M.O., Fernandes, N.M.M., Barbosa, J.M., Pinto, G.M., Benega, M.A.G., Taha-Tijerina, J.J., Andrade, R.J.E., Ribeiro, H., 2024. Thermomechanical properties of multifunctional polymer hybrid nanocomposites based on carbon nanotubes and nanosilica. Journal of Applied Polymer Science, e56054.
- Pinto, L.A., Backes, E.H., Harb, S.V., Pinto, G.M., da Cunha, D.A.L.V., Andrade, R.J.E., Fechine, G.J.M., Selistre-de-Araújo, H.S., Costa, L.C. and Pessan, L.A., 2024.

Shape memory thermoplastic polyurethane/polycaprolactone blend and composite with hydroxyapatite for biomedical application. Journal of Materials Research, 39(1), pp.90-106.

- Pinto, G.M., Santos, A.B., Helal, E., Ribeiro, H., David, E., Woellner, C.F., Demarquette, N.R. and Fechine, G.J., 2023. Exploring the relationship between interfacial adhesion, molecular dynamics, and the brill transition in fully bio-based polyamide 1010 nanocomposites reinforced by two-dimensional materials. Polymer, 289, p.126482.
- de Oliveira Cremonezzi, J.M., Pinto, G.M., Mincheva, R., Andrade, R.J.E., Raquez, J.M. and Fechine, G.J.M., 2023. The micromechanics of graphene oxide and molybdenum disulfide in thermoplastic nanocomposites and the impact to the polymer-filler interphase. Composites Science and Technology, 243, p.110236.
- Ribeiro, H., Taha-Tijerina, J.J., Gomez, O., Acosta, E., Pinto, G.M., Moraes, L.R., Fechine, G.J., Andrade, R.J., Reinoza, J., Padilla, V. and Lozano, K., 2023. Thermal Transport and Rheological Properties of Hybrid Nanofluids Based on Vegetable Lubricants. Nanomaterials, 13(20), p.2739.
- Pinto, G.M., Cremonezzi, J.M., Ribeiro, H., Andrade, R.J., Demarquette, N.R. and Fechine, G.J., 2023. From two-dimensional materials to polymer nanocomposites with emerging multifunctional applications: a critical review. Polymer Composites, 44(3), pp.1438-1470.
- Maldonado, M.P., Pinto, G.M., Costa, L.C. and Fechine, G.J., 2022. Enhanced thermally conductive TPU/graphene filaments for 3D printing produced by melt compounding. Journal of Applied Polymer Science, 139(25), p.e52405.
- de Souza, Z.S., Pinto, G.M., Silva, G.D.C., Demarquette, N.R., Fechine, G.J. and Sobrinho, M.A., 2021. Interface adjustment between poly (ethylene terephthalate) and graphene oxide in order to enhance mechanical and thermal properties of nanocomposites. Polymer Engineering & Science, 61(7), pp.1997-2011.
- Pinto, G.M., Silva, G.D.C., Santillo, C., Lavorgna, M., Maia, J.M. and Fechine, G.J., 2020. Crystallization kinetics, structure, and rheological behavior of poly (ethylene

terephthalate)/multilayer graphene oxide nanocomposites. Polymer Engineering & Science, 60(11), pp.2841-2851.

- Pinto, G.M., Silva, G.D.C. and Fechine, G.J., 2020. Effect of exfoliation medium on the morphology of multi-layer graphene oxide and its importance for Poly (Ethylene terephthalate) based nanocomposites. Polymer Testing, 90, p.106742.

CONFERENCE PRESENTATIONS

- G. M. Pinto, E. Helal, H. Ribeiro, E. David, N. R. Demarquette, G. J. M. Fechine. Effect of Temperature on the Tensile Behavior of Polyamide 1010 Nanocomposites Reinforced by Different Two-dimensional Material / 39th International Conference of the Polymer Processing Society (PPS39). Cartagena de Indias, Colombia – May 2024. (Oral)
- G. M. Pinto, E. Helal, H. Ribeiro, E. David, N. R. Demarquette, G. J. M. Fechine. Hybrid Multifunctional Nanocomposites Based on Polyamide 10.10 and 2D Nanomaterials / 17th Brazilian Polymer Conference (CBPOL 17). Joinville, SC, Brazil – October 2023. (Poster)
- G. M. Pinto, E. Helal, H. Ribeiro, E. David, N. R. Demarquette, G. J. M. Fechine. Use of Kramers-Kronig Transform and Vogel-Fulcher-Tammann Equation to Probe the Molecular Dynamics of Polyamide 10.10 Nanocomposites / Conference on Electrical Insulation and Dielectric Phenomena. New Jersey, NJ, USA. October 2023. (Oral)
- G. M. Pinto, E. Helal, H. Ribeiro, E. David, N. R. Demarquette, G. J. M. Fechine. Green Polyamide 1010 Nanocomposites Based on Hybrid Two-Dimensional Nanomaterials: Effects on Microstructure and Crystallization Kinetics / 38th International Conference of the Polymer Processing Society (PPS38). Olma Messen St. Gallen, Switzerland – May 2023. (Oral)
- G. M. Pinto, H. Ribeiro, E. David, N. R. Demarquette, G. J. M. Fechine. Effect of Different Two-dimensional Nanomaterials on the Microstructural Evolutions of Green Polyamide 1010 / ANTEC 2023. Denver, CO, USA – March 2023. (Poster)
- G. M. Pinto, H. Ribeiro, E. David, N. R. Demarquette, G. J. M. Fechine Microstructural Analysis of Nanocomposites Based on Green Polyamide and 2D Materials /

COLLOQUE ÉTUDIANT CREPEC. Montreal, QC, Canada - December 2022. (Poster)

- G. M. Pinto, G. C. Silva G. J. M. Fechine. Influence of Multi-Layer Graphene Oxide Distribution on the Microstructure and Mechanical Properties of Poly(Ethylene Terephthalate) Nanocomposites / 16th Brazilian Polymer Conference (CBPOL 16). Ouro Preto, MG, Brazil – October 2021. (Oral)
- G. M. Pinto, G. C. Silva G. J. M. Fechine, J. Maia. Effect of Different Shear Stresses on the Rheological Behavior of Poly(Ethylene Terephthalate)/Graphene Oxide Nanocomposites / 18th World Congress on Rheology (ICR 2020). Rio de Janeiro, RJ, Brazil – August 2020. (Oral)
- G. M. Pinto, G. C. Silva G. J. M. Fechine. Nanocompósitos Multifuncionais de PET/GO / 15th Brazilian Polymer Conference (CBPOL 15). Bento Gonçalves, RS, Brazil – October 2019. (Poster)

BIBLIOGRAPHY

Abd Malek, N. A., Alias, N., Md Saad, S. K., Abdullah, N. A., Zhang, X., Li, X., … Zhan, Y. (2020). Ultra-thin MoS2 nanosheet for electron transport layer of perovskite solar cells. *Optical Materials*, *104*, 109933. https://doi.org/10.1016/j.optmat.2020.109933

Acerce, M., Voiry, D., & Chhowalla, M. (2015). Metallic 1T phase MoS2 nanosheets as supercapacitor electrode materials. *Nature Nanotechnology*, *10*(4), 313–318. https://doi.org/10.1038/nnano.2015.40

Addou, R., & Colombo, L. (2022). Defects in Two-Dimensional Materials. In *Defects in Two-Dimensional Materials*. Elsevier.

Aghajani, A., Ehsani, M., Khajavi, R., Kalaee, M., & Zaarei, D. (2022). Thermally conductive and mechanically strengthened bio-epoxy/boron nitride nanocomposites: The effects of particle size, shape, and combination. *Polymer Composites*. https://doi.org/10.1002/PC.27081

Andrade, C. S., Godoy, A. P. S., Benega, M. A. G., Andrade, R. J. E. R. C. R. J. E., Andrade, R. J. E. R. C. R. J. E., Silva, W. M., … Taha-Tijerina, J. (2021). Micro scalable graphene oxide productions using controlled parameters in bench reactor. *Nanomaterials*, *11*(8), 1–11. https://doi.org/10.3390/nano11081975

Aoyama, S., Ismail, I., Park, Y. T., Yoshida, Y., Macosko, C. W., & Ougizawa, T. (2018). Polyethylene Terephthalate/Trimellitic Anhydride Modified Graphene Nanocomposites. *ACS Applied Nano Materials*. https://doi.org/10.1021/acsanm.8b01525

Asadian, H., & Shelesh-Nezhad, K. (2020). Simulation of dynamic mechanical and viscoelastic behavior in polymer/clay nanocomposites. *Polymer Composites*, *41*(3), 817–823. https://doi.org/10.1002/pc.25412

Ashok, K. G., & Kalaichelvan, K. (2020). Mechanical, ballistic impact, and water absorption behavior of luffa/graphene reinforced epoxy composites. *Polymer Composites*, *41*(11), 4716–4726. https://doi.org/10.1002/PC.25745

Azevedo, S., Kaschny, J. R., De Castilho, C. M. C., & De Brito Mota, F. (2007). A theoretical investigation of defects in a boron nitride monolayer. *Nanotechnology*, *18*(49), 495707. https://doi.org/10.1088/0957-4484/18/49/495707

Bai, J., Zhao, B., Zhou, J., Fang, Z., Li, K., Ma, H., … Sun, Y. (2019). Improved Electrochemical Performance of Ultrathin MoS $_2$ Nanosheet/Co Composites for Lithium-

Ion Battery Anodes. *ChemElectroChem*, *6*(6), 1930–1938. https://doi.org/10.1002/celc.201801891

Bai, L., Sharma, R., Cheng, X., & Macosko, C. W. (2018). Kinetic Control of Graphene Localization in Co-continuous Polymer Blends via Melt Compounding. *Langmuir*, *34*(3), 1073–1083. https://doi.org/10.1021/ACS.LANGMUIR.7B03085/ASSET/IMAGES/LARGE/LA-2017-03085D_0010.JPEG

Baird, M. E., Goldsworthy, G. T., & Creasey, C. J. (1971). Low frequency dielectric behaviour of polyamides. *Polymer*, *12*(3), 159–175. https://doi.org/10.1016/0032-3861(71)90042-5

Balandin, A. A. (2011). Thermal properties of graphene and nanostructured carbon materials. *Nature Materials*, *10*(8), 569–581. https://doi.org/10.1038/nmat3064

Balandin, A. A., Ghosh, S., Bao, W., Calizo, I., Teweldebrhan, D., Miao, F., & Lau, C. N. (2008). Superior Thermal Conductivity of Single-Layer Graphene. *Nano Letters*, *8*(3), 902–907. https://doi.org/10.1021/nl0731872

Banhart, F., Kotakoski, J., & Krasheninnikov, A. V. (2011). Structural defects in graphene. *ACS Nano*, *5*(1), 26–41. https://doi.org/10.1021/NN102598M/ASSET/IMAGES/LARGE/NN-2010-02598M_0003.JPEG

Baniasadi, H., Borandeh, S., & Seppälä, J. (2021). High-Performance and Biobased Polyamide/Functionalized Graphene Oxide Nanocomposites through In Situ Polymerization for Engineering Applications. *Macromolecular Materials and Engineering*, *2100255*, 2100255. https://doi.org/10.1002/mame.202100255

Barkan, T. (2019). Graphene: the hype versus commercial reality. *Nature Nanotechnology*, *14*(10), 904–906. https://doi.org/10.1038/s41565-019-0556-1

Bellussi, F. M., Sáenz Ezquerro, C., Laspalas, M., & Chiminelli, A. (2021). Effects of Graphene Oxidation on Interaction Energy and Interfacial Thermal Conductivity of Polymer Nanocomposite: A Molecular Dynamics Approach. *Nanomaterials*, *11*(7), 1709. https://doi.org/10.3390/nano11071709

Bertolazzi, S., Brivio, J., & Kis, A. (2011). Stretching and Breaking of Ultrathin MoS 2. *ACS Nano*, *5*(12), 9703–9709. https://doi.org/10.1021/nn203879f

Bhimanapati, G. R., Kozuch, D., & Robinson, J. A. (2014). Large-scale synthesis and functionalization of hexagonal boron nitride nanosheets. *Nanoscale*, *6*(20), 11671–11675. https://doi.org/10.1039/C4NR01816H

Billmeyer, F. W. (1949). Methods for estimating intrinsic viscosity. *Journal of Polymer Science*, *4*(1), 83–86. https://doi.org/10.1002/pol.1949.120040107

BIOVIA. (2023). *BIOVIA Materials Studio*. San Diego: Dassault Systèmes.

Bissessur, R, & Liu, P. (2006). Direct insertion of polypyrrole into molybdenum disulfide. *Solid State Ionics*, *177*(1–2), 191–196. https://doi.org/10.1016/j.ssi.2005.09.052

Bissessur, Rabin, Gallant, D., & Brüning, R. (2003). Novel nanocomposite material consisting of poly[oxymethylene-(oxyethylene)] and molybdenum disulfide. *Materials Chemistry and Physics*, *82*(2), 316–320. https://doi.org/10.1016/S0254-0584(03)00310-9

Bissessur, Rabin, & White, W. (2006). Novel alkyl substituted polyanilines/molybdenum disulfide nanocomposites. *Materials Chemistry and Physics*, *99*(2–3), 214–219. https://doi.org/10.1016/j.matchemphys.2005.10.012

Blase, X., Rubio, A., Louie, S. G., & Cohen, M. L. (1994). Stability and Band Gap Constancy of Boron Nitride Nanotubes. *Europhysics Letters (EPL)*, *28*(5), 335–340. https://doi.org/10.1209/0295-5075/28/5/007

Boden, A., Boerner, B., Kusch, P., Firkowska, I., & Reich, S. (2014). Nanoplatelet Size to Control the Alignment and Thermal Conductivity in Copper–Graphite Composites. *Nano Letters*, *14*(6), 3640–3644. https://doi.org/10.1021/nl501411g

Bose, S., Bhattacharyya, A. R., Kulkarni, A. R., & Pötschke, P. (2009). Electrical, rheological and morphological studies in co-continuous blends of polyamide 6 and acrylonitrile–butadiene–styrene with multiwall carbon nanotubes prepared by melt blending. *Composites Science and Technology*, *69*(3–4), 365–372. https://doi.org/10.1016/J.COMPSCITECH.2008.10.024

B.R., A., & Ghosh, D. (2023). Atomic investigation on optimal interfacial bonding for enhanced fracture properties in polymer nanocomposites. *Engineering Fracture Mechanics*, *281*, 109078. https://doi.org/10.1016/J.ENGFRACMECH.2023.109078

Bragaglia, M., Lamastra, F. R., Russo, P., Vitiello, L., Rinaldi, M., Fabbrocino, F., & Nanni, F. (2021). A comparison of thermally conductive polyamide 6-boron nitride composites produced via additive layer manufacturing and compression molding. *Polymer Composites*, *42*(6), 2751–2765. https://doi.org/10.1002/PC.26010

Brent, J. R., Savjani, N., & O'Brien, P. (2017). Synthetic approaches to two-dimensional transition metal dichalcogenide nanosheets. *Progress in Materials Science*, *89*, 411–478. https://doi.org/10.1016/j.pmatsci.2017.06.002

Burger, N., Laachachi, A., Ferriol, M., Lutz, M., Toniazzo, V., & Ruch, D. (2016). Review of thermal conductivity in composites: Mechanisms, parameters and theory. *Progress in Polymer Science*, *61*, 1–28. https://doi.org/10.1016/j.progpolymsci.2016.05.001

Carroll, B., Cheng, S., & Sokolov, A. P. (2017). Analyzing the Interfacial Layer Properties in Polymer Nanocomposites by Broadband Dielectric Spectroscopy. *Macromolecules*, *50*(16), 6149–6163. https://doi.org/10.1021/acs.macromol.7b00825

Castellanos-Gomez, A., Poot, M., Steele, G. A., van der Zant, H. S. J., Agraït, N., & Rubio-Bollinger, G. (2012). Elastic Properties of Freely Suspended MoS 2 Nanosheets. *Advanced Materials*, *24*(6), 772–775. https://doi.org/10.1002/adma.201103965

Chandrasekaran, S., Sato, N., Tölle, F., Mülhaupt, R., Fiedler, B., & Schulte, K. (2014). Fracture toughness and failure mechanism of graphene based epoxy composites. *Composites Science and Technology*, *97*, 90–99. https://doi.org/10.1016/j.compscitech.2014.03.014

Chauhan, V., Kärki, T., & Varis, J. (2022). Review of natural fiber-reinforced engineering plastic composites, their applications in the transportation sector and processing techniques. *Journal of Thermoplastic Composite Materials*, *35*(8), 1169–1209. https://doi.org/10.1177/0892705719889095

Chen, H., Ginzburg, V. V., Yang, J., Yang, Y., Liu, W., Huang, Y., … Chen, B. (2016). Thermal conductivity of polymer-based composites: Fundamentals and applications. *Progress in Polymer Science*, *59*, 41–85. https://doi.org/10.1016/j.progpolymsci.2016.03.001

Chen, Jin, Huang, X., Sun, B., & Jiang, P. (2019). Highly Thermally Conductive Yet Electrically Insulating Polymer/Boron Nitride Nanosheets Nanocomposite Films for Improved Thermal Management Capability. *ACS Nano*, *13*(1), 337–345. https://doi.org/10.1021/acsnano.8b06290

Chen, Junjie, & Li, L. (2020). Effect of oxidation degree on the thermal properties of graphene oxide. *Journal of Materials Research and Technology*, *9*(6), 13740–13748. https://doi.org/10.1016/j.jmrt.2020.09.092

Chen, S., Gorbatikh, L., & Seveno, D. (2021). Molecular Dynamics Simulations of Polyamide-6 Composite with Covalently Bonded Graphene Network for Thermal Conductivity Enhancement. *ACS Applied Nano Materials*. https://doi.org/10.1021/acsanm.1c02241

Chen, T., Qiu, J., Zhu, K., & Li, J. (2016). Electro-mechanical performance of polyurethane dielectric elastomer flexible micro-actuator composite modified with titanium dioxide-graphene hybrid fillers. *Materials & Design*, *90*, 1069–1076. https://doi.org/10.1016/j.matdes.2015.11.068

Chen, Xiaoming, Zhang, L., Park, C., Fay, C. C., Wang, X., & Ke, C. (2015). Mechanical strength of boron nitride nanotube-polymer interfaces. *Applied Physics Letters*, *107*(25), 253105. https://doi.org/10.1063/1.4936755

Chen, Xing, Wu, P., Rousseas, M., Okawa, D., Gartner, Z., Zettl, A., & Bertozzi, C. R. (2009). Boron Nitride Nanotubes Are Noncytotoxic and Can Be Functionalized for Interaction with Proteins and Cells. *Journal of the American Chemical Society*, *131*(3), 890–891. https://doi.org/10.1021/ja807334b

Chen, Y., Li, D., Yang, W., & Xiao, C. (2018). Enhancement of mechanical, thermal and tribological properties of AAPS-modified graphene oxide/ polyamide 6 nanocomposites. *Composites Part B: Engineering*, *138*, 55–65. https://doi.org/10.1016/j.compositesb.2017.09.058

Chen, Z., Xu, C., Ma, C., Ren, W., & Cheng, H.-M. (2013). Lightweight and Flexible Graphene Foam Composites for High-Performance Electromagnetic Interference Shielding. *Advanced Materials*, *25*(9), 1296–1300. https://doi.org/10.1002/adma.201204196

Cheng, M., Ramasubramanian, A., Rasul, M. G., Jiang, Y., Yuan, Y., Foroozan, T., … Shahbazian-Yassar, R. (2021). Direct Ink Writing of Polymer Composite Electrolytes with Enhanced Thermal Conductivities. *Advanced Functional Materials*, *31*(4), 2006683. https://doi.org/10.1002/adfm.202006683

Cheng, S., Carroll, B., Bocharova, V., Carrillo, J. M., Sumpter, B. G., & Sokolov, A. P. (2017). Focus: Structure and dynamics of the interfacial layer in polymer nanocomposites with attractive interactions. *Journal of Chemical Physics*, *146*(20), 203201. https://doi.org/10.1063/1.4978504/13608249/203201_1_ACCEPTED_MANUSCRIPT.PDF

Cheng, S., Carroll, B., Lu, W., Fan, F., Carrillo, J. M. Y., Martin, H., … Sokolov, A. P. (2017). Interfacial Properties of Polymer Nanocomposites: Role of Chain Rigidity and Dynamic Heterogeneity Length Scale. *Macromolecules*, *50*(6), 2397–2406. https://doi.org/10.1021/acs.macromol.6b02816

Cheng, S., Holt, A. P., Wang, H., Fan, F., Bocharova, V., Martin, H., … Sokolov, A. P. (2016). Unexpected Molecular Weight Effect in Polymer Nanocomposites. *Physical Review Letters*, *116*(3), 1–5. https://doi.org/10.1103/PhysRevLett.116.038302

Chhowalla, M., Shin, H. S., Eda, G., Li, L.-J., Loh, K. P., & Zhang, H. (2013). The chemistry of two-dimensional layered transition metal dichalcogenide nanosheets. *Nature Chemistry*, *5*(4), 263–275. https://doi.org/10.1038/nchem.1589

Chiu, F. C., & Huang, I. N. (2012). Phase morphology and enhanced thermal/mechanical properties of polyamide 46/graphene oxide nanocomposites. *Polymer Testing*, *31*(7), 953–962. https://doi.org/10.1016/j.polymertesting.2012.06.014

Cho, J., Lee, H., Nam, K.-H., Yeo, H., Yang, C.-M., Seong, D. G., … Kim, S. Y. (2020). Enhanced electrical conductivity of polymer nanocomposite based on edge-selectively functionalized graphene nanoplatelets. *Composites Science and Technology*, *189*, 108001. https://doi.org/10.1016/j.compscitech.2020.108001

Choi, Y. K., Park, S. J., Park, S., Kim, S., Kern, N. R., Lee, J., & Im, W. (2021). CHARMM-GUI Polymer Builder for Modeling and Simulation of Synthetic Polymers. *Journal of Chemical Theory and Computation*, *17*(4), 2431. https://doi.org/10.1021/ACS.JCTC.1C00169

Chouhan, A., Mungse, H. P., & Khatri, O. P. (2020). Surface chemistry of graphene and graphene oxide: A versatile route for their dispersion and tribological applications. *Advances in Colloid and Interface Science*, *283*, 102215. https://doi.org/10.1016/J.CIS.2020.102215

Clifton, S., Thimmappa, B. H. S., Selvam, R., & Shivamurthy, B. (2020). Polymer nanocomposites for high-velocity impact applications-A review. *Composites Communications*, *17*, 72–86. https://doi.org/10.1016/j.coco.2019.11.013

Coleman, J. N., Lotya, M., O'Neill, A., Bergin, S. D., King, P. J., Khan, U., … Nicolosi, V. (2011). Two-Dimensional Nanosheets Produced by Liquid Exfoliation of Layered Materials. *Science*, *331*(6017), 568–571. https://doi.org/10.1126/science.1194975

Correa, C. A., Razzino, C. A., & Hage, E. (2007). Role of Maleated Coupling Agents on the Interface Adhesion of Polypropylene—Wood Composites. *Journal of Thermoplastic Composite Materials*, *20*(3), 323–339. https://doi.org/10.1177/0892705707078896

Cui, X., Ding, P., Zhuang, N., Shi, L., Song, N., & Tang, S. (2015). Thermal Conductive and Mechanical Properties of Polymeric Composites Based on Solution-Exfoliated Boron Nitride and Graphene Nanosheets: A Morphology-Promoted Synergistic Effect. *ACS*

Applied Materials & Interfaces, *7*(34), 19068–19075. https://doi.org/10.1021/acsami.5b04444

Cui, Y., Gong, H., Wang, Y., Li, D., & Bai, H. (2018). A Thermally Insulating Textile Inspired by Polar Bear Hair. *Advanced Materials*, *30*(14). https://doi.org/10.1002/adma.201706807

Czaderna-Lekka, A., & Kozanecki, M. (2021). Molecular dynamics of poly(2-(2-methoxyethoxy)ethyl methacrylate) hydrogels studied by broadband dielectric spectroscopy. *Polymer*, *222*, 123618. https://doi.org/10.1016/j.polymer.2021.123618

Danda, C., Amurin, L. G., Muñoz, P. A. R., Nagaoka, D. A., Schneider, T., Troxell, B., … Maia, J. M. (2020). Integrated Computational and Experimental Design of Ductile, Abrasion-Resistant Thermoplastic Polyurethane/Graphene Oxide Nanocomposites. *ACS Applied Nano Materials*, *3*(10), 9694–9705. https://doi.org/10.1021/acsanm.0c01740

de Oliveira, Y. D. C., Amurin, L. G., Valim, F. C. F., Fechine, G. J. M., & Andrade, R. J. E. (2019). The role of physical structure and morphology on the photodegradation behaviour of polypropylene-graphene oxide nanocomposites. *Polymer*, *176*(May), 146–158. https://doi.org/10.1016/j.polymer.2019.05.029

Dean, C. R., Young, A. F., Meric, I., Lee, C., Wang, L., Sorgenfrei, S., … Hone, J. (2010). Boron nitride substrates for high-quality graphene electronics. *Nature Nanotechnology*, *5*(10), 722–726. https://doi.org/10.1038/nnano.2010.172

Dickinson, R. G., & Pauling, L. (1923). The Crystal Structure of Molybdenite. *Journal of the American Chemical Society*, *45*(6). https://doi.org/10.1021/ja01659a020

Ding, J.-H., Zhao, H.-R., & Yu, H.-B. (2018). High-yield synthesis of extremely high concentrated and few-layered boron nitride nanosheet dispersions. *2D Materials*, *5*(4), 045015. https://doi.org/10.1088/2053-1583/aad51a

Dittrich, B., Wartig, K.-A., Hofmann, D., Mülhaupt, R., & Schartel, B. (2013). Flame retardancy through carbon nanomaterials: Carbon black, multiwall nanotubes, expanded graphite, multi-layer graphene and graphene in polypropylene. *Polymer Degradation and Stability*, *98*(8), 1495–1505. https://doi.org/10.1016/j.polymdegradstab.2013.04.009

Dong, H., Liu, M., Chen, X., Han, G., Li, L., Lu, F., … Tao, H. (2022). Mechanical properties of in situ modified graphene nanosheets-reinforced polypropylene. *Polymer Composites*, *43*(7), 4687–4699. https://doi.org/10.1002/PC.26721

Du, G., Guo, Z., Wang, S., Zeng, R., Chen, Z., & Liu, H. (2010). Superior stability and high capacity of restacked molybdenum disulfide as anode material for lithium ion batteries. *Chemical Communications*, *46*(7), 1106–1108. https://doi.org/10.1039/b920277c

Eda, G., Yamaguchi, H., Voiry, D., Fujita, T., Chen, M., & Chhowalla, M. (2011). Photoluminescence from Chemically Exfoliated MoS 2. *Nano Letters*, *11*(12), 5111–5116. https://doi.org/10.1021/nl201874w

Evans, A. M., Giri, A., Sangwan, V. K., Xun, S., Bartnof, M., Torres-Castanedo, C. G., … Hopkins, P. E. (2021). Thermally conductive ultra-low-k dielectric layers based on two-dimensional covalent organic frameworks. *Nature Materials*, *20*(8), 1142–1148. https://doi.org/10.1038/s41563-021-00934-3

Falin, A., Cai, Q., Santos, E. J. G., Scullion, D., Qian, D., Zhang, R., … Li, L. H. (2017). Mechanical properties of atomically thin boron nitride and the role of interlayer interactions. *Nature Communications*, *8*(1), 15815. https://doi.org/10.1038/ncomms15815

Fechine, G. J. M., Martin-Fernandez, I., Yiapanis, G., Bentini, R., Kulkarni, E. S., Bof De Oliveira, R. V., … Özyilmaz, B. (2015). Direct dry transfer of chemical vapor deposition graphene to polymeric substrates. *Carbon*, *83*, 224–231. https://doi.org/10.1016/j.carbon.2014.11.038

Ferreira, E. H. C., Andrade, R. J. E., & Fechine, G. J. M. (2019). The “superlubricity State” of Carbonaceous Fillers on Polyethylene-Based Composites in a Molten State. *Macromolecules*, *52*(24), 9620–9631. https://doi.org/10.1021/acs.macromol.9b01746

Ferreira, E. H. C., de Lima, L. P., & Fechine, G. J. M. (2020a). The “Superlubricity State” of Carbonaceous Fillers on Polymer Composites. *Macromolecular Chemistry and Physics*, *221*(16), 1–7. https://doi.org/10.1002/macp.202000192

Ferreira, E. H. C., de Lima, L. P., & Fechine, G. J. M. (2020b). The “Superlubricity State” of Carbonaceous Fillers on Polymer Composites. *Macromolecular Chemistry and Physics*, *221*(16), 1–7. https://doi.org/10.1002/macp.202000192

Ferreira Junior, J. C., Moghimian, N., Gutiérrez, G., Helal, E., Ajji, A., Barra, G. M. de O., & Demarquette, N. R. (2022). Effects of an industrial graphene grade and surface finishing on water and oxygen permeability, electrical conductivity, and mechanical properties of high-density polyethylene (HDPE) multilayered cast films. *Materials Today Communications*, *31*, 103470. https://doi.org/10.1016/j.mtcomm.2022.103470

Fu, X., Yao, C., & Yang, G. (2015). Recent advances in graphene/polyamide 6 composites: A review. *RSC Advances*, *5*(76), 61688–61702. https://doi.org/10.1039/c5ra09312k

Furimsky, E. (1980). Role of MoS2 and WS2 in Hydrodesulfuritation. *Catalysis Reviews*, *22*(3). https://doi.org/10.1080/03602458008067538

Galpaya, D., Wang, M., Liu, M., Motta, N., Waclawik, E., & Yan, C. (2012). Recent Advances in Fabrication and Characterization of Graphene-Polymer Nanocomposites. *Graphene*, *01*(02), 30–49. https://doi.org/10.4236/graphene.2012.12005

Gálvez, O., Toledano, O., Hermoso, F. J., Linares, A., Sanz, M., Rebollar, E., … Ezquerra, T. A. (2023). Inter and intra molecular dynamics in poly(trimethylene 2,5-furanoate) as revealed by infrared and Broadband Dielectric Spectroscopies. *Polymer*, *268*, 125699. https://doi.org/10.1016/j.polymer.2023.125699

Gao, Q., & Jian, Z. (2020). Fragility and Vogel-Fulcher-Tammann parameters near glass transition temperature. *Materials Chemistry and Physics*, *252*, 123252. https://doi.org/10.1016/j.matchemphys.2020.123252

Garcia, P. S., de Oliveira, Y. D. C., Valim, F. C. F., Kotsilkova, R., Ivanov, E., Donato, R. K., … Andrade, R. J. E. (2021). Tailoring the graphene oxide chemical structure and morphology as a key to polypropylene nanocomposite performance. *Polymer Composites*, *42*(11), 6213–6231. https://doi.org/10.1002/PC.26297

Geng, Y., Wang, S. J., & Kim, J.-K. (2009). Preparation of graphite nanoplatelets and graphene sheets. *Journal of Colloid and Interface Science*, *336*(2), 592–598. https://doi.org/10.1016/j.jcis.2009.04.005

George, E., Joy, J., & Anas, S. (2021). Acrylonitrile-based polymer/graphene nanocomposites: A review. *Polymer Composites*, *42*(10), 4961–4980. https://doi.org/10.1002/PC.26224

Ghosh, S., Bao, W., Nika, D. L., Subrina, S., Pokatilov, E. P., Lau, C. N., & Balandin, A. A. (2010). Dimensional crossover of thermal transport in few-layer graphene. *Nature Materials*, *9*(7), 555–558. https://doi.org/10.1038/nmat2753

Godoy, A. P., Amurim, L. G., Mendes, A., Gonçalves, E. S., Ferreira, A., de Andrade, C. S., … Andrade, R. J. E. (2021). Enhancing the electromagnetic interference shielding of flexible films with reduced graphene oxide-based coatings. *Progress in Organic Coatings*, *158*, 106341. https://doi.org/10.1016/j.porgcoat.2021.106341

Golberg, D., Bando, Y., Huang, Y., Terao, T., Mitome, M., Tang, C., & Zhi, C. (2010). Boron Nitride Nanotubes and Nanosheets. *ACS Nano*, *4*(6), 2979–2993. https://doi.org/10.1021/nn1006495

Göldel, A., Kasaliwal, G., & Pötschke, P. (2009). Selective Localization and Migration of Multiwalled Carbon Nanotubes in Blends of Polycarbonate and Poly(styrene-acrylonitrile). *Macromolecular Rapid Communications*, *30*(6), 423–429. https://doi.org/10.1002/MARC.200800549

Göldel, A., Marmur, A., Kasaliwal, G. R., Pötschke, P., & Heinrich, G. (2011). Shape-dependent localization of carbon nanotubes and carbon black in an immiscible polymer blend during melt mixing. *Macromolecules*, *44*(15), 6094–6102. https://doi.org/10.1021/MA200793A/ASSET/IMAGES/MEDIUM/MA-2011-00793A_0012.GIF

Gómez-Navarro, C., Burghard, M., & Kern, K. (2008). Elastic Properties of Chemically Derived Single Graphene Sheets. *Nano Letters*, *8*(7), 2045–2049. https://doi.org/10.1021/nl801384y

Gong, L., Young, R. J., Kinloch, I. A., Riaz, I., Jalil, R., & Novoselov, K. S. (2012). Optimizing the Reinforcement of Polymer-Based Nanocomposites by Graphene. *ACS Nano*, *6*(3), 2086–2095. https://doi.org/10.1021/nn203917d

Gouzman, I., Grossman, E., Verker, R., Atar, N., Bolker, A., & Eliaz, N. (2019, May 3). Advances in Polyimide-Based Materials for Space Applications. *Advanced Materials*, Vol. 31, p. 1807738. Wiley-VCH Verlag. https://doi.org/10.1002/adma.201807738

Govindaraj, P., Fox, B., Aitchison, P., & Hameed, N. (2019a). A Review on Graphene Polymer Nanocomposites in Harsh Operating Conditions [Review-article]. *Industrial and Engineering Chemistry Research*, *58*(37), 17106–17129. https://doi.org/10.1021/acs.iecr.9b01183

Govindaraj, P., Fox, B., Aitchison, P., & Hameed, N. (2019b). A Review on Graphene Polymer Nanocomposites in Harsh Operating Conditions [Review-article]. *Industrial and Engineering Chemistry Research*, *58*(37), 17106–17129. https://doi.org/10.1021/acs.iecr.9b01183

Guerra, V., Wan, C., & McNally, T. (2019). Thermal conductivity of 2D nano-structured boron nitride (BN) and its composites with polymers. *Progress in Materials Science*, Vol. 100. https://doi.org/10.1016/j.pmatsci.2018.10.002

Guerreiro, M., Rompante, J., Leite, A. C., Fernandes, L. P., Santos, R. M., Paiva, M. C., & Covas, J. A. (2021). Development of electrically conductive polymer nanocomposites for the automotive cable industry. *Polímeros*, *31*(2). https://doi.org/10.1590/0104-1428.20210017

Guo, Y., Ruan, K., Shi, X., Yang, X., & Gu, J. (2020). Factors affecting thermal conductivities of the polymers and polymer composites: A review. *Composites Science and Technology*, *193*, 108134. https://doi.org/10.1016/j.compscitech.2020.108134

Hagita, K., & Morita, H. (2019). Effects of polymer/filler interactions on glass transition temperatures of filler-filled polymer nanocomposites. *Polymer*, *178*, 121615. https://doi.org/10.1016/j.polymer.2019.121615

Han, D. D., Zhang, Y. L., Liu, Y., Liu, Y. Q., Jiang, H. B., Han, B., … Sun, H. B. (2015). Bioinspired Graphene Actuators Prepared by Unilateral UV Irradiation of Graphene Oxide Papers. *Advanced Functional Materials*, *25*(28), 4548–4557. https://doi.org/10.1002/adfm.201501511

Han, Y., Shi, X., Yang, X., Guo, Y., Zhang, J., Kong, J., & Gu, J. (2020). Enhanced thermal conductivities of epoxy nanocomposites via incorporating in-situ fabricated hetero-structured SiC-BNNS fillers. *Composites Science and Technology*, *187*, 107944. https://doi.org/10.1016/j.compscitech.2019.107944

Han, Z., & Fina, A. (2011). Thermal conductivity of carbon nanotubes and their polymer nanocomposites: A review. *Progress in Polymer Science*, *36*(7), 914–944. https://doi.org/10.1016/j.progpolymsci.2010.11.004

He, J., Wang, H., Qu, Q., Su, Z., Qin, T., Da, Y., & Tian, X. (2020). Construction of interconnected SiC particles attached rGO structure in epoxy composites to achieve significant thermal conductivity enhancement. *Materials Today Communications*, *25*, 101584. https://doi.org/10.1016/j.mtcomm.2020.101584

Helal, E., Amurin, L. G., Carastan, D. J., de Sousa, R. R., David, E., Fréchette, M., & Demarquette, N. R. (2017). Interfacial molecular dynamics of styrenic block copolymer-based nanocomposites with controlled spatial distribution. *Polymer*, *113*, 9–26. https://doi.org/10.1016/j.polymer.2017.02.025

Helal, E., Demarquette, N. R., Amurin, L. G., David, E., Carastan, D. J., & Fréchette, M. (2015). Styrenic block copolymer-based nanocomposites: Implications of nanostructuration and nanofiller tailored dispersion on the dielectric properties. *Polymer*, *64*, 139–152. https://doi.org/10.1016/j.polymer.2015.03.026

Helal, Emna, Kurusu, R. S., Moghimian, N., Gutierrez, G., David, E., & Demarquette, N. R. (2019). Correlation between morphology, rheological behavior, and electrical behavior of conductive cocontinuous LLDPE/EVA blends containing commercial graphene nanoplatelets. *Journal of Rheology*, *63*(6), 961–976. https://doi.org/10.1122/1.5108919

Hennrich, F., Krupke, R., Arnold, K., Rojas Stütz, J. A., Lebedkin, S., Koch, T., … Kappes, M. M. (2007). The Mechanism of Cavitation-Induced Scission of Single-Walled Carbon Nanotubes. *The Journal of Physical Chemistry B*, *111*(8), 1932–1937. https://doi.org/10.1021/jp065262n

Hernandez, Y., Nicolosi, V., Lotya, M., Blighe, F. M., Sun, Z., De, S., … Coleman, J. N. (2008). High-yield production of graphene by liquid-phase exfoliation of graphite. *Nature Nanotechnology*, *3*(9), 563–568. https://doi.org/10.1038/nnano.2008.215

Hirsch, A., & Hauke, F. (2018). Post-Graphene 2D Chemistry: The Emerging Field of Molybdenum Disulfide and Black Phosphorus Functionalization. *Angewandte Chemie*, *130*(16), 4421–4437. https://doi.org/10.1002/ange.201708211

Holinski, R., & Gänsheimer, J. (1972). A study of the lubricating mechanism of molybdenum disulfide. *Wear*, *19*(3), 329–342. https://doi.org/10.1016/0043-1648(72)90124-X

Holt, A. P., Griffin, P. J., Bocharova, V., Agapov, A. L., Imel, A. E., Dadmun, M. D., … Sokolov, A. P. (2014). Dynamics at the polymer/nanoparticle interface in poly(2-vinylpyridine)/ silica nanocomposites. *Macromolecules*, *47*(5), 1837–1843. https://doi.org/10.1021/ma5000317

Hong, S. K., Kim, K. Y., Kim, T. Y., Kim, J. H., Park, S. W., Kim, J. H., & Cho, B. J. (2012). Electromagnetic interference shielding effectiveness of monolayer graphene. *Nanotechnology*, *23*(45), 455704. https://doi.org/10.1088/0957-4484/23/45/455704

Horváth, L., Magrez, A., Golberg, D., Zhi, C., Bando, Y., Smajda, R., … Schwaller, B. (2011). In Vitro Investigation of the Cellular Toxicity of Boron Nitride Nanotubes. *ACS Nano*, *5*(5), 3800–3810. https://doi.org/10.1021/nn200139h

Hou, J., Li, G., Yang, N., Qin, L., Grami, M. E., Zhang, Q., … Qu, X. (2014). Preparation and characterization of surface modified boron nitride epoxy composites with enhanced thermal conductivity. *RSC Advances*, *4*(83). https://doi.org/10.1039/c4ra07394k

Hu, X., Qian, W., Li, X., Fei, G., Luo, G., Wang, Z., & Xia, H. (2019). A novel method to prepare homogeneous biocompatible graphene-based PDMS composites with enhanced mechanical, thermal and antibacterial properties. *Polymer Composites*, *40*(S2), E1397–E1406. https://doi.org/10.1002/PC.25019

Huang, C., Qian, X., & Yang, R. (2018). Thermal conductivity of polymers and polymer nanocomposites. *Materials Science and Engineering: R: Reports*, *132*, 1–22. https://doi.org/10.1016/J.MSER.2018.06.002

Huang, H., Zhang, Z. X., Zhang, X. T., Yan, L., Yang, S. K., Xiao, L. X., … Chen, D. Q. (2022a). A facile strategy to improve the mechanical and thermal conductivity of PA6 nanocomposites by introducing graphene oxide/sodium benzoate compounding nucleator. *Journal of Applied Polymer Science*, *139*(10). https://doi.org/10.1002/app.51761

Huang, H., Zhang, Z. X., Zhang, X. T., Yan, L., Yang, S. K., Xiao, L. X., … Chen, D. Q. (2022b). A facile strategy to improve the mechanical and thermal conductivity of PA6 nanocomposites by introducing graphene oxide/sodium benzoate compounding nucleator. *Journal of Applied Polymer Science*, *139*(10), 1–11. https://doi.org/10.1002/app.51761

Huang, J., Zhou, J., & Liu, M. (2022). Interphase in Polymer Nanocomposites. *JACS Au*. https://doi.org/10.1021/jacsau.1c00430

Huang, T., Zeng, X., Yao, Y., Sun, R., Meng, F., Xu, J., & Wong, C. (2016). Boron nitride@graphene oxide hybrids for epoxy composites with enhanced thermal conductivity. *RSC Advances*, *6*(42), 35847–35854. https://doi.org/10.1039/c5ra27315c

Hummers, W. S., & Offeman, R. E. (1958). Preparation of Graphitic Oxide. *Journal of the American Chemical Society*, *80*(6), 1339–1339. https://doi.org/10.1021/ja01539a017

Humphrey, W., Dalke, A., & Schulten, K. (1996). VMD: Visual molecular dynamics. *Journal of Molecular Graphics*, *14*(1), 33–38. https://doi.org/10.1016/0263-7855(96)00018-5

Hussain, F., Hojjati, M., Okamoto, M., & Gorga, R. E. (2006). Review article: Polymer-matrix nanocomposites, processing, manufacturing, and application: An overview. *Journal of Composite Materials*, *40*(17), 1511–1575. https://doi.org/10.1177/0021998306067321

Hussein, A., Sarkar, S., Lee, K., & Kim, B. (2017). Cryogenic fracture behavior of epoxy reinforced by a novel graphene oxide/poly(p-phenylenediamine) hybrid. *Composites Part B: Engineering*, *129*, 133–142. https://doi.org/10.1016/j.compositesb.2017.07.085

Jain, A., Ong, S. P., Hautier, G., Chen, W., Richards, W. D., Dacek, S., … Persson, K. A. (2013). Commentary: The Materials Project: A materials genome approach to accelerating materials innovation. *APL Materials*, *1*(1), 011002. https://doi.org/10.1063/1.4812323

Jan, R., May, P., Bell, A. P., Habib, A., Khan, U., & Coleman, J. N. (2014). Enhancing the mechanical properties of BN nanosheet–polymer composites by uniaxial drawing. *Nanoscale*, *6*(9), 4889. https://doi.org/10.1039/c3nr06711d

Jang, S. K., Youn, J., Song, Y. J., & Lee, S. (2016). Synthesis and Characterization of Hexagonal Boron Nitride as a Gate Dielectric. *Scientific Reports*, *6*(1), 30449. https://doi.org/10.1038/srep30449

Japić, D., Kulovec, S., Kalin, M., Slapnik, J., Nardin, B., & Huskić, M. (2022). Effect of Expanded Graphite on Mechanical and Tribological Properties of Polyamide 6/Glass Fibre Composites. *Advances in Polymer Technology*, *2022*, 1–8. https://doi.org/10.1155/2022/9974889

Jawaid, A., Nepal, D., Park, K., Jespersen, M., Qualley, A., Mirau, P., … Vaia, R. A. (2016). Mechanism for Liquid Phase Exfoliation of MoS2. *Chemistry of Materials*, *28*(1), 337–348. https://doi.org/10.1021/acs.chemmater.5b04224

Jeong, J.-M., Kang, H. G., Kim, H.-J., Hong, S. B., Jeon, H., Hwang, S. Y., … Kim, D. H. (2018). Hydraulic Power Manufacturing for Highly Scalable and Stable 2D Nanosheet Dispersions and Their Film Electrode Application. *Advanced Functional Materials*, *28*(43), 1802952. https://doi.org/10.1002/adfm.201802952

Jia, F., Fagbohun, E. O., Wang, Q., Zhu, D., Zhang, J., Gong, B., & Cui, Y. (2021). Improved Thermal Conductivity of Styrene Acrylic Resin with Carbon Nanotubes, Graphene and Boron Nitride hybrid fillers. *Carbon Resources Conversion*. https://doi.org/10.1016/j.crcon.2021.05.001

Jia, J., Sun, X., Lin, X., Shen, X., Mai, Y.-W., & Kim, J.-K. (2014). Exceptional Electrical Conductivity and Fracture Resistance of 3D Interconnected Graphene Foam/Epoxy Composites. *ACS Nano*, *8*(6), 5774–5783. https://doi.org/10.1021/nn500590g

Jiang, T., Kuila, T., Kim, N. H., & Lee, J. H. (2014). Effects of surface-modified silica nanoparticles attached graphene oxide using isocyanate-terminated flexible polymer chains on the mechanical properties of epoxy composites. *J. Mater. Chem. A*, *2*(27), 10557–10567. https://doi.org/10.1039/C4TA00584H

Jimenez, A. M., Altorbaq, A. S., Müller, A. J., & Kumar, S. K. (2020). Polymer Crystallization under Confinement by Well-Dispersed Nanoparticles. *Macromolecules*, *53*(22), 10256–10266. https://doi.org/10.1021/acs.macromol.0c01479

Jiménez, I., Jankowski, A., Terminello, L. J., Carlisle, J. A., Sutherland, D. G. J., Doll, G. L., … Himpsel, F. J. (1998). Near-edge x-ray absorption fine structure study of bonding

modifications in BN thin films by ion implantation. *Applied Physics Letters*, *68*(20), 2816. https://doi.org/10.1063/1.116334

Jiménez, I., Jankowski, A., Terminello, L., Sutherland, D., Carlisle, J., & Doll, G. (1997). Core-level photoabsorption study of defects and metastable bonding configurations in boron nitride. *Physical Review B*, *55*(18), 12025. https://doi.org/10.1103/PhysRevB.55.12025

Jing, L., Li, H., Tay, R. Y., Sun, B., Tsang, S. H., Cometto, O., … Tok, A. I. Y. (2017). Biocompatible Hydroxylated Boron Nitride Nanosheets/Poly(vinyl alcohol) Interpenetrating Hydrogels with Enhanced Mechanical and Thermal Responses. *ACS Nano*, *11*(4), 3742–3751. https://doi.org/10.1021/acsnano.6b08408

Jo, I., Pettes, M. T., Kim, J., Watanabe, K., Taniguchi, T., Yao, Z., & Shi, L. (2013). Thermal Conductivity and Phonon Transport in Suspended Few-Layer Hexagonal Boron Nitride. *Nano Letters*, *13*(2), 550–554. https://doi.org/10.1021/nl304060g

Jo, I., Pettes, M. T., Ou, E., Wu, W., & Shi, L. (2014). Basal-plane thermal conductivity of few-layer molybdenum disulfide. *Applied Physics Letters*, *104*(20), 201902. https://doi.org/10.1063/1.4876965

Jo, S., Kim, T., Iyer, V. G., & Im, W. (2008). CHARMM-GUI: A web-based graphical user interface for CHARMM. *Journal of Computational Chemistry*, *29*(11), 1859–1865. https://doi.org/10.1002/JCC.20945

Joensen, P., Frindt, R. F., & Morrison, S. R. (1986). Single-layer MoS2. *Materials Research Bulletin*, *21*(4), 457–461. https://doi.org/10.1016/0025-5408(86)90011-5

Johnson, R. W., Evans, J. L., Jacobsen, P., Thompson, J. R. R., & Christopher, M. (2004). The Changing Automotive Environment: High-Temperature Electronics. *IEEE Transactions on Electronics Packaging Manufacturing*, *27*(3), 164–176. https://doi.org/10.1109/TEPM.2004.843109

Jung, I., Dikin, D. A., Piner, R. D., & Ruoff, R. S. (2008). Tunable Electrical Conductivity of Individual Graphene Oxide Sheets Reduced at "Low" Temperatures. *Nano Letters*, *8*(12), 4283–4287. https://doi.org/10.1021/nl8019938

Jyoti, J., Singh, B. P., Arya, A. K., & Dhakate, S. R. (2016). Dynamic mechanical properties of multiwall carbon nanotube reinforced ABS composites and their correlation with entanglement density, adhesion, reinforcement and C factor. *RSC Advances*, *6*(5), 3997–4006. https://doi.org/10.1039/C5RA25561A

Kadhim, N., Zaman, A., Jiang, M., Li, Y., Yang, X., Qiu, J., & Zhou, Z. (2021). A cast-in-place fabrication of high performance epoxy composites cured in an in-situ synthesized 3D foam of nanofibers. *Composites Part B: Engineering*, *205*, 108495. https://doi.org/10.1016/j.compositesb.2020.108495

Kalupgian, C. D. (2021). *Fotodegradação e Fotoestabilização de Filmes de Nanocompósitos De PEAD/h-BN*. Universidade Presbiteriana Mackenzie, São Paulo.

Kang, S., Kim, J., Park, J. H., Jung, I., & Park, M. (2020). Multiwalled carbon nanotube pretreatment to enhance tensile properties, process stability, and filler dispersion of polyamide 66 nanocomposites. *Composites Part B: Engineering*, *198*, 108204. https://doi.org/10.1016/j.compositesb.2020.108204

Karger-Kocsis, J., Mahmood, H., & Pegoretti, A. (2020). All-carbon multi-scale and hierarchical fibers and related structural composites: A review. *Composites Science and Technology*, *186*, 107932. https://doi.org/10.1016/j.compscitech.2019.107932

Kausar, A. (2017). Polyamide 1010/Polythioamide Blend Reinforced with Graphene Nanoplatelet for Automotive Part Application. *Advances in Materials Science*, *17*(3), 24–36. https://doi.org/10.1515/adms-2017-0013

Kausar, Ayesha. (2017). Exploration on high performance polyamide 1010/polyurethane blends filled with functional graphene nanoplatelet: physical properties and technical application. *Journal of the Chinese Advanced Materials Society*, *5*(2), 133–147. https://doi.org/10.1080/22243682.2017.1305915

Kausar, Ayesha. (2018). Composite coatings of polyamide/graphene: microstructure, mechanical, thermal, and barrier properties. *Composite Interfaces*, *25*(2), 109–125. https://doi.org/10.1080/09276440.2017.1340020

Kausar, Ayesha. (2019). In-situ modified graphene reinforced polyamide 1010/poly(ether amide): mechanical, thermal, and barrier properties. *Materials Research Innovations*, *23*(4), 191–199. https://doi.org/10.1080/14328917.2017.1409392

Kavimani, V., Stalin, B., Gopal, P. M., Ravichandran, M., Karthick, A., & Bharani, M. (2021). Application of r-GO-MMT Hybrid Nanofillers for Improving Strength and Flame Retardancy of Epoxy/Glass Fibre Composites. *Advances in Polymer Technology*, *2021*, 1–9. https://doi.org/10.1155/2021/6627743

Kee, J., Kim, D., Kim, H., & Koo, J. (2023). Enhanced thermal conductivity of polyamide nanocomposites involving expanded graphite–carbon nanotube network structure using

supercritical CO_2. *Advanced Composite Materials*, 1–11. https://doi.org/10.1080/09243046.2022.2161479

Kelly, A., & Macmillan, N. H. (1986). *Strong Solids*. Clarendon Press.

Keridou, I., Cailloux, J., Martínez, J. C., Santana, O., Maspoch, M. L., Puiggalí, J., & Franco, L. (2020). Biphasic polylactide/polyamide 6,10 blends: Influence of composition on polyamide structure and polyester crystallization. *Polymer*, *202*, 122676. https://doi.org/10.1016/j.polymer.2020.122676

Khan, U., O'Neill, A., Lotya, M., De, S., & Coleman, J. N. (2010). High-Concentration Solvent Exfoliation of Graphene. *Small*, *6*(7), 864–871. https://doi.org/10.1002/smll.200902066

Kim, H., Abdala, A. A., & Macosko, C. W. (2010). Graphene/Polymer Nanocomposites. *Macromolecules*, *43*(16), 6515–6530. https://doi.org/10.1021/ma100572e

Kim, J. E., Han, T. H., Lee, S. H., Kim, J. Y., Ahn, C. W., Yun, J. M., & Kim, S. O. (2011). Graphene Oxide Liquid Crystals. *Angewandte Chemie*, *123*(13), 3099–3103. https://doi.org/10.1002/ange.201004692

Kim, J., Kim, J., Song, S., Zhang, S., Cha, J., Kim, K., … Jeon, S. (2017). Strength dependence of epoxy composites on the average filler size of non-oxidized graphene flake. *Carbon*, *113*, 379–386. https://doi.org/10.1016/j.carbon.2016.11.023

Kinloch, I. A., Suhr, J., Lou, J., Young, R. J., & Ajayan, P. M. (2018). Composites with carbon nanotubes and graphene: An outlook. *Science*, *362*(6414), 547–553. https://doi.org/10.1126/science.aat7439

Kiziltas, A., Liu, W., Tamrakar, S., & Mielewski, D. (2021). Graphene Nanoplatelet Reinforcement for Thermal and Mechanical Properties Enhancement of Bio-based Polyamide 6, 10 Nanocomposites for Automotive Applications. *Composites Part C: Open Access*, 100177. https://doi.org/10.1016/j.jcomc.2021.100177

Klonos, P. A., Nosach, L. V., Voronin, E. F., Pakhlov, E. M., Kyritsis, A., & Pissis, P. (2019). Glass Transition and Molecular Dynamics in Core-Shell-Type Nanocomposites Based on Fumed Silica and Polysiloxanes: Comparison between Poly(dimethylsiloxane) and Poly(ethylhydrosiloxane). *Journal of Physical Chemistry C*, *123*(46), 28427–28436. https://doi.org/10.1021/acs.jpcc.9b07247

Kong, W., Kum, H., Bae, S.-H., Shim, J., Kim, H., Kong, L., … Kim, J. (2019). Path towards graphene commercialization from lab to market. *Nature Nanotechnology*, *14*(10), 927–938. https://doi.org/10.1038/s41565-019-0555-2

Korkees, F., Aldrees, A., Barsoum, I., & Alshammari, D. (2021). Functionalised graphene effect on the mechanical and thermal properties of recycled PA6/PA6,6 blends. *Journal of Composite Materials*. https://doi.org/10.1177/0021998320987897

Kovtyukhova, N. I., Perea-López, N., Terrones, M., & Mallouk, T. E. (2017). Atomically Thin Layers of Graphene and Hexagonal Boron Nitride Made by Solvent Exfoliation of Their Phosphoric Acid Intercalation Compounds. *ACS Nano*, *11*(7), 6746–6754. https://doi.org/10.1021/acsnano.7b01311

Kovtyukhova, N. I., Wang, Y., Lv, R., Terrones, M., Crespi, V. H., & Mallouk, T. E. (2013). Reversible Intercalation of Hexagonal Boron Nitride with Brønsted Acids. *Journal of the American Chemical Society*, *135*(22), 8372–8381. https://doi.org/10.1021/ja403197h

Kremer, F., & Schönhals, A. (2003a). *Broadband Dielectric Spectroscopy* (F. Kremer & A. Schönhals, Eds.). Berlin, Heidelberg: Springer Berlin Heidelberg. https://doi.org/10.1007/978-3-642-56120-7

Kremer, F., & Schönhals, A. (2003b). *Broadband Dielectric Spectroscopy*. Berlin, Heidelberg: Springer Berlin Heidelberg. https://doi.org/10.1007/978-3-642-56120-7

Krishna, S., Sreedhar, I., & Patel, C. M. (2021). Molecular dynamics simulation of polyamide-based materials – A review. *Computational Materials Science*, *200*(September), 110853. https://doi.org/10.1016/j.commatsci.2021.110853

Kuang, Z., Chen, Y., Lu, Y., Liu, L., Hu, S., Wen, S., … Zhang, L. (2015). Fabrication of Highly Oriented Hexagonal Boron Nitride Nanosheet/Elastomer Nanocomposites with High Thermal Conductivity. *Small*, *11*(14), 1655–1659. https://doi.org/10.1002/smll.201402569

Kubát, J., Rigdahl, M., & Welander, M. (1990). Characterization of interfacial interactions in high density polyethylene filled with glass spheres using dynamic-mechanical analysis. *Journal of Applied Polymer Science*, *39*(7), 1527–1539. https://doi.org/10.1002/APP.1990.070390711

Kuciel, S., Kuźnia, P., & Jakubowska, P. (2016). Properties of composites based on polyamide 10.10 reinforced with carbon fibers. *Polimery/Polymers*, *61*(2), 106–112. https://doi.org/10.14314/polimery.2016.106

Kuciel, S., Kuźniar, P., & Liber-Kneć, A. (2012). Polyamides from renewable sources as matrices of short fiber reinforced biocompositesle. *Polimery*, *57*(9).

Kuester, S., Demarquette, N. R., Ferreira, J. C., Soares, B. G., & Barra, G. M. O. (2017). Hybrid nanocomposites of thermoplastic elastomer and carbon nanoadditives for electromagnetic shielding. *European Polymer Journal*, *88*, 328–339. https://doi.org/10.1016/j.eurpolymj.2017.01.023

Kuilla, T., Bhadra, S., Yao, D., Kim, N. H., Bose, S., & Lee, J. H. (2010). Recent advances in graphene based polymer composites. *Progress in Polymer Science*, *35*(11), 1350–1375. https://doi.org/10.1016/j.progpolymsci.2010.07.005

Kumar, R., Goel, N., & Kumar, M. (2017). UV-Activated MoS2 Based Fast and Reversible NO2 Sensor at Room Temperature. *ACS Sensors*, *2*(11), 1744–1752. https://doi.org/10.1021/ACSSENSORS.7B00731/ASSET/IMAGES/LARGE/SE-2017-00731S_0006.JPEG

Kurusu, R. S., Helal, E., Moghimian, N., David, E., & Demarquette, N. (2018). The Role of Selectively Located Commercial Graphene Nanoplatelets in the Electrical Properties, Morphology, and Stability of EVA/LLDPE Blends. *Macromolecular Materials and Engineering*, *303*(9), 1800187. https://doi.org/10.1002/mame.201800187

Kyulavska, M., Toncheva-Moncheva, N., & Rydz, J. (2017). Biobased polyamide ecomaterials and their susceptibility to biodegradation. *Handbook of Ecomaterials*.

Lahiri, D., Hec, F., Thiesse, M., Durygin, A., Zhang, C., & Agarwal, A. (2014). Nanotribological behavior of graphene nanoplatelet reinforced ultra high molecular weight polyethylene composites. *Tribology International*, *70*, 165–169. https://doi.org/10.1016/J.TRIBOINT.2013.10.012

Łątka, Ł., Goc, K., Kapusta, C., & Zapotoczny, S. (2021). Enhanced Thermal Conductivity of Polyamide-Based Nanocomposites Containing Graphene Oxide Sheets Decorated with Compatible Polymer Brushes. *Materials*, *14*(4), 751. https://doi.org/10.3390/ma14040751

Layek, R. K., & Nandi, A. K. (2013). A review on synthesis and properties of polymer functionalized graphene. *Polymer*, *54*(19), 5087–5103. https://doi.org/10.1016/j.polymer.2013.06.027

Lee, C., Wei, X., Kysar, J. W., & Hone, J. (2008). Measurement of the Elastic Properties and Intrinsic Strength of Monolayer Graphene. *Science*, *321*(5887), 385–388. https://doi.org/10.1126/science.1157996

Lee, D., Lee, B., Park, K. H., Ryu, H. J., Jeon, S., & Hong, S. H. (2015). Scalable Exfoliation Process for Highly Soluble Boron Nitride Nanoplatelets by Hydroxide-Assisted Ball Milling. *Nano Letters*, *15*(2), 1238–1244. https://doi.org/10.1021/nl504397h

Lee, G. Do, Wang, C. Z., Yoon, E., Hwang, N. M., Kim, D. Y., & Ho, K. M. (2005). Diffusion, coalescence, and reconstruction of vacancy defects in graphene layers. *Physical Review Letters*, *95*(20), 205501. https://doi.org/10.1103/PHYSREVLETT.95.205501/FIGURES/4/MEDIUM

Lee, P., Kim, S. Y., Ko, Y. K., Ha, J. U., Jeoung, S. K., Shin, D., … Kim, M. (2022). Tribological Properties of Polyamide 46/Graphene Nanocomposites. *Polymers*, *14*(6), 1139. https://doi.org/10.3390/polym14061139

Leeladhar, Raturi, P., & Singh, J. P. (2018). Sunlight-driven eco-friendly smart curtain based on infrared responsive graphene oxide-polymer photoactuators. *Scientific Reports*, *8*(1), 3687. https://doi.org/10.1038/s41598-018-21871-3

Lei, W., Mochalin, V. N., Liu, D., Qin, S., Gogotsi, Y., & Chen, Y. (2015). Boron nitride colloidal solutions, ultralight aerogels and freestanding membranes through one-step exfoliation and functionalization. *Nature Communications*, *6*(1), 8849. https://doi.org/10.1038/ncomms9849

Lei, W., Zhang, H., Wu, Y., Zhang, B., Liu, D., Qin, S., … Chen, Y. (2014). Oxygen-doped boron nitride nanosheets with excellent performance in hydrogen storage. *Nano Energy*, *6*, 219–224. https://doi.org/10.1016/j.nanoen.2014.04.004

Levinta, N., Corobea, M. C., Vuluga, Z., Nicolae, C. A., Gabor, A. R., Raditoiu, V., … Teodorescu, M. (2020). Bio-Based polyamide 1010 with a halogen-free flame retardant based on melamine-gallic acid complex. *Polymers*, *12*(7), 1–19. https://doi.org/10.3390/polym12071482

Li, B., & Zhong, W.-H. (2011). Review on polymer/graphite nanoplatelet nanocomposites. *Journal of Materials Science*, *46*(17), 5595–5614. https://doi.org/10.1007/s10853-011-5572-y

Li, F., Hua, Y., Qu, C.-B., Xiao, H.-M., & Fu, S.-Y. (2016). Greatly enhanced cryogenic mechanical properties of short carbon fiber/polyethersulfone composites by graphene oxide coating. *Composites Part A: Applied Science and Manufacturing*, *89*, 47–55. https://doi.org/10.1016/j.compositesa.2016.02.016

Li, Haoxiang, Wu, H., Zhang, W., Zhao, X., Zhang, L., & Gao, Y. (2021). Rheological mechanism of polymer nanocomposites filled with spherical nanoparticles: Insight from

molecular dynamics simulation. *Polymer*, *231*, 124129. https://doi.org/10.1016/j.polymer.2021.124129

Li, He, Wang, J., Gao, S., Chen, Q., Peng, L., Liu, K., … Liu, K. (2017). Superlubricity between MoS2 Monolayers. *Advanced Materials*, *29*(27), 1701474. https://doi.org/10.1002/ADMA.201701474

Li, J., Sham, M., Kim, J., & Marom, G. (2007). Morphology and properties of UV/ozone treated graphite nanoplatelet/epoxy nanocomposites. *Composites Science and Technology*, *67*(2), 296–305. https://doi.org/10.1016/j.compscitech.2006.08.009

Li, M., Zhou, H., Zhang, Y., Liao, Y., & Zhou, H. (2017). The effect of defects on the interfacial mechanical properties of graphene/epoxy composites. *RSC Adv.*, *7*(73), 46101–46108. https://doi.org/10.1039/C7RA08243F

Li, M., Zhou, H., Zhang, Y., Liao, Y., & Zhou, H. (2018). Effect of defects on thermal conductivity of graphene/epoxy nanocomposites. *Carbon*, *130*, 295–303. https://doi.org/10.1016/j.carbon.2017.12.110

Li, P., Zhang, Z., Yang, M., Yuan, J., & Jiang, W. (2021). MoS2-decorated talc hybrid for improving the tribological property of Nomex/PTFE fabric composites. *Polymer Composites*, *42*(11), 5839–5849. https://doi.org/10.1002/PC.26264

Li, Q., Chen, L., Gadinski, M. R., Zhang, S., Zhang, G., Li, H. U., … Wang, Q. (2015). Flexible high-temperature dielectric materials from polymer nanocomposites. *Nature*, *523*(7562), 576–579. https://doi.org/10.1038/nature14647

Li, Q., Liu, F., Yang, T., Gadinski, M. R., Zhang, G., Chen, L.-Q., & Wang, Q. (2016). Sandwich-structured polymer nanocomposites with high energy density and great charge–discharge efficiency at elevated temperatures. *Proceedings of the National Academy of Sciences*, *113*(36), 9995–10000. https://doi.org/10.1073/pnas.1603792113

Li, R., Yang, X., Li, J., Shen, Y., Zhang, L., Lu, R., … Zhang, T. (2022). Review on polymer composites with high thermal conductivity and low dielectric properties for electronic packaging. *Materials Today Physics*, *22*, 100594. https://doi.org/10.1016/j.mtphys.2021.100594

Li, Shengtao, Yu, S., & Feng, Y. (2016). Progress in and prospects for electrical insulating materials. *High Voltage*, *1*(3), 122–129. https://doi.org/10.1049/HVE.2016.0034

Li, Shengzhao, Yang, T., Zou, H., Liang, M., & Chen, Y. (2017). Enhancement in thermal conductivity and mechanical properties via large-scale fabrication of boron nitride

nanosheets. *High Performance Polymers*, *29*(3), 315–327. https://doi.org/10.1177/0954008316643766

Li, Wanli, Liu, J., Hao, C., Jiang, K., Xu, D., & Wang, D. (2008). Interaction of thermoplastic polyurethane with polyamide 1212 and its influence on the thermal and mechanical properties of TPU/PA1212 blends. *Polymer Engineering & Science*, *48*(2), 249–256. https://doi.org/10.1002/pen.20853

Li, Wu, Carrete, J., & Mingo, N. (2013). Thermal conductivity and phonon linewidths of monolayer MoS 2 from first principles. *Applied Physics Letters*, *103*(25), 253103. https://doi.org/10.1063/1.4850995

Li, X., Hao, X., Zhao, M., Wu, Y., Yang, J., Tian, Y., & Qian, G. (2013). Exfoliation of Hexagonal Boron Nitride by Molten Hydroxides. *Advanced Materials*, *25*(15), 2200–2204. https://doi.org/10.1002/adma.201204031

Liang, H., Liao, Q., Chen, N., Liang, Y., Lv, G., Zhang, P., … Qu, L. (2019). Thermal Efficiency of Solar Steam Generation Approaching 100 % through Capillary Water Transport. *Angewandte Chemie*, *131*(52), 19217–19222. https://doi.org/10.1002/ange.201911457

Lin, B. Z., Ding, C., Xu, B. H., Chen, Z. J., & Chen, Y. L. (2009). Preparation and characterization of polythiophene/molybdenum disulfide intercalation material. *Materials Research Bulletin*, *44*(4), 719–723. https://doi.org/10.1016/j.materresbull.2008.09.031

Lin, Q.-Y., Jing, G., Zhou, Y.-B., Wang, Y.-F., Meng, J., Bie, Y.-Q., … Liao, Z.-M. (2013). Stretch-Induced Stiffness Enhancement of Graphene Grown by Chemical Vapor Deposition. *ACS Nano*, *7*(2), 1171–1177. https://doi.org/10.1021/nn3053999

Lin, X., Shen, X., Zheng, Q., Yousefi, N., Ye, L., Mai, Y.-W., & Kim, J.-K. (2012). Fabrication of Highly-Aligned, Conductive, and Strong Graphene Papers Using Ultralarge Graphene Oxide Sheets. *ACS Nano*, *6*(12), 10708–10719. https://doi.org/10.1021/nn303904z

Lin, Y., Lang, F., Zeng, D., Yi-Lan, Y. O. U., Li, D., & Xiao, C. (2020). Effects of modified graphene on property optimization in thermal conductive composites based on PPS/PA6 blend. *Soft Materials*, *00*(00), 1–11. https://doi.org/10.1080/1539445X.2020.1856873

Liu, C., Chen, C., Wang, H., Chen, M., Zhou, D., Xu, Z., & Yu, W. (2019). Synergistic Effect of Irregular Shaped Particles and Graphene on the Thermal Conductivity of Epoxy Composites. *Polymer Composites*, *40*(S2), E1294–E1300. https://doi.org/10.1002/PC.24968

Liu, G. D., Wu, J. P., Dong, H. M., & Zhang, H. Q. (2020). Nonlinear modification of vogel-fulcher-tamman (VFT) model and its application in enthalpy relaxation of glassy polystyrene. *Journal of Non-Crystalline Solids*, *528*, 119761. https://doi.org/10.1016/j.jnoncrysol.2019.119761

Liu, Jialin, Hui, D., & Lau, D. (2022). Two-dimensional nanomaterial-based polymer composites: Fundamentals and applications. *Nanotechnology Reviews*, *11*(1), 770–792. https://doi.org/10.1515/ntrev-2022-0041

Liu, Juan, Zeng, J., Zhu, C., Miao, J., Huang, Y., & Heinz, H. (2020). Interpretable molecular models for molybdenum disulfide and insight into selective peptide recognition. *Chemical Science*, *11*(33), 8708. https://doi.org/10.1039/D0SC01443E

Liu, L., Zhou, M., Jin, L., Li, L., Mo, Y., Su, G., … Tian, Y. (2019). Recent advances in friction and lubrication of graphene and other 2D materials: Mechanisms and applications. *Friction*, *7*(3), 199–216. https://doi.org/10.1007/S40544-019-0268-4/METRICS

Liu, P., Cottrill, A. L., Kozawa, D., Koman, V. B., Parviz, D., Liu, A. T., … Strano, M. S. (2018). Emerging trends in 2D nanotechnology that are redefining our understanding of "Nanocomposites." *Nano Today*, *21*, 18–40. https://doi.org/10.1016/j.nantod.2018.04.012

Liu, W., Ullah, B., Kuo, C.-C., & Cai, X. (2019). Two-Dimensional Nanomaterials-Based Polymer Composites: Fabrication and Energy Storage Applications. *Advances in Polymer Technology*, *2019*, 1–15. https://doi.org/10.1155/2019/4294306

Liu, Y., Ge, X., & Li, J. (2020). Graphene lubrication. *Applied Materials Today*, *20*, 100662. https://doi.org/10.1016/J.APMT.2020.100662

Lotz, B. (2021). Original Crystal Structures of Even-Even Polyamides Made of Pleated and Rippled Sheets. *Macromolecules*, *54*(2), 551–564. https://doi.org/10.1021/acs.macromol.0c02404

Lu, L., Yang, B., & Liu, J. (2020). Flexible multifunctional graphite nanosheet/electrospun-polyamide 66 nanocomposite sensor for ECG, strain, temperature and gas measurements. *Chemical Engineering Journal*, *400*(March), 125928. https://doi.org/10.1016/j.cej.2020.125928

Lu, X., Detrez, F., Yvonnet, J., & Bai, J. (2021). Identification of elastic properties of interphase and interface in graphene-polymer nanocomposites by atomistic simulations. *Composites Science and Technology*, 108943. https://doi.org/10.1016/j.compscitech.2021.108943

Luo, W., Wang, Y., Hitz, E., Lin, Y., Yang, B., & Hu, L. (2017). Solution Processed Boron Nitride Nanosheets: Synthesis, Assemblies and Emerging Applications. *Advanced Functional Materials*, *27*(31), 1701450. https://doi.org/10.1002/adfm.201701450

Ma, P.-C., Siddiqui, N. A., Marom, G., & Kim, J.-K. (2010). Dispersion and functionalization of carbon nanotubes for polymer-based nanocomposites: A review. *Composites Part A: Applied Science and Manufacturing*, *41*(10), 1345–1367. https://doi.org/10.1016/j.compositesa.2010.07.003

Madhad, H. v, Mishra, N. S., Patel, S. B., Panchal, S. S., Gandhi, R. A., & Vasava, D. v. (2021). Graphene/graphene nanoplatelets reinforced polyamide nanocomposites: A review. *High Performance Polymers*, 095400832110112. https://doi.org/10.1177/09540083211011216

Madhad, H. v., & Vasava, D. v. (2019). Review on recent progress in synthesis of graphene–polyamide nanocomposites. *Journal of Thermoplastic Composite Materials*, (October). https://doi.org/10.1177/0892705719880942

Madinehei, M., Kuester, S., Kaydanova, T., Moghimian, N., & David, É. (2021). Influence of Graphene Nanoplatelet Lateral Size on the Electrical Conductivity and Electromagnetic Interference Shielding Performance of Polyester Nanocomposites. *Polymers*, *13*(15), 2567. https://doi.org/10.3390/polym13152567

Mak, K. F., Lee, C., Hone, J., Shan, J., & Heinz, T. F. (2010). Atomically thin MoS2: A new direct-gap semiconductor. *Physical Review Letters*, *105*(13). https://doi.org/10.1103/PhysRevLett.105.136805

Marciano de Oliveira Cremonezzi, J., Ribeiro, H., Jorge Espanhol Andrade, R., & José Macedo Fechine, G. (2022). Characterization strategy for graphene oxide and molybdenum disulfide: Proceedings based on the ISO/TS 21356-1:2021 standard. *FlatChem*, *36*, 100448. https://doi.org/10.1016/J.FLATC.2022.100448

Marian, M., Berman, D., Rota, A., Jackson, R. L., Rosenkranz, A., Marian, M., … Rosenkranz, A. (2022). Layered 2D Nanomaterials to Tailor Friction and Wear in Machine Elements—A Review. *Advanced Materials Interfaces*, *9*(3), 2101622. https://doi.org/10.1002/ADMI.202101622

Marset, D., Dolza, C., Boronat, T., Montanes, N., Balart, R., Sanchez-Nacher, L., & Quiles-Carrillo, L. (2020). Injection-Molded parts of partially biobased polyamide 610 and biobased halloysite nanotubes. *Polymers*, *12*(7), 1–15. https://doi.org/10.3390/polym12071503

Martinez, L., Andrade, R., Birgin, E. G., & Martínez, J. M. (2009). PACKMOL: A package for building initial configurations for molecular dynamics simulations. *Journal of Computational Chemistry*, *30*(13), 2157–2164. https://doi.org/10.1002/JCC.21224

Mayo, S. L., Olafson, B. D., & Goddard, W. A. (1990). DREIDING: a generic force field for molecular simulations. *The Journal of Physical Chemistry*, *94*(26), 8897–8909. https://doi.org/10.1021/j100389a010

McCall, D. W., & Anderson, E. W. (1960). Dielectric properties of linear polyamides. *The Journal of Chemical Physics*, *32*(1), 237–241. https://doi.org/10.1063/1.1700907

McKeen, L. W. (2012). Polyamides (Nylons). In *Film Properties of Plastics and Elastomers* (pp. 157–188). Elsevier. https://doi.org/10.1016/B978-1-4557-2551-9.00008-6

McNally, T., & Pötschke, P. (2011). *Polymer–Carbon Nanotube Composites: Preparation, Properties and Applications*. Elsevier.

Md Said, N. H., Liu, W. W., Khe, C. S., Lai, C. W., Zulkepli, N. N., & Aziz, A. (2021). Review of the past and recent developments in functionalization of graphene derivatives for reinforcement of polypropylene nanocomposites. *Polymer Composites*, *42*(3), 1075–1108. https://doi.org/10.1002/PC.25922

Medeiros, G. S., Muñoz, P. A. R. R., de Oliveira, C. F. P. P., da Silva, L. C. E. E., Malhotra, R., Gonçalves, M. C., … Fechine, G. J. M. M. (2020). Polymer Nanocomposites Based on Poly(ε-caprolactone), Hydroxyapatite and Graphene Oxide. *Journal of Polymers and the Environment*, *28*(1), 331–342. https://doi.org/10.1007/s10924-019-01613-w

Mehra, N., Mu, L., Ji, T., Yang, X., Kong, J., Gu, J., & Zhu, J. (2018). Thermal transport in polymeric materials and across composite interfaces. *Applied Materials Today*, *12*, 92–130. https://doi.org/10.1016/J.APMT.2018.04.004

Meng, F., Huang, F., Guo, Y., Chen, J., Chen, X., Hui, D., … Zhou, Z. (2017). In situ intercalation polymerization approach to polyamide-6/graphite nanoflakes for enhanced thermal conductivity. *Composites Part B: Engineering*, *117*, 165–173. https://doi.org/10.1016/j.compositesb.2017.02.043

Meng, W., Huang, Y., Fu, Y., Wang, Z., & Zhi, C. (2014). Polymer composites of boron nitride nanotubes and nanosheets. *J. Mater. Chem. C*, *2*(47), 10049–10061. https://doi.org/10.1039/C4TC01998A

Meng, X., Wang, M., Cong, C., Ye, H., & Zhou, Q. (2019). Synergistic effects of multiwalled carbon nanotube/molybdenum disulfide hybrid particles on the mechanical and wear

performance of epoxy. *Polymer Composites*, *40*(S2), E1642–E1648. https://doi.org/10.1002/PC.25110

Mensah, B., Gupta, K. C., Kim, H., Wang, W., Jeong, K.-U., & Nah, C. (2018). Graphene-reinforced elastomeric nanocomposites: A review. *Polymer Testing*, *68*, 160–184. https://doi.org/10.1016/j.polymertesting.2018.04.009

Michell, R. M., & Müller, A. J. (2016). Confined crystallization of polymeric materials. *Progress in Polymer Science*, *54–55*, 183–213. https://doi.org/10.1016/j.progpolymsci.2015.10.007

Mir, S. M., Jafari, S. H., Khonakdar, H. A., Krause, B., Pötschke, P., & Taheri Qazvini, N. (2016). A promising approach to low electrical percolation threshold in PMMA nanocomposites by using MWCNT-PEO predispersions. *Materials & Design*, *111*, 253–262. https://doi.org/10.1016/J.MATDES.2016.08.073

Mittal, G., Dhand, V., Rhee, K. Y., Park, S. J., & Lee, W. R. (2015). A review on carbon nanotubes and graphene as fillers in reinforced polymer nanocomposites. *Journal of Industrial and Engineering Chemistry*, *21*, 11–25. https://doi.org/10.1016/j.jiec.2014.03.022

Mohan, V. B., Lau, K. tak, Hui, D., & Bhattacharyya, D. (2018). Graphene-based materials and their composites: A review on production, applications and product limitations. *Composites Part B: Engineering*, *142*(December 2017), 200–220. https://doi.org/10.1016/j.compositesb.2018.01.013

Momma, K., & Izumi, F. (2011). VESTA 3 for three-dimensional visualization of crystal, volumetric and morphology data. *Urn:Issn:0021-8898*, *44*(6), 1272–1276. https://doi.org/10.1107/S0021889811038970

Moore, A. L., & Shi, L. (2014). Emerging challenges and materials for thermal management of electronics. *Materials Today*, *17*(4), 163–174. https://doi.org/10.1016/j.mattod.2014.04.003

Morishita, T., & Okamoto, H. (2016). Facile Exfoliation and Noncovalent Superacid Functionalization of Boron Nitride Nanosheets and Their Use for Highly Thermally Conductive and Electrically Insulating Polymer Nanocomposites. *ACS Applied Materials & Interfaces*, *8*(40), 27064–27073. https://doi.org/10.1021/acsami.6b08404

Mouloua, D., Kotbi, A., Deokar, G., Kaja, K., El Marssi, M., EL Khakani, M. A., & Jouiad, M. (2021). Recent Progress in the Synthesis of MoS2 Thin Films for Sensing,

Photovoltaic and Plasmonic Applications: A Review. *Materials*, *14*(12), 3283. https://doi.org/10.3390/ma14123283

Mousavi, M. R., Tehran, A. C., & Shelesh-Nezhad, K. (2020). Study on morphology, mechanical, thermal and viscoelastic properties of PA6/TPU/CNT nanocomposites. *Plastics, Rubber and Composites*, *49*(9), 400–413. https://doi.org/10.1080/14658011.2020.1784588

Mun, S. C., Kim, M. J., Cobos, M., Gu, L., & Macosko, C. W. (2019). Strategies for interfacial localization of graphene/polyethylene-based cocontinuous blends for electrical percolation. *AIChE Journal*, *65*(6), e16579. https://doi.org/10.1002/AIC.16579

Muñoz, P. A. R., de Oliveira, C. F. P., Amurin, L. G., Rodriguez, C. L. C., Nagaoka, D. A., Tavares, M. I. B., … Fechine, G. J. M. (2018). Novel improvement in processing of polymer nanocomposite based on 2D materials as fillers. *Express Polymer Letters*, *12*(10), 930–945. https://doi.org/10.3144/expresspolymlett.2018.79

Muraru, S., Burns, J. S., & Ionita, M. (2020). GOPY: A tool for building 2D graphene-based computational models. *SoftwareX*, *12*, 100586. https://doi.org/10.1016/J.SOFTX.2020.100586

Naskar, A. K., Keum, J. K., & Boeman, R. G. (2016). Polymer matrix nanocomposites for automotive structural components. *Nature Nanotechnology*, *11*(12), 1026–1030. https://doi.org/10.1038/nnano.2016.262

Nie, X., Sang, X., Fu, Y., Shi, X., Zheng, K., & Ma, Y. (2022). Exfoliation of hexagonal boron nitride assisted with hierarchical ionic fragments by ball-milling for achieving high thermally conductive polymer nanocomposite. *Polymer Composites*, *43*(2), 946–954. https://doi.org/10.1002/PC.26424

Novoselov, K. S., Geim, A. K., Morozov, S. V., Jiang, D., Zhang, Y., Dubonos, S. V., … Firsov, A. A. (2004). Electric field in atomically thin carbon films. *Science*, *306*(5696), 666–669. https://doi.org/10.1126/SCIENCE.1102896/SUPPL_FILE/NOVOSELOV.SOM.PDF

Nunes, M. A. B. S., de Matos, B. R., Silva, G. G., Ito, E. N., de Melo, T. J. A., & Fechine, G. J. M. (2021). Hybrids nanocomposites based on a polymer blend (linear low-density polyethylene/poly(ethylene-co-methyl acrylate) and carbonaceous fillers (graphene and carbon nanotube). *Polymer Composites*, *42*(2), 661–677. https://doi.org/10.1002/pc.25856

Oh, Kyounghwan, Kim, H., & Seo, Y. (2020). Long-Living Anions Could Dramatically Change the Overall Physical Properties of a Polyamide (Nylon 6) Synthesized by a Novel Process. *ACS Omega*, *5*(28), 17463–17470. https://doi.org/10.1021/acsomega.0c01962

Oh, Kyunghwan, Kim, H., & Seo, Y. (2019). Effect of Diamine Addition on Structural Features and Physical Properties of Polyamide 6 Synthesized by Anionic Ring-Opening Polymerization of ε-Caprolactam. *ACS Omega*, *4*(17), 17117–17124. https://doi.org/10.1021/acsomega.9b01342

Oliveira, C. F. P., Muñoz, P. A. R., Santos, M. C. C., Medeiros, G. S., Simionato, A., Nagaoka, D. A., … Fechine, G. J. M. (2019). Tuning of surface properties of poly(vinyl alcohol)/graphene oxide nanocomposites. *Polymer Composites*, *40*(S1), E312–E320. https://doi.org/10.1002/pc.24659

O'Neill, A., Bakirtzis, D., & Dixon, D. (2014). Polyamide 6/Graphene composites: The effect of in situ polymerisation on the structure and properties of graphene oxide and reduced graphene oxide. *European Polymer Journal*, *59*, 353–362. https://doi.org/10.1016/j.eurpolymj.2014.07.038

Öner, M., Keskin, G., Kızıl, G., Pochat-Bohatier, C., & Bechelany, M. (2019). Development of poly(3-hydroxybutyrate-co-3-hydroxyvalerate)/boron nitride bionanocomposites with enhanced barrier properties. *Polymer Composites*, *40*(1), 78–90. https://doi.org/10.1002/PC.24603

Pan, B., Li, N., Chu, G., Wei, F., Liu, J., Zhang, J., & Zhang, Y. (2014). Tribological investigation of MC PA6 reinforced by boron nitride of single layer. *Tribology Letters*, *54*(2), 161–170. https://doi.org/10.1007/S11249-014-0324-1/FIGURES/9

Pandey, J. C., & Singh, M. (2021). Dielectric polymer nanocomposites: Past advances and future prospects in electrical insulation perspective. *SPE Polymers*, (June), 1–21. https://doi.org/10.1002/pls2.10059

Papageorgiou, D. G., Kinloch, I. A., & Young, R. J. (2015). Graphene/elastomer nanocomposites. *Carbon*, *95*, 460–484. https://doi.org/10.1016/j.carbon.2015.08.055

Pasupathi, M. K., Alagar, K., P, M. J. S., M.M, M., & Aritra, G. (2020). Characterization of Hybrid-nano/Paraffin Organic Phase Change Material for Thermal Energy Storage Applications in Solar Thermal Systems. *Energies*, *13*(19), 5079. https://doi.org/10.3390/en13195079

Pathmanathan, K., Cavaillé, J.-Y., & Johari, G. P. (1992). The dielectric properties of dry and water-saturated nylon-12. *Journal of Polymer Science Part B: Polymer Physics*, *30*(4), 341–348. https://doi.org/10.1002/polb.1992.090300404

Paton, K. R., Varrla, E., Backes, C., Smith, R. J., Khan, U., O'Neill, A., … Coleman, J. N. (2014). Scalable production of large quantities of defect-free few-layer graphene by shear exfoliation in liquids. *Nature Materials*, *13*(6), 624–630. https://doi.org/10.1038/nmat3944

Peddamallu, N., Sridharan, K., Nakayama, T., & Sarathi, R. (2019). Understanding the fundamental properties of epoxy molybdenum disulfide nanocomposites. *Polymer Composites*, *40*(4), 1556–1563. https://doi.org/10.1002/PC.24898

Petrény, R., & Mészáros, L. (2020). The effect of microstructure on the dynamic mechanical properties of carbon fiber and carbon nanotube reinforced multi-scale composites with a polyamide 6 matrix. *IOP Conference Series: Materials Science and Engineering*, *903*(1). https://doi.org/10.1088/1757-899X/903/1/012021

Pham, T., Li, G., Bekyarova, E., Itkis, M. E., & Mulchandani, A. (2019). MoS 2 -Based Optoelectronic Gas Sensor with Sub-parts-per-billion Limit of NO 2 Gas Detection. *ACS Nano*, *13*(3), 3196–3205. https://doi.org/10.1021/ACSNANO.8B08778/ASSET/IMAGES/LARGE/NN-2018-087785_0007.JPEG

Pinto, Gabriel M., Cremonezzi, J. M. O., Ribeiro, H., Andrade, R. J. E., Demarquette, N. R., & Fechine, G. J. M. (2023, March 1). From two-dimensional materials to polymer nanocomposites with emerging multifunctional applications: A critical review. *Polymer Composites*. John Wiley and Sons Inc. https://doi.org/10.1002/pc.27213

Pinto, Gabriel M., Santos, A. B., Helal, E., Ribeiro, H., David, E., Woellner, C. F., … Fechine, G. J. M. (2023). Exploring the relationship between interfacial adhesion, molecular dynamics, and the brill transition in fully bio-based polyamide 1010 nanocomposites reinforced by two-dimensional materials. *Polymer*, *289*, 126482. https://doi.org/10.1016/j.polymer.2023.126482

Pinto, Gabriel M., Silva, G. da C., & Fechine, G. J. M. (2020). Effect of exfoliation medium on the morphology of multi-layer graphene oxide and its importance for Poly(Ethylene terephthalate) based nanocomposites. *Polymer Testing*, *90*(July), 106742. https://doi.org/10.1016/j.polymertesting.2020.106742

Pinto, Gabriel M., Silva, G. da C., Santillo, C., Lavorgna, M., Maia, J. M., & Fechine, G. J. M. (2020). Crystallization kinetics, structure, and rheological behavior of poly(ethylene

terephthalate)/multilayer graphene oxide nanocomposites. *Polymer Engineering & Science*, *60*(11), 2841–2851. https://doi.org/10.1002/pen.25516

Pinto, Gabriel Matheus, Helal, E., Ribeiro, H., David, E., Demarquette, N. R., & Fechine, G. J. M. (2024). Effect of Environmental Temperature and Semi-Crystalline Order on the Toughening of Polyamide 1010 by 2D Nanomaterials. *Submitted to Polymer Composites*.

Pleşa, I., Noţingher, P. V., Schlögl, S., Sumereder, C., & Muhr, M. (2016). Properties of Polymer Composites Used in High-Voltage Applications. *Polymers 2016, Vol. 8, Page 173*, *8*(5), 173. https://doi.org/10.3390/POLYM8050173

Plimpton, S. (1995). Fast Parallel Algorithms for Short-Range Molecular Dynamics. *Journal of Computational Physics*, *117*(1), 1–19. https://doi.org/10.1006/jcph.1995.1039

Pötschke, P., Bhattacharyya, A. R., & Janke, A. (2004). Carbon nanotube-filled polycarbonate composites produced by melt mixing and their use in blends with polyethylene. *Carbon*, *42*(5–6), 965–969. https://doi.org/10.1016/J.CARBON.2003.12.001

Pötschke, P., Kretzschmar, B., & Janke, A. (2007). Use of carbon nanotube filled polycarbonate in blends with montmorillonite filled polypropylene. *Composites Science and Technology*, *67*(5), 855–860. https://doi.org/10.1016/J.COMPSCITECH.2006.02.034

Potts, J. R., Dreyer, D. R., Bielawski, C. W., & Ruoff, R. S. (2011). Graphene-based polymer nanocomposites. *Polymer*, *52*(1), 5–25. https://doi.org/10.1016/j.polymer.2010.11.042

Punetha, V. D., Rana, S., Yoo, H. J., Chaurasia, A., McLeskey, J. T., Ramasamy, M. S., … Cho, J. W. (2017). Functionalization of carbon nanomaterials for advanced polymer nanocomposites: A comparison study between CNT and graphene. *Progress in Polymer Science*, *67*, 1–47. https://doi.org/10.1016/j.progpolymsci.2016.12.010

Qin, W., Vautard, F., Drzal, L. T., & Yu, J. (2015). Mechanical and electrical properties of carbon fiber composites with incorporation of graphene nanoplatelets at the fiber–matrix interphase. *Composites Part B: Engineering*, *69*, 335–341. https://doi.org/10.1016/j.compositesb.2014.10.014

Qiu, S., Hu, Y., Shi, Y., Hou, Y., Kan, Y., Chu, F., … Xing, W. (2018). In situ growth of polyphosphazene particles on molybdenum disulfide nanosheets for flame retardant and friction application. *Composites Part A: Applied Science and Manufacturing*, *114*, 407–417. https://doi.org/10.1016/J.COMPOSITESA.2018.08.012

Qu, J., Fan, L., Mukerabigwi, J. F., Liu, C., & Cao, Y. (2021). A silicon rubber composite with enhanced thermal conductivity and mechanical properties based on nanodiamond and boron nitride fillers. *Polymer Composites*, *42*(9), 4390–4396. https://doi.org/10.1002/PC.26156

Quiles-Carrillo, L., Balart, R., Boronat, T., Torres-Giner, S., Puglia, D., Dominici, F., & Torre, L. (2021). Development of Compatibilized Polyamide 1010/Coconut Fibers Composites by Reactive Extrusion with Modified Linseed Oil and Multi-functional Petroleum Derived Compatibilizers. *Fibers and Polymers*, *22*(3), 728–744. https://doi.org/10.1007/s12221-021-0024-z

Quiles-Carrillo, Luis, Boronat, T., Montanes, N., Balart, R., & Torres-Giner, S. (2019). Injection-molded parts of fully bio-based polyamide 1010 strengthened with waste derived slate fibers pretreated with glycidyl- and amino-silane coupling agents. *Polymer Testing*, *77*. https://doi.org/10.1016/j.polymertesting.2019.04.022

Radisavljevic, B., Radenovic, A., Brivio, J., Giacometti, V., & Kis, A. (2011). Single-layer MoS2 transistors. *Nature Nanotechnology*, *6*(3), 147–150. https://doi.org/10.1038/nnano.2010.279

Rafiq, R., Cai, D., Jin, J., & Song, M. (2010). Increasing the toughness of nylon 12 by the incorporation of functionalized graphene. *Carbon*, *48*(15), 4309–4314. https://doi.org/10.1016/j.carbon.2010.07.043

Ramesh, C. (1999). New crystalline transitions in nylons 4,6, 6,10, and 6,12 using high temperature x-ray diffraction studies. *Macromolecules*, *32*(11), 3721–3726. https://doi.org/10.1021/MA981284Z

Ramezani, A., Seyfi, J., Razavi Aghjeh, M. K., Mohammadloo, H. E., Mousavi, S. R., & Khonakdar, H. A. (2022). Poly(vinylidene fluoride)/molybdenum disulfide nanocomposite coatings: Studying the surface properties and corrosion protection. *Polymer Composites*. https://doi.org/10.1002/PC.27077

Randhawa, K. S., & Patel, A. D. (2020). Enhancing tribo-mechanical properties & thermal stability of PA6 by h-BN fillers. *E-Polymers*, *20*(1), 733–745. https://doi.org/10.1515/EPOLY-2020-0069/ASSET/GRAPHIC/J_EPOLY-2020-0069_FIG_012.JPG

Rao, C. N. R., Maitra, U., & Waghmare, U. v. (2014). Extraordinary attributes of 2-dimensional MoS2 nanosheets. *Chemical Physics Letters*, *609*, 172–183. https://doi.org/10.1016/j.cplett.2014.06.003

Rastegar, S., & Montazeri, A. (2022). Atomistic insights into the toughening role of surface-treated boron nitride nanosheets in PLA-based nanocomposites. *European Polymer Journal*, *168*, 111071. https://doi.org/10.1016/j.eurpolymj.2022.111071

Rasul, M. G., Kiziltas, A., Arfaei, B., & Shahbazian-Yassar, R. (2021). 2D boron nitride nanosheets for polymer composite materials. *Npj 2D Materials and Applications*, *5*(1), 56. https://doi.org/10.1038/s41699-021-00231-2

Ravindran, A., Feng, C., Huang, S., Wang, Y., Zhao, Z., & Yang, J. (2018). Effects of Graphene Nanoplatelet Size and Surface Area on the AC Electrical Conductivity and Dielectric Constant of Epoxy Nanocomposites. *Polymers*, *10*(5), 477. https://doi.org/10.3390/polym10050477

Reiss, T., Hjelt, K., & Ferrari, A. C. (2019). Graphene is on track to deliver on its promises. *Nature Nanotechnology*, *14*(10), 907–910. https://doi.org/10.1038/s41565-019-0557-0

Ren, Y., Ren, L., Li, J., Lv, R., Wei, L., An, D., … Wong, C. P. (2020). Enhanced thermal conductivity in polyamide 6 composites based on the compatibilization effect of polyether-grafted graphene. *Composites Science and Technology*, *199*, 108340. https://doi.org/10.1016/j.compscitech.2020.108340

Ribeiro, H., Trigueiro, J. P. C., Lopes, M. C., Pedrotti, J. J., Woellner, C. F., Silva, W. M., … Ajayan, P. M. (2018). Enhanced thermal conductivity and mechanical properties of hybrid MoS2/h-BN polyurethane nanocomposites. *Journal of Applied Polymer Science*, *135*(30), 10–13. https://doi.org/10.1002/app.46560

Ribeiro, H., Trigueiro, J. P. C., Owuor, P. S., Machado, L. D., Woellner, C. F., Pedrotti, J. J., … Ajayan, P. M. (2018). Hybrid 2D nanostructures for mechanical reinforcement and thermal conductivity enhancement in polymer composites. *Composites Science and Technology*, *159*, 103–110. https://doi.org/10.1016/j.compscitech.2018.01.032

Ribeiro, H., Trigueiro, J. P. C., Silva, W. M., Woellner, C. F., Owuor, P. S., Cristian Chipara, A., … Ajayan, P. M. (2019). Hybrid MoS2/h-BN Nanofillers As Synergic Heat Dissipation and Reinforcement Additives in Epoxy Nanocomposites. *ACS Applied Materials and Interfaces*, *11*(27), 24485–24492. https://doi.org/10.1021/acsami.7b09945

Ribeiro, H., Trigueiro, J. P. C., Woellner, C. F., Pedrotti, J. J., Miquita, D. R., Silva, W. M., … Ajayan, P. M. (2020a). Higher thermal conductivity and mechanical enhancements in hybrid 2D polymer nanocomposites. *Polymer Testing*, *87*(March), 1–9. https://doi.org/10.1016/j.polymertesting.2020.106510

Ribeiro, H., Trigueiro, J. P. C., Woellner, C. F., Pedrotti, J. J., Miquita, D. R., Silva, W. M., … Ajayan, P. M. (2020b). Higher thermal conductivity and mechanical enhancements in hybrid 2D polymer nanocomposites. *Polymer Testing*, *87*(xxxx), 106510. https://doi.org/10.1016/j.polymertesting.2020.106510

Ries, M., Possart, G., Steinmann, P., & Pfaller, S. (2021). A coupled MD-FE methodology to characterize mechanical interphases in polymeric nanocomposites. *International Journal of Mechanical Sciences*, 106564. https://doi.org/10.1016/j.ijmecsci.2021.106564

Rittigstein, P., Priestley, R. D., Broadbelt, L. J., & Torkelson, J. M. (2007). Model polymer nanocomposites provide an understanding of confinement effects in real nanocomposites. *Nature Materials 2007 6:4*, *6*(4), 278–282. https://doi.org/10.1038/nmat1870

Rodriguez, C. L. C., Kessler, F., Dubey, N., Rosa, V., & Fechine, G. J. M. (2017). CVD graphene transfer procedure to the surface of stainless steel for stem cell proliferation. *Surface and Coatings Technology*, *311*, 10–18. https://doi.org/10.1016/j.surfcoat.2016.12.111

Rodriguez, C. L. C., Muñoz, P. A. R., Donato, K. Z., Seixas, L., Donato, R. K., & Fechine, G. J. M. (2020). Understanding the unorthodox stabilization of liquid phase exfoliated molybdenum disulfide. *Physical Chemistry Chemical Physics*, *22*, 1457–1465. https://doi.org/10.1039/c9cp06422b

Rodriguez, C. L. C., Nunes, M. A. B. S., Garcia, P. S., & Fechine, G. J. M. (2021). Molybdenum disulfide as a filler for a polymeric matrix at an ultralow content: Polystyrene case. *Polymer Testing*, *93*(October 2020), 106882. https://doi.org/10.1016/j.polymertesting.2020.106882

Román-Manso, B., Figueiredo, F. M., Achiaga, B., Barea, R., Pérez-Coll, D., Morelos-Gómez, A., … Miranzo, P. (2016). Electrically functional 3D-architectured graphene/SiC composites. *Carbon*, *100*, 318–328. https://doi.org/10.1016/j.carbon.2015.12.103

Ronchi, R. M., de Lemos, H. G., Nishihora, R. K., Cuppari, M. G. D. V., & Santos, S. F. (2023). Tribology of polymer-based nanocomposites reinforced with 2D materials. *Materials Today Communications*, *34*, 105397. https://doi.org/10.1016/J.MTCOMM.2023.105397

Rouhi, S. (2016). Molecular dynamics simulation of the adsorption of polymer chains on CNTs, BNNTs and GaNNTs. *Fibers and Polymers*, *17*(3), 333–342. https://doi.org/10.1007/s12221-016-5676-8

Ruiz-Vargas, C. S., Zhuang, H. L., Huang, P. Y., van der Zande, A. M., Garg, S., McEuen, P. L., … Park, J. (2011). Softened Elastic Response and Unzipping in Chemical Vapor Deposition Graphene Membranes. *Nano Letters*, *11*(6), 2259–2263. https://doi.org/10.1021/nl200429f

Rusu, D., Boyer, S., Lacrampe, M., & Krawczak, P. (2011). Bioplastics for automotive applications. *Handbook Bioplast Biocompos Eng Appl*, *81*, 397.

Salunke, D. R., & Gopalan, V. (2021). Thermal and Electrical behaviors of Boron Nitride/Epoxy reinforced polymer matrix composite—A review. *Polymer Composites*, *42*(4), 1659–1669. https://doi.org/10.1002/PC.25952

Santhosha, A. L., Nayak, P. K., Pollok, K., Langenhorst, F., & Adelhelm, P. (2019). Exfoliated MoS_2 as Electrode for All-Solid-State Rechargeable Lithium-Ion Batteries. *The Journal of Physical Chemistry C*, *123*(19), 12126–12134. https://doi.org/10.1021/acs.jpcc.9b01816

Sarac, E. C., Poudeh, L. H., Zanjani, J. S. M., Letofsky-Papst, I., Cebeci, F. Ç., Aydin, I., … Okan, B. S. (2019). Performance Comparison of CVD Grown Carbon Nanofiber Based on Single- and Multi-Layer Graphene Oxides in Melt-Compounded PA6.6 Nanocomposites. *Open Journal of Composite Materials*, *09*(02), 99–123. https://doi.org/10.4236/ojcm.2019.92005

Sarkar, D., Das, D., Das, S., Kumar, A., Patil, S., Nanda, K. K., … Shukla, A. (2019). Expanding Interlayer Spacing in MoS_2 for Realizing an Advanced Supercapacitor. *ACS Energy Letters*, *4*(7), 1602–1609. https://doi.org/10.1021/acsenergylett.9b00983

Sattar, M. A. (2021). Interface Structure and Dynamics in Polymer-Nanoparticle Hybrids: A Review on Molecular Mechanisms Underlying the Improved Interfaces. *ChemistrySelect*, *6*(20), 5068–5096. https://doi.org/10.1002/slct.202100831

Sayed-Ahmad Baraza, Y. (2019). *Theoretical and Experimental studies of structure and functionalization of 2D Nanomaterials*. Nantes.

Seki, Y., Kizilkan, E., İşbilir, A., Sarikanat, M., & Altay, L. (2021). Enhanced in-plane and through-plane thermal conductivity and mechanical properties of polyamide 4.6 composites loaded with hybrid carbon fiber, synthetic graphite and graphene. *Polymer Composites*, *42*(9), 4630–4642. https://doi.org/10.1002/PC.26174

Senturk, O., & Palabiyik, M. (2023). Exploring the tribological properties of PA6/GO nanocomposites produced by in situ polymerization. *Journal of Materials Science*, *58*(25), 10318–10339. https://doi.org/10.1007/S10853-023-08662-6/FIGURES/5

Seyed Esfahani, S. A., Ghahramani, N., Mehranpour, M., & Nazockdast, H. (2021). Rheological, thermal, and electrical characterization polyamide/polypropylene blend composites containing hybrid filler: Boron nitride and reduced graphene oxide. *SPE Polymers*, *2*(2), 134–144. https://doi.org/10.1002/pls2.10041

Shanker, A., Li, C., Kim, G.-H., Gidley, D., Pipe, K. P., & Kim, J. (2017). High thermal conductivity in electrostatically engineered amorphous polymers. *Science Advances*, *3*(7), e1700342. https://doi.org/10.1126/sciadv.1700342

Shen, H., Yi, E., Heywood, S., Parkinson, D. Y., Chen, G., Tamura, N., … Doeff, M. M. (2020). Scalable Freeze-Tape-Casting Fabrication and Pore Structure Analysis of 3D LLZO Solid-State Electrolytes. *ACS Applied Materials & Interfaces*, *12*(3). https://doi.org/10.1021/acsami.9b11780

Shen, X., Wang, Z., Wu, Y., Liu, X., He, Y.-B., & Kim, J.-K. (2016). Multilayer Graphene Enables Higher Efficiency in Improving Thermal Conductivities of Graphene/Epoxy Composites. *Nano Letters*, *16*(6), 3585–3593. https://doi.org/10.1021/acs.nanolett.6b00722

Shen, X., Wang, Z., Wu, Y., Liu, X., & Kim, J.-K. (2016). Effect of functionalization on thermal conductivities of graphene/epoxy composites. *Carbon*, *108*, 412–422. https://doi.org/10.1016/j.carbon.2016.07.042

Shen, X., Zheng, Q., & Kim, J.-K. K. (2021). Rational design of two-dimensional nanofillers for polymer nanocomposites toward multifunctional applications. *Progress in Materials Science*, *115*, 100708. https://doi.org/10.1016/j.pmatsci.2020.100708

Shen, X.-J., Liu, Y., Xiao, H.-M., Feng, Q.-P., Yu, Z.-Z., & Fu, S.-Y. (2012). The reinforcing effect of graphene nanosheets on the cryogenic mechanical properties of epoxy resins. *Composites Science and Technology*, *72*(13), 1581–1587. https://doi.org/10.1016/j.compscitech.2012.06.021

Shi, K., Liu, Z., Wei, Y. Y., Wang, W., Ju, X. J., Xie, R., & Chu, L. Y. (2015). Near-Infrared Light-Responsive Poly(N-isopropylacrylamide)/Graphene Oxide Nanocomposite Hydrogels with Ultrahigh Tensibility. *ACS Applied Materials and Interfaces*, *7*(49), 27289–27298. https://doi.org/10.1021/acsami.5b08609

Shim, S. H., Kim, K. T., Lee, J. U., & Jo, W. H. (2012). Facile method to functionalize graphene oxide and its application to poly(ethylene terephthalate)/graphene composite. *ACS Applied Materials and Interfaces*, *4*(8), 4184–4191. https://doi.org/10.1021/am300906z

Shin, D. H., Shin, S. H., & Choi, S.-H. (2020). Self-powered and flexible perovskite photodiode/solar cell bifunctional devices with MoS2 hole transport layer. *Applied Surface Science*, *514*, 145880. https://doi.org/10.1016/j.apsusc.2020.145880

Singh, A. K., Kumar, P., Late, D. J., Kumar, A., Patel, S., & Singh, J. (2018). 2D layered transition metal dichalcogenides (MoS_2): Synthesis, applications and theoretical aspects. *Applied Materials Today*, *13*, 242–270. https://doi.org/10.1016/j.apmt.2018.09.003

Soares, Y. C. F., Yokoyama, D. D., Costa, L. C., de Oliveira Cremonezzi, J. M., Ribeiro, H., Naccache, M. F., & Andrade, R. J. E. (2023). Multifunctional hexagonal boron nitride dispersions based in xanthan gum for use in drilling fluids. *Geoenergy Science and Engineering*, *221*, 111311. https://doi.org/10.1016/j.petrol.2022.111311

Soccio, M., Martínez-Tong, D. E., Alegría, A., Munari, A., & Lotti, N. (2017). Molecular dynamics of fully biobased poly(butylene 2,5-furanoate) as revealed by broadband dielectric spectroscopy. *Polymer*, *128*, 24–30. https://doi.org/10.1016/j.polymer.2017.09.007

Sorrentino, A., Altavilla, C., Merola, M., Senatore, A., Ciambelli, P., & Iannace, S. (2015). Nanosheets of MoS2-oleylamine as hybrid filler for self-lubricating polymer composites: Thermal, tribological, and mechanical properties. *Polymer Composites*, *36*(6), 1124–1134. https://doi.org/10.1002/PC.23444

Souza, Z. S. B., Pinto, G. M., Silva, G. da C., Demarquette, N. R., Fechine, G. J. M., & Sobrinho, M. A. M. (2021). Interface adjustment between poly(ethylene terephthalate) and graphene oxide in order to enhance mechanical and thermal properties of nanocomposites. *Polymer Engineering & Science*, (January), pen.25715. https://doi.org/10.1002/pen.25715

Stankovich, S., Dikin, D. A., Piner, R. D., Kohlhaas, K. A., Kleinhammes, A., Jia, Y., … Ruoff, R. S. (2007). Synthesis of graphene-based nanosheets via chemical reduction of exfoliated graphite oxide. *Carbon*, *45*(7), 1558–1565. https://doi.org/10.1016/j.carbon.2007.02.034

Steeman, P. A. M., & Maurer, F. H. J. (1992). Dielectric properties of polyamide-4,6. *Polymer*, *33*(20), 4236–4241. https://doi.org/10.1016/0032-3861(92)90263-V

Steeman, P. A. M., & Van Turnhout, J. (1997). A numerical Kramers-Kronig transform for the calculation of dielectric relaxation losses free from Ohmic conduction losses. *Colloid and Polymer Science*, *275*(2), 106–115. https://doi.org/10.1007/s003960050059

Strugova, D., David, É., & Demarquette, N. R. (2022). Linear viscoelasticity of PP/PS/MWCNT composites with co-continuous morphology. *Journal of Rheology*, *66*(4), 671–681. https://doi.org/10.1122/8.0000441

Strugova, D., Ferreira Junior, J. C., David, É., & Demarquette, N. R. (2021). Ultra-low percolation threshold induced by thermal treatments in co-continuous blend-based pp/ps/mwcnts nanocomposites. *Nanomaterials*, *11*(6). https://doi.org/10.3390/nano11061620

Su, L. S., & Tsai, J. L. (2021). Characterizing the mechanical properties of nanocomposites with aligned graphene. *Polymer Composites*, *42*(8), 4005–4014. https://doi.org/10.1002/PC.26112

Su, Z., Wang, H., Tian, K., Huang, W., Xiao, C., Guo, Y., … Tian, X. (2018). The combination of π-π interaction and covalent bonding can synergistically strengthen the flexible electrical insulating nanocomposites with well adhesive properties and thermal conductivity. *Composites Science and Technology*, *155*, 1–10. https://doi.org/10.1016/j.compscitech.2017.09.018

Suk, J. W., Piner, R. D., An, J., & Ruoff, R. S. (2010). Mechanical Properties of Monolayer Graphene Oxide. *ACS Nano*, *4*(11), 6557–6564. https://doi.org/10.1021/nn101781v

Sun, H., Mumby, S. J., Maple, J. R., & Hagler, A. T. (1994). An ab Initio CFF93 All-Atom Force Field for Polycarbonates. *Journal of the American Chemical Society*, *116*(7), 2978–2987. https://doi.org/10.1021/ja00086a030

Sun, J., & Du, S. (2019). Application of graphene derivatives and their nanocomposites in tribology and lubrication: a review. *RSC Advances*, *9*(69), 40642–40661. https://doi.org/10.1039/C9RA05679C

Sun, R., Li, L., Zhang, H., & Yang, J. (2020). Effect of hydrogen functionalization on interfacial behavior of defective-graphene/polymer nanocomposites. *Polymer Composites*, *41*(4), 1291–1298. https://doi.org/10.1002/PC.25454

Sun, X., Huang, C., Wang, L., Liang, L., Cheng, Y., Fei, W., & Li, Y. (2021). Recent Progress in Graphene/Polymer Nanocomposites. *Advanced Materials*, *33*(6), 1–28. https://doi.org/10.1002/adma.202001105

Taha-Tijerina, J., Ribeiro, H., Aviña, K., Martínez, J. M., Godoy, A. P., Cremonezzi, J. M. de O., … Castro, S. (2020). Thermal Conductivity Performance of 2D h-BN/MoS2/-Hybrid Nanostructures Used on Natural and Synthetic Esters. *Nanomaterials*, *10*(6), 1160. https://doi.org/10.3390/nano10061160

Tajaddod, N., Song, K., Green, E. C., Zhang, Y., & Minus, M. L. (2016). Exfoliation of Boron Nitride Platelets by Enhanced Interfacial Interaction with Polyethylene. *Macromolecular Materials and Engineering*, *301*(3). https://doi.org/10.1002/mame.201500284

Tanaka, T., Montanari, G. C., & Mulhaupt, R. (2004). Polymer nanocomposites as dielectrics and electrical insulation-perspectives for processing technologies, material characterization and future applications. *IEEE Transactions on Dielectrics and Electrical Insulation*, *11*(5), 763–784. https://doi.org/10.1109/TDEI.2004.1349782

Tang, Y., Zhang, P., Zhu, M., Li, J., Li, Y., Wang, Z., & Huang, L. (2019). Temperature Effects on the Dielectric Properties and Breakdown Performance of h-BN/Epoxy Composites. *Materials*, *12*(24), 4112. https://doi.org/10.3390/ma12244112

Tashiro, K., & Yoshioka, Y. (2004). Molecular dynamics simulation of the structural and mechanical property changes in the Brill transition of nylon 10/10 crystal. *Polymer*, *45*(12), 4337–4348. https://doi.org/10.1016/j.polymer.2004.03.082

Tokarczyk, M., Kowalski, G., Witowski, A. M., Koziński, R., Librant, K., Aksienionek, M., … Ciepielewski, P. (2014). Structural and electronic properties of graphene oxide and reduced graphene oxide papers prepared by high pressure and high temperature treatment. *Acta Physica Polonica A*, *126*(5), 1190–1194. https://doi.org/10.12693/APhysPolA.126.1190

Tong, Z., Zhuo, W., Zhou, J., Huang, R., & Jiang, G. (2017). Crystallization behavior and enhanced toughness of poly(ethylene terephthalate) composite with noncovalent modified graphene functionalized by pyrene-terminated molecules: a comparative study. *Journal of Materials Science*, *52*(17), 10567–10580. https://doi.org/10.1007/s10853-017-1173-8

Turchanin, A., Beyer, A., Nottbohm, C. T., Zhang, X., Stosch, R., Sologubenko, A., … Gölzhäuser, A. (2009). One nanometer thin carbon nanosheets with tunable conductivity and stiffness. *Advanced Materials*, *21*(12), 1233–1237. https://doi.org/10.1002/adma.200803078

Uzoma, P. C., Hu, H., Khadem, M., & Penkov, O. V. (2020). Tribology of 2D Nanomaterials: A Review. *Coatings 2020, Vol. 10, Page 897*, *10*(9), 897. https://doi.org/10.3390/COATINGS10090897

Valorosi, F., De Meo, E., Blanco-Varela, T., Martorana, B., Veca, A., Pugno, N., … Palermo, V. (2020). Graphene and related materials in hierarchical fiber composites: Production techniques and key industrial benefits. *Composites Science and Technology*, *185*, 107848. https://doi.org/10.1016/j.compscitech.2019.107848

Vanroy, B., Wübbenhorst, M., & Napolitano, S. (2013). Crystallization of thin polymer layers confined between two adsorbing walls. *ACS Macro Letters*, *2*(2), 168–172. https://doi.org/10.1021/MZ300641X/SUPPL_FILE/MZ300641X_SI_001.PDF

Varrla, E., Backes, C., Paton, K. R., Harvey, A., Gholamvand, Z., McCauley, J., & Coleman, J. N. (2015). Large-Scale Production of Size-Controlled MoS 2 Nanosheets by Shear Exfoliation. *Chemistry of Materials*, *27*(3), 1129–1139. https://doi.org/10.1021/cm5044864

Verdejo, R., Bernal, M. M., Romasanta, L. J., & Lopez-Manchado, M. A. (2011). Graphene filled polymer nanocomposites. *J. Mater. Chem.*, *21*(10), 3301–3310. https://doi.org/10.1039/C0JM02708A

Vikraman, D., Arbab, A. A., Hussain, S., Shrestha, N. K., Jeong, S. H., Jung, J., … Kim, H.-S. (2019). Design of WSe 2 /MoS 2 Heterostructures as the Counter Electrode to Replace Pt for Dye-Sensitized Solar Cell. *ACS Sustainable Chemistry & Engineering*, *7*(15), 13195–13205. https://doi.org/10.1021/acssuschemeng.9b02430

Wadkin-Snaith, D., Mulheran, P., & Johnston, K. (2023). Filler-induced heterogeneous nucleation of polymer crystals investigated by molecular dynamics simulations. *Polymer*, *281*, 126113. https://doi.org/10.1016/j.polymer.2023.126113

Wang, G., Fu, Y., Guo, A., Mei, T., Wang, J., Li, J., & Wang, X. (2017). Reduced Graphene Oxide-Polyurethane Nanocomposite Foam as a Reusable Photoreceiver for Efficient Solar Steam Generation. *Chemistry of Materials*, *29*(13), 5629–5635. https://doi.org/10.1021/acs.chemmater.7b01280

Wang, H., Mi, X., Li, Y., & Zhan, S. (2020, January 1). 3D Graphene-Based Macrostructures for Water Treatment. *Advanced Materials*, Vol. 32, p. 1806843. Wiley-VCH Verlag. https://doi.org/10.1002/adma.201806843

Wang, J., Jin, X., Li, C., Wang, W., Wu, H., & Guo, S. (2019). Graphene and graphene derivatives toughening polymers: Toward high toughness and strength. *Chemical Engineering Journal*, *370*(December 2018), 831–854. https://doi.org/10.1016/j.cej.2019.03.229

Wang, J., Li, C., Zhang, X., Xia, L., Zhang, X., Wu, H., & Guo, S. (2017). Polycarbonate toughening with reduced graphene oxide: Toward high toughness, strength and notch resistance. *Chemical Engineering Journal*, *325*, 474–484. https://doi.org/10.1016/J.CEJ.2017.05.090

Wang, N., Yang, G., Wang, H., Yan, C., Sun, R., & Wong, C.-P. (2019). A universal method for large-yield and high-concentration exfoliation of two-dimensional hexagonal boron nitride nanosheets. *Materials Today*, *27*, 33–42. https://doi.org/10.1016/j.mattod.2018.10.039

Wang, R., Wu, L., Zhuo, D., Zhang, J., & Zheng, Y. (2018). Fabrication of Polyamide 6 Nanocomposite with Improved Thermal Conductivity and Mechanical Properties via Incorporation of Low Graphene Content. *Industrial & Engineering Chemistry Research*, *57*(32), 10967–10976. https://doi.org/10.1021/acs.iecr.8b01070

Wang, S., Luo, Z., Liang, J., Hu, J., Jiang, N., He, J., & Li, Q. (2022). Polymer Nanocomposite Dielectrics: Understanding the Matrix/Particle Interface. *ACS Nano*, *16*(9), 13612–13656. https://doi.org/10.1021/ACSNANO.2C07404/ASSET/IMAGES/LARGE/NN2C07404_0018.JPEG

Wang, T., Zhuo, J., Du, K., Chen, B., Zhu, Z., Shao, Y., & Li, M. (2014). Electrochemically Fabricated Polypyrrole and MoSx Copolymer Films as a Highly Active Hydrogen Evolution Electrocatalyst. *Advanced Materials*, *26*(22), 3761–3766. https://doi.org/10.1002/adma.201400265

Wang, X., Kalali, E. N., & Wang, D.-Y. (2015). An in situ polymerization approach for functionalized MoS $_2$ /nylon-6 nanocomposites with enhanced mechanical properties and thermal stability. *Journal of Materials Chemistry A*, *3*(47), 24112–24120. https://doi.org/10.1039/C5TA06071K

Wang, X.-B., Weng, Q., Wang, X., Li, X., Zhang, J., Liu, F., … Bando, Y. (2014). Biomass-Directed Synthesis of 20 g High-Quality Boron Nitride Nanosheets for Thermoconductive Polymeric Composites. *ACS Nano*, *8*(9), 9081–9088. https://doi.org/10.1021/nn502486x

Wang, Yafei, Chang, Z., Gao, K., Li, Z., Hou, G., Liu, J., & Zhang, L. (2021). Designing high thermal conductivity of polydimethylsiloxane filled with hybrid h-BN/MoS2 via molecular dynamics simulation. *Polymer*, *224*, 123697. https://doi.org/10.1016/j.polymer.2021.123697

Wang, Yinrui, & Xie, Y. (2020). Electroactive FeS2-modified MoS2 nanosheet for high-performance supercapacitor. *Journal of Alloys and Compounds*, *824*, 153936. https://doi.org/10.1016/j.jallcom.2020.153936

Wang, Z., Shen, X., Akbari Garakani, M., Lin, X., Wu, Y., Liu, X., … Kim, J. K. (2015). Graphene aerogel/epoxy composites with exceptional anisotropic structure and properties. *ACS Applied Materials and Interfaces*, *7*(9), 5538–5549. https://doi.org/10.1021/acsami.5b00146

Wei, J., Zang, Z., Zhang, Y., Wang, M., Du, J., & Tang, X. (2017). Enhanced performance of light-controlled conductive switching in hybrid cuprous oxide/reduced graphene oxide (Cu_2O/rGO) nanocomposites. *Optics Letters*, *42*(5), 911. https://doi.org/10.1364/ol.42.000911

Wei, S. N., Liu, X., Yan, J., Zhong, M., Joseph, P., Zhang, J., & Zhang, R. C. (2022). A study of the mechanical performance of nanocomposites of polyethylene containing exfoliated boron nitride nanoplatelets. *Polymer Composites*, *43*(9), 6276–6286. https://doi.org/10.1002/PC.26936

Weng, Q., Wang, X., Wang, X., Bando, Y., & Golberg, D. (2016). Functionalized hexagonal boron nitride nanomaterials: emerging properties and applications. *Chemical Society Reviews*, *45*(14), 3989–4012. https://doi.org/10.1039/C5CS00869G

Woodward, R. I., Murray, R. T., Phelan, C. F., de Oliveira, R. E. P., Runcorn, T. H., Kelleher, E. J. R., … de Matos, C. J. S. (2017). Characterization of the second- and third-order nonlinear optical susceptibilities of monolayer MoS2 using multiphoton microscopy. *2D Materials*, *4*(1). https://doi.org/10.1088/2053-1583/4/1/011006

Wu, S., Ladani, R. B., Zhang, J., Bafekrpour, E., Ghorbani, K., Mouritz, A. P., … Wang, C. H. (2015). Aligning multilayer graphene flakes with an external electric field to improve multifunctional properties of epoxy nanocomposites. *Carbon*, *94*, 607–618. https://doi.org/10.1016/J.CARBON.2015.07.026

Wu, X., Liu, W., Shi, F. guo, Yang, L., & Zhang, C. (2022). Constructing three-dimensional boron nitride network for highly thermally conductive epoxy resin composites. *Polymer Composites*, *43*(3), 1711–1717. https://doi.org/10.1002/PC.26490

Wurm, A., Ismail, M., Kretzschmar, B., Pospiech, D., & Schick, C. (2010). Retarded Crystallization in Polyamide/Layered Silicates Nanocomposites caused by an Immobilized Interphase. *Macromolecules*, *43*(3), 1480–1487. https://doi.org/10.1021/ma902175r

Wypych, F., & Schöllhorn, R. (1992). 1T-MoS_2, a new metallic modification of molybdenum disulfide. *J. Chem. Soc., Chem. Commun.*, (19). https://doi.org/10.1039/C39920001386

Xiang, M., Li, C., & Ye, L. (2018). Reactive melt processing of polyamide 6/reduced graphene oxide nano-composites and its electrically conductive behavior. *Journal of Industrial and Engineering Chemistry*, *62*, 84–95. https://doi.org/10.1016/j.jiec.2017.12.047

Xiang, M., Li, C., & Ye, L. (2019). Polyamide 6/reduced graphene oxide nano-composites prepared via reactive melt processing: formation of crystalline/network structure and

electrically conductive properties. *Journal of Polymer Research*, *26*(5), 1–14. https://doi.org/10.1007/s10965-019-1765-x

Xiao, M., & Du, B. X. (2016). Review of high thermal conductivity polymer dielectrics for electrical insulation. *High Voltage*, *1*(1), 34–42. https://doi.org/10.1049/HVE.2016.0008

Xiao, R., Wu, G., & Lin, Y. (2023). Rationalizing the interfacial layer in polymer nanocomposites: Correlation between enthalpy and dielectric relaxation. *Polymer*, *270*, 125765. https://doi.org/10.1016/J.POLYMER.2023.125765

Xin, Y., Duan, F., & Mu, X. (2020). Effects of defects on the interfacial shear characteristics between graphene and poly (methyl methacrylate). *Polymer Composites*, *41*(10), 4297–4306. https://doi.org/10.1002/PC.25712

Xu, F., Chen, R., Lin, Z., Qin, Y., Yuan, Y., Li, Y., … He, X. (2018). Superflexible Interconnected Graphene Network Nanocomposites for High-Performance Electromagnetic Interference Shielding. *ACS Omega*, *3*(3), 3599–3607. https://doi.org/10.1021/acsomega.8b00432

Xu, J.-T., Wang, Q., & Fan, Z.-Q. (2005). Non-isothermal crystallization kinetics of exfoliated and intercalated polyethylene/montmorillonite nanocomposites prepared by in situ polymerization. *European Polymer Journal*, *41*(12), 3011–3017. https://doi.org/10.1016/j.eurpolymj.2005.04.042

Xu, L., Tan, X., Xu, R., Xie, J., & Lei, C. (2019). Influence of functionalized molybdenum disulfide (MoS2) with triazine derivatives on the thermal stability and flame retardancy of intumescent Poly(lactic acid) system. *Polymer Composites*, *40*(6), 2244–2257. https://doi.org/10.1002/PC.25032

Xu, W. hua, He, Y., Xie, H., Qin, S., Tan, L. cao, Wu, T., & Qu, J. ping. (2021). Ultrafast Fabrication of Graphene-Reinforced Nanocomposites via Synergy of Steam Explosion and Alternating Convergent-Divergent Flow. *Small*, *17*(28), 2100017. https://doi.org/10.1002/SMLL.202100017

Xu, Z., & Gao, C. (2011). Aqueous Liquid Crystals of Graphene Oxide. *ACS Nano*, *5*(4), 2908–2915. https://doi.org/10.1021/nn200069w

Yang, B., Wang, S., Li, H., Song, Z., Liu, L., & Li, Y. (2021a). A molecular dynamics study on the effect of TSW defective graphene on the glass transition temperature of polymer materials. *Polymer Bulletin*, (0123456789). https://doi.org/10.1007/s00289-021-03631-y

Yang, B., Wang, S., Li, H., Song, Z., Liu, L., & Li, Y. (2021b). A molecular dynamics study on the effect of TSW defective graphene on the glass transition temperature of polymer materials. *Polymer Bulletin*, (0123456789). https://doi.org/10.1007/s00289-021-03631-y

Yang, J., Shi, G., Tu, Y., & Fang, H. (2014). High correlation between oxidation loci on graphene oxide. *Angewandte Chemie*, *53*(38), 10190–10194. https://doi.org/10.1002/ANIE.201404144

Yang, L., Chen, W., Yu, Q., & Liu, B. (2021). Mass production of two-dimensional materials beyond graphene and their applications. *Nano Research*, *14*(6), 1583–1597. https://doi.org/10.1007/s12274-020-2897-3

Yang, X., Tan, S., Li, G., & Zhou, E. (2001). Dependence of the brill transition on the crystal size of nylon 10 10. *Macromolecules*, *34*(17), 5936–5942. https://doi.org/10.1021/ma002091q

Ye, L., Xu, H., Zhang, D., & Chen, S. (2014). Synthesis of bilayer MoS2 nanosheets by a facile hydrothermal method and their methyl orange adsorption capacity. *Materials Research Bulletin*, *55*, 221–228. https://doi.org/10.1016/J.MATERRESBULL.2014.04.025

Yin, X., & Hu, G. (2015). Effects of organic montmorillonite with different interlayer spacing on mechanical properties, crystallization and morphology of polyamide 1010/nanometer calcium carbonate nanocomposites. *Fibers and Polymers*, *16*(1), 120–128. https://doi.org/10.1007/s12221-015-0120-z

Yin, X., Hu, G., Luo, Y., & Fan, X. (2017). Influence of synergism caused by organic montmorillonite and nanometer calcium carbonate on mechanical properties and crystallization of polyamide 1010-based composites. *Fibers and Polymers*, *18*(7), 1314–1322. https://doi.org/10.1007/s12221-017-1074-0

Yoo, B. M., Shin, H. J., Yoon, H. W., & Park, H. B. (2014). Graphene and graphene oxide and their uses in barrier polymers. *Journal of Applied Polymer Science*, *131*(1). https://doi.org/10.1002/app.39628

Yoshioka, Y., & Tashiro, K. (2003). Structural change in the Brill transition of Nylon m/n (1) Nylon 10/10 and its model compounds. *Polymer*, *44*(22), 7007–7019. https://doi.org/10.1016/j.polymer.2003.04.001

Young, R. J., Kinloch, I. A., Gong, L., & Novoselov, K. S. (2012). The mechanics of graphene nanocomposites: A review. *Composites Science and Technology*, *72*(12), 1459–1476. https://doi.org/10.1016/j.compscitech.2012.05.005

Yousefi, N., Lin, X., Zheng, Q., Shen, X., Pothnis, J. R., Jia, J., … Kim, J. K. (2013). Simultaneous in situ reduction, self-alignment and covalent bonding in graphene oxide/epoxy composites. *Carbon*, *59*, 406–417. https://doi.org/10.1016/j.carbon.2013.03.034

Yousefi, N., Sun, X., Lin, X., Shen, X., Jia, J., Zhang, B., … Kim, J. K. (2014). Highly aligned graphene/polymer nanocomposites with excellent dielectric properties for high-performance electromagnetic interference shielding. *Advanced Materials*, *26*(31), 5480–5487. https://doi.org/10.1002/adma.201305293

Yu, B., Fan, J., He, J., Liu, Y., Wang, R., Qi, K., … Luo, Z. (2022). Boron Nitride Nanosheets: Large-Scale Exfoliation in Naoh-Licl Solution and Their Highly Thermoconductive Insulating Nanocomposite Paper with Pi Via Electrospinning-Electrospraying. *SSRN Electronic Journal*. https://doi.org/10.2139/SSRN.4156642

Yu, J., Zhao, W., Wu, Y., Wang, D., & Feng, R. (2018). Tribological properties of epoxy composite coatings reinforced with functionalized C-BN and H-BN nanofillers. *Applied Surface Science*, *434*, 1311–1320. https://doi.org/10.1016/J.APSUSC.2017.11.204

Yu, L., & Yu, H. (2015). Light-powered tumbler movement of graphene oxide/polymer nanocomposites. *ACS Applied Materials and Interfaces*, *7*(6), 3834–3839. https://doi.org/10.1021/am508970k

Yu, X., Cheng, H., Zhang, M., Zhao, Y., Qu, L., & Shi, G. (2017, August 1). Graphene-based smart materials. *Nature Reviews Materials*, Vol. 2, pp. 1–13. Nature Publishing Group. https://doi.org/10.1038/natrevmats.2017.46

Yu, Z., & Drzal, L. T. (2020). Functionalized graphene oxide as coupling agent for graphene nanoplatelet/epoxy composites. *Polymer Composites*, *41*(3), 920–929. https://doi.org/10.1002/PC.25423

Yuan, D., Wang, B., Wang, L., Wang, Y., & Zhou, Z. (2013). Unusual toughening effect of graphene oxide on the graphene oxide/nylon 11 composites prepared by in situ melt polycondensation. *Composites Part B: Engineering*, *55*, 215–220. https://doi.org/10.1016/j.compositesb.2013.05.055

Zakaria, M. R., Md Akil, H., Omar, M. F., Abdul Kudus, M. H., Mohd Sabri, F. N. A., & Abdullah, M. M. A. B. (2020). Enhancement of mechanical and thermal properties of carbon fiber epoxy composite laminates reinforced with carbon nanotubes interlayer using electrospray deposition. *Composites Part C: Open Access*, *3*, 100075. https://doi.org/10.1016/j.jcomc.2020.100075

Zang, C.-G., Zhu, X.-D., & Jiao, Q.-J. (2015). Enhanced mechanical and electrical properties of nylon-6 composite by using carbon fiber/graphene multiscale structure as additive. *Journal of Applied Polymer Science*, *132*(19), n/a-n/a. https://doi.org/10.1002/app.41968

Zeng, H., Gao, C., Wang, Y., Watts, P. C. P., Kong, H., Cui, X., & Yan, D. (2006). In situ polymerization approach to multiwalled carbon nanotubes-reinforced nylon 1010 composites: Mechanical properties and crystallization behavior. *Polymer*, *47*(1), 113–122. https://doi.org/10.1016/j.polymer.2005.11.009

Zeng, M., Xiao, Y., Liu, J., Yang, K., & Fu, L. (2018). Exploring Two-Dimensional Materials toward the Next-Generation Circuits: From Monomer Design to Assembly Control. *Chemical Reviews*, *118*(13), 6236–6296. https://doi.org/10.1021/acs.chemrev.7b00633

Zeng, Y., Li, T., Yao, Y., Li, T., Hu, L., & Marconnet, A. (2019). Thermally Conductive Reduced Graphene Oxide Thin Films for Extreme Temperature Sensors. *Advanced Functional Materials*, *29*(27), 1901388. https://doi.org/10.1002/adfm.201901388

Zhang, Hao, Moon, Y. K., Zhang, X. Q., Liu, J. S., Zhang, H. X., & Yoon, K. B. (2017). Facile preparation of functionalized MoS2/polyethylene nanocomposites through in situ polymerization with MoS2 containing Ziegler–Natta catalyst. *European Polymer Journal*, *87*, 60–68. https://doi.org/10.1016/j.eurpolymj.2016.12.010

Zhang, He xin, Seo, D. H., Lee, D. E., & Yoon, K. B. (2021). Fabrication of highly thermal conductive PA6/hBN composites via in-situ polymerization process. *Journal of Polymer Research*, *28*(2). https://doi.org/10.1007/s10965-020-02378-w

Zhang, J., Lei, W., Schutz, J., Liu, D., Tang, B., Wang, C. H., & Wang, X. (2019). Improving the gas barrier, mechanical and thermal properties of poly(vinyl alcohol) with molybdenum disulfide nanosheets. *Journal of Polymer Science, Part B: Polymer Physics*, *57*(7), 406–414. https://doi.org/10.1002/polb.24799

Zhang, L., Deng, H., & Fu, Q. (2018). Recent progress on thermal conductive and electrical insulating polymer composites. *Composites Communications*, *8*, 74–82. https://doi.org/10.1016/j.coco.2017.11.004

Zhang, Q., Lin, D., Deng, B., Xu, X., Nian, Q., Jin, S., … Cheng, G. J. (2017). Flyweight, Superelastic, Electrically Conductive, and Flame-Retardant 3D Multi-Nanolayer Graphene/Ceramic Metamaterial. *Advanced Materials*, *29*(28), 1605506. https://doi.org/10.1002/adma.201605506

Zhang, S.-L., Wang, G.-B., Jiang, Z.-H., Wang, D., Ma, R.-T., & Wu, Z.-W. (2005). Impact properties, phase structure, compatibility, and fracture morphology of polyamide-

1010/thermoplastic poly(ester urethane) elastomer blends. *Journal of Polymer Science Part B: Polymer Physics*, *43*(10), 1177–1185. https://doi.org/10.1002/polb.20410

Zhang, S.-L., Wang, G.-B., Jiang, Z.-H., Wang, D., Ma, R.-T., Wu, Z.-W., & Lab, A. G. M. (2005). Impact properties, phase structure, compatibility, and fracture morphology of polyamide-1010/thermoplastic poly (ester urethane) elastomer blends. *Wiley Online Library*, *43*(10), 1177–1185. https://doi.org/10.1002/polb.20410

Zhang, X., Geng, B., Chen, H., Chen, Y., Wang, Y., Zhang, L., … Chen, J. (2018). Extraordinary toughness enhancement of poly(lactic acid) by incorporating very low loadings of noncovalent functionalized graphene-oxide via masterbatch-based melt blending. *Chemical Engineering Journal*, *334*, 2014–2020. https://doi.org/10.1016/J.CEJ.2017.11.102

Zhao, B., Zhao, C., Hamidinejad, M., Wang, C., Li, R., Wang, S., … Park, C. B. (2018). Incorporating a microcellular structure into PVDF/graphene–nanoplatelet composites to tune their electrical conductivity and electromagnetic interference shielding properties. *Journal of Materials Chemistry C*, *6*(38), 10292–10300. https://doi.org/10.1039/C8TC03714K

Zhao, C., Ang, J. M., Liu, Z., & Lu, X. (2017). Alternately stacked metallic 1T-MoS2/polyaniline heterostructure for high-performance supercapacitors. *Chemical Engineering Journal*, *330*, 462–469. https://doi.org/10.1016/j.cej.2017.07.129

Zhao, G., Han, S., Wang, A., Wu, Y., Zhao, M., Wang, Z., & Hao, X. (2015). "Chemical Weathering" Exfoliation of Atom-Thick Transition Metal Dichalcogenides and Their Ultrafast Saturable Absorption Properties. *Advanced Functional Materials*, *25*(33), 5292–5299. https://doi.org/10.1002/adfm.201501972

Zhi, C., Bando, Y., Tang, C., Honda, S., Kuwahara, H., & Golberg, D. (2006). Boron nitride nanotubes/polystyrene composites. *Journal of Materials Research*, *21*(11), 2794–2800. https://doi.org/10.1557/jmr.2006.0340

Zhishen, M., Qingbo, M., Jinhua, F., Hongfang, Z., & Donglin, C. (1993). Crystal structure and thermodynamic parameters of Nylon-1010. *Polymer International*, *32*(1), 53–60. https://doi.org/10.1002/pi.4990320110

Zhou, K., Liu, J., Zeng, W., Hu, Y., & Gui, Z. (2015). In situ synthesis, morphology, and fundamental properties of polymer/MoS_2 nanocomposites. *Composites Science and Technology*, *107*, 120–128. https://doi.org/10.1016/j.compscitech.2014.11.017

Zhou, K., Tang, G., Gao, R., & Guo, H. (2018). Constructing hierarchical polymer@MoS2 core-shell structures for regulating thermal and fire safety properties of polystyrene nanocomposites. *Composites Part A: Applied Science and Manufacturing*, *107*, 144–154. https://doi.org/10.1016/j.compositesa.2017.12.026

Zhou, M. Y., Liu, J., & Zhang, L. Q. (2022, October 31). Structure and properties of polymer/two-dimensional nanomaterials studied via molecular dynamics simulation: a review. *Molecular Systems Design and Engineering*, Vol. 8, pp. 11–31. Royal Society of Chemistry. https://doi.org/10.1039/d2me00121g

Zhou, S., Shi, Y., Bai, Y., Liang, M., & Zou, H. (2020). Preparation of thermally conductive polycarbonate/boron nitride composites with balanced mechanical properties. *Polymer Composites*, *41*(12), 5418–5427. https://doi.org/10.1002/PC.25805

Zhou, W., Zou, X., Najmaei, S., Liu, Z., Shi, Y., Kong, J., … Idrobo, J. C. (2013). Intrinsic structural defects in monolayer molybdenum disulfide. *Nano Letters*, *13*(6), 2615–2622. https://doi.org/10.1021/nl4007479

Zhu, Y., Murali, S., Cai, W., Li, X., Suk, J. W., Potts, J. R., & Ruoff, R. S. (2010). Graphene and graphene oxide: Synthesis, properties, and applications. *Advanced Materials*, *22*(35), 3906–3924. https://doi.org/10.1002/adma.201001068